AUC GEOGRAPHICA

48
2/2013

CONTENTS

THE CAUSES AND MECHANISMS OF MORAINE-DAMMED LAKE FAILURES IN THE CORDILLERA BLANCA, NORTH AMERICAN CORDILLERA, AND HIMALAYAS

ADAM EMMER[1], ALEJO COCHACHIN[2]

[1] Charles University in Prague, Faculty of Science, Department of Physical Geography and Geoecology
[2] Unidad de Glaciologia y Recursos Hydricos del Autoridad Nacional de Agua

ABSTRACT

Glacial lake outburst floods (GLOFs) from moraine-dammed lake failures represent a significant threat to inhabitants of high mountain areas across the globe. The first part of this paper summarises the causes and mechanisms of moraine-dammed lake failures through a review of the scientific literature and unpublished reports. There are eight main causes, of which five are characterised as dynamic and three as long-term, and these are associated with around twenty failure mechanisms. The dynamic causes are slope movements into the lake, earthquakes, flood waves from a lake situated upstream, blocking of underground outflow channels, and intensive rainfall or snowmelt. The long-term causes are the melting of buried ice, the impact of hydrostatic pressure, and the effect of time. These causes (triggers) and the consequent mechanisms of dam failure are described in detail. The second part compares the historical moraine-dammed lake failures within three regions between 1900 and 2009: the Cordillera Blanca of Peru, the North American Cordillera, and the Himalayas. It has been found that dynamic causes are around four times more common than long-term causes although significant regional differences have been observed. The most frequent causes in these regions were found to be slope movements in which the displaced material was dominated by solid-state water (ice falls, ice avalanches, and snow avalanches). The other causes tended to show distinct regional patterns while the temporal distribution of events also differs according to region. In the North American Cordillera and Himalayas moraine dam failures occur exclusively during the summer season while in the Cordillera Blanca they are more evenly distributed with the exception of the dry season. This reflects the general climatic setting of each of the study regions.

Keywords: moraine-dammed lakes, natural dam failures, GLOFs, natural hazards, high mountain areas

1. Introduction

In this study moraine-dammed lakes are defined as natural freshwater reservoirs dammed by material accumulated from a glacier (the moraine). This type of lake is not considered to be particularly stable because the morainic material forming the dam is usually unconsolidated and, therefore, even a relatively weak trigger can cause the dam to fail, leading to a glacial lake outburst flood (GLOF) (e.g. Costa & Schuster 1988; Richardson & Reynolds 2000a; Shrestha 2010). This form of flood describes the sudden water release from any form of glacial lake (e.g. bedrock-dammed, moraine-dammed, or ice-dammed) irrespective of its cause (Benn & Evans 1998). These floods are characterised by peak discharges that are many times higher than those of a hydrometeorological flood (Clauge & Evans 2000). They, therefore, have the potential to be highly catastrophic. GLOFs may occur as a result of dam failure (moraine-dammed or ice-dammed) or dam overflow (all types of glacial lake).

The study of moraine-dammed lake failure is complex and requires interdisciplinary cooperation. It is appreciated that two main groups of parameters are decisive in contributing to a moraine dam failure, the first is that of dam stability and the second is the possibility of a triggering event (Richardson & Reynolds 2000a; Hegglin & Huggel 2008). These are difficult to assess and quantify which leads to problems in estimating the probability

of a moraine dam failure (hazard assessment) (Emmer & Vilímek 2013). It is possible for a moraine dam failure to be total or partial and, therefore, a given lake can be subjected to repeated GLOFs (O'Connor et al. 2001; Bajracharya et al. 2007a). GLOFs represent an increasingly significant threat in high-mountain areas because the number of potentially dangerous glacial lakes is increasing as a result of global climate change and concurrent glacier retreat (e.g. Evans & Clauge 1994; Bolch et al. 2008; Ives et al. 2010).

GLOFs from moraine-dammed lake failures have been studied in high-mountain regions all over the world including the Himalaya (Vuichard & Zimmerman 1987; Kattelmann & Watanabe 1997; Bajracharya et al. 2007a,b), Hindu-Kush (Iturrizaga 2005; Ives et al. 2010), Karakoram (Hewitt 1982), Tian-Shan (Janský et al. 2009; Narama et al. 2010; Bolch et al. 2011), Caucasus Mts. (Petrakov et al. 2007), Cascade Range (O'Connor et al. 2001), British Columbia (Clauge & Evans 2000; Kershaw et al. 2005), Peruvian Andes (Zapata 1984; Vilímek et al. 2005a; Carey et al. 2011; Klimeš 2012), Patagonia (Harrison et al. 2006; Dussaillant et al. 2009) as well as in the European Alps (Haeberli et al. 2001; Huggel et al. 2004) and Scandinavia (Breien et al. 2008). The objectives of this paper are to provide an overview of moraine-dammed lake failures, to investigate their causes and mechanisms, and to compare the temporal aspect of these events within three

regions: the Cordillera Blanca of Peru, the North American Cordillera, and Himalaya. These areas were chosen because they have a long history of moraine-dammed lake research and there is, therefore, a greater chance of acquiring information about GLOFs. The flooding that occurs as a result of moraine-dammed lake failures poses a significant threat in high mountain regions and by comparing events it is possible to recognise the regional specifics that are necessary in order to build an optimal regionally focused hazard assessment.

2. Materials and methods

The causes (triggers) and mechanisms of moraine-dammed lake failures are summarised following an extensive search of the published scientific literature and unpublished reports from the archive of the Autoridad Nacional de Agua in Huaraz, Peru. These causes and consequent mechanisms of dam failure are described in detail with examples given for each. The similarities and disparities that exist between the particular causes have been investigated as well as the temporal characteristics of events in the Cordillera Blanca of Peru, the North American Cordillera, and Himalaya. The GLOF database (GLOFs database 2012) has been used as the basis for this comparative analysis: the details of around ninety-five moraine dam failures within the three study areas have been compiled for the period 1900 to 2009. The causes of the GLOFs are known in sixty of these cases (twenty in Cordillera Blanca of Peru, eleven in the North American Cordillera, and twenty-nine in Himalaya) but unknown in the other instances. The precise dates of the GLOFs are known in sixty-six of the cases and can be attributed to a year in seventy-five instances. The temporal characteristics of the GLOFs are considered both in terms of their monthly and annual distributions.

3. The causes and mechanisms of moraine-dammed lake failures

There is a close relationship between various types of natural hazards and moraine-dammed lake failures that result in GLOFs. The former, the various natural hazards, often represent the cause of the latter, the lake failures. These relationships are summarised in Figure 1. Yamada (1998) divided the process of moraine dam failure into two groups: the first consisted of dam failure caused by a dynamic initiating event while the second consisted of spontaneous "dam self-destruction". The latter group are caused by long-term degradation of the dam without a dynamic initiating event. This grouping is followed here and the causes of moraine dam failure are classifies as either dynamic causes or long-term.

3.1 The dynamic causes of moraine-dammed lake failures

The dynamic causes are slope movements into the lake, earthquakes, a flood wave from a lake situated upstream, blocking of underground outflow channels, and intensive rainfall or snowmelt. In this group the time interval between the trigger and the moraine dam failure ranges from minutes in the case of, for example, a slope movement into the lake to hours or days in the case of, for example, intensive rainfall or snowmelt. These dynamic causes were termed "quasicoincidental" by O'Connor et al. (2001) as it is not possible to accurately predict the time or place in which they will occur.

The slope movement into the lake includes various types of mass-movement such as icefalls, avalanches, rockfalls, landslides, debris flows, and mudflows. The mass of material entering the lake causes water displacement in the form of surge (displacement) waves (Richardson & Reynolds 2000a) and these can reach heights of tens of metres (Plafker & Eyzaguirre 1979 in Costa & Schuster
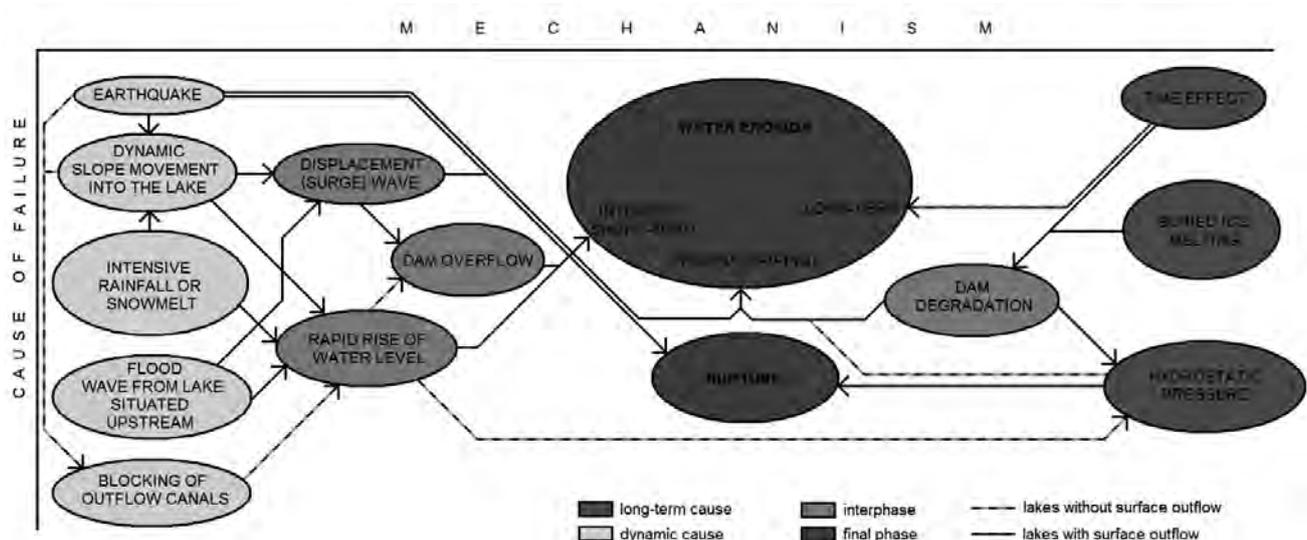

Fig. 1 The causes and mechanisms that underpin the process of moraine dam failure.

1988). The waves have a considerable impact on the stability of the moraine-dam (e.g. Kattelmann & Watanabe 1997; Clauge & Evans 2000). The slope movement into the lake and its related displacement wave may lead to two different mechanisms of dam failure. The first is that of immediate dam rupture following the impact of the displacement wave and this represents the most catastrophic scenario while the second is that of dam failure due to an increase in outflow channel discharge. The second mechanism is essentially caused by the increased water level within the lake which increases the outflow channel discharge and causes increased incision which then, in turn, increases the discharge and increases the incision. This "positive feedback" (Yamada 1998) continues until the outflow channel is either able to resist the incision due to structural changes or until the lake empties (Clauge & Evans 2000). However, if the displacement wave has the necessary energy and moraine dam is at the same time sufficiently resistant, flooding may result from dam overflow (Kershaw et al. 2005). This may happen without significant damage to the moraine dam and an example occurred on 22nd April 2002 as a result of rockfall into lake Safuna Alta in the Cordillera Blanca (Hubbard et al. 2005). It is possible for dam overflow and outflow channel incision caused by sudden rise of the water level to occur during the same flood event. Kershaw et al. (2005) presented stratigraphical and sedimentological evidence from the Queen Bess lake GLOF on 12th August 1997 that indicated both scenarios. The first phase of flooding was represented by dam overflow during which the bulk of the flood volume escaped (Clauge & Evans 2000) while the second phase was represented by dam incision and final failure. The time interval between these phases was in order of minutes (Evans et al. 2002).

It is possible for an earthquake to directly initiate a moraine-dammed lake failure as the shock can cause sufficient damage to a dam for it to fail (Clauge & Evans 2000) while there is also the chance that the seismic activity may initiate slope movements. In some cases it is not known whether dam failure was caused directly by an earthquake or if it was caused by slope movements initiated by an earthquake and this is particularly difficult distinguish in the case of historical events (Strasser et al. 2008). There is also the chance that an earthquake could change the internal structure of the moraine dam causing internal erosion in the form of piping which may then lead to the emptying of the lake (Lliboutry et al. 1977). In contrast, changes in the internal structure of the dam may serve to reduce infiltration through the moraine by blocking underground outflow channels. This may be dangerous in instances where the lake does not have a surface outflow as there is then a continuous rise in lake water level. It was seen at lake Parón (Cordillera Blanca) when an earthquake in 1966 inhibited flow along underground channels and the water level rose steadily until next strong earthquake in 1970 when discharge turned into the values before 1966 event (Lliboutry et al. 1977).

The flood wave from an upstream lake can cause dam failure on a lake situated downstream. The flood wave can often transform easily into different types of flows because of its high erosion and transport potential (Cenderelli & Wohl 2001; Breien et al. 2008). It produces a displacement wave or a significant rise in the water level when entering the downstream lake and this has the same consequences as a slope movement into the lake. A dam failure may occur as a result of the direct impact of the displacement wave or following incision of the outflow channels. The overall flood volume often considerable in these cases as there are inputs from two lakes. This was seen in the Cordillera Blanca following the Palcacocha outburst flood which destroyed the downstream lake Jircacocha on 13th December 1941 (Vilímek et al. 2005b) (Figure 2). The catastrophic debris-flow incorporated water from both lakes and destroyed one-third of the city of Huaraz claiming about 6000 lives (Lliboutry et al. 1977). However, in some cases, the downstream lake may absorb the flood wave if it has a sufficiently large accommodation space. It is known that lake Parón in the Cordillera Blanca has been able to absorb outburst floods from two lakes, the first from lake Chacrucocha prior to 1950 and second from lake Artesoncocha in 1951 (Lliboutry et al. 1977; Carey et al. 2012).

The blocking of underground outflow channels can be caused by four mechanisms: clogging by sediments brought into the lake by its tributaries; clogging by material brought into the lake during mass-movements; freezing of outflow channels (O'Connor et al. 2001); and blocking of outflow channels caused by the changing internal structure of dam due to an earthquake (Lliboutry et al. 1977). The water level of the lake starts to rise if the channels are blocked and this leads to the same mechanism of dam failure as occurs during intense rainfall or snowmelt – dam rupture caused when the lithostatic pressure exceeds that of hydrostatic pressure (Richardson & Reynolds 2000a). There will also be increased erosion in instances of dam overflow. However, unlike the rise in water level caused by intense rainfall or snowmelt, the blocking of underground outflow channels usually causes the water level to increase until the lake basin is full. This occurs unless the hydrostatic pressure exceeds the lithostatic pressure as blocked channels do not usually unblock spontaneously. The moraine dam failure at lake Zhangzhanbo in Tibet on 11th July 1981 was caused by blocking of underground outflow channels (Ding & Liu 1992; Yamada 1998).

It is also clear that intense rainfall or snowmelt will lead to a rise in the water level of the lake. This cause depends on many factors of which the variability and extremity of the precipitation are perhaps the most significant or, alternatively, the variability and extremity of air temperature in relation to snowmelt (Yamada 1998). If a lake has surface runoff the increasing water level may lead to an increase in the erosion of the outflow channels and to the cycle of "positive feedback" (see above). If a lake does not
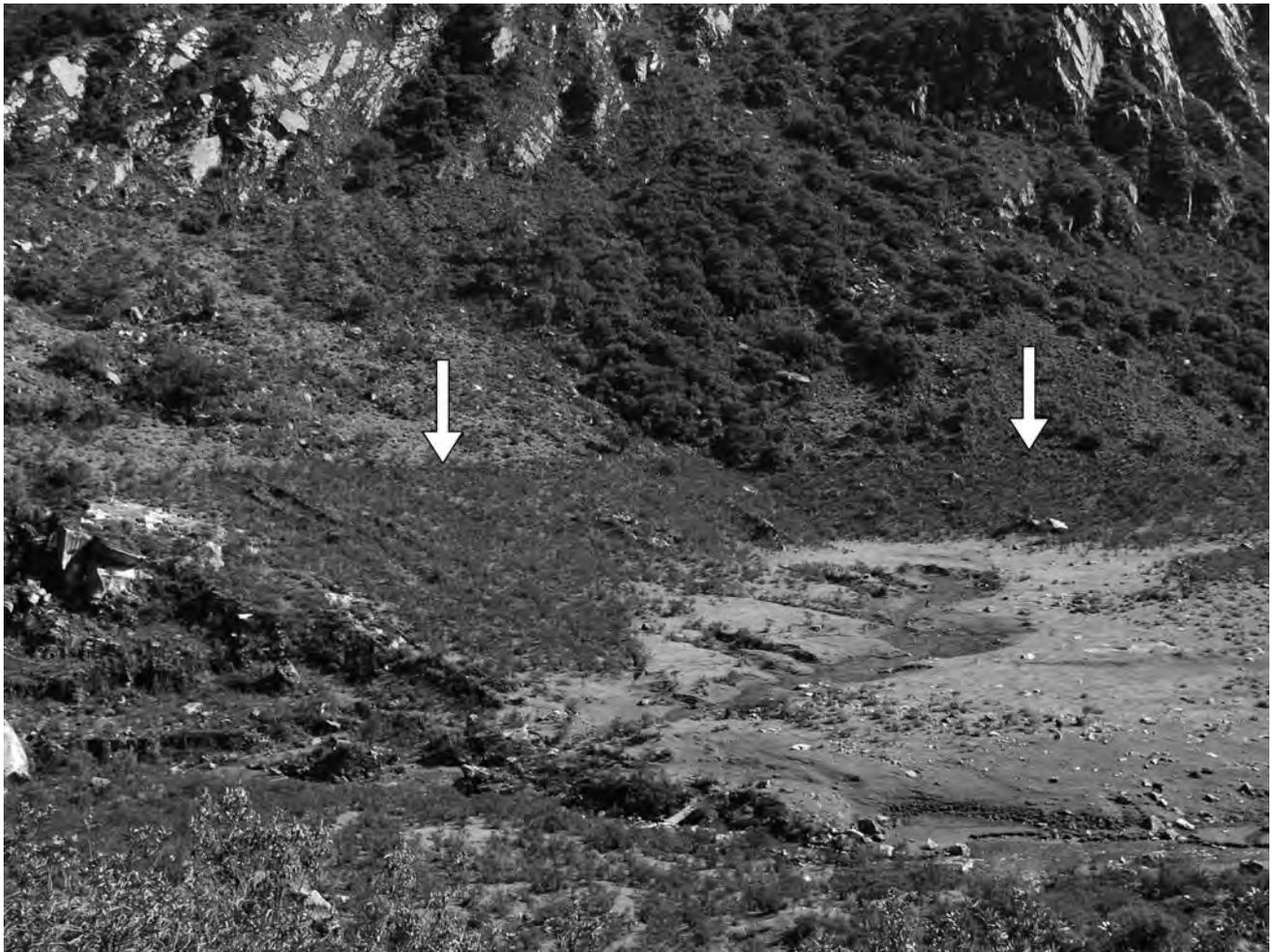
Fig. 2 The former lake basin of Jircacocha in the Cordillera Blanca. Its dam failed after the arrival of a flood wave from lake Palcacocha. The horizontal line indicated by arrows shows the former water level.

have surface runoff then the most important factor is the dam freeboard which is defined as the vertical elevation between the lake level and the lowest point on the dam crest. The rise in lake water level can lead to two different mechanisms of dam destruction. The first mechanism is dam rupture due to the increased hydrostatic pressure. This happens when the hydrostatic pressure overcomes the lithostatic pressure, which keeps the components of the dam together (Richardson & Reynolds 2000a). The second is dam overflow from which the subsequent erosion may induce dam failure (Kattelmann & Watanabe 1997). The failure of a dam under the Dallier glacier in the Cascade Range provides an example of one that occurred as a result of intense rainfall or snowmelt (O'Connor et al. 2001). It is also well known that intense rainfall also a major trigger for slope movements, which may initiate moraine dam failure.

3.2 The long-term causes of moraine-dammed lake failures

The long-term causes of dam destruction are the ice melting of buried ice, the impact of hydrostatic pressure, and the effect of time. It is difficult to accurately constrain which of these long-term issues ultimately leads to the destruction of the dam. This led Yamada (1998) to group these under the title of "self-destruction" due to the absence of an initial external dynamic event (Yamada 1998; Bajracharya et al. 2007b). The long-term causes also weaken the resistance of the dam to dynamic causes: while the impact of hydrostatic pressure and the effect of time have some influence on the moraine dam they are not often the main cause of dam destruction. The degradation of a moraine dam is a function of time and this function does not constitute a single process. It is, instead, a group of processes that may lead to the degradation of a dam over a protracted period and which affects the moraine slope stability, dam freeboard, internal structure etc. In combination with, for example, intense rainfall, the effect of time may lead to mass movements on moraine slopes (Awal et al. 2010). If a lake is associated with a surface outflow, its sequential erosion may cause the lake to empty, without a significant GLOF (Yamada 1998). If a lake is not associated with a surface outflow, the internal erosion of outflow channels through piping may also cause the lake to empty, without a significant GLOF (Clauge & Evans 2000; Haeberli et al. 2001).

Fig. 3 An example of an uncovered ice lens in the protruding basal moraine of the developing lake Llaca in the Cordillera Blanca.

The term "buried ice" describes an ice lens integrated into the body of the moraine dam (Figure 3). It is possible for this to represent up to 90% of the dam volume (Costa & Schuster 1988). The melting of this buried ice weakens the stability of the dam as it disrupts its structural integrity and may also decrease the dam freeboard (Richardson & Reynolds 2000b; Huggel et al. 2002). The disruption of the structural integrity of the dam enables rupture by hydrostatic pressure while it also decreases the ability of the dam to withstand other causes that would not normally represent a significant problem. For example, the long-term degradation of the moraine dam leads to a decrease in the freeboard which, in combination with moderate rainfall or snowmelt, may lead to dam destruction.

The hydrostatic pressure is the pressure exerted by the gravitational force acting on a water column at certain depth. The water dammed in a moraine-dammed lake affects the dam by this pressure and its long-term affect may lead to the dam failure (Yamada 1998). This cause becomes especially significant if the moraine dam is weakened by, for example, buried ice melting while deep lakes are more susceptible to rupture caused by hydrostatic pressure. The destruction caused by the systematic effect of hydrostatic pressure occurs when the moraine dam is no longer able to resist the hydrostatic pressure, i.e. the hydrostatic pressure exceeds the lithostatic pressure (Richardson & Reynolds 2000a). This may be caused by an increase in the lake water level or the protracted degradation of the moraine dam (Yamada 1998; Jaboyedoff et al. 2004 in Vilímek et al. 2005a). The increase in lake water level may be caused by intense rainfall or snowmelt or the blocking of underground outflow channels (Costa & Schuster 1988; Grabs & Hanish 1993; Janský et al. 2006). It is also possible to increase the hydrostatic pressure by basal ice melting and lake deepening (Watanabe & Rothacher 1996). In cases where dam degradation occurs as a result of buried ice melting, intense slope erosion, or changes in the internal structure of the dam, rupture by hydrostatic pressure may occur without a significant change in the pressure (Richardson & Reynolds 2000a). These all represent examples of "dam self-destruction" and may occur without a dynamic trigger. This happened in 1994 at lake Lugge Tsho in Bhutan (Watanabe & Rothacher 1996). The impact of hydrostatic pressure has a specific position in the categorisation of mechanisms of dam destruction as both dynamic and long-term causes can lead to dam rupture caused by hydrostatic pressure (Figure 1).

4. The comparative analysis

The comparative analysis investigates historical moraine-dammed lakes failures between 1900 and 2009 from three regions: the Cordillera Blanca of Peru, the North American Cordillera, and Himalaya. The basic characteristics of these regions are listed in Table 1. These regions are commonly characterised by glacier retreat at present which is leading to the formation and

Tab. 1 The basic characteristics of the studied regions.

Region	Mountains	Coordinates	Highest peak(s)	Climatic settings
Cordillera Blanca	Cordillera Blanca (Peru) Cordillera Huayhuash (Peru)	8°–10° S 77°–78° W	Huascarán (6768 m asl)	Tropical High Mountain Climate – Wet & Dry Seasons
North American Cordillera	Coast Mountains (CAN) Rocky Mountains (CAN) Cascade Range (USA)	30°–50° N 120°–135° W	Mt. Waddington (4019 m asl) Mt. Rainier (4392 m asl)	Temperate High Mountain Climatic Zone – 4 Seasons
Himalaya	Himalaya (China, India, Nepal, Bhutan)	27°–35° N 75°–95° E	Mt. Everest/ Sagarmatha (8848 m asl)	Temperate High Mountain Climatic Zone – 4 Seasons

development of new potentially dangerous moraine-dammed lakes. The threat of GLOFs in these areas is real while the downstream valleys are often settled.

4.1 The spatial analysis

It is important to assess whether there are differences regarding the causes of moraine-dammed lake failures across the three study regions. The slope movements have been divided into two subgroups for this purpose: the first incorporates slope movements in which the displaced material was dominated by solid-state water (ice falls, ice avalanches, and snow avalanches) while the second incorporates movements in which the displaced material was dominated by rock or liquid-state water (rockfalls, landslides, and various types of flows). It should be noted that the failure mechanisms for these two subgroups are identical. Furthermore, the concept of dam failure stemming from a combination of long-term causes without an evident dynamic cause ("dam self-destruction" (Yamada 1998) suggests that it will always be difficult to define the precise cause of failure (i.e. there is no distinguishing between the ice melting of buried ice, the impact of hydrostatic pressure, and the effect of

time). Indeed, unless a lake is continuously monitored, it is often difficult to determine the cause of a contemporary GLOF, and even more so in the case of historical events. Therefore, while a single cause may be the most commonly ascribed, there is a possibility that it in part reflects the ease with which it can be identified. The comparison of dynamic and long-term causes (Table 2) shows that, across all three regions, dynamic causes prevail over long-term causes by a ratio of 4 : 1. There are, however, significant regional differences. In the Cordillera Blanca all of the twenty dam failures resulted from a dynamic event while more than two-fifths resulted from a long-term cause in Himalaya ("dam self-destruction").

The most frequent cause of failure in three regions of interest was found to be slope movements in which the displaced material was dominated by solid-state water (ice falls, ice avalanches, and snow avalanches) (Figure 4). This finding corresponds with those of previous studies (e.g. Costa & Schuster 1988; Ding & Liu 1992; Clauge & Evans 2000; Jiang et al. 2004; Awal et al. 2010). The second and the third most frequent causes tend to show distinct regional patterns with the second most common cause being slope movements dominated by solid rock or water in the Cordillera Blanca of Peru, intensive rainfall

Tab. 2 The dynamic and long-term causes of moraine-dammed lake failures (60 instances where causes of the moraine dam failures are known).

Region	Dynamic Causes		Long-term Causes		Total number of events
	Number of events	%	Number of events	%	
Cordillera Blanca	20	100.0	0	0.0	20
North American Cordillera	10	90.9	1	10.1	11
Himalaya	17	58.6	12	41.4	29
Total	47	78.3	13	21.7	60
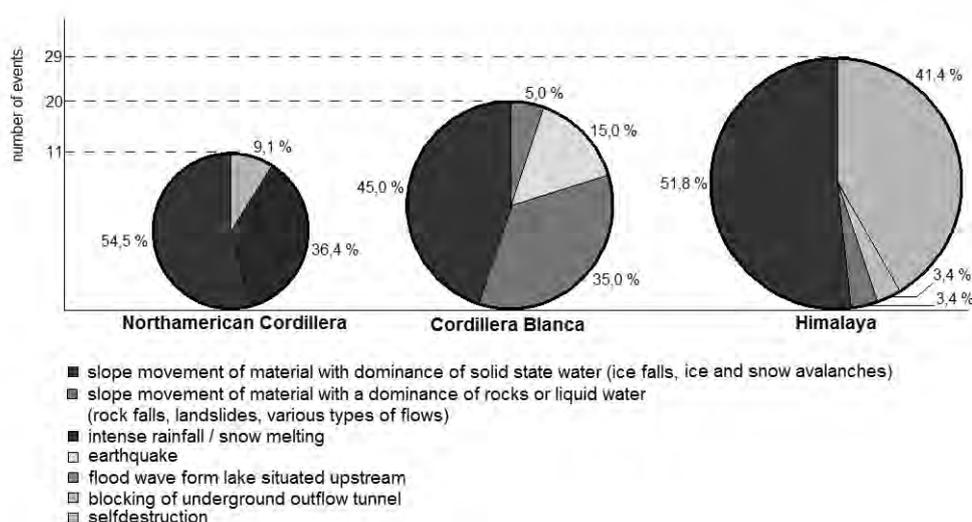
Fig. 4 A representation of the causes of moraine-dammed lake failures in the Cordillera Blanca, the North American Cordillera, and Himalaya.

or snowmelt in the North American Cordillera, and self-destruction in Himalaya. It is of interest to note that intensive rainfall or snowmelt is only recorded as a trigger in the North American Cordillera and it may be that this reflects the particular climatic setting of the region. The moraine-dammed lakes in the North American Cordillera are situated between 1400 and 2400 m asl (O'Connor et al. 2001) whereas in the Cordillera Blanca and Himalaya they generally occur between 4000 and 5000 m asl (Lliboutry et al. 1977; Yamada 1998). The intensity of the combined rainfall and snowmelt may be greater in the North American Cordillera during the summer due to these lower elevations. Thereafter, only one moraine-dammed lake failure in the North American Cordillera was attributed to dam self-destruction.

The trigger of dam self-destruction represents the second most frequent cause of moraine dam failures in Himalaya. This may reflect the significant volumes of buried ice that occur in many moraine dam bodies in this region (Yamada 1998; Bajracharya et al. 2007b). The melting of buried ice leads to degradation of moraine dam and this may lead to its failure, especially in combination with the affect of hydrostatic pressure impact, without a dynamic triggering event (see above). Thereafter, one moraine dam failure in the region was caused by the blocking of underground outflow channels and one by a slope movement into a lake in which the displaced material was dominated by rock or liquid-state water. The second most frequent cause of moraine-dammed lake failures in the Cordillera Blanca were slope movements into lakes in which the displaced material was dominated by rock. In fact, slope movements account for 80% of all moraine dam failures in this region while 15% could

be attributed to an earthquake. Thereafter, one dam failure was caused by the propagation of a flood wave which resulted from the failure of an upstream dam.

4.2 The temporal analysis

This section focuses on the temporal distribution of 66 moraine-dammed lake failures and GLOFs over months (Figure 5) and 75 moraine-dammed lake failures and GLOFs over years (Figure 6). The monthly differences in the distribution of GLOFs shown in Figure 5 clearly reflect the general climatic setting of each of the study regions. The temporal distribution of moraine dam failures is similar in the North American Cordillera and Himalaya as dam failures occur exclusively during the summer season from June to September. The lake water levels are higher at this time because the warmer temperatures melt glacial ice and, thereby, reduce the dam freeboard. In the Cordillera Blanca, with its alternating wet and dry seasons, moraine dam failures are more evenly distributed but cluster during the wet season from December to May. The lake water levels are again higher at this time because there is a considerable amount of precipitation while the temperatures are also slightly warmer than they are during the dry season. These data indicate that the moraine dam failures occur most commonly during the warmer times of the year and corroborate the notion the most frequent cause of moraine dam failures are dynamic slope movements in which the displaced material was dominated by solid-state water (ice falls, ice avalanches, and snow avalanches).

The annual distribution of moraine dam failures has been analysed using a dataset of seventy-five events
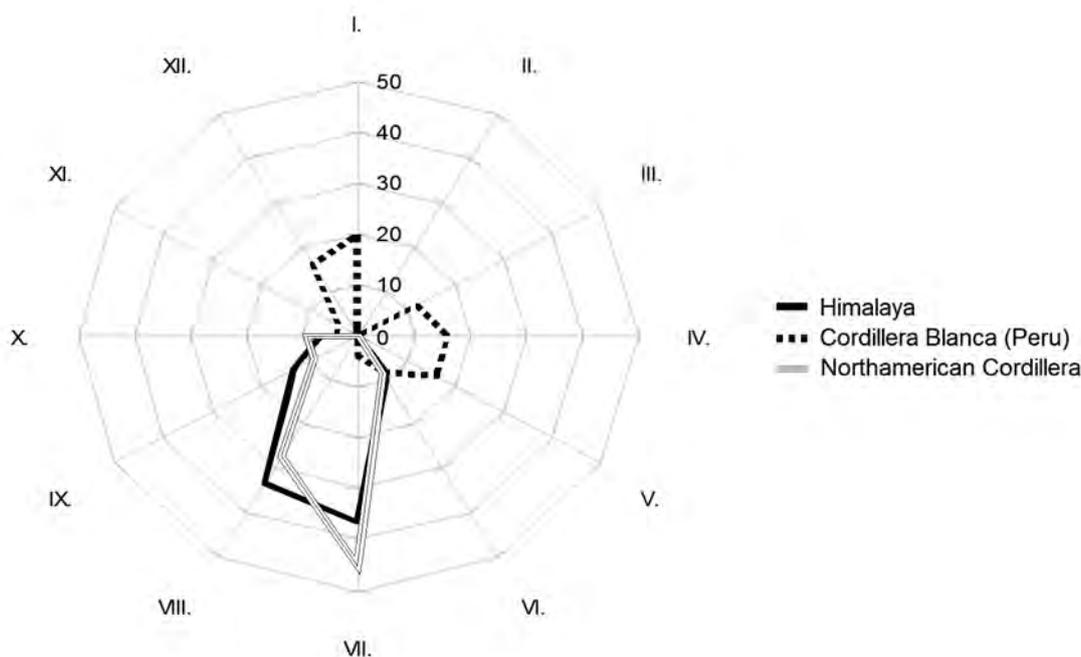
Fig. 5 The distribution of moraine dam failures plotted according to month (66 instances overall).

for which the year of failure is known. In the period between 1900 and 1924 only one moraine-dam failure was recorded – this occurred at lake Zhanlonba in China during 1902 (Ding & Liu 1992) (Figure 6). In the period between 1935 and 1944 eight moraine-dam failures were recorded in the Cordillera Blanca region. These events claimed thousands of lives and caused considerable damage to infrastructure as well as leading to a series of investigations into moraine-dammed lakes (Zapata 2002; Carey 2005). These investigations called for remedial work at thirty-five sites in the form of artificial dams, concrete outlets, tunnels, etc. (Reynolds 2003; Carey et al. 2012). It may also be one of the reasons for the decreased number of moraine dam failures in the following years. In the period between 1970 and 1974 five failures were recorded in the region. These were all triggered by the catastrophic earthquake that occurred in Cordillera Blanca on 31st May 1970. The next moraine dam failure did not occur for another twenty-seven years. This protracted period of stability is thought to reflect the extensive remedial works and rupture of the most unstable lake dams following the earthquake in 1970. The annual distribution of moraine dam failure in Himalaya is more regular with at least two failures in each five-year period between 1955 and 2004. There was a maximum of six failures in the five-year period between 1980 and 1984. The annual distribution of moraine dam failures in the North American Cordillera is also broadly constant with no peaks evident.

5. Discussion

There are a number of published lists of moraine-dammed lake failures for specific regions such as those that have been compiled for the Cordillera Blanca (Zapata 2002), the North American Cordillera (Clague & Evans 2000; O'Connor et al. 2001), and Himalaya (Yamada 1998; Ives et al. 2010). These lists have been updated and supplemented with as much data as it was possible to attain. There is, however, a paucity of events both at the beginning and at the end of the period from 1900 to 2009. The paucity of events at the beginning of this period may reflect an absence of moraine-dammed lake failures at that time or, more likely, that such events were not recorded if the areas in which they occurred were uninhabited or if no significant damage occurred. The paucity of events at the end of this period may again reflect an absence of moraine-dammed lake failures but is more likely to reflect the amount of time it takes for the data to be processed and published. In a number of instances the cause of the moraine-dammed lake failure is not known with certainty and it is only possible to attribute a probable cause. It is, nonetheless, evident that the most common causes are slope movements in which the displaced material is dominated by solid-state water (ice falls, ice avalanches, and snow avalanches). This finding corresponds with those of previous studies (e.g. Costa & Schuster 1988; Ding & Liu 1992; Clague & Evans 2000; Jiang et al. 2004; Awal et al. 2010).
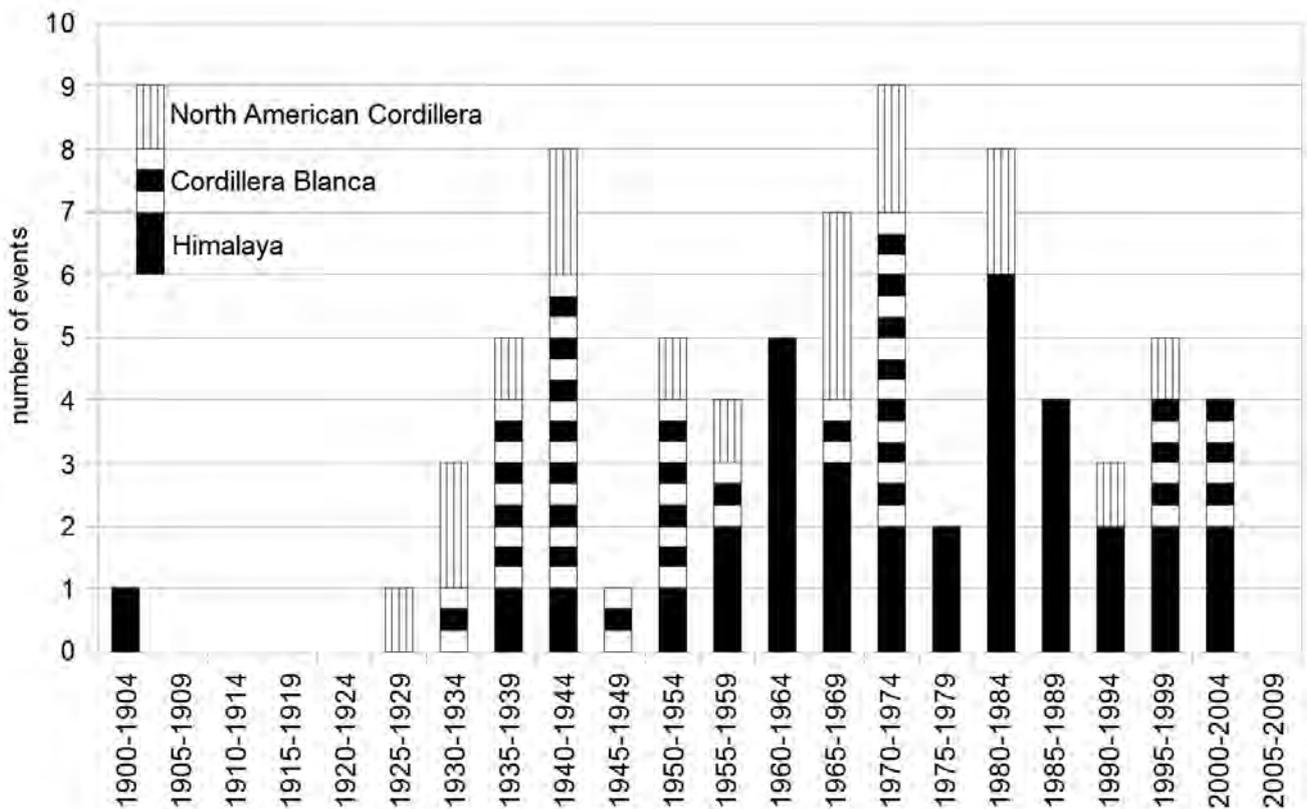

Fig. 6 The distribution of moraine dam failures plotted according to year (75 instances overall).

6. Conclusions

There are eight main causes, of which five are characterised as dynamic and three as long-term, and these are associated with around twenty failure mechanisms. The dynamic causes are slope movements into the lake (e.g. icefalls, avalanches, rockfalls, landslides, and other types of flow), earthquakes, a flood wave from a lake situated upstream, blocking of underground outflow channels, and intensive rainfall or snowmelt. The long-term causes are the ice melting of buried ice, the impact of hydrostatic pressure, and the effect of time. It is, therefore, clear that GLOFs are associated closely to various types of natural hazard. The similarities and disparities between the particular causes were investigated as well as the temporal characteristics of events in the Cordillera Blanca of Peru, the North American Cordillera, and Himalaya. It was found that dynamic causes are around four times more common than long-term causes although significant regional differences are seen: in the Cordillera Blanca of Peru all dam failures resulted from a dynamic event while more than two-fifths resulted from a long-term cause in Himalaya. The most frequent causes of GLOFs from moraine-dammed lakes were found to be slope movements in which the displaced material was dominated by solid-state water (ice falls, ice avalanches, and snow avalanches). This accounted for around half of all events irrespective of the specific study area. The other causes tended to show distinct regional patterns with the second most common cause being slope movements dominated by solid rock or water in the Cordillera Blanca of Peru, intensive rainfall or snowmelt in the North American Cordillera, and self-destruction in Himalaya. The temporal distribution of moraine dam failures is similar in the North American Cordillera and Himalaya as dam failures occur exclusively during the summer season from June to September while in the Cordillera Blanca they are more evenly distributed but cluster during the wet season from December to May. These patterns clearly reflect the general climatic setting of each of the study regions. The annual distribution of these failures is broadly constant with no particular trends yet evident. The recognition of these regional differences is necessary in order to build optimal regionally focused methods for moraine-dammed lakes hazard assessment in the future.

Acknowledgements

REFERENCES

AWAL, R., NAKAGAWA, H., FUJITA, M., KAWAIKE, K., BABA, Y., ZHANG, H. (2010): Experimental study on glacial lake outburst floods due to waves overtopping and erosion of moraine dam. Annuals of Disaster Prevention Research Institute 53, 583–594.

BAJRACHARYA, B., SHRESTHA, A. B., RAJBHANDARI, L. (2007a): Glacial lake outburst floods in the Sagarmatha region. Mountain Research and Development 27, 336–344.

BAJRACHARYA, S. R., MOOL, P. K., SHRESTHA, B. R. (2007b): The impact of global warming on the glaciers of the Himalaya. In: International Symposium on Geo-disasters, Infrastructure Management and Protection of World Heritage Sites 25–26 Nov 2006. Kathmandu: International Centre for Integrated Mountain Development (ICIMOD), 231–242.

BENN, D. I., EVANS, D. J. A. (1998): Glaciers & Glaciation. London, Hodder Education.

BOLCH, T., BUCHROITHNER, M. F., PETERS, J., BASSLER, M., BAJRACHARYA, S. (2008): Identification of glacier motion and potentially dangerous glacial lakes in the Mt. Everest region/Nepal using spaceborne imagery. Natural Hazards and Earth System Sciences 8, 1329–1340.

BOLCH, T., PETERS, J., YEROGOV, A., PRADHAN, B., BUCHROITHNER, M., BLAGOVESHCHENSKY, V. (2001): Identification of potentially dangerous glacial lakes in the northern Tien Shan. Natural Hazards 59, 1691–1714.

BREIEN, H., DE BLASIO, F. V., ELVERHØI, A., HØEG, K. (2008): Erosion and morphology of a debris flow caused by a glacial lake outburst flood, Western Norway. Landslides 5, 271–280.

CAREY, M. (2005): Living and dying with glaciers: people's historical vulnerability to avalanches and outburst floods in Peru. Global and Planetary Change 47, 122–134.

CAREY, M., FRENCH, A., O'BRIEN, E. (2012): Unintended effects of technology on climate change adaptation: an historical analysis of water conflicts below Andean Glaciers. Journal of Historical Geography 38, 181–191.

CAREY, M., HUGGEL, C., BURY, J., PORTOCARRERO, C., HAEBERLI, W. (2011): An integrated socio-environmental framework for glacial hazard management and climate change adaptation: lessons from Lake 513, Cordillera Blanca, Peru. Climatic Change 112, 733–767.

CENDERELLI, D. A., WOHL, E. E. (2001): Peak discharge estimates of glacial-lake outburst floods and "normal" climatic floods in the Mount Everest region, Nepal. Geomorphology 40, 57–90.

CLAUGE, J. J., EVANS, S. G. (2000): A review of catastrophic drainage of moraine-dammed lakes in British Columbia. Quaternary Science Reviews 19, 1763–1783.

COSTA, J. E., SCHUSTER, R. L. (1988): The formation and failure of natural dams. Geological Society of America Bulletin 100, 1054–1068.

DING, Y., LIU, J. (1992): Glacial lake outburst flood disasters in China. Annals of Glaciology 16, 180–184.

DUSSAILLANT, A., BENITO, G., BUYTAETR, W., CARLING, P., MEIER, C., ESPINOZA, F. (2010): Repeated glacial-lake outburst floods in Patagonia: an increasing hazard? Natural Hazards 54, 469–481.

EMMER, A., VILÍMEK, V. (2013): Hazard assessment of GLOFs for moraine-dammed lakes: an example from Cordillera Blanca, Peru. Natural Hazards and Earth System Sciences, 13, 1551–1565.

EVANS, S. G., CLAUGE, J. J. (1994): Recent climatic change and catastrophic geomorphic processes in mountain environments. Geomorphology 10, 107–128.

EVANS, S. G. CLAUGE, J. J., HUNGR, O., GEERTSEMA, M. (2002): Climate change and geomorphological hazards in the Canadian Cordillera; the anatomy of impacts and some tools for adaptation, Climate Change Action Fund Project A099. Scientific Report 1999–2001: Summary of Activities and Results.

GLOFs DATABASE (2012): <glofs-database.com>. Last accessed: 10/2012.

GRABS, W. E., HANISCH, J. (1993): Objectives and prevention methods for glacier lake outburst floods (GLOFs). In: Snow and Glacier Hydrology (Proceedings of the Kathmandu Symposium, November 1992), Great Yarmouth (UK), 341–352.

HAEBERLI, W., KÄÄB, A., MÜHLL, D. V., TEYSSEIRE, P. (2001): Prevention of outburst floods from periglacial lakes at Grubengletscher, Valais, Swiss Alps. Journal of Glaciology 47, 111–122.

HARRISON, S., GLASSER, N., WINCHESTER, V., HARESIGN, E., WARREN, C., JANSSON, K. A. (2006): Glacial lake outburst flood associated with recent mountain glacier retreat, Patagonian Andes. Holocene 16, 611–620.

HEGGLIN, E., HUGGEL, C. (2008): An integrated assessment of vulnerability to glacial hazards – a case study in the Cordillera Blanca, Peru. Mountain Research and Development 28, 299–309.

HEWITT, K. J. (1982): Natural dams and outburst floods of the Karakoram Himalaya. In: Hydrological Aspects of Alpine and High Mountain Areas (Proceedings of the Exeter Symposium, July 1982), Great Yarmouth (UK), 259–269.

HUBBARD, B., HEALD, A., REYNOLDS, J. M., QUINCEY, D., RICHARDSON, S. D., ZAPATA, M. L., SANTILLAN, N. P., HAMBREY, M. J. (2005): Impact of a rock avalanche on a moraine-dammed proglacial lake: Laguna Safuna Alta, Cordillera Blanca, Peru. Earth Surface Processes and Landforms 30, 1251–1264.

HUGGEL, C., HAEBERLI, W., KÄÄB, A., BIERI, D., RICHARDSON, S. (2004): An assessment procedure for glacial hazards in the Swiss Alps. Canadian Geotechnical Journal 41, 1068–1083.

HUGGEL, C., KÄÄB, A., HAEBERLI, W., TEYSSEIRE, P., PAUL, F. (2002): Remote sensing based assessment of hazards from glacier lake outbursts: a case study in the Swiss Alps. Canadian Geotechnical Journal 39, 316–330.

ITURRIZAGA, L. (2005): Historical glacier-dammed lakes and outburst floods in the Karamba valley (Hindukush-Karakoram). Geo Journal 63, 1–47.

IVES, J. D., SHRESTHA, B. R., MOOL, P. K. (2010): Formation of Glacial Lakes in the Hindu Kush-Himalayas and GLOF Risk Assessment. Kathmandu (Nepal), International Centre for Integrated Mountain Development (ICIMOD).

JABOYEDOFF, M., BAILLIFARD, F., BARDOU, E., GIROD, F. (2004): The effect of weathering on Alpine rock instability. Quarterly Journal of Engineering Geology and Hydrogeology 37, 95–103.

JANSKÝ, B., ENGEL, Z., ŠOBR, M., BENEŠ, V., ŠPAČEK, K., YEROKHIN, S. (2009): The evolution of Petrov lake and moraine dam rupture risk (Tien-Shan, Kyrgyzstan). Natural Hazards 50, 83–96.

JANSKÝ, B., ŠOBR, M., YEROKHIN, S. (2006): Typology of high mountain lakes of Kyrgyzstan with regard to the risk of their rupture. Limnological Review 6, 135–140.

JIANG, Z. X., CUI, P., JIANG, L. W. (2004): Critical hydrological conditions for overflow burst of moraine lake. Chinese Geographical Science 14, 39–47.

KATTELMANN, R., WATANABE, T. (1997): Draining Himalayan glacial lakes before they burst. In: Destructive Water: Water-Caused Natural Disasters, their Abatement and Control (Proceedings of the Conference held at Anaheim, California, June 1996), 337–343.

KERSHAW, J. A., CLAUGE, J. J., EVANS, S. G. (2005): Geomorphic and sedimentological signature of a two-phase outburst flood from moraine-dammed Queen Bess Lake, British Columbia, Canada. Earth Surface Processes and Landforms 30, 1–25.

KLIMEŠ, J. (2012): Geomorphology and natural hazards of the selected glacial valleys, Cordillera Blanca, Peru. AUC Geographica 47, 25–31.

LLIBOUTRY, L., MORALES, B. A., PAUTRE, A., SCHNEIDER, B. (1977): Glaciological problems set by the control of dangerous lakes in Cordillera Blanca, Peru. I. Historical failures of moranic dams, their causes and prevention. Journal of Glaciology 18, 239–254.

NARAMA, C., DUISHONAKUNOV, M., KÄÄB, A., DAIYROV, M., ABDRAKHMATOV, K. (2010): The 24 July 2008 outburst flood at the western Zyndan glacier lake and recent regional changes in glacier lakes of the Teskey Ala-Too range, Tien Shan, Kyrgyzstan, Natural Hazards and Earth System Sciences 10, 647–659.

O'CONNOR, J. E., HARDISON, J. H., COSTA, J. E. (2001): Debris flows from failures of Neoglacial-age moraine dams in the Three Sisters and Mount Jefferson Wilderness areas, Oregon. Reston (Virginia): U. S. Geological Survey.

PETRAKOV, D. A., KRYLENKO, I. V., CHERNOMORETS, S. S., TUTUBALINA, O. V., KRYLENKO, I. N., SAKHMINA, M. S. (2007): Debris flow hazard of glacial lakes in the Central Caucasus. In: Chen & Major (eds.) Debris-Flow Hazards Mitigation: Mechanics, Prediction, and Assessment. Millpress, Netherlands, 703–714.

PLAFKER, G., EYZAGUIRRE, V. R. (1979): Rock avalanche and wave at Chungar, Peru. In: Rockslide and Avalanches. Elsevier, 269–279.

REYNOLDS, J. M. (2003): Development of glacial hazard and risk minimisation protocols in rural environments: methods of glacial hazard assessment and management in the Cordillera Blanca, Peru. Flintshire (UK), Reynolds Geo-Sciences Ltd.

RICHARDSON, S. D., REYNOLDS, J. M. (2000a): An overview of glacial hazards in the Himalayas. Quaternary International 65–66, 31–47.

RICHARDSON, S. D., REYNOLDS, J. M. (2000b): Degradation of ice-cored moraine dams: implications for hazard development. In: Debris-Covered Glaciers (Proceedings of a workshop held at Seattle, Washington, USA, September 2000), 187–197.

SHRESTHA, A. B. (2010): Managing flash flood risk in Himalaya-information sheet # 1/10. Kathmandu (Nepal), International Centre for Integrated Mountain Development (ICIMOD).

STRASSER, M., SCHINDLER, C., ANSELMETTI, F. S. (2008): Late Pleistocene earthquake-triggered moraine dam failure and outburst of Lake Zurich, Switzerland. Journal of Geophysical Research 113, 1–16.

VILÍMEK, V., KLIMEŠ, J, ZAPATA, M. L. (2005a): Glacial lake outburst flood in the areas of Huarás, Cordillera Blanca, Peru. Studia Geomorphologica Carpatho-Balcanica 39, 115–124.

VILÍMEK, V., ZAPATA, M. L., KLIMEŠ, J, PATZELT, Z., SANTILLAN, N. (2005b): Influence of glacial retreat on natural hazards of the Palcacocha Lake area, Peru. Landslides 2, 107–115.

VUICHARD, D., ZIMMERMANN, M. (1987): The 1985 catastrophic drainage of a moraine-dammed lake, Khumbu Himal, Nepal: cause and consequences. Mountain Research and Development 7, 91–110.

WATANABE, T., ROTHACHER, D. (1996): The 1994 Lugge Tsho glacial lake outburst flood, Bhutan Himalaya. Mountain Research and Development 16, 77–81.

YAMADA, T. (1998): Glacier Lake and its Outburst Flood in the Nepal Himalaya. Tokyo, Japanese Society of Snow and Ice.

ZAPATA, M. L. (1984): Avalanchas y aluviones en la departmento de Ancash, Huaráz (Peru), Electroperú, S. A.

ZAPATA, M. L. (2002): La dinamica glaciar en lagunas de la Cordillera Blanca. Acta Montana 19, 37–60.

RÉSUMÉ

Analýza příčin a mechanismů destrukcí hrází jezer hrazených morénami v pohořích Cordillera Blanca (Peru), Severoamerická Kordillera a Himaláj

Příspěvek je členěn do dvou částí. První část má rešeršní charakter a shrnuje rozličné příčiny a mechanismy destrukcí (protržení) hrází jezer hrazených morénami. Pět dymanických příčin (různé typy svahových pohybů, zemětřesení, povodňová vlna z výše položeného jezera, intenzivní dešťové srážky / tání sněhu, ucpání podzemních odtokových kanálů) a tři dlouhodobé příčiny (odtávání pohřbeného ledu, působení hydrostatického tlaku a dlouhodobá degradace tělesa hráze v čase) jsou popsány spolu s mechanismy vedoucími k destrukcím morénových hrází, a to včetně konkrétních příkladů ze zájmových oblastí. Ve druhé části příspěvku je provedena srovnávací analýza těchto událostí mezi oblastmi pohoří Cordillera Blanca (Peru), Severoamerická Kordillera a pohoří Himaláj. Na základě vytvořené databáze protržených morénových hrází mezi lety 1900 a 2009 je zhodnoceno jednak zastoupení různých příčin, jednak časová distribuce těchto událostí. Nejfrekventovanější příčinou ve všech studovaných oblastech byl dynamický svahový pohyb do jezera. Zastoupení a výskyt dalších příčin se však mezi jednotlivými oblastmi výrazně liší. Časová distribuce událostí výrazně odlišuje oblast Cordillera Blanca od zbývajících dvou, což do určité míry odráží roční chod klimatu a na něj vázaných příčin destrukcí morénových hrází.

Adam Emmer
Charles University in Prague
Faculty of Science
Department of Physical Geography and Geoecology
Albertov 6
128 43 Prague 2
Czech Republic
E-mail: aemmer@seznam.cz

Alejo Cochachin
Unidad de Glaciologia y Recursos Hydricos
de Autoridad Nacional de Agua
Av. Confraternidad 167
Independencia – Huaraz, Peru

MASS DISTRIBUTION OF EARTH LANDFORMS DETERMINED BY ASPECTS OF THE GEOPOTENTIAL AS COMPUTED FROM THE GLOBAL GRAVITY FIELD MODEL EGM 2008

JAN KALVODA[1], JAROSLAV KLOKOČNÍK[2],
JAN KOSTELECKÝ[3], ALEŠ BEZDĚK[2]

[1] Charles University in Prague, Faculty of Science, Department of Physical Geography and Geoecology
[2] Astronomical Institute, Academy of Sciences of the Czech Republic
[3] Research Institute of Geodesy, Topography and Cartography

ABSTRACT

Correlations of large-scale landform patterns with some aspects of the geopotential as computed from the global gravity field model EGM 2008, particularly the radial second derivatives of the disturbing gravitational potential Γ_{33}, the strike angle θ_S and virtual deformations of the ellipse of deformation, are demonstrated. Selected regions with documentation of aspects from EGM 2008 are the Nepal Himalaya and its neighbouring areas, the collision zone of East-Asian and West-Pacific lithospheric plates, the contact region of north-eastern Africa, south-western Asia and south-eastern Europe, morphotectonic contact between the Bohemian Massif, Eastern Alps and the Western Carpathians in Central Europe and regions of ancient rapid events indicated by relics of large impact craters Vredefort, Chicxulub and Popigai. It is suggested that landform patterns with very conspicuous combinations of significantly high positive or negative values of Γ_{33} are under the strong influence of rapid and/or intensive geomorphic processes. These geophysical signatures supported by values of the strike angle θ_S and virtual dilatations or compressions of the ellipse of deformation reflect the regional dynamics of Earth surface evolution as characterised by a very effective integration of tectonic and climate-driven morphogenetic processes.

Keywords: Earth landforms, gravity field model EGM 2008, mass distribution, geodynamics, geomorphic processes

1. Introduction

Progress in satellite geodesy and dynamics of the Earth's artificial satellites, involves satellite altimetry and space-born gradiometry data, together with an extensive, nearly global and often very precise database of terrestrial gravity anomalies. It enables the parameters of the static gravity field of the Earth (the so called harmonic geopotential coefficients or Stokes parameters represented by spherical expansion) to be reliably determined to a high degree and order, and detailed geoid undulations and other quantities derivable from the harmonic coefficients to be observed with high accuracy and resolution. The National Geospatial-Intelligence Agency of the USA developed the *E*arth *G*ravity *F*ield *M*odel 2008 (EGM 2008, Pavlis et al. 2008a,b, 2012) combined from the GRACE satellite data and gravity anomalies over the world (excluding Antarctica) to degree $n_{max} = 2190$.

Global combined gravity field models of the Earth, based on satellite and terrestrial data, can today have worldwide high resolution and precision. The EGM 2008 (Pavlis et al. 2008a,b, 2012) uses satellite multiyear inter-satellite range-rate data from a near polar orbiting tandem of satellites called GRACE (Gravity Recovery and Climate Experiment, NASA + GFZ) with extensive gravity anomalies derived from terrestrial gravimeters and satellite altimetry. EGM 2008 reaches a resolution of 5 × 5 arcmin, which is ~9 km of half-wavelength on the Earth's surface at the equator, and, with the exception of Antarctica and some other areas, a precision of the order 1 miliGal. Such a model offers new opportunities to many applications in

geodesy, geophysics, geology, geomorphology and physical geography. The new data coming from the gradiometer on board GOCE (Gravity Field and Steady-State Ocean Circulation Explorer, ESA's gravity mission, Floberghagen et al. 2011) improve the middle-wavelength part (from ~120 to ~250 degrees) of future gravity models where satellite terrestrial data are wanting. The newest gravity field models from 2010–2011 also comprise gradiometry data from the satellite GOCE mission instead of data from GRACE (e.g. EIGEN 6C, Förste et al. 2011). They have only at maximum about half the resolution in comparison with EGM 2008 (Klokočník et al. 2012). Progress in the quality of quantities derived from their harmonic geopotential coefficients has been noted only in Antarctica.

In the presented paper, using the harmonic geopotential coefficients of the EGM 2008, are computed: the detailed geoid undulations N [m], the gravity anomalies Δg [1 mGal = 10^{-5} m s^{-2}], the full Marussi tensor of the second derivatives of the disturbing potential (also known as Full Tensor Gradiometry [1 E = 1 Eötvös = 10^{-9} s^{-2}]), namely its radial component Γ_{33} (sometimes denoted T_{zz} or T_{rr}) in spherical harmonics, the invariants of the gravity field I_0, I_1, I_2, computable from the components of the Marussi tensor, their specific ratio I and the strike angle θ_S, utilizing the theory of Pedersen and Rasmussen (1990) and Beiki and Pedersen (2010). A virtual dilatation or contraction of the ellipse of deformation is added. Some of these quantities are functionals of the geopotential in a mathematical sense and some of them are not. Therefore, they are concisely designated in the paper as *aspects* of the geopotential.

In our project selected large-scale landform patterns are surveyed using a set of parameters computed from EGM 2008. The first recently published experimental results consisted in computing two anomalous parameters of the gravitational field in EGM 2008 (e.g. Kalvoda et al. 2010; Klokočník et al. 2010a), namely the gravity anomaly Δg and the second-order radial derivative Γ_{33} of the disturbing gravitational potential. The latter is not available directly from scattered ground gravity surveys. The second order derivatives and the invariants provide evidence about details of near-surface (not deep) structures. The Marussi tensor was already used in local scales (a few kilometers) for petroleum, metal, diamond, ground water etc. explorations (e.g. Mataragio and Kieley 2009; Murphy and Dickinson 2009). The full Marussi tensor is a richer source of information than standard single gravity anomalies. This extra information can be applied by tensor imaging techniques to enhance a target anomaly definition, as tested for local features (minerals, oil and gas industry), e.g., by Dickinson et al. (2009). Theoretical and experimental studies mentioned above were our stimulation to examine larger regions – in other words, to advance from local gradiometric measurements to the global gravity field models. Previously the gravity anomalies or the second derivatives were derived from gravimeters or gradiometers on airplanes. Recently, Beiki and Pedersen (2010) tested an approach to the larger area (ca 500 × 500 km) of the Vredefort impact crater in South Africa. These authors also used local measurements (a gradiometer on board of an airplane) but not Stokes parameters.

We computed the aspects listed above, based on a global gravity field model. The resolution achieved by the EGM 2008 is applicable and valuable for regional (10^2–10^3 km) and large-scale surveys and geo-applications. The local scale (~1 km) is below the resolution of the EGM 2008. Tests of the sensitivity of the aspects of the EGM 2008 to selected landform patterns were realized by Klokočník et al. (2008a,b, 2010a,b) using especially large impact craters and by Kalvoda et al. (2010) in Himalayan regions with very conspicuous relief features of active orogeny and intensive climate-morphogenetic processes. The aim of the paper is to present examples of computed aspects of the EGM 2008 with suggestions of various geomorphological and geodynamic interpretations.

2. Theory, data and computations

2.1 Description of theory

The disturbing static gravitational potential outside the Earth masses in spherical coordinates in spherical expansion reads

$$V(r,\varphi,\lambda) = \frac{GM}{r} \sum_{l=2}^{\infty} \sum_{m=0}^{l} \left(\frac{R}{r}\right)^l (C'_{l,m} \cos m\lambda + S_{l,m} \sin m\lambda) P_{l,m}(\sin \varphi), \quad (1)$$

where GM is a product of the universal gravity unit and the mass of the Earth (known from satellite analyses as a geocentric gravitational constant), r is the radial distance of an external point where V is computed, the symbol R is for the radius of the Earth (which can be approximated by the semi-major axis of a reference ellipsoid), $P_{l,m}(\sin \varphi)$ are Legendre associated functions, l and m are the degree and order of the harmonic expansion, (φ, λ) are geocentric latitude and longitude, $C'_{l,m}$ and $S_{l,m}$ are harmonic geopotential coefficients (Stokes parameters), fully normalized, $C'_{l,m} = C_{l,m} - C^{el}_{l,m}$, where $C^{el}_{l,m}$ belongs to the reference ellipsoid.

Gravity gradient tensor $\boldsymbol{\Gamma}$ (*the Marussi tensor*) is a tensor of the second derivatives of the disturbing potential V and is computed by means of $C'_{l,m}$, $S'_{l,m}$ of the particular gravity field model known to the maximum degree $l_{\max}$ (see below details about EGM 2008):

$$\boldsymbol{\Gamma} = \begin{bmatrix} \Gamma_{11} & \Gamma_{12} & \Gamma_{13} \\ \Gamma_{21} & \Gamma_{22} & \Gamma_{23} \\ \Gamma_{31} & \Gamma_{32} & \Gamma_{33} \end{bmatrix} = \begin{bmatrix} \dfrac{\partial^2 V}{\partial x^2} & \dfrac{\partial^2 V}{\partial x \partial y} & \dfrac{\partial^2 V}{\partial x \partial z} \\ \dfrac{\partial^2 V}{\partial y \partial x} & \dfrac{\partial^2 V}{\partial y^2} & \dfrac{\partial^2 V}{\partial y \partial z} \\ \dfrac{\partial^2 V}{\partial z \partial x} & \dfrac{\partial^2 V}{\partial z \partial y} & \dfrac{\partial^2 V}{\partial z^2} \end{bmatrix} \quad (2)$$

The outside of the source $\boldsymbol{\Gamma}$ satisfies Laplace's equation, the trace of the tensor is zero, $\boldsymbol{\Gamma}$ is symmetric, and contains just five independent components. These can be conveniently computed by means of the formulae in Hotine (1969). The horizontal components help identify the shape and geological setting of a target body. The quantity Γ_{33} is best suited for target body detection; Γ_{33} helps to define isopath/density relationships of a body mass with relation to its geological setting (e.g., Murphy and Dickinson 2009).

Under any coordinate transformation, $\boldsymbol{\Gamma}$ preserves *three invariants*

$$I_0 = \text{trace}(\boldsymbol{\Gamma}) = \Gamma_{11} + \Gamma_{22} + \Gamma_{33}, \quad (3)$$

$$I_1 = \Gamma_{11}\Gamma_{22} + \Gamma_{22}\Gamma_{33} + \Gamma_{33}\Gamma_{11} - \Gamma_{12}^2 - \Gamma_{23}^2 - \Gamma_{13}^2, \quad (4)$$

$$I_2 = \det(\boldsymbol{\Gamma}) = \Gamma_{11}(\Gamma_{22}\Gamma_{33} - \Gamma_{23}^2) + \Gamma_{12}(\Gamma_{23}\Gamma_{13} - \Gamma_{12}\Gamma_{33}) + \Gamma_{13}(\Gamma_{12}\Gamma_{23} - \Gamma_{13}\Gamma_{22}). \quad (5)$$

Pedersen and Rasmussen (1990) defined the *ratio I* of the invariants I_1 and I_2 as

$$0 \le I = -(I_2 / 2)^2 / (I_1 / 2)^3 \le 1. \quad (6)$$

It lies between zero and unity for any potential field. If the causative body is strictly 2-D, then I is equal to zero. The *strike angle* θ_S is determined through

$$\tan 2\theta_S = 2\frac{\Gamma_{12}(\Gamma_{11} + \Gamma_{22}) + \Gamma_{13}\Gamma_{23}}{\Gamma_{11}^2 + \Gamma_{22}^2 + \Gamma_{13}^2 - \Gamma_{23}^2} = 2\frac{-\Gamma_{12}\Gamma_{33} + \Gamma_{13}\Gamma_{23}}{\Gamma_{13}^2 - \Gamma_{23}^2 + \Gamma_{33}(\Gamma_{11} - \Gamma_{22})} \quad (7)$$

within a multiple of π/2. The strike angle indicates how gradiometer measurements rotate within the main directions of the underground structures. Provided that I is

small, the strike angle may indicate a dominant 2-D structure. For more details see, e.g., Pedersen and Rasmussen (1990) or Beiki and Pedersen (2010).

To define the term *virtual deformation*, we will utilize an analogy with the tidal deformation. If there is tidal potential T, then horizontal shifts (deformations) exist due to it and they can be expressed as follows in North-South direction (latitude direction)

$$u_\Phi = l_S \frac{1}{g} \frac{\partial T}{g \partial \varphi} \quad , \tag{8}$$

in East-West direction (longitudinal direction)

$$u_\Lambda = l_S \frac{1}{g \cos \varphi} \frac{\partial T}{\partial \lambda} \quad , \tag{9}$$

where g is gravity acceleration $9.81\,\mathrm{m\ s^{-2}}$, l_S is the elastic coefficient (Shida number) expressing the elastic properties of the Earth as a whole planet ($l_S = 0.08$), φ and λ are the geocentric coordinates of a point P where we measure T. The potential T is in $[\mathrm{m^2\ s^{-2}}]$ and in our case, T is represented by (1), (8) and (9). This mechanism is applied to a standard Earth model (here EGM 2008), but real values of the Shida parameters l for the Earth's surface are not known.

We apply the apparatus of mechanics of continuum to derive the main directions of the tension (e.g. Brdička et al. 2000). The tensor of deformation E is defined as a gradient of shift. Let us select a local coordinate system (x,y) in P by the equations

$$\mathrm{d}\varphi = \mathrm{d}x,$$
$$\mathrm{d}\lambda \cos \varphi = \mathrm{d}y.$$

Then it holds that

$$E = \begin{pmatrix} \varepsilon_{11} & \varepsilon_{12} \\ \varepsilon_{21} & \varepsilon_{22} \end{pmatrix} = grad\left(d\right) = \begin{pmatrix} \dfrac{\partial u_x}{\partial x} & \dfrac{\partial u_x}{\partial y} \\ \dfrac{\partial u_y}{\partial x} & \dfrac{\partial u_y}{\partial y} \end{pmatrix}$$

$$d = Ex + t,$$

where d is the vector of shift, E the gradient of shift, x the vector of the coordinates and t the vector of translation.

The tensor of deformation can be separated into two parts:

$$E = e + \Omega = (e_{ij}) + (\Omega_{ij}), \tag{10}$$

where e is the symmetrical tensor and Ω the anti-symmetrical tensor of deformation, respectively. We will need e:

$$e = \begin{pmatrix} e_{11} & e_{12} \\ e_{21} & e_{22} \end{pmatrix} = \begin{pmatrix} \varepsilon_{11} & \dfrac{(\varepsilon_{12} + \varepsilon_{21})}{2} \\ \dfrac{(\varepsilon_{12} + \varepsilon_{21})}{2} & \varepsilon_{22} \end{pmatrix} \tag{11}$$

and the parameters of deformation
$\Delta = e_{11} + e_{22}$ (total dilatation), $\gamma_1 = e_{11} - e_{22}$ (pure cut),
$\gamma_2 = 2e_{12}$ (technical cut),
$\gamma = (\gamma_1{}^2 + \gamma_2{}^2)^{1/2}$ (total cut), $a = \frac{1}{2}\,(\Delta + \gamma)$ (major semi-axis of ellipse of deformation),
$b = \frac{1}{2}\,(\Delta - \gamma)$ (minor semi-axis of ellipse of deformation),
$\alpha = \frac{1}{2} \operatorname{atan}(\gamma_2/\gamma_1)$ (direction of main axis of deformation).

In relevant sketch maps of presented complex figures, the semi-axis of deformation ellipse a and b are expressed together with their relative size. Values of l_S are not known, and, therefore, only main directions of the virtual deformations (and not also their amplitudes) are demonstrated. The plotted quantities are a and b expressed in the figures as small crosses.

Virtual deformations of the ellipse of deformations, calculated using the tensor of deformation E (Eqn. 8–11), are geometrically expressed by its dilatation or compression. Virtual dilatations of the ellipse of deformation indicates uplifted regions at the geoid, whose mass has (according to the pattern of values of the gravitational potential) a tendency to disintegration. On the contrary, virtual compression of the ellipse of deformation indicates lowered zones and/or areas at the geoid. Natural processes which are the cause of these states of the near-surface part of the geoid, are certainly very diverse as a consequence of regionally heterogenous integration of morphotectonic and erosion-denudational processes. The suggested interpretation of the field of virtual deformations of the ellipse of deformation is also in agreement with regional patterns of the values of Δg, Γ_{33} and θ_S.

2.2 Quality of data and computations

The EGM 2008 (Pavlis et al. 2008a,b, 2012) is a combined solution (from satellite and terrestrial data) complete to the degree and order 2160 in a spherical harmonic expansion. It also contains additional coefficients extending to the degree 2190 and order 2159. *Satellite data* to the EGM 2008 come only from the GRACE A/B SST (low-low satellite-to-satellite tracking). The *terrestrial data* base of EGM 2008 is very extensive and consists of several sources (gravimetric measurements, anomalies derived from altimetry, models or fill-in data from digital models of the terrain) when nothing better was available. EGM 2008 is probably the best currently available combination gravity field model of the Earth. Nevertheless, it does not yield a homogeneous gravity anomaly field. For example, no terrestrial data in EGM 2008 are available for Antarctica. Only poorer data (the "*fill-in*" set from satellite topography, of lower precision, resolution and reliability) over high mountain belts are available (Pavlis et al. 2012). Although the data in EGM 2008 are in general of high quality, there are still large variations of the precision of the geoid undulation, gravity anomalies, and other quantities derived from C_{lm}, S_{lm} of EGM 2008. Pavlis et al. (2008a) documented the accuracy estimates (see also Figures 1 and 2 in Kalvoda et al. 2010) for the gravity anomalies in EGM 2008, their variability over latitude and longitude from covariance analysis. The accuracy and resolution of the derivatives of the EGM 2008 geopotential for some of the mountain belts and other regions with the fill-in data can be several times lower than for the best covered areas.

Plotting is important for visualizing our results; we make use of strongly non-linear scales to emphasize various features which otherwise might remain hidden. A note about the units of plotted functionals: *mGal* for the gravity anomalies and/or disturbances, E = Eötvös for the second order potential derivatives. The invariants I_1 and I_2 have units $[s^{-4}]$ and $[s^{-6}]$ and the ratio I is spaceless. The strike angle θ_S is expressed in degrees and its demonstration in red means its direction to the East and in blue to the West of the meridian.

3. Selected results of screening: aspects of the EGM 2008 in varied regions of the Earth

A systematic screening was performed of correlations between aspects of the geopotential, as represented by the EGM 2008, and large-scale landform patterns displaying varied near-surface geological structures as well as climate-morphogenetic processes. Results of the screening are represented by means of examples from regions of various planation surfaces, high mountain ranges, collision zones of oceanic and continental lithospheric plates, volcanic chains and large impact craters. Selected regions with demonstration of aspects from EGM 2008 are as follows: the Nepal Himalaya and its neighbouring regions, the collision zone of East-Asian and West-Pacific lithospheric plates, the contact region of north-eastern Africa, south-western Asia and south-eastern Europe, morphotectonic contact between the Bohemian Massif, Eastern Alps and the Western Carpathians in Central Europe and regions of ancient rapid events indicated by relics of large impact craters Vredefort, Chicxulub and Popigai.

By means of the evaluation of an extensive set of graphical representations of values of selected aspects of the geopotential (computed from the EGM 2008), it was found that the most effective information for geo-applications is provided by 1) the radial second derivative of the disturbing gravitational Γ_{33}, 2) the strike angle θ_S, and 3) virtual deformations of the ellipse of deformation (Klokočník et al. 2013). Variable values of Γ_{33} display significant gravitational signatures of extensive differences and changes in mass density and/or rock massif and regolith distributions. Local directions of strike angle θ_S and virtual deformations of the ellipse of deformation form clusters, stripes and also zones with frequent space changes. These configurations can reflect and/or be closely related to directions of tectonic pressures in rock massifs of the Earth's landforms.

The Nepal Himalaya and its neighbouring regions

Strong coincidences were identified between the large-scale landform configuration of the Himalaya and the extension of regions with very high positive values of the radial second derivative of the disturbing gravitational potential Γ_{33} and the most likely in combination with conspicuous areas of high negative values of Γ_{33} in

their close neighbourhood (Kalvoda et al. 2010). Specific configuration and sharp differences in orographical patterns of the Himalaya are indicated by a large range of values of Γ_{33} approximately between +1100 E and −760 E. It is a conspicuous reflection of high mountain massifs (Figure I in Colour appendix) divided by large canyon-like valleys of antecedent origin with very active deep-side erosion and related morphogenetic processes. High-mountain landforms and rapid exhumation of deep crystalline rocks in the Himalayan region of the collision orogeny are the result of morphotectonic processes, as well as denudation and erosional efficiency under variable palaeoclimatic conditions which occurred during the late Cenozoic (compare e.g. Kalvoda 1992, 2007).

A comparison of Δg and Γ_{33} records displaying the southern Himalayan foredeep, the Gangetic Plain is also very instructive. Negative gravity anomalies Δg (Figure Ia) are sensitive to geological structure driven by a long-term subduction of the Indian sub-continent under the Asian continental plate. On the contrary, the second order derivatives $\boldsymbol{\Gamma}$ (Figures Ib, c, d) reflect the near-surface mass distribution and flat accumulation landforms of the Gangetic Plain and dissected relief of the Siwalik Hills. Mountain ranges of the Himalaya are also demonstrated by the invariants (Figures Ie, f, g), namely by zones of the significantly negative I_1 (Figure Ie) and positive I_2 (Figure If). The eastern directions of the strike angle θ_S (Figure Ih, i) are very noticeable in the Gangetic Plain and the Siwalik Hills and its prevailingly western directions in the Himalayan and Tibetan regions. The main patterns of virtual deformations (Figure Ij), which are presented by dilatations and contractions of the ellipse of deformation, follow the extremely dissected relief of the Himalaya. Virtual dilatations of the ellipse of deformation are concentrated in mountain vaults, and, on the contrary, its virtual contractions indicate strikingly cut-down areas of the mountainous landscape.

The collision zone of the East-Asian and West-Pacific lithospheric plates

The main large-scale morphostructural patterns of the active collision zone between the Pacific (oceanic) and Asian (continental) plates are quite well expressed by the functionals Δg (Figure IIa), Γ_{33} (Figure IIb) and also partially by strike angle θ_S (Figure IIc). Mountain chains of Japanese islands, including the huge massifs of stratovolcanoes, can be determined in Figures IIa, b, especially by the stripes and clusters of positive values of Δg and Γ_{33}. A striking feature drawn in Figures IIa, b, c, d is a remarkable arc of deep tectonic trenches connected with the active subduction of the Western-Pacific oceanic plate under the eastern margin of the Asian continental plate.

Virtual deformations derived from the ellipse of deformation (Figure IId) follow the positions of elevations and depressions of land and submarine reliefs. Demonstrated patterns of these virtual deformations are very similar to the occurrence of gravity anomalies

Δg (Figure IIa). The topographical features of the Kuril Islands, the Japanese Islands and groups of submarine volcanic massifs in the western part of the Pacific Ocean are especially noticeable, as expressed by positive values of Δg and/or virtual dilatations (compare Figures IIa and IId). The Kuril and Japanese trenches are indicated by negative values of Δg and/or virtual contractions of the ellipse of deformation.

Contact region of north-eastern Africa, south-western Asia and south-eastern Europe

The complicated geological and landform patterns of the large contact region between these continents can be estimated especially from configurations of highly positive or negative values of Δg (Figure IIIa), Γ_{33} (Figure IIIb) and the strike angle θ_S (Figure IIIc). The main orographical patterns including the mountain ranges between the Balkans and the Iranian Highland as well as tectonic basins (e.g. in the Mediterranean Sea west of Cyprus and between Crete and the northern coast of Africa) are conspicuously expressed by Δg (Figure IIIa) and by virtual dilatations and contractions of the ellipse of deformation (Figure IIId). Also remarkable are zones with significantly high positive values of Γ_{33} (Figure IIIb) combined with high negative values in close neighbourhoods. It is especially well rendered in regions of the Caucasus and the Elborz mountains (compare also Chapter 4 with details in Figure XI) as well as the narrow tectonic suture with the Dead Sea.

Conspicuous morphotectonic contact between the Bohemian Massif, the Eastern Alps and the Western Carpathians in Central Europe

An example of a varied geological and landform patterns is presented especially in Figures IVa, b, displaying Δg and Γ_{33} for the Bohemian Massif and its surrounding areas. This part of central Europe includes an extensive region of the geological contact between the Hercynian structures of the Bohemian Massif and the Tertiary Alpine and the Carpathian orogens to the south and/or east of them (compare e.g. Golonka et al. 2006). A combination of the gravity signatures Δg and Γ_{33} mediates an effective expression of the deeper and near-surface parts of the Earth's crust and landform patterns. There is a possibility that clusters of western and/or eastern directions of the strike angle θ_S (Figure IVc) could be a reflection of assumed pressures and tensions in rock massifs of these large morphotectonic units. Figure IVd shows the virtual deformations of the ellipse of deformation with pronounced patterns of mountain belts and highlands (virtual dilatations) and the mainly tectonically conditioned network of valleys and basins (virtual compressions) with active erosion and/or accumulation processes.

Regions of the Vredefort, Chicxulub and Popigai impact craters

The gravity signal of various impact craters on the Earth has been studied by, among others, Klokočník et al. (2010a,b). These authors suggested that some of the studied craters can not be single but double or multiple craters (Chicxulub and Popigai).

Vredefort, located in South Africa, is the largest confirmed impact crater on the Earth. Due to its large age (2×10^9 years), the area underwent substantial structural-geological and erosion changes. Therefore, the impact crater is "fragmented" (Figures VIa, b, d). This indefinite state is especially manifested by the strike angle θ_S (Figure Vc).

Chicxulub is a large multi-ring impact crater in the north Yucatan at $\varphi = 21°20'$ N and $\lambda = 270°30'$ E. Hildebrand et al. (1995, 1998) estimated its diameter as 170 km based on measured gravity profiles and by the location of rings of cenotes. Sharpton et al. (1993) identified two more distant rings in their gravity profiles and also interpreted a 300 km-diameter crater. It is a relatively young impact structure (age $\sim 60 \times 10^6$ years) but completely buried under the surface and covered by Tertiary limestone. The Chicxulub impact crater was discovered by gravity anomalies measured during oil prospecting (for details and references see Klokočník 2008; Klokočník et al. 2010a,b). The geographical position and main structural patterns of the Chicxulub crater are well expressed using the gravity signatures Δg (Figure VIa), Γ_{33} (Figure VIb) and virtual deformations (Figures VIc, d). Virtual dilatations and compressions of the ellipse of deformation very closely follow the variable morphostructural, erosion and accumulation landform patterns of the Mexican and Caribean areas (Figures VIc, d), including details of the round structures of the Chicxulub impact crater. Figures VIc, d show the virtual deformations of the ellipse of deformation in Mexico and the Caribbean (Campech bank) and in a detail the round structure of the compressed zone around the Chicxulub crater, coinciding with the negative anomalies and radial second derivatives. Two circular-like features of the Chicxulub crater are clearly visible (FigureVIb) with strong negative values of Γ_{33} as well as a central part and two rings with positive values of Γ_{33}. The outer ring has a diameter of 160–180 km. A hypothetical second (smaller) Chicxulub crater can also be identified – with some uncertainty – as a relief depression manifested by local virtual compressions of the ellipse of deformation (Figure VId).

The *Popigai* impact crater ($\varphi = 71°39'$ N, $\lambda = 111°11'$ E) in Siberia, with a diameter of about 100 km and age $\sim 35 \times 10^6$ years (Pilkington et al. 2002; Masaitis et al. 2005), is partly visible on the surface. According to Klokočník et al. (2010a,b), the Popigai crater is probably not single (compare the gravity anomalies Δg and second radial derivative Γ_{33} in Figures VIIa, b), but double and may be a multiple crater. In Figures VIIc, d, the strike angle θ_S and the virtual deformations of the ellipse of deformation in the Popigai area are displayed, with striking circular structure of the impact crater (virtual compression) surrounded by irregular topographical elevations.

4. Discussion

The presented examples of aspects of the EGM 2008 in geodynamically varied regions of the Earth enable the expression of some general findings and related remarks. The long-term activity of climate-morphogenetic processes in tectonically calm regions and in areas of active epeirogenesis resulted in the development of large planation surfaces and lowlands which are very close to geophysical levels of the same gravitational potential (Kalvoda et al. 2010). Therefore, it was found that on large-scale planation surfaces and topographically similar landforms, smoothed by denudation or accumulation of different genesis and age, values of the second derivatives of the disturbing gravitational potential Γ_{33} are only in the range of approximately ±100 E. On the contrary, regions of active orogeny and related morphotectonic processes are characterised by conspicuous compressions of rock massifs in the near-surface part of the Earth's crust and a very variable topographic mass distribution. These landform patterns are displayed by significantly high positive and/or negative values of Γ_{33}.

High negative values of Γ_{33} have been indicated in regions of tectonically conditioned discontinuities or sinking of the Earth's surface and in regions with very intense erosion of rocks and transport of regolith. For example, the Lake Baikal rift zone is well observed as a strong and prolonged negative gravity anomaly Δg and the radial second derivatives Γ_{33} (Figures VIIIa, b). This significant orogenetic region also involves dissected mountainous relief evolving by intensive morphogenetic processes. Moreover, there are interesting landform patterns NW of Lake Baikal indicating an intersection of several tectonic faults.

The range of geomorphologic applications of EGM 2008 clearly depends on the quality of the regional gravity data as well as variability of the Earth surface processes. For example, landform patterns of the Grand Canyon in Arizona, originated by the intensive erosion processes of the Colorado River network along fault zones during long-term neotectonic uplifts of geological formations, are well expressed by EGM 2008 (Figures IXa, b). From various tests with volcanic mountains, the stratovolcanoes Popocatepetl and Iztaccihuatl are the most visible, as shown in Figures Xa, b. There are positive second derivatives Γ_{33} located in the areas of the volcanoes, surrounded by "rings" around them with negative Γ_{33}.

Similar opinion can be expressed as an explanation of striking anomalies of the invariants. In regions with very noticeable features of active morphotectonic and erosion processes, very significant negative values I_1 and, on the contrary, positive values of I_2 were identified (compare Figures Ie, f, g). Similarly, it is possible to express and verify the hypothesis that directions of strike angle θ_S to a certain degree represent, or are in a harmony with, the prevailing directions of tectonic pressures and tensions in the near-surface part of the Earth's crust. Significant

coincidences were also detected between regional patterns of Γ_{33} and virtual deformations of the ellipse of deformation.

Landform patterns of the Earth provide regional evidence of the nature of very dynamic landscape evolution, including intense morphotectonic processes, variable rates of denudation, sediment transfer and deposition. Gravity data are therefore very valuable for establishing a better understanding of the processes driving uplift and erosion, especially in the regions with active orogenetic processes. Detected various large-scale configurations of selected functionals of the EGM 2008, which are particularly conspicuous on graphical representations of Γ_{33} and θ_S values, give evidence of the long-term operation of certain complexes of morphogenetic processes producing the evolution of not only distinctive topographic features, but also, especially, of specific relief types of the Earth.

It is worth noting that striking coincidences between different aspects of the EGM 2008, representing regional geomorphic and structural-geological features of the Earth, are systematically identified. Examples of natural relations between selected aspects of the EGM 2008 suitable for variable geo-applications are demonstrated in Figure XI (the region of the southern part of the Caspian Sea) and Figure XII (the Ghawar oil fields in Saudi Arabia).

Selected aspects of the EGM 2008 in Figures XIa, b, c clearly indicate a continuation of an extensive morphotectonic depression (approximately of W–E direction, see also Figure III) originated between the southern Caucasus and the Iranian mountain belts. The Eastern part of the indicated graben-like zone forms a sedimentary basin of the southern part of the Caspian Sea situated at a foot of the very steep northern slopes of the Elborz mountains.

Similarly, a group of the aspects of the EGM 2008, expressed in the Ghawar region (Figure XII) in Saudi Arabia with one of the largest oil fields in the world (Al-Anazi 2007), can be well correlated with geomorphologic features and the structural-geological situation. Figures XIIa, b represent a detailed view of the values of the derivatives in a relatively small area of the Ghawar oil fields in Saudi Arabia (~100 km long in a south-north direction). Conspicuous harmony between a course of zones with positive values of Γ_{33} (Figure XIIa) and virtual dilatations of the ellipse of deformation (Figure XIIb) testify in favour of the existence of matter elevation situated in a nearly longitudinal direction. This elevation is clearly surrounded on the western and eastern sides by zones of negative values of Γ_{33} and/or virtual compressions of the ellipse of deformation, which can be interpreted as a manifestation of linear near-surface depressions.

Correlation of the displayed values of aspects of the geopotential as computed by means of the EGM 2008 on a sub-continental scale with their details in smaller regions (e.g. Figures XI and XII) as parts of a very large region (Figure III) confirms very good possibilities of an integrated approach to various geo-applications. Records

of the present state of quantitative characteristics of the near-surface part of the geoid also make it possible to assess the recent dynamics of landform processes, notwithstanding the fact that calculations and their interpretations are based on the static gravity field model EGM 2008. For example, virtual dilatations of the ellipse of deformations give evidence of a tendency to gradual disintegration of topographical elevations. Moreover, significantly negative values of Γ_{33} indicate zones of rapid erosion processes which are very often connected with active epeirogenetic or orogenetic uplifts. A possibility to use all groups of the functions of the geopotential, computed from EGM 2008, substantially increases the quality of their geodynamic interpretation. Although computed aspects are based on a one common gravity field model, represented in the paper by EGM 2008, they have very diverse morphogenetic features. All these findings can also be accepted as a recommendation for varied geo-applications.

5. Conclusions

An extensive screening of gravity signatures computed from EGM 2008 and their comparison with morphotectonic patterns and orographical features on a large scale was realized. From the methodological and interpretative points of view, it was confirmed that distributions of values of the second derivatives of the disturbing gravitational potential Γ_{33} very precisely represent a near-surface (topographical) mass distribution. In this sense, a set of values of Γ_{33} and their regional configurations are a consequence of landform evolution and reflections of both former and recent morphostructural and climate-morphogenetic processes (Kalvoda et al. 2010). Correlations of large-scale landform configurations with some aspects of the EGM 2008, particularly the radial second derivatives of the disturbing gravitational potential Γ_{33}, the strike angle θ_S and virtual deformation of the ellipse of deformation, are demonstrated in the selected regions of the Earth. These regions are characterized by large-scale planation surfaces, high mountain ranges, collision zones of oceanic and continental lithospheric plates, volcanic chains and impact craters.

It is suggested that landform patterns with very conspicuous combinations of significantly high positive or negative values of Γ_{33} are under the strong influence of rapid and/or intensive geomorphic processes. Strong coincidences between a large-scale landform configuration of selected regions and the extension of areas with very high positive values of the radial second derivative of the disturbing gravitational potential Γ_{33}, and the most likely in combination with conspicuous areas of high negative values of Γ_{33} in their close neighbourhood, have been identified. These geophysical signatures supported by values of the strike angle θ_S and virtual dilatations or compressions of the ellipse of deformation reflect the regional dynamics of Earth surface evolution as characterised by a very effective integration of tectonic and climate-driven morphogenetic processes.

Experimental studies of varied aspects of the geopotential as computed from the EGM 2008 are continuing. Topics are not only to determine the utmost limit of their interpretations but also to find new applications of the EGM 2008. Comparison of aspects of the geopotential computed by means of the EGM 2008 on a sub-continental scale with their details in smaller regions confirms advantages of an integrated approach to geo-applications.

Acknowledgements

REFERENCES

AL-ANAZI, B. D. (2007): What you know about the Ghawar Oil Field, Saudi Arabia? CSEG Recorder, April, 40–43.

BEIKI, M., PEDERSEN, L. B. (2010): Eigenvector Analysis of Gravity Gradient Tensor to Locate Geologic Bodies, Geophysics, 75, 6, 137–149.

BRDIČKA, M., SAMEK, L., SOPKO, B. (2000): Mechanika kontinua (Continuum Mechanics), Academia, Praha.

DICKINSON, J. L., BREWSTER, J. R., ROBINSON, J. W., MURPHY, C. A. (2009): Imaging Techniques for Full Tensor Gravity Gradiometry Data, 11th SAGA Biennal Technological Meeting & Exhibition, Swaziland, 16th–18th September, 84–88.

FLOBERGHAGEN, R., FEHRINGER, M., LAMARRE, D., MUZI, D., FROMMKNECHT, B., STEIGER, CH., PIÑEIRO, J., DA COSTA, A. (2011): Mission design, operation and exploitation of the gravity field and steady-state ocean circulation explorer mission. Journal of Geodesy, 85, 749–758.

FÖRSTE, CH., BRUINSMA, S., SHAKO, R., MARTY, J.-C., FLECHTNER, F., ABRIKOSOV, O., DAHLE, CH., LEMOINE, J. M., NEUMAYER, H., BIANCALE, R., BARTHELMES, F., KÖNIG, R., BALMINO, G. (2011): EIGEN-6A new combined global gravity field model including GOCE data from the collaboration of GFZ-Potsdam and GRGS-Toulouse, EGU General Assembly 2011, 3rd–8th April 2011, Vienna, Austria.

GOLONKA, J., PICHA, F. J. (eds.) (2006): The Carpathians and their foreland: geology and hydrocarbon resources. American Association of Petroleum Geologists, Edition: Memoir, 84, 600 pp., Tulsa.

HILDEBRAND, A. R., PILKINGTON, M., CONNORS, M., ORTIZ-ALEMAN, C., CHAVEZ, R. E. (1995): Size and structure of the Chicxulub crater revealed by horizontal gravity gradients and cenotes. Nature, 376, 415–417.

HILDEBRAND, A. R. and 10 others (1998): Mapping Chicxulub craters structure with gravity and seismic reflection data. In: Grady, M. M. (Ed.): Meteorites: Flux with Time and Impact Effects. Geological Society of London, Special Publications, 140, 155–176.

HOTINE, M. (1969): Mathematical Geodesy, ESSA, US. Dept. Comm., Environ. Sci. Services Admin., Monograph 2, Washington, D.C.

HOLMES, S. A., PAVLIS, N. K., NOVÁK, P. (2006): A Fortran Program for Very-high Degree Harmonic Synthesis, version 05/01/2006.

KALVODA, J. (1992): Geomorphological Record of the Quaternary Orogeny in the Himalaya and the Karakoram. In: Development in Earth Surface Processes 3, Elsevier, 315 pp., Amsterdam.

KALVODA, J. (2007): Dynamics of landform evolution in the Makalu – Barun region, Nepal Himalaya. Geografický časopis, 59, 2, 85–106, Bratislava.

KALVODA, J., KLOKOČNÍK, J, KOSTELECKÝ, J. (2010): Regional correlation of the Earth Gravitational Model 2008 with morphogenetic patterns of the Nepal Himalaya, Acta Universitatis Carolinae, Geographica, XLV, 2, 53–78, Prague.

KLOKOČNÍK, J. (ed.) (2008): Detection of Hidden Impact (Meteoritic) Structures: Introduction Study and Simulations Before the GOCE Launch, Report: Grant ESA/PECS C-98056 "GOCE – Specific Tasks on Fine Gravity Field Structure of the Earth", Report of Astronom. Inst. Czech Acad. Sci., Ondřejov Obs., 101 pp.

KLOKOČNÍK, J., KOSTELECKÝ, J., WAGNER, C. A. (2008a): Improvement in the radial accuracy of altimeter-satellite orbits to the geopotential. Earth-Science Reviews, 91, 1–4, 106–120.

KLOKOČNÍK, J., NOVÁK, P., PEŠEK, I., KOSTELECKÝ, J., WAGNER, C. A. (2008b): EGM 08: tests of the model and simulations for GOCE. IAG Symposium on Gravity, Geoid and Earth Observations, Chania, Crete, 23th–27th June, Greece.

KLOKOČNÍK, J., NOVÁK, P., KOSTELECKÝ, J., WAGNER, C. A. (2010a): Detection of Earth impact craters aided by the detailed global gravitational model EGM 2008. Acta Geodynamica et Geomaterialia, 7, 1 (157), 71–97, Prague.

KLOKOČNÍK, J., KOSTELECKÝ, J., PEŠEK, I., NOVÁK, P., WAGNER, C. A., SEBERA, J. (2010b): Candidates for Multiple Impact Craters? Popigai and Chicxulub as seen by the Global High Resolution Gravitational Field Model EGM08, Solid Earth EGU, 1, 71–83, doi: 10.5194/se-1-71-2010.

KLOKOČNÍK, J., KOSTELECKÝ, J., SEBERA, J., BEZDĚK, A. (2012): Comparison of EIGEN 6C and EGM 2008 Gravity Field Models via Marussi Tensor, computed for Selected Areas on the Earth, EGU General Assembly 2012, 22nd–27th April, Vienna, Austria.

KLOKOČNÍK, J., KOSTELECKÝ, J., KALVODA, J., SEBERA, J., BEZDĚK, A. (2012): Towards a System of Data Systems in Geoscience: Marussi Tensor and Invariants of the Earth Gravity Field from Recent Global Gravity Models EGM 2008 and EIGEN 6C based on Satellite (GRACE or GOCE) and Terrestrial Data. Poster, the Japan Geoscience Union Meeting 2012, 20th–25th May, Makuhari, Chiba, Japan.

KLOKOČNÍK, J., KALVODA, J., KOSTELECKÝ, J., BEZDĚK, A. (2013): Gravity Disturbances, the Marussi Tensor, Invariants and Other Functions of the Geopotential as Represented by the Global Gravity Field Model EGM 2008 and Suggestions for Geo-applications. Poster, ESA Living Planet Symposium, 9th–13th September, 2013, Edinburgh.

MASAITIS, V. L., NAUMOV, M. V., MASHCHAK, M. S. (2005): Original Diameter and Depth of Erosion of the Popigai Impact Crater, Russia. In: Kenkmann, T., Hörz, F., Deutsch, A. (Eds.), Large Meteorite Impacts III, The Geological Society of America, Special paper, 384, 131–140.

MATARAGIO, J., KIELEY, J. (2009): Application of Full Tensor Gradient Invariants in Detection of Intrusion-Hosted Sulphide Mineralization: Implications for Deposition Mechanisms, Minig Geoscience, EAGE 1st break, vol. 27, 95–98.

MORITZ, H. (1984): Geodetic Reference System 1980. Bulletin Géodesique, 58, 388–398.

MURPHY, C. A., DICKINSON, J. L. (2009): Exploring Exploration Play Models with FTG Gravity Data, 11th SAGA Biennal Technological Meeting & Exhibition, 16–18th September, Swaziland, 89–91.

PAVLIS, N. K., HOLMES, S. A., KENYON, S. C., FACTOR, J. K. (2008a): EGM2008: An Overview of Its Development and Evaluation, National Geospatial-Intelligence Agency, USA. The International Conference of Gravity, Geoid and Earth Observation 2008, 23th–27th June, Chania, Crete, Greece.

PAVLIS, N. K., HOLMES, S. A., KENYON, S. C., FACTOR, J. K. (2008b): An Earth Gravitational Model to Degree 2160: EGM2008, EGU General Assembly 2008, 13th–18th April, Vienna, Austria.

PAVLIS, N. K., HOLMES, S. A., KENYON, S.C., FACTOR, J. K. (2012): The Development and Evaluation of the Earth Gravitational Model 2008 (EGM2008), Journal of Geophysical Research, 117, B04406, doi: 10.1029/2011JB008916.

PEDERSEN, B. D., RASMUSSEN, T. M. (1990): The Gradient Tensor of Potential Field Anomalies: Some implications on data Collection and Data Processing of Maps. Geophysics, 55, #12, 1558–1566.

PILKINGTON, M., PESONEN, L. J., GRIEVE, R. A. F., MASAITIS, V. L. (2002): Geophysics and Petrophysics of the Popigai Impact Structure, Siberia. In: Plado, J., Pesonene, L. J. (Eds.): Impacts in Precambrian Shields, Springer-Verlag, 87–107.

RABUS, B., EINEDER, M., ROTH, A., BAMLER, R. (2003): The Shuttle radar topography mission – a new class of digital elevation models acquired by spaceborne radar. Photogrammetry and Remote Sensing, 57, 241–262.

RUMMEL, R., COLOMBO, O. L. (1985): Gravity Field Determination from Satelite Gradiometry, Bulletin Géodesique, 59, 233–246.

SEBERA, J., WAGNER, C. A., BEZDĚK, A., KLOKOČNÍK, J. (2012): Guide to Direct Gravitational Field Modelling with Hotine's equations, Journal of Geodesy, on-line, 1–16, doi: 10.1007/s00190-012-0591-2.

SHARPTON, V. L. et al. (1993): Chicxulub multi-ring impact basin: Size and other characteristics derived from gravity analysis. Science, 261, 1564–1567.

RÉSUMÉ

Rozložení hmoty povrchových tvarů Země zjištěné aspekty geopotenciálu vypočtenými z globálního modelu tíhového pole EGM 2008

V práci jsou porovnány povrchové tvary Země s vybranými aspekty (deriváty) geopotenciálu vypočtenými z globálního mode-lu tíhového pole EGM 2008, a to zvláště s radiální složkou porucho-vého tíhového potenciálu Γ_{33}, úhlem posunu θ_S a virtuální dilatací či kompresí elipsy deformace. Byl proveden systematický skríning aspektů geopotenciálu určených z EGM 2008 a jejich korelace s rozsáhlými povrchovými tvary, které jsou důsledkem geologic-ké stavby a klimato-morfogenetických procesů. Výsledky tohoto skríningu a korelací jsou ukázány na příkladech oblastí se zarov-nanými povrchy, vysokých pohoří, kolizních zón, oceánských

a pevninských litosférických desek, vulkanických masivů a velkých impaktních kráterů. Vybrané regionální příklady korelace aspektů geopotenciálu vypočtených z EGM 2008 s uspořádáním povrchových tvarů Země jsou Nepálský Himálaj, kolizní zóna Východoasijské a Západopacifické litosférické desky, styčná zóna severovýchodní Afriky, jihozápadní Asie a jihovýchodní Evropy, morfotektonický kontakt mezi Českým masivem, Východními Alpami a Západními Karpatami ve střední Evropě a území s relikty velkých impaktních kráterů Vredefort, Chicxulub a Popigai. Dále je navržena a dokumentována interpretace, že rozsáhlé povrchové tvary s velmi nápadnou kombinací vysoce kladných a záporných hodnot poruchového tíhového potenciálu Γ_{33} jsou silně ovlivněny intenzivními geomorfologickými procesy. Tyto geofyzikální charakteristiky, podpořené specifickými hodnotami úhlu posunu θ_S a virtuální dilatace či komprese elipsy deformace, jsou reflexí dynamiky vývoje zemského povrchu, která je podmíněna velmi efektivní integrací morfotektonických a klimato-morfogenetických procesů.

Jan Kalvoda
Charles University in Prague, Faculty of Science
Albertov 6, CZ-128 43, Prague 2, Czech Republic
E-mail: kalvoda@natur.cuni.cz

Jaroslav Klokočník
Astronomical Institute, Academy of Sciences of the Czech Republic
Fričova 298, CZ-251 65, Ondřejov, Czech Republic
E-mail: jklokocn@asu.cas.cz

Jan Kostelecký
Research Institute of Geodesy, Topography and Cartography
CZ-250 66, Zdiby 98, Czech Republic
E-mail: kost@fsv.cvut.cz

Aleš Bezděk
Astronomical Institute, Academy of Sciences of the Czech Republic
Fričova 298, CZ-251 65, Ondřejov, Czech Republic
E-mail: bezdek@asu.cas.cz

COMPARISON OF METEOROLOGICAL CONDITIONS DURING MAY AND AUGUST 2010 FLOODS IN CENTRAL EUROPE

MAREK KAŠPAR[1], MILOSLAV MÜLLER[1,2],
JOZEF PECHO[3,4]

[1] Institute of Atmospheric Physics AS CR
[2] Charles University, Faculty of Science
[3] Technical University of Liberec
[4] Comenius University, Faculty of Mathematics, Physics and Informatics

Abstract

We compared May and August 2010 precipitation events that produced catastrophic flooding. In May, large rivers (Vistula, Oder) were affected, while smaller rivers (e.g. Lausitzer Neisse) were affected in August. Similarities in precipitation characteristics (duration of several days, daily total maximum of approximately 180 mm) can be explained by similarities in the meso-a scale (thermo-dynamic indicia connected with a cyclonic system of Mediterranean origin). These indicia were more significant in May (extreme and deep vertical wind speed, extreme northerly flux of moisture) than in August (strong but non-extreme northerly flux of moisture) when conditional instability was additionally detected. Obviously more intensive orographic enhancement in the first case and the strong effect of convection in the latter case produced differences in the return periods of precipitation totals (longer return periods in August). Subsequently, the hydrological response was rapid and particularly strong in smaller streams in August.

Keywords: flood, heavy precipitation, meteorological anomaly, return period, orographic precipitation enhancement

1. Introduction

In 2010, several significant flooding events occurred worldwide. From a global viewpoint, the most catastrophic one affected Pakistan in summer (Gaurav et al. 2011), causing 1760 deaths and 9.5 billion U.S. dollars in damage (MunichRe 2012). In Central Europe, summer flooding can also be very devastating, as it was, for example, in July 1997 and in August 2002 (Řezáčová et al. 2005). In 2010, the region experienced several catastrophic floods during the warmer half-year. The events were studied in detail in the affected countries by meteorological and hydrological authorities in the Czech Republic, Germany, Poland, and Slovakia. Cyclones moving along the Vb pathway (van Bebber 1891) were blamed for hundreds of millimeters of precipitation during several days both in May and in August. On the other hand, the events differed from each other not only in terms of the affected catchments but also the course of flooding. The aim of this paper is to elucidate the hydrological differences between the events with respect to meteorological causes and precipitation distribution. The structure of the paper is as follows: (1) a brief description of the events, (2) specification of data and methods, (3) determination of meteorological conditions both before and during the events by means of anomalies in synoptic-scale fields, (4) time/space/intensity analysis of precipitation, (5) conclusions and discussion of the results.

Flooding occurred in the eastern part of Central Europe in the second half of May 2010. The antecedent saturation of the region was high due to rains that occurred at the beginning of the month (Daňhelka and Šercl 2011). Extra-heavy rains that reached their maximum on 16 May were associated with a cyclone passing from the Mediterranean northeastward, becoming almost stationary over Ukraine for several days (Bissolli et al. 2011). The highest precipitation totals were recorded in the western sector of the cyclone at the state border between the Czech Republic, Slovakia, and Poland. This headwater area of the rivers Odra and Vistula is prone to flooding in summer (Čekal, Hladný 2008) due to (i) frequent Mediterranean cyclones trajectories and (ii) a specific configuration of mountain ranges supporting low-level convergence and uplifts of air (Kyselý and Picek 2007). Subsequently, the water stages were even higher than those during the catastrophic flood in July 1997 in some regions, mainly in the upper reaches of the Vistula River in Poland (Bissolli et al. 2011). In the Czech Republic, peak flows reached return periods of more than 50 years at some gauges (Figure 1). Moreover, because heavy precipitation fell over the Flysch Outer Western Carpathians, which are susceptible to landslides, it also had geomorphologic impacts. More than 150 mostly small landslides originated only in the eastern part of the Czech Republic, including a kilometer-long rockslide along the southern slope of Mt. Girová, the Beskydy Mts. (Pánek et al. 2011).

During the first decade of August 2010, flooding occurred in many rivers over the western part of the Czech Republic, with high return periods concentrated in a rather small region at the state border between the Czech Republic, Germany and Poland (Figure 1). Heavy rains reaching their maximum on 7 August were more concentrated in time than they were in May. They were associated with a rather shallow cyclone passing from the Mediterranean to the north. The most affected river basins were Lausitzer Neisse (a left-sided tributary of Oder) and the neighboring

right-sided tributaries of Elbe (Müller and Walther 2011). The water levels were the highest ever recorded at some smaller streams. Moreover, the flood caused the Niedów Dam on the river Witka to break.
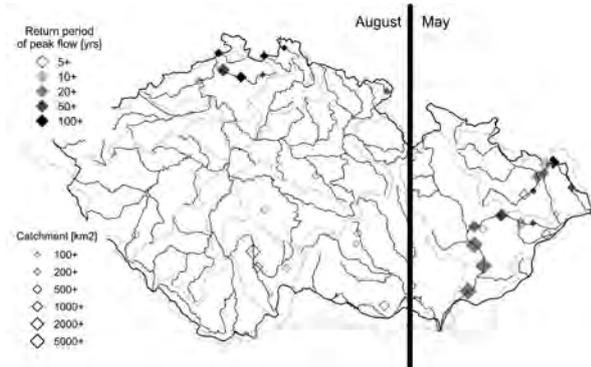
Fig. 1 Return periods of peak flows reached in May 2010 and in August 2010 in the Czech Republic (the right and the left part of the figure, respectively). The size of the sign represents the area of the catchment in km².

2. Data and methods

2.1 Meteorological data and their processing

Müller et al. (2009) demonstrate that heavy rains, which produce floods in major rivers in the Czech Republic, are regularly associated with the appearance of climatologically high or low values of certain thermo-dynamic variables in specific meso-*a* scale areas in Europe and the Northern Atlantic. Subsequent studies (e.g., Kašpar and Müller 2009; Müller and Kašpar 2010) come to similar conclusions within the broader region of Central Europe and indicate that such thermo-dynamic anomalies may be an effective indicator of causal synoptic processes. Based on these findings, we opted for a more in-depth analysis of the events using the method presented below.

We used the 6-hourly NCEP/NCAR Reanalysis data set (Kalnay et al. 1996) covering the area of interest, 0°–40° E by 40°–60° N, with a horizontal resolution of 2.5°. We limited ourselves to the 60-year period spanning from 1951 to 2010. We considered the values of basic variables directly offered by the data set at the following isobaric levels: 1000, 925, 850, 700, 600, 500, 400, and 300 hPa. These variables include air temperature, geopotential height, specific and relative humidity, zonal and meridional wind components, and vertical velocity. In addition to the basic variables, we calculated several variables derived from gradients, divergences, vorticities, fluxes, and Lagrangian tendencies.

We standardized the sample distributions of the values of all variables in each grid point and on each calendar day to reduce the effect of the climatological annual cycle. Moreover, we standardized the time series individually at 00, 06, 12 and 18 UTC to reduce the possible effects of a diurnal cycle. We used a standardization procedure that

eliminates the skewness and kurtosis in these distributions and set their mean to 0 and their standard deviation to 1. In the majority of cases, this is an adequate standardization procedure and yields the "near normality" of the resulting distributions (e.g., Jobson 1991).

First, we eliminated the skewness by a unified extension of the Box-Cox transformation proposed by Yeo and Johnson (2000). The extension is a non-linear power transformation defined as

$Y(x) = [(x + 1)^{\tilde{\alpha}} - 1]/\tilde{\alpha}, x \geq 0$ and $\tilde{\alpha} \neq 0$;
$Y(x) = 1n(x + 1), x \geq 0$ and $\tilde{\alpha} = 0$;
$Y(x) = -[(-x + 1)^{2-\tilde{\alpha}} - 1]/(2 - \tilde{\alpha}), x < 0$ and $\tilde{\alpha} \neq 2$;
$Y(x) = -1n(-x + 1), x < 0$ and $\tilde{\alpha} = 2$. (1)

In Eq. (1), $Y(x)$ is the transformed value of an original value x and is the time-smoothed transformation parameter corresponding to a given calendar day. We estimated the parameter for each calendar day by minimizing the skewness of the sample-transformed distribution of $Y(x)$. To smooth the parameter in time, we applied a 1-D Gaussian filter to the time series of the estimations of this parameter. For accuracy, we did not consider 29 February. For leap years, we used the corresponding to 28 February. On calendar days with the index j, the time-smoothed parameters were calculated by

$$\alpha_j = \frac{\sum_{jj=j-k}^{j+k} \alpha_{jj} G(jj, j)}{2k + 1},$$ (2)

where a_{jj} is the estimation of the parameter on the calendar day with the index jj and the discrete Gaussian function $G(jj,j)$ is given by

$$G(jj, j) = \frac{1}{\sqrt{2\pi} s} e^{-\frac{(jj-j)^2}{2s^2}}.$$ (3)

After some testing, we subjectively selected Gaussian smoothing with a standard deviation $s = 30$ days and time window $k = 3s = 90$ days. The smoothing of the parameter is sufficient to significantly reduce the effect of outliers and to eliminate the high-frequency time oscillations over periods of less than roughly three months. On the other hand, the smoothing is reasonably strong in eliminating the annual cycle of the skewness of transformed distributions, which thus oscillates around zero.

Next, we removed the kurtosis by the modified Box-Cox transformation introduced for symmetric distributions by John and Draper (1980):

$Z(y) = \text{SIGN}[(|y - y_M| + 1)^{\tilde{\beta}} - 1]/\tilde{\beta}, \tilde{\beta} \neq 0$;
$Z(y) = \text{SIGN}[1n(|y - y_M| + 1)], \tilde{\beta} = 0$. (4)

In Eq. (4), $Z(y)$ is the transformed value of a value $y = Y(x)$ obtained by Eq. (1), y_M is the median of a given sample distribution of y, SIGN is the sign of the original value before taking absolute values and $\tilde{\beta}$ is the time-smoothed transformation parameter corresponding to a given calendar day. We estimated the parameter for each calendar day by minimizing the kurtosis of the sample-transformed distribution of $Z(y)$. To smooth the parameter in

time, we applied the 1-D Gaussian filter described by Eqs. (2) and (3) with standard deviation $s = 30$ days and time window $k = 3s = 90$ days.

Finally, we set the mean to 0 and the standard deviation to 1 by the application of the standard score

$$\hat{z} = \frac{z - \tilde{\mu}}{\tilde{\sigma}}, \tag{5}$$

where $\hat{z}$ is the standardized value of a value $z = Z(y)$ obtained by Eq. (4), $\tilde{\mu}$ is the time-smoothed mean and $\tilde{\sigma}$ is the time-smoothed standard deviation of the sample-transformed distribution of $Z(y)$ corresponding to a given calendar day. To smooth the parameters in time, we applied the 1-D Gaussian filter described by Eqs (2) and (3) with standard deviation $s = 10$ days and time window $k = 3s = 30$ days.

Because heavy rains in May and August 2010 were clearly conditioned by atmospheric processes occurring on a time scale longer than 6 hours, we additionally considered the daily means of the standardized variables using the formula

$$\hat{z}_d = \frac{0.5\hat{z}_{06}^d + \hat{z}_{12}^d + \hat{z}_{18}^d + \hat{z}_{00}^{d+1} + 0.5\hat{z}_{06}^{d+1}}{4}, \tag{6}$$

where the values of $\hat{z}$ at 06, 12 and 18 UTC on the day d and at 00 and 06 UTC on the following day $d + 1$ are included. We defined the daily period from 06 UTC to 06 UTC on the following day to ensure the agreement with the period during which daily precipitation totals were measured.

In the last step, we assessed the probability of not exceeding high and low values of each standardized variable at each grid point. We applied the three-parametric generalized extreme value (GEV) distribution (Coles 2001) using a block maxima approach.

Regarding high values, we assembled the quarterly maxima from 1951 to 2010 to ensure the sufficient independency of the sample and explanation of the distribution of 1% of the highest daily means $\hat{z}_d$ and 0.25% of the highest 6-hourly values . Hereinafter, these high values are referred to as $\hat{x}$. Then, we fitted the distribution of the maxima with the GEV distribution. We estimated the GEV parameters by the method using L-moments (Hosking and Wallis 1997). L-moments are the linear combinations of the realizations of a variable and represent a set of scale and shape statistics alternative to conventional (product) moments. The method using L-moments is computationally simpler and may give better estimations of the parameters for moderate sample sizes than the maximum likelihood method and the methods of conventional moments (Hosking et al. 1985).

The probability of not exceeding p of a value $\hat{x}$ is calculated by

$$p(\hat{x}) = \left[F(\hat{x})\right]^{4/(365.2425n)}, \tag{7}$$

where F denotes the cumulative distribution function of the GEV estimated from quarterly maxima and $n = 1$ for

daily means and $n = 4$ for 6-hourly dataset. Equation (7) presumes the independence of the dataset, which does not have to be fulfilled each time. Nevertheless, this can be neglected because of our purposes focused on the comparison of the events. Finally, the corresponding return period N in units of year can be estimated for the most extreme values $\hat{x}$ of as

$$N(\hat{x}) = \frac{1}{4\left(1 - F(\hat{x})\right)}. \tag{8}$$

Regarding low values, we employed the same procedure, but we used the re-analysis dataset multiplied by −1 as an input. The actual probability of not exceeding these values is then equal $1 - p$. We defined the positive and negative anomalies in a given variable as a contiguous space which is characterized by the probability of not exceeding the values of the variable equal to or greater than 0.99 (0.9975 for 6-hourly dataset) and equal to or less than 0.01 (0.0025 for 6-hourly dataset), respectively.

2.2 Precipitation data and their processing

We searched the daily precipitation totals of the entire territory of the Czech Republic (measured by the Czech Hydrometeorological Institute) and, in part, those of neighboring countries as well: Slovakia (by the Slovak Hydrometeorological Institute), Poland (by the Institute of Meteorology and Water Management), and Germany (by the German Weather Service). Apart from daily totals, we also searched two- and three-day precipitation totals.

To express the extremeness of precipitation totals at individual gauge stations within the Czech Republic, we determined the return periods of precipitation totals at more than 700 gauges. To this end, we again applied the three-parametric GEV distribution that was found to represent a suitable model for precipitation extremes in most regions of the Czech Republic (Kyselý and Picek 2007). We used the parameters of the GEV distribution estimated by means of the L-moment algorithm (Hosking and Wallis 1997) and the region-of-influence (ROI) method (Burn 1990; Gaál and Kyselý 2009). In contrast to local (at-site) frequency modeling, in which inference is drawn solely based on data observed at individual gauges, the ROI method makes use of regions, in which all regional data, weighted by a dissimilarity measure, are used to estimate the parameters of the distribution of extremes at a given gauge station. The advantage of the ROI method compared to the local analysis is that sampling variations in the estimates of model parameters and high quantiles may be substantially reduced, and the inference becomes more robust (for more details see Kyselý et al. 2011).

3. Analysis of thermo-dynamic anomalies

We performed the objective detection of positive and negative anomalies in thermodynamic variables

just before and during heavy rainfall episodes in May and August 2010. We focused on significant anomalies and their spatial extent in light of the probability of not exceeding high and low values at individual grid points. The anomalies, which can be interpreted in terms of synoptic-dynamic meteorology and illustrate both similar and different attributes among the episodes, are discussed in the following sub-sections.

3.1 May 2010 event

The development of the upper-level and lower-level thermo-baric fields just before and during the event is illustrated in Figure XIII (colour appendix). An omega block over the eastern North Atlantic and Western Europe preceded the onset of the causal cyclonic system. The block, which was distinguishable particularly at lower levels, enabled the formation of an upper-level cut-off low in the southern portion of a long-wave trough over Western Europe. The center of the low first appeared over the Balearic Islands at approximately 18 UTC on 14 May. At the same time, strong cyclogenesis initiated near the surface on the front (eastern) side of the low. Figure XIIIa indicates that cyclogenesis took place according to the classic Petterssen scheme of a type B development (Petterssen and Smebye 1971) as the upper-level low spread over a pre-existing lower-level baroclinic area. The strength of the cyclogenetic processes is characterized by intense cyclonic vorticity

advection at upper levels ahead of the low in Figure 2. In accordance with the quasigeostrophic approach, apparent vertically increasing vorticity advection ahead of the low triggered synoptic-scale ascending motions, leading to the increase and extension of cyclonic vorticity downward and downstream in a sloped zone. The completion of vertical coupling between the lower-level baroclinic area and the upper vorticity maximum led to the development of a vertically deep and thermally asymmetric cyclone.

While the cyclone propagated to the north-east across the Adriatic Sea and over eastern Romania (Figure XIIIb,c,d), it intensified partially due to lee effects south of the Alps and Carpathian Mountains (Bissolli et al. 2011). Such a cyclone pathway, which transports subtropical air of significant water vapor content northward, is well known for its role in bringing persistent and heavy rainfall to Central Europe (e.g., Mudelsee et al. 2004). However, the specific cyclone pathway is clearly only one of many ingredients important for producing extreme precipitation. Figures 3, 4, and 5 reveal some other thermo-dynamic indicia that could favor extreme precipitation during the event. One-day-averaged fields are used to stress the importance of the persistence of favorable thermo-dynamic conditions. Figure 3 shows extremely strong and vertically deep lifting on the western flank of the cyclone supporting precipitation throughout the troposphere over a large area of Central Europe. Upward motions at upper levels were linked to a baroclinic zone characterized by the widespread warm advection of moist air from the south and east directions, while upward motions at lower levels occurred in the relatively cold air mass southwest from the strong frontal zone (Figure 4). The upward motions at lower

Fig. 2 Three-dimensional projection of the maxima of absolute vorticity advection and maxima of the corresponding probability of not exceeding the values in the selected sub-region on 14 May 2010 at 18 UTC. The values of the advection are depicted by shading in $[10^{-9} \text{ s}^{-2}]$. Positive and negative values correspond to cyclonic and anticyclonic vorticity advection, respectively. The probabilities of not exceeding the values are evaluated at grid points in the 850–300 hPa layer and are depicted by symbols according to the legend. Corresponding return periods equal to or greater than 10 years are depicted inside the symbols.

Fig. 3 Same as Figure 2, but for the minimum vertical velocities in the p-system on 16 May 2010. The positive and negative values, in $[\text{Pa s}^{-1}]$, correspond to downward and upward motions, respectively.
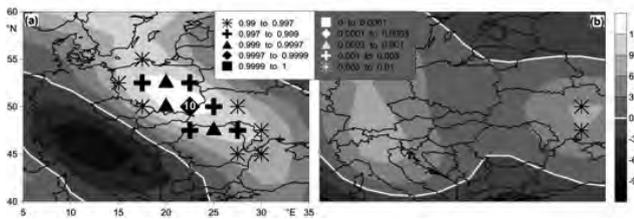
Fig. 4 Southwest to northeast temperature gradient and the corresponding probability of not exceeding the values at (a) 850 and (b) 500 hPa on 16 May 2010. The values of the gradient are depicted by shading in [10^{-6} K m^{-1}]. The positive and negative values correspond to the temperature increase and temperature decrease from the southwest to the northeast, respectively. The probabilities of not exceeding the values are depicted at grid points by symbols according to the legend.
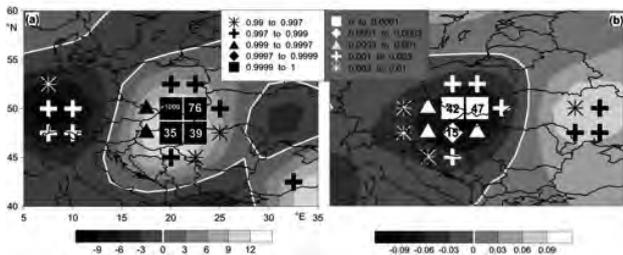
Fig. 5 Selected dynamic variables and the corresponding probability of not exceeding the values at 850 hPa on 16 May 2010. The values of the variables are depicted by shading, and the probabilities of not exceeding the values are depicted at grid points by symbols according to the legend. Corresponding return periods equal to or greater than 10 years are depicted inside the symbols. (a) Flow convergence in [10^{-6} s^{-1}]. The positive and negative values correspond to convergence and divergence, respectively. (b) Meridional flux of moisture in [kg m^{-2} s^{-1}]. The positive and negative values correspond to southerly and northerly moisture flux, respectively.

levels were linked to extremely strong air convergence (Figure 5a) resulting from the confluence to and difluence from the area of enhanced horizontal pressure gradient. Figure 5b shows a strong northerly moisture flux at lower levels, which was linked to strong northerly flow in the area of enhanced horizontal pressure gradient and which supplemented moisture fluxes from the south and east directions at upper levels. Apart from the significant supply of moisture to the area of upward motions, the northerly moisture flux most likely played a role in the orographic enhancement of precipitation on the northern slopes of mountains where additional uplift triggered particularly high rainfall intensities (Section 4).

3.2 August 2010 event

Figure XIV indicates that upper level thermo-baric conditions played a significant role in the development of the causal cyclonic system. The onset of the event was characterized by the deepening of an initially shallow upper level trough with the axis extending from the eastern North Atlantic to the western Mediterranean

(Figure XIVa). The spreading of the trough to the southeast over a pre-existing baroclinic area supported lower-level cyclogenesis apparent over northern Italy at 18 UTC on 5 August (Figure XIVb). Figure 6 demonstrates the strength and extent of the cyclogenetic processes on the front side of the through using quasi-geostrophic thinking (see Sect. 3.1). It is evident that intense cyclonic vorticity advection affected only the highest tropospheric levels. Therefore, the significant increase in cyclonic vorticity advection with height was limited to upper and middle levels. As a result, a thermally asymmetric cyclone developed particularly at these levels. The cyclone extended down to the surface layer as well; however, there, the cyclonic circulation was weak (Figure XIVb).
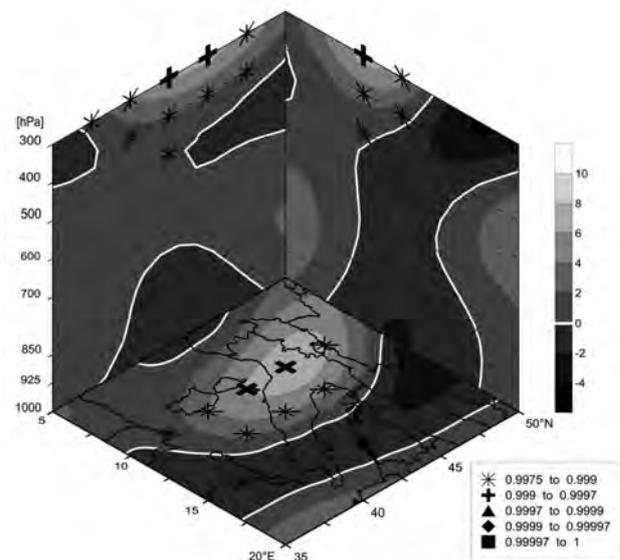
Fig. 6 Same as Figure 2, but for 5 August 2010 at 06 UTC.

While the cyclone slowly moved initially to the east and later to the northeast over the eastern part of central Europe, it weakened (Figure XIVc,d). At the same time, however, the horizontal temperature gradient sharpened between colder air over Western Europe and very warm air over Eastern Europe. Figure 7 reveals a strong and widespread southwest to northeast temperature gradient, which led to the rapid strengthening of baroclinity over Central Europe. In addition, aerological sounding at the central European station Prague-Libuš indicates a vertically deep conditional instability on 7 August 00 UTC, with the values of CAPE and CIN equaling 190 J kg^{-1} and −5 J kg^{-1}, respectively (www .weather.uwyo.edu/upperair). The combination of the synoptic-scale baroclinity and upward motions in the baroclinic zone (Figure 8) with the conditional instability in the sub-synoptic scale could favor the convection of precipitation during an earlier stage of the event.
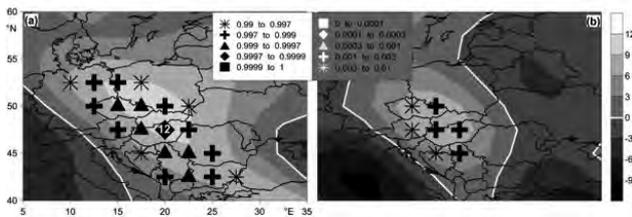
**Fig. 7** Same as Figure 4, but for 6 August 2010.
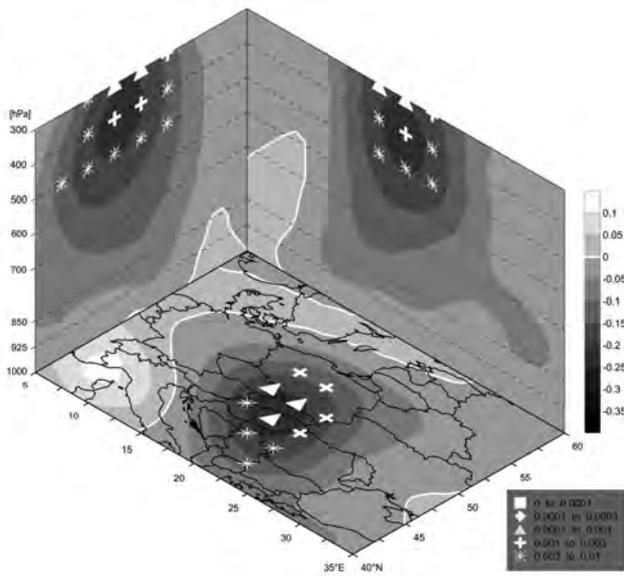
**Fig. 8** Same as Figure 3, but for 6 August 2010.
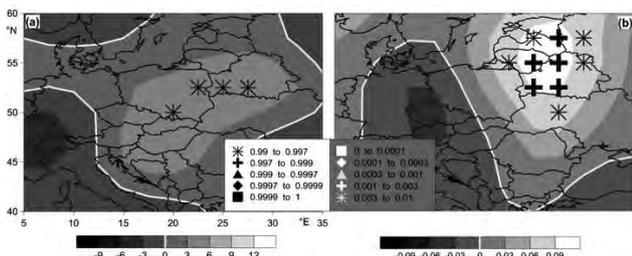
Fig. 9 Same as Figure 5, but for (a) flow convergence on 6 August 2010 and (b) meridional flux of moisture on 7 August 2010.

Figures 8 and 9 complete the description of the extremeness of thermo-dynamic conditions in the meso-a scale. Strong and persistent upward motions occurred only at upper levels (Figure 8), where they were related to well-developed cyclonic circulation. By contrast, non-extreme upward motions connected with strong but rather non-extreme air convergence (Figure 9a) occurred inside the baroclinic zone at lower levels. Due to the weakened horizontal pressure gradient there, the northerly moisture flux to the rainfall area was also non-extreme (Figure 9b). Unlike in the May 2010 event, both extreme and non-extreme (but still favorable) thermo-dynamic indicia can be identified. Therefore, their combined effect was most likely much more crucial in the production of extreme precipitation than the effect of individual ones.

4. Precipitation analysis

The daily precipitation totals observed during the studied events are depicted in Figure XV. From this point of view, the events appear rather similar. Apart from large regions with daily totals of tens of millimeters, there was a limited area with higher precipitation both in May and in August. In May, it was concentrated around the Moravskoslezske Beskydy Mts.; in August, the main affected area was situated around the Jizerske hory Mts. and the Luzicke hory Mts. The highest daily totals were also very similar: 185.2 mm at the Polish gauge Straconka (on 16 May) and 179.0 mm at the Czech gauge Hejnice (on 7 August).

However, there is a substantial difference between the events regarding the return periods of precipitation totals (Figure 10). For example, the daily total of 100 mm had the return period approximately 20 years in May while about 100 years at most gauges in August. It means that in the latter event, precipitation affected a region where heavy rains are significantly less frequent. This fact is even more visible if we compare 3-day totals. In May, they were about twice as high as in August, whereas respective return periods were still longer in August.
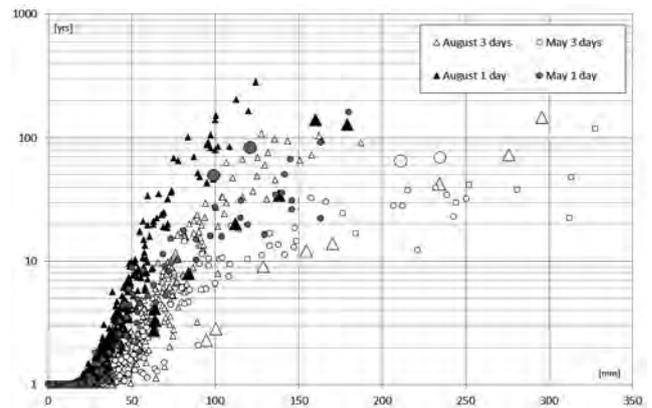

Fig. 10 Maximum one-day and three-day precipitation totals (x-axis) and their return periods (y-axis) at Czech gauge stations during the studied events. Outstanding values discussed in text are marked with big signs.

Nevertheless, several gauges recorded high precipitation totals in August but reached significantly shorter return periods in comparison to other gauges (Figure 10). Three of them even belonged to the highest totals (both daily and 3-day) which were detected in August. In fact, their return periods were similar to those from May! No analogous anomaly occurred in May when only two gauges reached slightly higher return periods than other gauges, despite of similar totals.

Therefore we also studied the relationship between reached precipitation totals and their return periods (if available) on one hand and the position of respective gauges on the other hand (Figure XVI). The above mentioned gauges with high totals but rather short return periods in August were concentrated in the eastern part

of the affected area where the Jizerske hory Mts. and the Giant Mts. constitute a significant barrier for northern winds. Here, as well as in the Moravskoslezske Beskydy Mts. in May, we can recognize a significant role of the orographic enhancement of precipitation. The leeward (~southern) side of the mountains was affected by the precipitation shadow. High precipitation totals occurred not only on the tops of mountains but also both in front of and just behind them. For example, the aforementioned gauges Straconka and Hejnice are situated at an altitude only approximately 400 meters above sea level but still in the vicinity of much higher mountain ranges. On the contrary, the larger (western) part of the area mostly affected by precipitation in August is obviously less orographically exposed.

This result well corresponds with the meteorological conditions described in Section 3. In May, meteorological conditions were characterized by extremely strong thermo-dynamic anomalies. One of these anomalies was a strong moisture flux from the north, which generally supports the orographic enhancement of precipitation along the northern slopes of mountains.

In August, on the contrary, thermo-dynamic anomalies were less significant in the meso-a scale. On the other hand, we can assume a significant role of convection during the latter event because of the detected conditional instability in the area of a strong baroclinic zone.

5. Conclusions

We compared two Central European heavy precipitation events that produced catastrophic flooding in the warm season of 2010. Both precipitation events lasted several days and were characterized by similar maxima of daily totals. These observations can be explained by similarities in meteorological conditions. In both cases, thermo-dynamic indicia in the meso-a scale were detected that are favorable for the production and prolongation of heavy rains. The indicia were connected with a cyclonic system of the Mediterranean origin. The final effects of the indicia were a significant supply of moisture highlighted by strong northerly moisture fluxes into the area of strong upward motions.

Despite these similarities, the events differed from the viewpoint of the hydrological course. While large rivers (Vistula, Oder) also overflowed in May, the August event was limited to smaller streams (Lausitzer Neisse); nevertheless, the peak flows in August can be hardly compared with any other known flood that occurred before. These differences can be explained by dissimilarities in the character and the distribution of precipitation.

In May, heavy rains affected the headwater area of the rivers Oder and Vistula, which is prone to long-lasting, synoptically driven, and orographically enhanced precipitation. Therefore, the return periods of precipitation totals were only approximately 20 years at the majority of

gauges, regardless of considering daily or three-day precipitation totals. Indeed, the meteorological conditions were characterized by extremely strong thermo-dynamic anomalies. One of these anomalies was a strong moisture flux from the north, which generally supports the orographic enhancement of precipitation along the northern slopes of mountains.

In August, on the contrary, thermo-dynamic anomalies were less significant in the meso-a scale. Nevertheless, precipitation was also enhanced by orography in part of the most affected area. On the other hand, daily totals of approximately 100 mm were also reached at many gauges with significantly lower orographic effects. We attribute this observation to the effect of convection, which can be assumed because of the detected conditional instability in the area of a strong baroclinic zone. Because the intense precipitation extended to an area with low orographic exposure, the return periods of daily totals in this limited area were much higher than in May. Subsequently, the hydrological response was rapid and particularly strong at smaller streams there.

Acknowledgements

REFERENCES

BISSOLLI, P., FRIEDRICH, K., RAPP, J., ZIESE, M. (2011): Flooding in eastern central Europe in May 2010 – reasons, evolution and climatological assessment. Weather 66(6), 147–153. DOI: 10.1002/wea.759

BURN, D. H. (1990): Evaluation of regional flood frequency analysis with a region of influence approach. Water Resources Research 26(10), 2257–2265. DOI: 10.1029/WR026i010p02257

ČEKAL, R., HLADNÝ, J. (2008): Analysis of flood occurrence seasonality on the Czech Republic territory with directional characteristics method. Acta Universitatis Carolinae Geographica 43(1–2), 3–14.

COLES, S. (2001): An introduction to statistical modeling of extreme values. London, Springer Verlag.

DAŇHELKA, J., ŠERCL, P. (2011): Floods in the Czech Republic in 2010. Meteorologické zprávy 64(1), 4–9. [in Czech, with an English abstract]

GAÁL, L., KYSELÝ, J. (2009): Comparison of region-of-influence methods for estimating high quantiles of precipitation in a dense dataset in the Czech Republic. Hydrology and Earth System Sciences 13(11), 2203–2219.

GAURAV, K., SINHA, R., PANDA, P. K. (2011): The Indus flood of 2010 in Pakistan: a perspective analysis using remote

sensing data. Natural Hazards 59(3), 1815–1826. DOI: 10.1007/s11069-011-9869-6

HASTINGS, D. A., DUNBAR, P. K., ELPHINGSTONE, G. M., BOOTZ, M., MURAKAMI, H., MARUYAMA, H., MASAHARU, H., HOLLAND, P., PAYNE, J., BRYANT, N. A., LOGAN, T. L., MULLER, J.-P., SCHREIER, G., MACDONALD, J. S. (1999): The Global Land One-kilometer Base Elevation (GLOBE) Digital Elevation Model, Version 1.0. National Oceanic and Atmospheric Administration, National Geophysical Data Center, 325 Broadway, Boulder, Colorado 80305-3328, U.S.A. Digital data base on the World Wide Web (URL: http://www.ngdc.noaa.gov/mgg/topo/globe.html) and CD-ROMs.

HOSKING, J. R. M., WALLIS, J. R. (1997): Regional frequency analysis: an approach based on L-moments. Cambridge, Cambridge University Press.

HOSKING, J. R. M., WALLIS, J. R., WOOD, E. F. (1985): Estimation of the generalized extreme value distribution by the method of probability-weighted moments. Technometrics 27(3), 251–261. DOI: 10.2307/1269706

JOBSON, J. D. (1991): Applied Multivariate Data Analysis: Regression and experimental design. London, Springer Verlag.

JOHN, J. A., DRAPER, N. R. (1980): An alternative family of transformations. Applied Statistics 29(2), 190–197.

KALNAY, E., KANAMITSU, M., KISTLER, R., COLLINS, W., DEAVEN, D., GANDIN, L., IREDELL, M., SAHA, S., WHITE, G., WOOLLEN, J., ZHU, Y., CHELLIAH, M., EBISUZAKI, W., HIGGINS, W., JANOWIAK, J., MO, K. C., ROPELEWSKI, C., WANG, J., LEETMAA, A., REYNOLDS, R., JENNE, R., JOSEPH, D. (1996): The NCEP/NCAR 40-Year Reanalysis Project. Bulletin of the American Meteorological Society 77(3), 437–471. DOI: 10.1175/1520-0477(1996)077<0437:TNYRP>2.0.CO;2

KAŠPAR, M., MÜLLER, M. (2009): Cyclogenesis in the Mediterranean basin: a diagnosis using synoptic-dynamic anomalies. Nat. Hazards Earth Syst. Sci. 9(3), 957–965.

KYSELÝ, J., GAÁL, L., PICEK, J. (2011): Comparison of regional and at-site approaches to modelling probabilities of heavy precipitation. International Journal of Climatology 31(10), 1457–1472. DOI: 10.1002/joc.2182

KYSELÝ, J., PICEK, J. (2007): Regional growth curves and improved design value estimates of extreme precipitation events in the Czech Republic. Climate Research 33(3), 243–255. DOI: 10.3354/cr033243

MUDELSEE, M., BÖRNGEN, M., TETZLAFF, G., GRÜNEWALD, U. (2004): Extreme floods in central Europe over the past 500 years: Role of cyclone pathway "Zugstrasse Vb". J. Geophys. Res. 109(D23101), 21 pp. DOI: 10.1029/2004JD005034

MÜLLER, M., KAŠPAR, M. (2010): Quantitative aspect in circulation type classifications – an example based on evaluation of moisture flux anomalies. Phys. Chem. Earth 35(9–12), 484–490. DOI: 10.1016/j.pce.2009.09.004

MÜLLER, M., KAŠPAR, M., ŘEZÁČOVÁ, D. SOKOL, Z. (2009): Extremeness of meteorological variables as an indicator of extreme precipitation events. Atmos. Research 92(3), 308–317. DOI: 10.1016/j.atmosres.2009.01.010

MÜLLER, U., WALTHER, P. (2011): The Neisse Flood 2010 – Analysis and Consequences. Wasserwirtschaft 101(11), 10–14. [in German]

MUNICHRE (2011): NatCatSERVICE. Available at www.munichre.com. [Cited 2013-03-01]

PÁNEK, T., BRÁZDIL, R., KLIMEŠ, J., SMOLKOVÁ, V., HRADECKÝ, J., ZAHRADNÍČEK, P. (2011): Rainfall-induced landslide event of May 2010 in the eastern part of the Czech Republic. Landslides 8(4), 507–516. DOI: 10.1007/s10346-011-0268-6

PETTERSSEN, S., SMEBYE, S. J. (1971): On the development of extratropical cyclones. Q. J. R. Meteorol. Soc. 97(414), 457–482. DOI: 10.1002/qj.49709741407

ŘEZÁČOVÁ, D., KAŠPAR, M., MÜLLER, M., SOKOL, Z., KAKOS, V., HANSLIAN, D., PEŠICE, P. (2005): A comparison of flood precipitation episode in August 2002 with historic extreme precipitation events on the Czech territory. Atmos. Res. 77(1–4), 354–366. DOI: 10.1016/j.atmosres.2004.10.008

VAN BEBBER, W. (1891): Die Zugstrassen der barometrischen Minima. Met. Z. 8, 361–366. [In German]

YEO, I.-K., JOHNSON, R. A. (2000): A new family of power transformations to improve normality or symmetry. Biometrika 87(4), 954–959. DOI: 10.1093/biomet/87.4.954

RÉSUMÉ

Srovnání meteorologických podmínek ve střední Evropě během povodní v květnu a srpnu 2010

Článek porovnává některé aspekty dvou případů silných srážek ve střední Evropě v roce 2010, které zde způsobily významné povodně: v květnu především na Visle a Odře a jejich přítocích, v srpnu spíše na menších tocích, jako je Lužická Nisa. Podobnost některých srážkových charakteristik (vícedenní trvání, maximální denní úhrn přibližně 180 mm) může být vysvětlena podobností meteorologických veličin v meso-a měřítku (termodynamické anomálie spojené s cyklonou středomořského původu). Tyto anomálie byly výraznější při květnové události (extrémní vertikální rychlost větru skrz celou troposféru, extrémní tok vlhkosti od severu) než při události srpnové (silný, ne však extrémní tok vlhkosti od severu), kdy byla naopak dodatečně detekována podmíněná instabilita. Zjevně výraznější orografické navýšení srážek v prvním případě a silný podíl konvekce v druhém případě způsobily odlišnosti v dosažených dobách opakování srážkových úhrnů, které byly při srpnové události větší. Následně i hydrologická odezva na menších tocích byla rychlá a silná.

Marek Kašpar
Institute of Atmospheric Physics
Boční II. 1401
141 31 Praha 4
Czech Republic
E-mail: kaspar@ufa.cas.cz

CREVICE-TYPE CAVES AS INDICATORS OF SLOPE FAILURES: A REVIEW PAYING A SPECIAL ATTENTION TO THE FLYSCH CARPATHIANS OF CZECHIA, POLAND, AND SLOVAKIA

JAN LENART, TOMÁŠ PÁNEK

University of Ostrava, Faculty of Science, Department of Physical Geography and Geoecology

ABSTRACT

The occurrence and evolution of crevice-type caves is one of the most spectacular phenomena in the progression of slope failures in distinct types of rocks. Crevices are common manifestations of disintegration of anisotropic flysch rocks in the area of the Carpathians. This paper presents the issues of the close connection between the evolution of gravitational slope deformations and the formation of crevice-type caves. Furthermore, it presents a contemporary view on the regional distribution of crevice-type caves in this area and outlines the recent progress and future possibilities of the investigation of this phenomenon. Based on the vertical distribution of different morphological zones within the caves and the main modes of their evolution, we can distinguish three basic types of crevice-type caves: (i) translational/spreading type, (ii) toppling type and (iii) rotational type.

Keywords: pseudokarst, crevice-type cave, gravitational slope deformations, Carpathians, flysch

1. Introduction

Caves belong to the forms of pseudokarst phenomena (Halliday 2007). Most extensive and widespread pseudokarst caves are crevice-type caves that are formed during the evolution of slope failures by the disintegration of rock blocks (Vítek 1978; Wagner et al. 1990; Baroň et al. 2003a; Margielewski and Urban 2003; Bella 2011). Margielewski and Urban (2003) consider the crevices to be free space between two rock blocks when at least one of them is affected by slope movement. Most commonly, crevice-type caves accompany the evolution of deep-seated gravitational slope deformations (DSGSDs), i.e. types of large-scale mass movements affecting large volumes of rock masses (Němčok 1972; Dramis and Sorriso-Valvo 1994), generally some tens of meters-deep (e.g. Hutchinson 1988: at least 30 m). The mass movements are mostly slow or extremely slow with an average velocity lower than 18 mm per year, but in their catastrophic stage they can reach very high speed (Varnes 1978). However, besides DSGSDs, the crevice-type caves can also be produced within the shallow and medium-deep (<30 m according to Hutchinson 1988) structurally-predisposed landslides (Margielewski 2009). Table 1 specifies the preparatory factors of landslide progression.

The crevice-type caves of equal genesis may occur in distinct types of rocks. The crevices very often open into incoherent sedimentary flysch deposits such as sandstones and conglomerates with intercalations of shales. However, they can be observed also in granites, quartzites, gneiss and other lithologies (Vítek 1978). Crevices originate also in carbonate rocks (limestones and dolomites). Typically, crevices and crevice-type caves occur within the areas built by anisotropic rigid rocks underlain by plastic shales (Pánek et al. 2009b, 2010).

Tab. 1 Preparatory factors of the opening of crevices within the landslide progression

Preparatory factors of opening of crevices within the landslide progression	
long-term	**lithological conditions** – Baroň et al. (2003b, 2004); Bubík et al. (2004); Margielewski (2004); Rybář et al. (2006); Margielewski et al. (2007)
	Tectonics – Pánek and Duras (2002); Pánek et al. (2007); Margielewski et al. (2007); Rybář et al. (2006 a 2008)
	denudation ratio and slope relaxation caused by incision of rivers – Margielewski et al. (2007); Rybář et al. (2008)
	macroclimate – Margielewski (2006b)
short-term	**seismic activity*** – Martino and Mugnozza (2005); Bozzano et al. (2011); Klimeš et al. (2012)
	heavy downpours* – Krejčí et al. (2002); Pánek et al. (2011b)
	groundwater content – Baroň and Kašperáková (2006); Medveďová et al. (2008)
	water from snow melting flushes* – Krejčí et al. (2004)
* also triggering factors	

This paper presents close connection between the evolution of gravitational slope deformations and crevice-type caves on an example of the flysch Carpathians. In summary, this work:

(1) provides a review of the genesis of crevice-type caves as an important geomorphic element within gravitationally disrupted slopes of the Carpathians;

originated in soluble or insoluble rocks (including karst) by the influence of gravitationally or tectonically induced widening of fissures (Panoš 2001). The term *rock-slide cave* is closest to the perception of a typical crevice-type cave evolved in the area of the Carpathians (Panoš 2001). Different terminology concerning crevice-type caves is displayed in Table 2.

Tab. 2 Different terminology concerning crevice-type caves

crevice-type cave	Margielewski and Urban (2003); Klassek (2004); Margielewski et al. (2007); Pánek et al. (2007)
joint cave	Wagner et al. (1990)
fissure cave	Kunský (1957); Kirchner and Krejčí (2002); Krejčí et al. (2012)
gull fissure cave	Bella (2011)
cleft cave	Panoš (2001); Pokorný and Holec (2009)
cambering cave	Bella (2011)
crevasse cave	Bella (1998); Baroň et al. (2003a); Petro et al. (2011)
landslide cave	Bella (2011)

(2) presents a contemporary view on the regional distribution of crevice-type caves in the flysch Carpathians of Czechia, Poland and Slovakia; and

(3) outlines recent progress and future possibilities and directions in the investigation of this phenomenon.

The terms of movements used in this paper agree with the classification of mass movements by Cruden and Varnes (1996).

2. Crevice-type caves – central topic of pseudokarst phenomena

The term 'pseudokarst' has recently been used to refer to forms resembling karst morphology, but primarily produced by a process other than dissolution (Halliday 2007). A pseudokarst cave is any cave that only originated in insoluble rocks by mechanical forces (Panoš 2001). Pseudokarst caves are then distinguished as fissure caves, cave niches, bedding-type caves, crevice-type caves, talus-type caves and combined-type caves. Crevice pseudokarst is one of eight types of pseudokarsts established in 1997 by the working session within 12th International Congress of Speleology (Kempe and Halliday 1997).

Crevice-type caves originate by the gravitational movement of tectonically or lithologically predisposed rock masses (Panoš 2001). These caves are mostly regularly narrow-shaped ('A' and 'V' or 'H' letter in cross-section) with high walls and flat ceilings or floors. The corridors may reach significant lengths: tens or hundreds of meters (Vítek 1978, 1981; Wagner et al. 1990). Within the crevice-type cave evolution, other processes such as water erosion, frost weathering, rockfall or seasonal temperature change might play an important role (Vítek 1981; Margielewski et al. 2007; Klimeš et al. 2012). Under such circumstances, the crevice-type cave is any cave that

3. Crevice-type caves in the flysch Carpathians

The flysch Carpathians are predominantly formed by Mesozoic and Palaeogene sediments which were folded during the lower and middle Miocene alpine orogeny phases (Menčík et al. 1983; Żytko et al. 1989; Lexa et al. 2000; Krejčí et al. 2004). The described mountain range is situated in the territory of the Czech Republic, Slovakia and Poland (Figure 1). Most of the crevice-type caves are situated in the area of the Outer Carpathians, but there are some localities, which pertains to the Inner Carpathians (Figure 1). The flysch rocks consist of thick-bedded sandstones or conglomerates with mica, glauconitic and calcific admixture and thin-bedded intercalations of shales (mudstones, siltstones) with a predominant content of illite and kaolinite clay minerals (Menčík et al. 1983; Eliáš 2000; Margielewski and Urban 2003; Pánek et al. 2011a; Petro et al. 2011). Ridges often have a character of monoclinal ridges and cuestas (Menčík et al. 1983), especially within the Silesian Unit (e.g. Moravskoslezské Beskydy Mts, Beskid Sląski Mts) characterised by steep northern slopes and gentle, long southern slopes predisposed by bedding planes (Krejčí et al. 2004). The flysch massif is strongly disrupted by joints and faults trending in the E-W, N-S, NW-SE and NE-SW directions (Menčík et al. 1983; Krejčí et al. 2002; Bubík et al. 2004; Petro et al. 2011) and WNW-ESE direction (Menčík et al. 1983; Pánek and Duras 2002). In terms of the strike characteristics of the beds, these joints and faults are classified as L (longitudinal), T (transversal) and D1 + D2 (two diagonal systems) (Mastella et al. 1997).

Slope deformations are common features in the flysch Carpathians (Kirchner and Krejčí 2002; Baroň et al. 2004; Margielewski 2006b, 2009; Rybář et al. 2008; Petro et al. 2011). The susceptibility of this region to

mass movements is given by (i) overall disequilibrium of flysch nappes that are not in balance with the underlying basement consisting of soft Neogene deposits (Krejčí et al. 2004), (ii) strong anisotropy of flysch rocks creating conditions for the evolution of slip surfaces (Margielewski 2006b) and (iii) high precipitation that (also due to summer heavy downpours and rapid snow melt at the end of winter) generate high pore pressures within the rock mass (Pánek et al. 2011b). Typical slope movements are represented by deep-seated gravitational slope deformations and structurally-induced landslides, very often accompanied by crevice-type rock-slide caves (Margielewski 2009). These caves, which were already known during the Wallachian colonization in 16–17th century (Četyna 1966), have systematically been mapped since the mid-20th century. As many as 23 caves were described in the Polish Carpathians in 1954 (Klassek 2004). The centre of exploration in this region was situated in the Beskid Śląski Mts where the first group of cavers was established. At the same time, the first cave in the Czech

Carpathians was described in 1953 (Tučník 1953). The Czech group of cavers was established in 1969 (Wagner et al. 1990). In Slovakia, the main research started in the 1990s (Bella et al. 2004). The longest and deepest caves have been detected and explored quite recently. It is for example The Wiślańska cave (explored in 2003; Szura 2009) and Miecharska cave in Poland (explored in 2004; Szura 2006) and The Pod Spišskou cave in Slovakia (explored in 2004, Majerníčková et al. 2005). In the Czech Republic, the largest caves were mapped by Foldyna and Pavlica (Foldyna 1968; Foldyna and Pavlica 1968) and by Wagner et al. (1990). The distribution of the caves is shown in Figure 1. Table 3 summarises the most remarkable caves of surveyed Carpathian flysch. The overall number of crevice-type caves in the area of the flysch Carpathians (Poland, Czechia and Slovakia) is higher than 1520 caves: 1350 caves in Poland (Klassek 2004; Ganszer 2012); 120 caves in Czechia (Wagner et al. 1990; Baroň 2001; Hromas et al. 2009); and 50 caves in Slovakia (Bella et al. 2004; Majerníčková et al. 2005).

Tab. 3 The largest crevice-type caves of the flysch Carpathians in Czechia, Poland and Slovakia

cave	l [m]	d [m]	country	source
Wiślańska	2 275	41	Poland	Ganszer (2012)
Miecharska	1 838	55.8	Poland	Ganszer (2012)
W Trzech Kopcach	1 244	32.6	Poland	Ganszer (2012)
Ostra – Rolling Stones	855.5	60*	Poland	Ganszer (2012)
Pod Spišskou	740	25	Slovakia	Majerníčková et al. (2005)
Drwali – Słowiańska	601	23.8	Poland	Ganszer (2012)
Dująca	582	18	Poland	Ganszer (2012)
Głęboka w Stołowie	554	25	Poland	Ganszer (2012)
Cyrilka	520	16	Czechia	Lenart and Wagner (2012)
Kněhyňská *	280	57.5	Czechia	Wagner et al. (1990)
l – length; d – denivelation; * – the biggest denivelation				

Fig. 1 The approximate distribution of crevice-type caves in the Carpathian flysch of Czechia, Poland and Slovakia – black dots: caves; for 1–10 see Table 3.

4. Evolution and morphology of crevice-type caves

4.1 The origin of crevices in the flysch Carpathians – historical overview

The research of gravitational slope deformations and crevice-type caves has been interconnected in the last ten years (e.g. the case studies of Baroň et al. 2003a; Margielewski and Urban 2003; Pánek et al. 2007, 2010; Klimeš et al. 2012). Thanks to open crevices, we have a unique chance to study the internal structure of landslide bodies from within and to perform a more detailed analysis of slope deformations (Margielewski and Urban 2003; Baroň et al. 2004; Margielewski 2006b). The evolution of slope deformations and occurrence of crevices in anisotropic rock massifs is predisposed by tectonic and lithological discontinuities (e.g. shear fractures, faults, joints, fissures, schistosity and bedding planes; Kirchner and Krejčí 2002; Di Luzio et al. 2004; Margielewski 2006b; Brideau et al. 2009; Jaboyedoff et al. 2009) and driven by various gravitational mechanisms like lateral spreading, toppling, sagging (*sackung*), rotational and translational sliding, and/or composite movement (e.g. Kleczkowski 1955; Němčok et. al. 1972; Varnes 1978; Hutchinson 1988; EPOCH 1993; Cruden and Varnes 1996). Crevice-type caves usually indicate the initial forms of the evolution of gravitational slope deformations (Margielewski and Urban 2003; Margielewski et al. 2007; Margielewski 2009).

First researchers dealing with crevice-types caves in the flysch Carpathians attributed their genesis to the joined effect of Pleistocene periglacial climate and mass movements within tectonically jointed rock mass (Novosad 1956, 1966; Foldyna 1968; Foldyna and Pavlica 1968; Wagner et al. 1990). In spite of the fact that Novosad (1956, 1966) attributed the origin of crevice-type caves to mass movements, he stressed the role of periglacial frost weathering during the Pleistocene cold stages. At the turn of a new millennium, there was a significant progress in the ideas concerning both genesis and age of crevice-type caves (e.g. Margielewski and Urban 2000; Baroň et al. 2003a). In accordance with recent observations, the age of crevice-type caves in the flysch Carpathians is placed especially to the humid periods of the Quaternary, including the Holocene (Margielewski 2003, 2006a; Margielewski et al., 2010; Pánek et al. 2011a, 2011b).

During the evolution of landslides along sliding surfaces, the crevices open and the caves are formed (Margielewski 2004). Within a more advanced stage of the progression of slope deformations, the cave begins to be more unstable in connection with fallen rocks, collapses and sediments fillings. According to Margielewski and Urban (2003) and Margielewski et al. (2007), crevice-type caves are generally extensional (dilation-related) fissures developed in the upper part of slope deformations as initial forms of other landslide headscarps.

Some crevice-type caves evolve by the process of fissure macro-dilatancy (Reynolds 1985; Kwaśniewski 1986) that is accompanied by abnormal growth of rock volume during the deformation (Margielewski et al. 2007) and that precedes the evolution of sliding surface (Margielewski 2009). However, recent observations have revealed that crevice-type caves do not only develop as initial fissures. Baroň (2000) distinguishes the initial cave stage above or right within the landslide headscarp where narrow but high crevices are still in the opening phase; the mature cave stage with wider passages and gradually collapsing roofs and the senile stage characterised by the cave system downfall due to rock collapse (Figure 2), but this distinction seems to be rather subjective than scientific. Sometimes the opened crevice is consequently narrowing because of secondary movement of blocks (Foldyna 1968; Wagner et al. 1990; Baroň et al. 2003a). In the light of hitherto investigation, crevice-type caves play a role as primary fissures of incipient landslides (e.g. Jaskinia Malinowska cave, Margielewski and Urban 2003), as a secondary opening fissures within the landslide body (initiation of secondary gravitational movement; e.g. Jaskinia Dolny Waserszlog cave, Pánek et al. 2010) or subsequently narrowing fissures within the landslide body (e.g. Zbojnická cave, Baroň 2001).
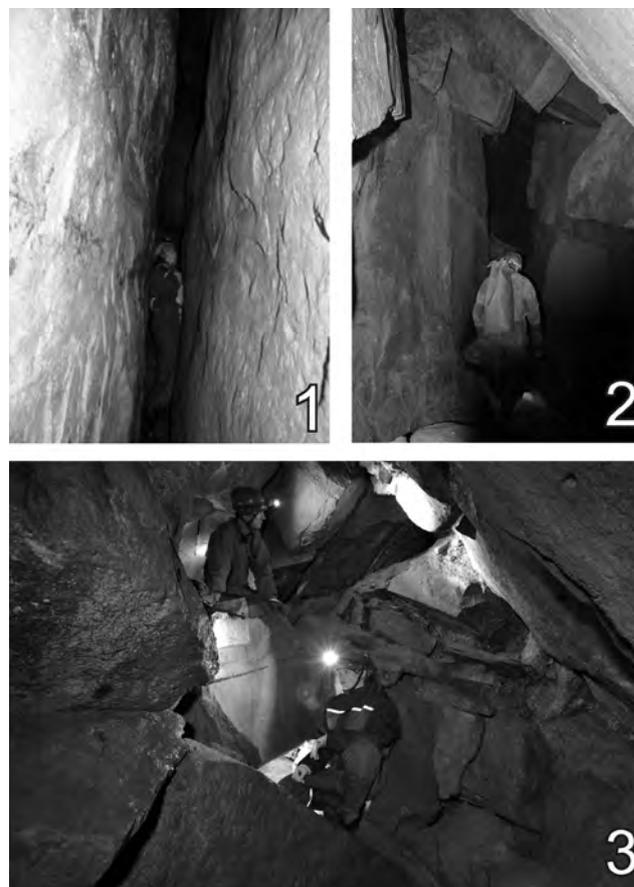

Fig. 2 Stages of cave evolution.

4.2 Basic morphological types and models of the evolution of crevice-type caves

According to recent observations and investigation of crevices, these are frequently present in the internal structure of slope deformations, but only rarely accessible by man. The main crevices are usually narrow but high and narrowing to the bottom or to the top. In some cases the wall face is curved, which is described by the long-term extensional-compressional incidence of tectonic stress (Jaroszewski 1972). With the continuous deformation of the upper part (toppling, lateral spreading and translational slide) the flat ceiling collapses and drops into the opened structure, whereas the rigid beds or boulders form the resulting shape of the ceiling (Margielewski and Urban 2000). According to the vertical distribution of different morphological zones, there are two basic models presented.

(i) Model of translationally, spreading or toppling-induced crevice-type cave:

The simple cross-section of the cave can be presented by an elementary model of the vertical cave (Figure 3) which consists of several levels (Wagner et al. 1990; Margielewski and Urban 2004). First, there is the upper zone of collapsed boulders and debris with small space between them. This zone, which is usually reflected by surface features (sinkholes, trenches), originates from trench walls and overhanging bed collapse. Upslope and downslope walls of crevices are very often disturbed by joints. In such context, main corridors of caves are disturbed joints widened by slope movements. The upper corridors of caves are usually more fissured because of the long-term relaxation of rock massif (Margielewski and Urban 2004). The second layer is described as a zone of wide chambers. This is a rather fissured and relaxed part of massif with longitudinal (L), transversal (T) and diagonal (D_1 and D_2) cracks (terminology after Mastella et al. 1997). The third layer (intermediate zone) is formed by sub-vertical pits with a depth about several meters, connected together by narrowings, filled by boulders and debris. This is followed by the fourth zone which is represented by one narrow crevice described as a tension crack of the landslide (Margielewski and Urban 2004). This is the case of crevice formed by lateral spreading and translational sliding. In the case of toppling process, the crevice narrows to the top and the ceiling is often cluttered with boulders. The fifth (lowermost) vertical layer can be observed in some vertical caves. It is recognizable by narrow crevices, very often differing in their direction from the initial fissure (e.g. Margielewski and Urban 2004). In some specific cases some of the levels are missing or there is a combination of the same type of zones in the caves with a complicated composition (e.g. Wagner et al. 1990).
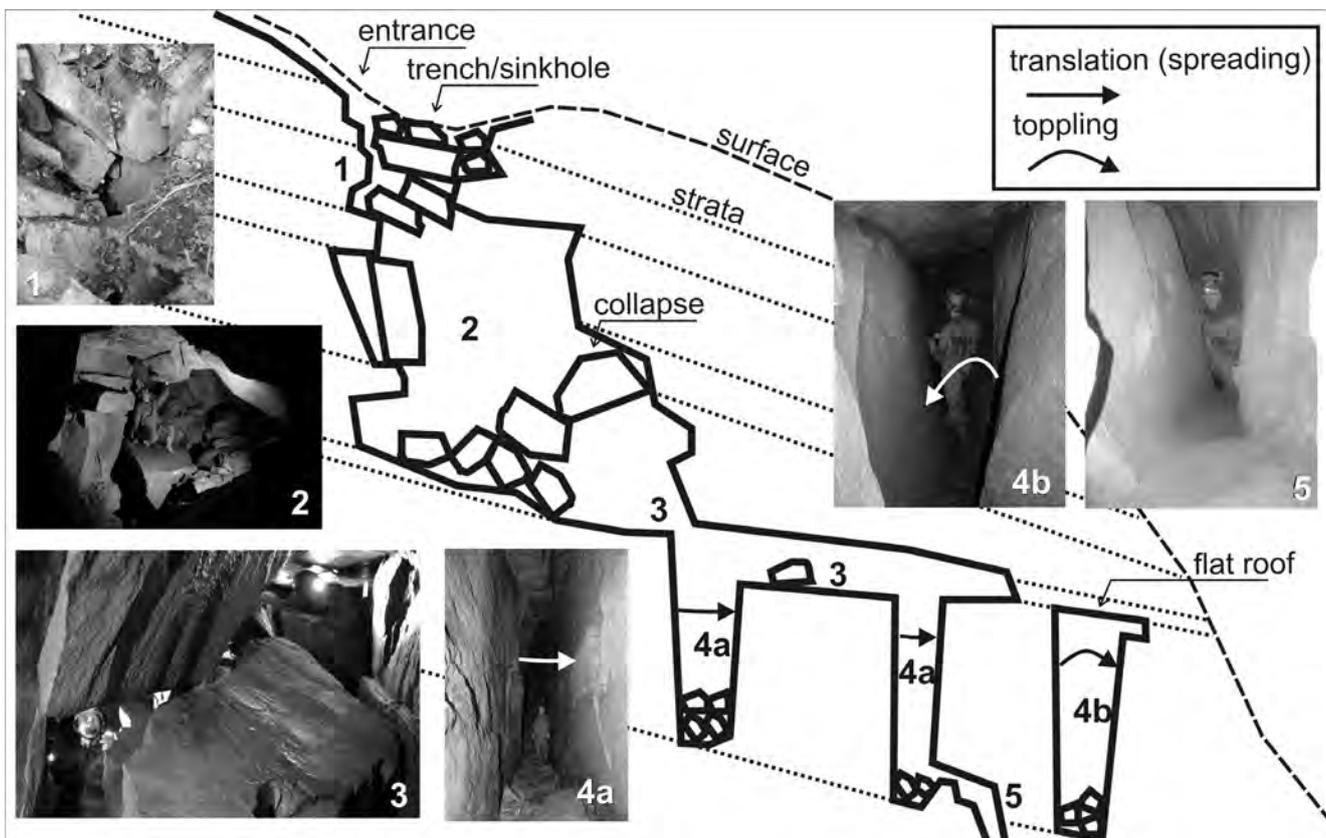

Fig. 3 Model of translationally, spreading, or toppling-induced crevice-type cave – 1: zone of collapsed boulders and debris (the Marná cave, photo: O. Lenart); 2: zone of wide chambers (The Kněhyňská cave, photo: J. Wagner); 3: intermediate zone (The Kněhyňská cave, photo: J. Lenart); 4a: zone of narrow crevices (The Miecharska cave, photo: J. Wagner); 4b: zone of narrow crevices with flat roofs (The Cyrilka cave, photo: O. Lenart); 5: the lowermost vertical layer terminated by narrowing (The Naděje cave, photo: V. Škarpich)

(ii) Model of a rotationally induced crevice-type cave

With the continuous movement of the lower part of crevice (in case of rotational slides), the ordering of vertical zones is different. The ceiling of the cave is narrowing and the bottom is widened and filled with sediments and debris (Figure 4). Sometimes the lower fragments of walls are collapsing. In the first stage of cave, there are often no surface manifestations of deformations and the terrain is flat. This is because the opening of crevices begins from the massif interior and progresses upwards (e.g. Margielewski and Urban 2000).

Due to the frequent subhorizontal bedding of flysch massif (the case e.g. of Silesian Unit in the Outer Western Carpathians), all the types of caves can be combined and blended together. For instance, the zone of rotational-type of crevice-type caves (the zone of debris, boulders and sediment) is followed downwards by the zone of translational-type of crevice-type caves (the zone of wide chambers) within the complex slide. These basic models are complicated by the subsidence of huge rock blocks (10^2–10^3 m³) in the case of very deep and wide extension of flysch massif. Such vertical zones were distinguished in the Diabla Dziura cave (Rożnów Foothill, Poland) by Margielewski and Urban (2004) and in the Velká Ondrášova jeskyně cave (Moravskoslezské Beskydy Mts, CR) by Kotouč (2011). The upper zone of such caves is highly fissured by the relaxation of rock massif. This zone is followed by the intermediate and lower zones which are created only by a single tension cracks. Finally, there is the lowermost zone of fissures which often differs in the direction contrary to the rest of the cave. Both the presented types of models and their modifications create a typical vertical morphological zonation of crevice-type caves occurring in the area of the flysch Carpathians.
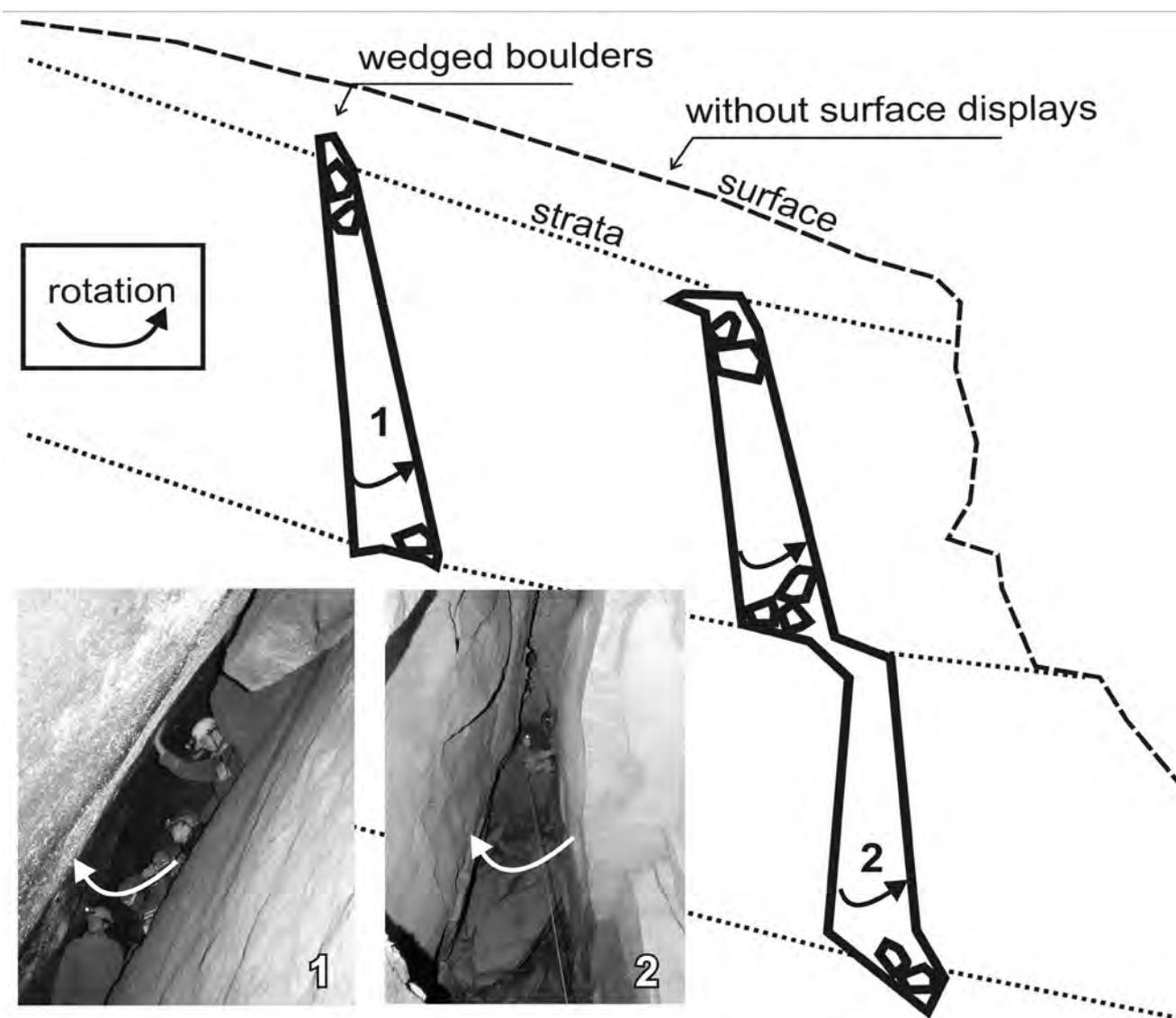
Fig. 4 Model of rotationally induced crevice-type cave – 1: crevice narrowing to the top, with wedged boulders (the Velryba cave, photo J. Lenart); 2: high narrowing crevice (the Kněhyňská cave – the Big Abyss, photo J. Wagner).

4.3 Morphological features and structures within the caves

There are three main types of corridor shapes formed by distinct gravitational movement of flysch massif: (i) 'V-letter-shaped' corridors, where the upper part of crevice is significantly wider than the lower part, (ii) 'A-letter-shaped' crevices, where the ceiling is significantly narrower than the bottom and (iii) 'H-letter-shaped' forms with no difference in the width between the lower and the upper parts of crevice. The first type indicates toppling, the second rotational slides and the third lateral spreading and incipient translational sliding (Margielewski and Urban 2003). Using this approach, there is a problem with large subsided and fissured rock blocks which can indicate a type of movement erroneously. This mistake can partially be eliminated by observing and correlating bedding planes which can usually be detected in the conditions of flysch rocks very well (Figure 3-1, 2, 3 and Figure 5-d, f). Subtle morphology of cave corridors is shaped by water erosion caused by episodic inflows (Urban 2005).

As for the vertical caves, each horizon (cave level detached according to thickness of sandstone/conglomerate beds) is usually shifted staircase (Figure 3 and 4). The elevation of bedding planes, sedimentary intercalations or boundaries in sedimentary sequences between
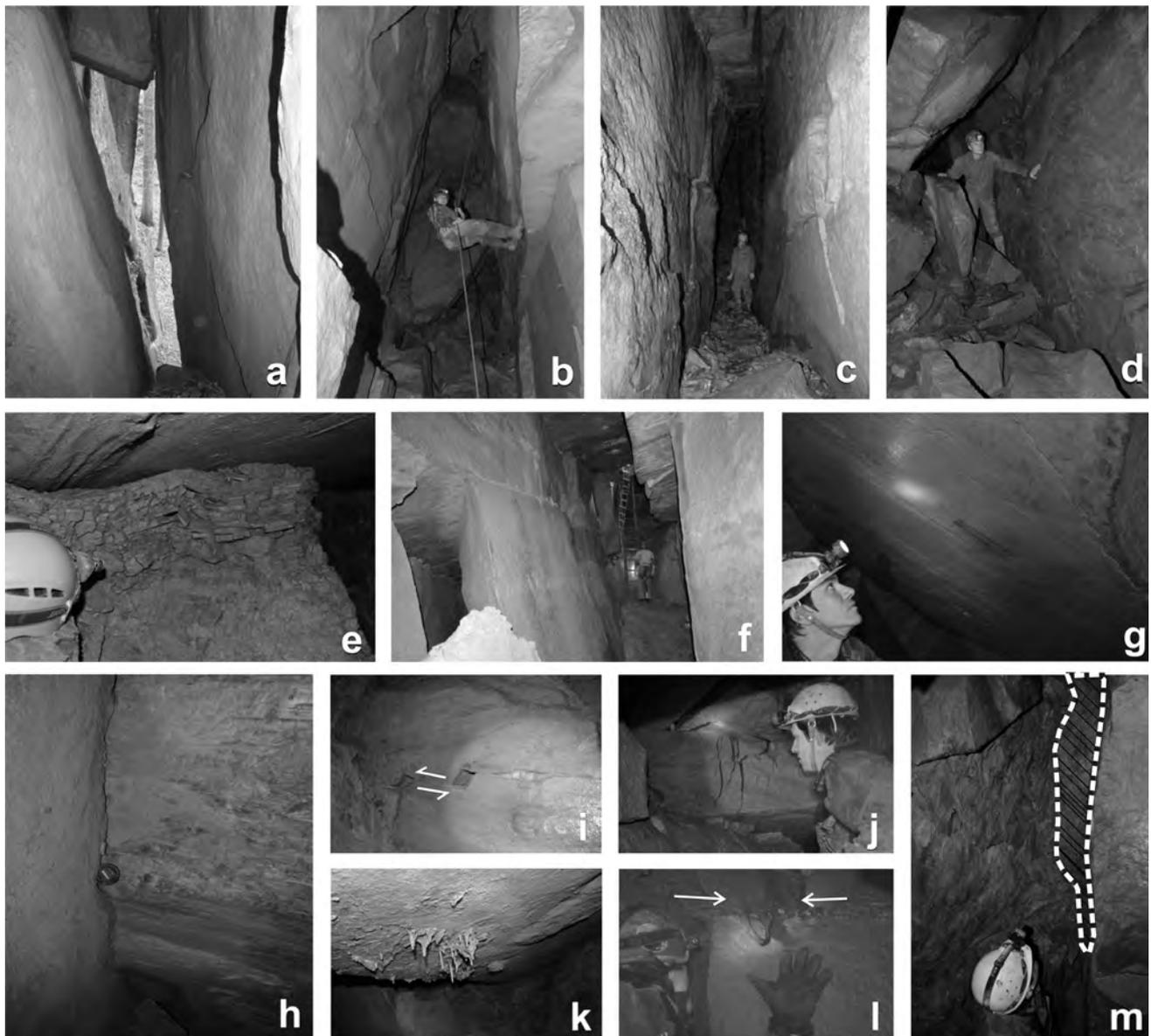
Fig. 5 Morphological features and structures within the caves – a: V-letter-shaped corridor (the Velryba cave); b: A-letter-shaped corridor (the Kněhyňská cave); c: H-letter-shaped corridor (the Miecharska cave); d: corridor filled with fallen blocks (the Kněhyňská cave); e: strata of shales folded by the movement of sandstone block (the Pod Spišskou cave); f: corridor created by interbedded movement of blocks (the Pod Spišskou cave); g: striations on lower surface (the Wiślańska cave); h: slickensided surface with secondarily produced minerals (the Čertova díra cave); i: disrupted walls with the signs of strike-slip movement (the Pod Spišskou cave); j: stressed material of sandstone block (the Wiślańska cave); k: small stalactites (the Pod Spišskou cave); l: compressed root within a narrowing crack (the Salajka cave); m: zones of tectonic breccia within the fault zone (the Kněhyňská cave); photo: a, e–m: J. Lenart; b–d: J. Wagner.
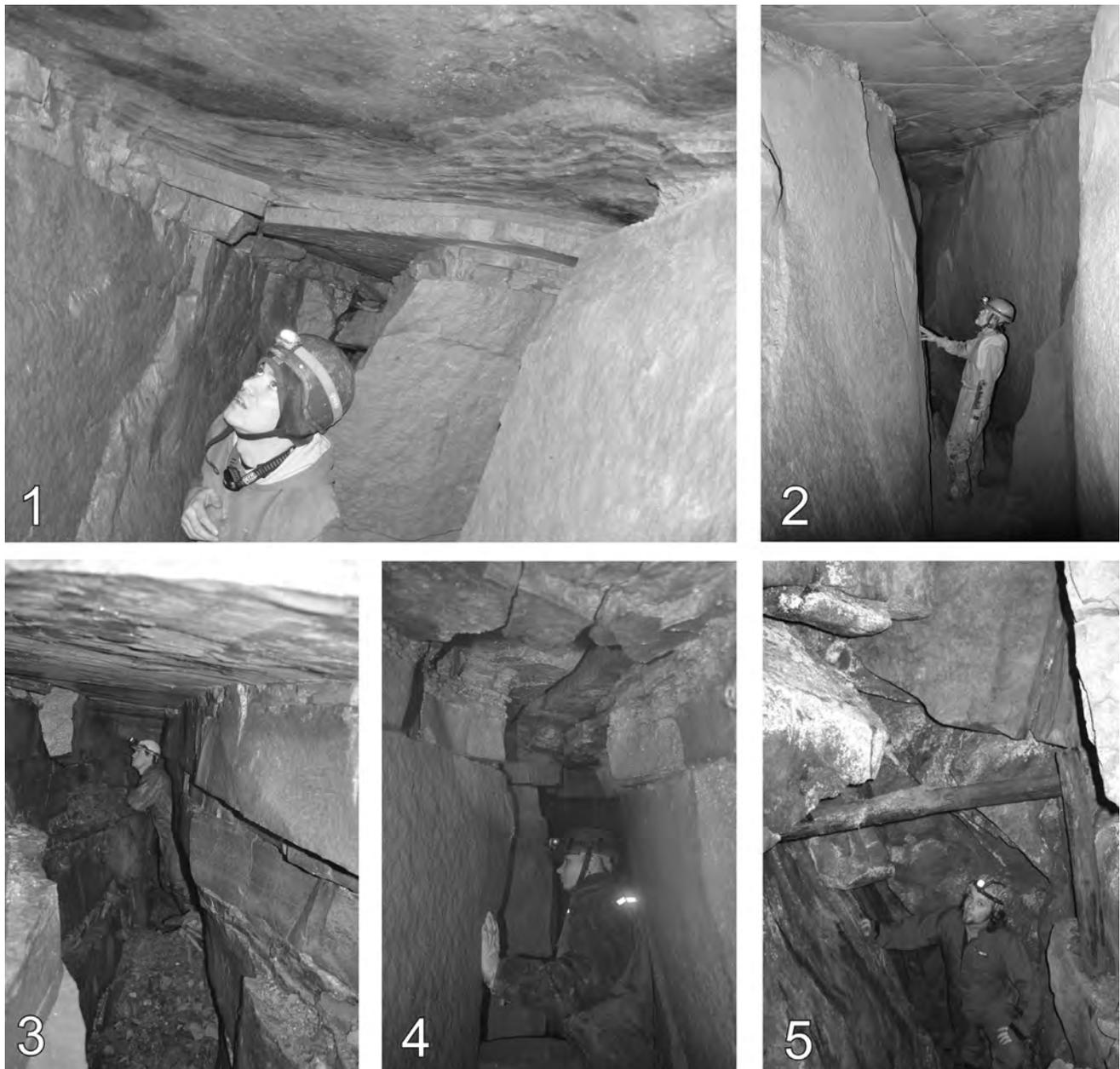
Fig. 6 Different types of ceilings within the crevices – 1: flat ceiling with the strata of shales (the Cyrilka cave, photo J. Lenart); 2: flat sandstone ceiling (the Pod Spišskou cave, photo J. Lenart); 3: flat sandstone ceiling (the Čertova díra cave, photo J. Lenart); 4: partly collapsed and fissured ceiling (the Salajka cave, photo J. Lenart); 5: ceiling created by wedged boulders (the Pod Úplazem cave, photo J. Wagner).

two opposite walls sometimes significantly change along the crevice. These are signs of vertical displacement or rotational movements (Margielewski and Urban 2003). A typical feature of horizontally established caves is a creep (translation) between sandstone/conglomerate beds. During this process, regularly shaped rooms with flat roofs are created by the movement of blocks along the bedding planes (Figure 6-1, 2, 3). In the case of advanced and combined stage of cave evolution, there could be 'corridor-like' areas created between fallen, tilted and cracked rock blocks and boulders (Figure 6-4, 5). Extensive rooms, horizons and corridors are typically connected with each other only by narrow and small crawl spaces (Figure 3-3, 5).

Generally, we can distinguish several microforms and structures commonly occurring in the crevice-type caves (Figure 5). They include (i) forms and structures related to tectonic and gravitational movements within the rock mass, (ii) forms and structures related to fluvial activity, (iii) speleothems and other secondary cave infill and (iv) forms related to biogenic activity.

(i) Faults and fault zones represent shearing planes originated by tectonic deformations. Cave systems are very often laterally limited by them, or the fault zones cross the cave. There are zones of mylonites and tectonic breccia occurring sporadically at the margins of the caves where the fault zone enters the massif (Figure 5-m). The direction of tectonic

pressure is expressed by the presence of striations and slickensides, tectoglyphs with ribs, hackle marks and Riedel shears (Davis et al. 1999; Katz et al. 2004; Margielewski et al. 2007). Locally, the whole walls of cave chambers are covered by these features, sometimes with more than one generation of striations (Figure 5-g, h). The direction of striations is often sub-horizontal (on cave walls) or there is a concordant direction of striations with the dip of strata (these are visible on cave ceilings). Faults pass to main corridors and crevices almost perpendicularly. Gravitationally induced movement can trigger the detachment of huge regularly-shaped boulders by pressure incidence on rock wall. While the boulders wedge into the widened crevice, small sub-vertical striations can occur on the walls, what indicates the widening of corridor. The displacement of sedimentary layers and intercalations, striations and other markers can be detectable along fractures analogously to fresh breaks affecting speleothems in karst caves (Jurková and Briestenský 2008). Within the tectonic jointing and gravitational sliding and rotating of blocks, there can also be two types of folding of shales (Figure 5-e): a) folding induced by the pressure of sliding blocks as a reduced form of compression folds (Baroň et al. 2006; Margielewski et al. 2007; Margielewski et al. 2008); b) folding induced by the subsidence of strata into the crevice. Margielewski (2004) reconstructed the rotational character of slope deformation based on the observation of gravitationally induced folds within the Muronka Mt. cave (Beskid Śląski Mts).

(ii) The forms and structures related to fluvial activity are represented by small shallow pools in many caves (proportions usually $< 100 \times 100$ cm) filled with sand or mud (Kotouč 2011; Lenart and Wagner 2012). Underground spring water can create gutters, whereas egutation pits are often created in mud and sand. In some specific cases systems of subterranean drainage evolve with underground fluxes of water and sediments along sliding surfaces (Margielewski et al. 2007).

(iii) Secondary speleothems are sometimes represented in crevice-type caves (Figure 5-k.; e.g. Bosák 2003; Cílek et al. 2003; Majerníčková et al. 2005; Urban et al. 2007a; Bruthans et al. 2009; Lenart and Wagner 2012). The composition of cement within flysch rocks is highly variable – from pure siliceous to calcareous ($CaCO_3$ around 18%) (Urban et al. 2007a). Fruticose sinters of this origin were also mentioned by Demek (1963). Having discovered the same sinters, Cílek et al. (2003) supposed their origin in calcific soils of the early and middle Holocene period and considered them senile now. Out of the crevice-type caves of Polish Carpathians, Urban et al. (2007a) mentioned 7 types of secondary speleothems according to the terminology proposed by Hill and Forti (1997): (1) small (less than 10 cm long) stalactites with a thinly-laminated external part and a soft amorphous internal part with organic matter, (2) crenulated flowstones, (3) moonmilk, (4) crusts, (5) coatings, (6) crystals and (7) helictites. Besides precipitated speleothems, corridors are filled with rock debris, gravel, sand or clay (Wagner et al. 1990). In some microclimatically anomalous and periodically iced caves there are large sand accumulations caused by frost weathering and erosion due to water frozen in the cave (Lenart 2011). Entrance parts of caves (in some specific cases also the deeper parts) very often contain accumulations of organic material (leaves, wood, bones, and guano) (Wagner et al. 1990).

(iv) Biogenic indicators of movements occur in the caves only rarely. For example, the roots of trees which get into the cave are U-letter-shaped by the pressure of blocks in a narrowing crack (Figure 5-l). By contrast, the roots tensed between two opposite walls indicate the widening of crack.

5. Recent progress in crevice-type caves investigation in the light of new geochronological, monitoring and prospecting methods

5.1 Chronology of crevices

Last decades have been characterized by rapid development of geochronological techniques (Walker 2005). Suitable materials used for the determination of minimum ages of crevice-type caves are secondary speleothems originating especially within sandstones and conglomerates containing calcareous cement (e.g. Middle Godula beds, Eliáš 2000). The ages were stated for small stalactites from the crevice-type caves in the Polish Carpathians using radiocarbon and U/Th-series dating (Urban et al. 2007a, 2007b; Margielewski et al. 2012). These ages correspond with the Late Glacial and humid Holocene phases: Preboreal-Boreal transition, Atlantic, Early Subboreal and Subboreal-Subatlantic transition (Starkel 1977; Margielewski 2003, 2006a; Margielewski et al. 2010; Pánek et al. 2011a, 2011b). The dating of speleothems within pseudokarst caves is also underway in other regions. Bruthans et al. (2009) analyzed the calcite sinters of sandstone caves in the Bohemian paradise (Bohemian Massif, Czech Republic) using ^{14}C and/or U/Th dating methods. Sanjurjo-Sánchez and Vidal Romaní (2011) dated two opal-A speleothem samples taken from the NW Spain granites. The results of the TL and OSL dating show their Upper Pleistocene and Holocene age. All these methods supplement ordinary dating methods of mass movements (e.g. Lang et al. 1999) and make crevice-type caves potentially important elements for relative dating and minimal age estimation within the landslide bodies.

There are some possibilities of how to estimate the relative age of crevices. Examples from the Outer Western Carpathians show a relation between the lithology and secondary features occurring within the crevices. The walls of crevices are composed of turbidites of thick-bedded sandstones, conglomerates and thin-bedded shales exposed to water erosion (e.g. Bruthans et al. 2012). Fresh (erosive) or fossil (sometimes secondarily mantled by mineral covers) character of opened crevices is also an indirect indicator of cave (landslide) age. Margielewski and Urban (2004) supposed several generations of crevices according to the occurrence of mineral crusts on walls. Bruthans et al. (2009) used cave walls covered by sinter to observe the erosional rate of rock surface.

5.2 Recent movements and forms

Recent movements forming crevice-type caves are evidenced by (i) glass indicator cracking, (ii) measuring movements by optical-mechanical crack gauges, (iii) dilatometry measuring and (iv) direct observations of fallen boulders, collapses or slumps. A very simple, yet inaccurate technique of how to identify recent movements of rock massif and boulders in caves is by placing glass indicators on sites where the movement of blocks and boulders is expected (Figure 7; Wagner et al. 1990). Since 1978 many of these indicators have been installed into the caves of the Czech Outer Western Carpathians and they are presently cracked or destroyed by the movement of rocks and subsidence of blocks and boulders. In some cases the crack in the broken glass is in the orders of a few centimetres (e.g. the Kněhyňská jeskyně cave). This is an actual proof of recent gravitational movements, but it is often an example only of secondary movements within the cave. Long-term investigation of slow gravitational and tectonical movements is provided with the use of the optical-mechanical crack gauge TM-71 (Stemberk and Jánoš 2002; Stemberk et al. 2008; Petro et al. 2011; Klimeš et al. 2012). In this sense, the movements are detected in three axes (crack dilation, horizontal shear

Fig. 7 Glass indicator installed in the Cyrilka cave; photo: M. Řezák.

displacement, and vertical displacement) and two types of rotation (Klimeš et al. 2012). This method is also suitable to measure the activity of recent faults (Briestenský and Stemberk 2008). Klimeš et al. (2012) distinguished gravitationally and tectonically induced movement with seasonal fluctuations in the Cyrilka cave (Moravskoslezské Beskydy Mts, Czech Repuiblic) following the results of crack gauge measurement. Baroň et al. (2003a) used the methods of dilatometry – direct measuring of distances between cave walls. He detected seasonal fluctuations of movements depending on sudden precipitation following a dry period. He also measured the subsidence of rock blocks wedged in crevasses.

Recent movements within crevice-type caves can be summarized in three groups (according to the type of movement): (i) movements induced by landslide, (ii) seasonal movements and (iii) secondary movements of blocks and boulders. The gravitational movement determines the main trend of movements – their direction and velocity. The proper movement for crevice-type cave creation is very slow (creep) and the crevices are formed perpendicular to the movement direction (Baroň et al. 2003a; Margielewski and Urban 2003). Seasonal movements measured within the massif are caused by the volumetric change of rocks which are partly elastic. These cyclically fluctuating movements become evident as narrowing and widening of crevices. The rate of movements depends on the season (annual temperature dilations) and water content in rocks (Klimeš et al. 2012) and decreases with depth (Briestenský et al. 2010). The main gravitationally induced movement and seasonal elastic movement are accompanied by secondary movements of relaxed blocks, boulders and sediments. These collapses are triggered by the slow movement of landslide body and by seasonal changes in the volume of rocks (Wagner et al. 1990).

5.3 Detection of crevices

Recent progress in the exploration of new crevice-type caves in the flysch Carpathians is partly connected with the introduction of new prospecting methods (Lenart et al. 2011; Baroň et al. 2012). Underground crevices without (or with a small amount of) surface features can be detected by various techniques. These are especially: (i) microclimatic methods based on the temperature contrast and air flow measurement and (ii) geophysical sounding.

(i) Microclimatic methods

Every underground crevice cumulates warm air during summer (Hromas et al. 2009). In winter time this air rises up from the subsurface structures and melts the snow (Figure 8; Baroň et al. 2012). According to the occurrence of these places and their temperature, high resolution detection of caverns can be realized. The examples from the Outer Western Carpathians show that the largest cave systems have an average air temperature

around 7 °C (Wagner et al. 1990). Therefore, the temperature measured above the anticipated cave reveals the dimensions of subsurface structures (Baroň 2004). Since there is usually a debris layer overlapping and masking crevices, ascending warm air is the unique evidence of the occurrence of crevice-type caves and other relaxed zones within the bedrock. It can be demonstrated on the example of the Čertův Mlýn Mt. slope deformation (Moravskoslezské Beskydy Mts), where there is a string of melting spots running diagonally to the ridge outlines main gravitational morphostructures (e.g. scarps, trenches, and cracks) and a large extent of relaxed bedrock with potentially numerous crevice-type caves (Táborík 2007).

Dimensions of subsurface structures are also evidenced by the time necessary for the compensation of temperature between the surface and the cave interior (Lenart 2013). In the case of small caves, warm air gets exhausted during the winter, whereas in the case of large cave systems, warm air is usually never spent (Lenart 2013). There is also a difference between the places where the snow is only melted on debris and places where the warm air rises up by chimney-like effect actively – i.e. the case of blow holes (Baroň 2004). If a cave is accessible for man, the circulation of air can be surveyed within the cave system. The directions of air flow indicate the connections between the crevices and corridors and the lakes of cold air indicate the lowermost places of crevices or inflow of cold air from the outside through the fissures (Komárková et al. 2008; Hromas 2009; Lenart 2013). In the Outer Western Carpathians there are some localities, where underground crevices are characterised by strong outflow of cold air onto the surface (Lenart 2011). As for the future investigation of these phenomena, there is a great potential of thermography methods (Nakládal 2006; Baroň et al. 2012). Jian-Hong at al. (2005) and Tsung-Lin et al. (2009) used thermography for the location of weathered zones within concrete walls and for the estimation of the depth of fissures. Analogically, this method could be useful in the detection of subsurface crevices and their extent in natural conditions (Baroň et al. 2012).

(ii) Geophysical techniques

Air-filled voids and caverns represent major subsurface geophysical anomalies (Milsom 2005; Ezersky 2008; Pánek et al. 2010; Gambetta et al. 2011). In the last few years, near-surface geophysical methods (especially ground penetrating radar-GPR, electrical resistivity tomography-ERT, seismic refraction and

Fig. 8 Melting spot, NE slope of the Kněhyně Mt.; photo: P. Táborík.

microgravimetry) have become widely introduced into geomorphology (Schrott and Sass 2008). Recently there has been extensive geophysical investigation in crevice-type caves, especially in the context of the research of gravitational slope deformations (e.g. Baroň 2004; Pánek et al. 2010; Kotouč 2011). The most useful techniques seem to be ERT and GPR techniques (potentially, also microgravimetry), which are useful in the detection of the geometry of important subsurface structures connected with crevice-type caves such as sliding surfaces, relaxed zones, cavities, lithological boundaries, aquifers and faults (El-Qady et al. 2005; Hradecký at al. 2005; Pánek et al. 2010 and 2011a; Lenart et al. 2011).

Results of recent 2D and 3D ERT measurements in the sites of crevice-type cave show several challenges and limitations (Tábořík 2009). Future investigation and testing of ERT for the detection of crevice-type caves should be conducted using a combination of other methods – especially GPR and microgravimetry as recently usefully tested, for example, in karst terrains (e.g. Gambetta et al. 2011; Gómez-Ortiz and Martín-Crespo 2012).

6. Future challenges in the investigation of crevice-type caves

Many questions remain unanswered concerning the relationships between crevice-type caves and gravitational slope deformations. First, there is a problem of the absolute age of crevice-type forms and their relative age with respect to the succession of slope deformations. The question is, in which stage of slope deformation evolution the cave is established. Is it the early initial stage, as Margielewski and Urban (2003) suppose, or the advanced stage connected with the retrograde progression of an older landslide? Do crevice-type caves evolve just during the main (catastrophic) stage of landslide activity or during the creeping phase of the evolution of a slope failure (initial stage)? This could be revealed by the absolute dating of crevices (to date unrealizable). Very rewarding fact would be the information on relative tendencies of cave progression. Some of the caves evolve directly within the landslide body, some of them are established before the slope moved down rapidly and some of them originate above the landslide headscarp as a result of retrograde progression of slope deformation. Is there any rule stating which type of crevice will occur in a particular stage of slope failure evolution? The age of cave could be determined by investigation of the cave sediments (Hromas et al. 2009). In theory, there are two possible types of sediments to explore. Firstly, there are sediments containing both minerogenic and organic material washed down into the caves from the surface. In the location of a proper sedimentary profile we could use the method of biostratigraphy (Bosák 2003). Organic material would be dated directly by conventional and AMS radiocarbon methods (Bosák 2003). The second type of sediments is

chemogenic speleothems, which could be numerically dated by radiocarbon and/or U/Th-series techniques. In spite of the fact that the dating of secondary infill within crevice-type caves only reveals its minimum age (Bosák 2003; Urban et al. 2007a), it brings valuable information on the evolutionary stages of caves and their relation to the succession of slope failures. In the near future, we can expect the expansion of the database of dated speleothems from crevices in the flysch Carpathians bringing important data on the chronology of slope failures and correlation between the genesis of crevice-type caves and palaeoclimatological conditions.

There is also an important question related to the importance of karst processes during the evolution of crevice-type caves (Panoš 1963). Palaeogene sandstones and conglomerates susceptible to karstification are known from crevice-type caves in Slovakia and Poland (e.g. Urban et al. 2007a; Miháľ 2010). There are strong indicators of karstification of sandstones and conglomerates with calcium-rich cement within these crevices (Otvos 1976). Moreover, there is a possibility of coupling these processes with mechanical activity during slope movements. Could the dissolution of calcium-rich cement be one of the preparatory factors for sliding activity in non-karstic rocks? Experience from several world regions reveals that the dissolution of carbonate rocks decreases shear strength of rocks by reducing contact surfaces along bedding planes and other discontinuities (Chigira et al. 2012).

7. Conclusion

The research of gravitational slope deformations and crevice-type caves has become interconnected in the last ten years. Crevice-type caves in the flysch Carpathians of Czechia, Poland and Slovakia are formed by the propagation of both deep-seated and shallow, structurally predisposed gravitational slopes deformations. The crevice-type caves of the same genesis may occur in distinct types of rocks like incoherent sedimentary flysch rocks (sandstones and conglomerates with intercalations of shales), but examples from other settings reveal that they can also affect granites, quartzites, gneiss and other lithologies. Crevice-type caves are mostly regularly narrow-shaped ('A' and 'V' or 'H' letter in cross-section) with high walls and flat roofs or floors. Thanks to crevices, we can study the internal structure of the landslide body from the inside and make an analysis of slope deformations with more precise facts by means of speleological techniques. During the evolution of the slope movement along sliding surfaces the crevices open and caves are formed (i) as primary initial fissures of future landslides, (ii) as secondary opening fissures within the landslide body (initiation of secondary gravitational movement) or (iii) successively closing fissures within the landslide body. Based on the vertical distribution of different

morphological zones within caves, there are two basic modes of cave evolution- translation (spreading)- or toppling-induced crevice-type caves and rotationally-induced crevice-type caves. Hitherto dating of speleothems within crevice-type caves of the flysch Carpathians point to their genesis during the humid phases of the Late Glacial and the Holocene and their evolution continues during the present times. Actual movements in the caves detected by various monitoring techniques involve major gravitational downslope activity of landslides, seasonal, pulsation-type movements detected between the cave walls and secondary movements of blocks and boulders within cave passages and chambers.

Acknowledgements

REFERENCES

BAROŇ, I. (2000): Evolutionary relations between pseudokarst caves on Kopce hill near Lidečko. Speleo 32, 32–35. (in Czech)

BAROŇ, I. (2001): Pseudokarst caves. In: Pavelka, J., Trezner, J. (eds.): The Nature of Wallachia (The Vsetín district). Vsetín, ČSOP, 45–49. (in Czech)

BAROŇ, I. (2004): Deep seated gravitational deformation on the Kopce hill near Lidečko: Results of inventory and geophysical analysis. Geol. výzk. Mor. Slez. v r. 2003, 82–87. (in Czech)

BAROŇ, I., KAŠPERÁKOVÁ, D. (2006): Numerical analysis of gravitational breakup of Silesian nappe with the help of FDM on the example of Radhošť-Pustevny slope deformation. Zpr. o geol. výzk. v r. 2006. Praha, 49–52. (in Czech)

BAROŇ, I., BEČKOVSKÝ, D., MÍČA, L. (2012): Application of infrared thermography for mapping open fractures in deep-seated rockslides and unstable cliffs. Landslides (in print)

BAROŇ, I., CÍLEK, V., KREJČÍ, O., MELICHAR, R., HUBATKA, F. (2004): Structure and dynamics of deep-seated slope failures in the Magura Flysch Nappe, outer Western Carpathians (Czech republic). Nat. Haz. And Earth Syst. Sci. 4, 549–562.

BAROŇ, I., CÍLEK, V., MELICHAR, R. (2003a): Pseudokarst caves as an indicators of slope movements. Geol. výzk. Mor. Slez. v r. 2002. Brno, 84–87. (in Czech)

BAROŇ, I., CÍLEK, V., MELICHAR, R., MELKA, K. (2003b): Clay minerals in slope sediments of selected deep seated slope deformations of Vsetín and its surrounding. Geol. výzk. Mor. Slez. v r. 2002. Brno, 89–91. (in Czech)

BAROŇ, I., JÁNOŠ, V., KLIMEŠ, J., NOVOTNÝ, R., HUBATKA, F. (2006): Holocene flexure deformation of Godula formation by the slope movement. Zpr. o geol. výzk. v r. 2006. Praha, 46–49.

BELLA, P. (1998): Genetic types of caves in Slovakia. Acta Carsologica 27/2, Ljubljana, 15–23.

BELLA, P. (2011): Genetic types of caves. Verbum, Ružomberok. 220 p. (in Slovak)

BELLA, P., GAÁL, Ľ., HOLÚBEK, P. (2004): Caves in non-carbonate rocks of Slovakia: list, genetic types, values and protection. In: Proceedings of the 8th international symposium on pseudokarst. Slovak caves administration. Liptovský Mikuláš, 32–56.

BOSÁK, P. (2003): Karst processes from the beginning to the end: How can they be dated? Speleogenesis and Evolution of Karst Aquifers 1(3), 1–24.

BOZZANO, F., LENTI, L., MARTINO, S., MONTAGNA, A., PACIELLO, A. (2011): Earthquake triggering of landslides in highly jointed rock masses: Reconstruction of the 1783 Scilla rock avalanche (Italy). Geomorphology 129, 294–308.

BRIDEAU, M. A., YAN, M., STEAD, D. (2009): The role of tectonic damage and brittle rock fracture in the development of large rock slope failures. Geomorphology 103, 30–49.

BRIESTENSKÝ, M., STEMBERK, J. (2008): Monitoring of micromovements in the caves of the Western Slovakia. Slovenský kras 46/2, 333–339. (in Slovak)

BRIESTENSKÝ, M., KOŠŤÁK, B., STEMBERK, J., PETRO, Ľ., VOZÁR, J., FOJTÍKOVÁ, J. (2010): Active tectonics fault microdisplacement analyses: a comparison of results from surface and underground monitoring in western Slovakia. Acta Geodyn. Geomater. 7(4), 387–397.

BRUTHANS, J., CHURÁČKOVÁ, Z., JENČ, P., SCHWEIGSTIL-LOVÁ, J. (2009): Age and origin of secondary carbonates in some caves of Czech Paradise. Zpr. o geol. výzk. v r. 2008. Praha, 54–58. (in Czech)

BRUTHANS, J., SVĚTLÍK, D., SOUKUP, J., SCHWEIGSTILLOVÁ, J., VALEK, J., SEDLÁČKOVÁ, M., MAYO, A. L. (2012): Fast evolving conduits in clay-bonded sandstone: Characterization, erosion processes and significance for the origin of sandstone landforms. Geomorphology 177–178, 178–193.

BUBÍK, M., KREJČÍ, O., KIRCHNER, K. (2004): Geological past and present of Frýdek-Místek region. Muzeum Frýdek-Místek. 54 p. (in Czech)

ČETYNA, B. (1966): Radhošť. Kulturně historický přehled. Ostrava, 23–30. (in Czech)

CHIGIRA, M., WANG, WU, X. (2012): Landslides induced by the Wenchuan earthquake. In: Clague, J. J, Stead, D. (eds.): Landslides (Types, Mechanisms and Modeling). Cambridge University Press, 383–392.

CÍLEK, V., BAROŇ, I., LANGROVÁ, A. (2003): Rock crusts and coatings minerals of Magura flysch sandstones in Vsetín region. Geol. výzk. Mor. Slez. v r. 2002, Brno, 22–24. (in Czech)

CRUDEN, D. M., VARNES, D. J. (1996): Landslide types and processes. In: TURNER, A. K., SHUSTER, R. L. (Eds.): Landslides: Investigation and Mitigation. Transp. Res. Board, Spec. rep. 247, 36–75.

DAVIS, G. H., BUMP, A. P., GARCÍA, P. E., AHLGREN, S. G. (1999): Conjugate Riedel deformation band shear zones. Journal of Structural Geology 22, 169–190.

DEMEK, J. (1963): Caves in flysch sandstones of Moravian-Silesian Carpathians. Československý kras 15, 127–130. (in Czech)

DI LUZIO, E., SAROLI, M., ESPOSITO, C., BIANCHI-FASANI, G., CAVINATO, G. P., SCARASCIA-MUGNOZZA, G. (2004): Influence of structural framework on mountain slope deformation in the Maiella anticline (Central Apennines, Italy). Geomorphology 60, 417–432.

DRAMIS, F., SORRISO-VALVO, M. (1994): Deep-seated gravitational slope deformations, related landslides and tectonics. Engineering Geology 38, 231–243.

EL-QADY, G., HAFEZ, M., ABDALLA, M. A., USHIJIMA, K. (2005): Imaging subsurface cavities using geoelectric tomography and ground-penetrating radar. Journal of Cave and Karst Studies 67(3), 174–181.

ELIÁŠ, M. (2000): Relations between Pústevny sandstones and Malinów sandstones (Godula formation s.s.) in the Beskydy Mts. Geol. výzk. Mor. Slez. v r. 1999, 64–66. (in Czech)

EPOCH (European Community Programme) (1993): Temporal occurence and forecasting of landslides in the European community, (Ed. J.-C. Flageollet). 3 volumes, Contract No. 90 0025.

EZERSKY, M. (2008): Geoelectric structure of the Ein Gedi sinkhole occurrence site at the Dead Sea shore in Israel. Journal of Applied Geophysics 64, 56–69.

FOLDYNA, J. (1968): Pseudokarst in the Godula beds of Godula rock formation (Moravian-Silesian Beskyds). Sborník vědeckých prací VŠB v Ostravě, řada hornicko-geologická 14. Ostrava, 83–103. (in Czech)

FOLDYNA, J., PAVLICA, J. (1968): Pseudokarst of the Lysá hora Mt. and the Kněhyně Mt. Sborník vědeckých prací VŠB v Ostravě, řada hornicko-geologická 14. Ostrava, 69–82. (in Czech)

GAMBETTA, M., ARMADILLO, E., CARMISCIANO, C., STEFANELLI, P., COCCHI, L., TONTINI, F. C. (2011): Determining geophysical properties of a near-surface cave through integrated microgravity vertical gradient and electrical resistivity tomography measurements. Journal of cave and karst studies 73, 11–15.

GANSZER, J. (Ed.) (2012): Database of caves in Polish flysch Carpathians. SPELEOKLUB BIELSKO-BIAŁA. [online]. [cit. 2012-12-22]. Available from: http://jkf.m3.net.pl/index.php (in Polish)

GÓMEZ-ORTIZ, D., MARTÍN-CRESPO, T. (2012): Assessing the risk of subsidence of a sinkhole collapse using ground penetrating radar and electrical resistivity tomography. Engineering Geology 149–150, 1–12.

HALLIDAY, W. R. (2007): Pseudokarst in the 21st century. Journal of Cave and Karst Studies 69, 103–113.

HILL, C., FORTI, P. (1997): Cave minerals of the world. Huntsville, Nat. Speleol. Soc., 463 p.

HRADECKÝ, J., PÁNEK, T., DURAS, R. (2005): Morphological and geophysical demonstrations of the top of Smrk Mt. (1276 m) extension in the Moravian-Silesian Beskyds. Geol. výzk. Mor. Slez. v r. 2004. Brno, 106–110. (in Czech)

HROMAS, J. (ed.) et al. (2009): The caves. In: Mackovčin, P., Sedláček, M. (eds.): Protected ladscape areas of the Czech republic, svazek XIV. AOPK ČR and EkoCentrum Brno, Praha, 56–58. (in Czech)

HUTCHINSON, J. N. (1988): Morphological and geotechnical parameters of landslides in relation to geology and hydrogeology. Proceedings, Fifth International Symposium on Landslides, Rotterdam, 3–35.

JABOYEDOFF, M., COUTURE, R., LOCAT, P. (2009): Structural analysis of Turtle Mountain (Alberta) using digital elevation model: toward a progressive failure. Geomorphology 103, 5–16.

JAROSZEWSKI, W. (1972): Microstructural criteria of tectonics in non-orogenic regions on example of north-eastern mesozoic margin of Góry Świętokrzyskie Mts. Stud. Geol. Pol. 38, 1–215. (in Polish)

JIAN-HONG, W., HUNG-MING, L., DER-HER, L., SHIH-CHIEF, F. (2005): Integrity assessment of rock mass behind the shotcreted slope using thermography. Engineering geology 80, 164–173.

JURKOVÁ, N., BRIESTENSKÝ, M. (2008): Recent movements along tectonic failures in the Západní cave (Ještěd ridge, Northern Bohemia). Slovenský kras 46/2, 341–345.

KATZ, Y., WIENBERGER, R., AYDIN, A. (2004): Geometry and kinematic evolution of Riedel shear structures, Capitol Reef National Park, Utah. Journal of structural geology 26, 491–501.

KEMPE, S., HALLIDAY, W. R. (1997): Report on the discussion on pseudokarst. Proceedings of the 12th International Congress of Speleology, Basel, Switzerland, Speleoprojects.

KIRCHNER, K., KREJČÍ, O. (2002): Slope deformations and their significance for relief development in the middle part of the Outer Western Carpathians in Moravia. Moravian geographical reports 10, 10–19.

KLASSEK, G. (2004): Caves of the Polish flysch Carpathians. Proceedings of the 8th International Symposium on Pseudokarst: Teplý Vrch – Slovakia. Liptovský Mikuláš, 69–74.

KLECZKOWSKI, A. (1955): Landslides and similar phenomena. Warszawa, Wyd. Geol., 93 p. (in Polish)

KLIMEŠ, J., ROWBERRY, M. D., BLAHŮT, J., BRIESTENSKÝ, M., HARTVICH, F., KOŠŤÁK, B., RYBÁŘ, J., STEMBERK, J., ŠTĚPANČÍKOVÁ, P. (2012): The monitoring of slow-moving landslides and assessment of stabilisation measures using an optical–mechanical crack gauge. Landslides 9(3), 407–415.

KOMÁRKOVÁ, V., LENART, J., PÁNEK, T. (2008): The research of slope deformations in the Satina catchment (Moravskoslezské Beskydy Mts.). Stav geomorfologických výzkumů v roce 2008. Ústav geoniky AV ČR, v. v. i., oddělení environmentální geografie Brno, 23–24. (in Czech)

KOTOUČ, M. (2011): Predisposition and structure of the Lukšinec deep seated slope deformation (The Lysá hora massif): analysis of pseudokarst cave systems. Ostrava. Diplomová práce. Ostravská univerzita. Vedoucí práce doc. RNDr. Tomáš Pánek, PhD. (in Czech)

KREJČÍ, O., BAROŇ, I., BÍL, M., HUBATKA, F., JUROVÁ, Z., KIRCHNER, K. (2002): Slope movements in the Flysch Carpathians of Eastern Czech Republic triggered by extreme rainfalls in 1997: a case study. Physics and Chemistry of the Earth 27, 1567–1576.

KREJČÍ, O., HUBATKA, F., ŠVANCARA, J. (2004): Gravitational spreading of the elevated mountain ridges in the Moravian-Silesian Beskids. Acta Geodyn. Geomater. 135, 97–109.

KUNSKÝ, J. (1957): Types of pseudokarst features in Czechoslovakia. Československý kras 10, 108–125. (in Czech)

KWAŚNIEWSKI, M. (1986): Dilatancy as a symptom of rock destruction. Prz. Gór. 42(6), 184–190. (in Polish)

LANG, A., MOYA, J., COROMINAS, J., SCHROTT, L., DIKAU, R. (1999): Classic and new dating methods for assessing the temporal occurrence of mass movements. Geomorphology 30, 33–52.

LENART, J. (2011): Contribution to understanding of microclimate in the Ledová cave (Lukšinec hill, Moravskoslezské Beskydy Mts.) Speleofórum 30, 39–42. (in Czech)

LENART, J. (2013): Dynamics of crevice-type caves microclimate in Czech part of Outer Western Carpathians (on the examples). Slovenský kras 52, 2011–2018. (in Czech)

LENART, J., WAGNER, J. (2012): The half kilometre length was exceeded in the Cyrilka cave. Speleofórum 31, 53–57. (in Czech)

LEXA, J., BEZÁK, V., ELEČKO, M., MELLO, J., POLÁK, M., POTFAJ, M., VOZÁR, J. (Eds.) (2000): Geological Map of Western Carpathians and Adjacent Areas 1 : 500,000. Geological Survey of Slovak Republic, Bratislava.

MAJERNÍČKOVÁ, F., MAJERNÍČKOVÁ, G., IMRICH, P. (2005): The Levočské vrchy mountains – pseudokarst paradise. Bulletin of the Slovak Speleological Society, special edition 2005, 36–42.

MARGIELEWSKI, W. (2003): Late Glacial-Holocene paleoenvironmental changes in the Western Carpathians: case studies of landslide forms and deposits. Folia Quaternaria 74, 1–97.

MARGIELEWSKI, W. (2004): Types of gravitational displacements of rocks masses in the area of Polish flysch Carpathians. Prz. Geol. 52, 603–614. (in Polish)

MARGIELEWSKI, W. (2006a): Records of the Late Glacial–Holocene palaeoenvironmental changes in landslide forms and deposits of the Beskid Makowski and Beskid Wyspowy Mts. Area (Polish Outer Carpathians). Folia Quaternaria 76, 1–149.

MARGIELEWSKI, W. (2006b): Structural control and types of movements of rock mass in anisotropic rocks: case studies in the Polish Flysch Carpathians. Geomorphology 77, 47–68.

MARGIELEWSKI, W. (2009): Problems of structural landslides of flysch Carpathians in the light of unified classification of slope movements – the critical review. Prz. Geol. 57, 905–917. (in Polish)

MARGIELEWSKI, W., URBAN, J. (2000): Character of mass movements initiations in the flysch Carpathians on the basis of structural analyses of the selected crevice-type caves. Prz. Geol. 48, 3, 268–274. (in Polish)

MARGIELEWSKI, W., URBAN, J. (2003): Crevice-type caves as initial forms of rock landslide development in the Flysch Carpathians. Geomorphology 54, 325–338.

MARGIELEWSKI, W., URBAN, J. (2004): The crevice-type cave Diabla Dziura w Bukowcu (Pogórze Rożnowskie Mts., Central Carpathians) as an initial stadium of deep seated gravitational slope deformations evolution in the flysch Carpathians. Prz. Geol. 52, 1171–1178. (in Polish)

MARGIELEWSKI, W., KRĄPIEC, M., VALDE–NOWAK, P., ZERNITSKAYA, V. (2010): A Neolithic yew bow in the Polish Carpathians: Evidence of the impact of human activity on mountainous palaeoenvironment from the Kamiennik landslide peat bog. Catena 80, 141–153.

MARGIELEWSKI, W., SZURA, C., URBAN, J. (2008): Jaskinia Miecharska cave (Beskid Śląski Mts., Outer Carpathians): The largest non-karst cave in the flysch Carpathians. Zacisk, April 2008, 7–13.

MARGIELEWSKI, W., URBAN, J., SZURA, C. (2007): Jaskinia Miecharska cave (Beskid Śląski Mts., Polish Outer Carpathians): case study of a crevice-type cave developed on a sliding surface. Nature Conservation 63, 57–68.

MARGIELEWSKI, W., URBAN, J., HERCMAN, H., ŽÁK, K., ZERNITSKA, V., PAWLAK, J. (2012): Dating speleothems in sandstone caves – methodological aspects and practical interpretation, Polish Outer Carpathians case study. In: Duszyński, F., Świrad, Z. (eds.), Sandstone Landscapes III. Diversity, ecology and conservation. Stołowe Mts. National Park, 25-28.04.2012, Abstract Booklet. Kudowa-Zdrój, 40–41.

MARTINO, S., MUGNOZZA, G. S. (2005): The role of the seismic trigger in the Calitri landslide (Italy): historical reconstruction and dynamic analysis. Soil Dynamics and Earthquake Engineering 25, 933–950.

MASTELLA, L.,ZUCHIEWICZ, W., TOKARSKI, A. K., RUBIN-KIEWICZ, J., LEONOWICZ, P., SZCZĘSNY, R. (1997): Aplication of joint analysis for paleostress reconstructions in structuraly complicated settings: case study from Silesian nappe, Outer Carpathians, Poland. Prz. Geol. 45, 1064–1066.

MEDVEĎOVÁ, A., PROKEŠOVÁ, R., SNOPKOVÁ, Z., KORÓNY, S. (2008): Relief and underground water level variability in the landslide area (The Ľubietová case study). Geomorfologia Slovaca et Bohemica 8/2, 38–48. (in Slovak)

MENČÍK, E., ADAMOVÁ, M., DVOŘÁK, J., DUDEK, A., JETEL, J., JURKOVÁ, A., HANZLÍKOVÁ, E., HOUŠA, V., PESLOVÁ, H., RYBÁŘOVÁ, L., ŠMÍD, B., ŠEBESTA, J., TYRÁČEK, J., VAŠÍČEK, Z. (1983): Geology of the Moravskoslezské Beskydy Mts. And Podbeskydská pahorkatina foothills. Ústřední Ústav Geologický. Praha, 304 p. (in Czech)

MIHÁĽ, F. (2010): Karst features in the Paleogene sandstones and conglomerates near Spišské Tomášovce. Aragonit 15/1, 38–41. (in Slovak)

MILSOM, J. (2005): Field Geophysics, the Geological Field Guide Series (3rd ed.). Wiley, Chichester, 232 p.

NAKLÁDAL, P. (2006): Máca, read, and how to recover the caves by the thermocamera. Speleo 45, 9–15. (in Czech)

NĚMČOK, A. (1972): Gravitational slope deformation in high mountains. Proceedings of The 24th International Geological Congress. Montreal, vol. 13, 132–141.

NOVOSAD, S. (1956): The fosil breakup of the Lukšinec ridge near Lysá hora Mt. Časopis pro mineralogii a geologii, 1/2, 126–131. (in Czech)

NOVOSAD, S. (1966): The slope failure in the Godula beds of Moravskoslezské Beskydy Mts. Sborník geologických věd, HIG 5. Praha, 71–86. (in Czech)

OTVOS, E. G. (1976): „Pseudokarst" and „pseudokarst terrains": Problems of terminology. Geological Society of America Bulletin 87, 1021–1027.

PÁNEK, T., DURAS, R. (2002): The morphotectonics of the eastern marginal slope of The Ropice-range (The Moravskoslezské Beskydy Mts.). Moravian geographical reports 10, 20–27.

PÁNEK, T., HRADECKÝ, J., ŠILHÁN, K., SMOLKOVÁ, V., ALTOVÁ, V. (2009b): Time constraints for the evolution of a large slope collapse in karstified mountainous terrain of the southwestern Crimean Mountains, Ukraine. Geomorphology 108, 171–181.

PÁNEK, T., MARGIELEWSKI, W., TÁBOŘÍK, P., URBAN, J., HRADECKÝ, J., SZURA, C. (2010): Gravitationally induced caves and other discontinuities detected by 2D electrical resistivity tomography: Case studies from the Polish Flysch Carpathians. Geomorphology 123, 165–180.

PÁNEK, T., TÁBOŘÍK, P., HRADECKÝ, J. (2007): Gravitational break-up of the Čertův mlýn ridge (Moravskoslezské Beskydy Mts.) Geol. výzk. Mor. Slez. v r. 2006. Brno, 124–129. (in Czech)

PÁNEK, T., TÁBOŘÍK, P., KLIMEŠ, J., KOMÁRKOVÁ, V., HRA-DECKÝ, J., ŠŤASTNÝ, M. (2011a): Deep-seated gravitational slope deformations in the highest parts of the Czech Flysch Carpathians: Evolutionary model based on kinematic analysis, electrical imaging and trenching. Geomorphology 129, 92–112.

PÁNEK, T., ŠILHÁN, K., TÁBOŘÍK, P., HRADECKÝ, J., SMOLKOVÁ, V., LENART, J., BRÁZDIL, R., KAŠÍČKOVÁ, L., PAZDUR, A. (2011b): Catastrophic slope failure and its origins: Case of the May 2010 Girová Mountain long-runout rockslide (Czech Republic). Geomorphology 130, 352–364.

PANOŠ, V. (1963): Problems of karstification of non-carbonate rocks. Časopis pro mineralogii a geologii 10(1), 105–109. (in Czech)

PANOŠ, V. (2001): Karsological and speleological terminology. Knižné centrum. Žilina, 352 p. (in Czech)

PETRO, Ľ., BÓNA, J., KOVÁČIK, M., FUSSGÄNGER, E., ANTONICKÁ, B., IMRICH, P. (2011): The Cave under the Spišská hill: Preliminary monitoring results of the block movements. Mineralia Slovaca 43, 121–128.

POKORNÝ, R., HOLEC, M. (2009): The caves of Ústí region: Non-karstic underground objects in the tertiary vulcanites, their origin, characteristics and biota. Nakladatelství XYZ. Praha, 278 p. (in Czech)

REYNOLDS, O. (1985): On the dilatancy of media composed of rigid particles in contact. Phil. Mag. 5(20), 469–481.

RYBÁŘ, J., JÁNOŠ, V., KLIMEŠ, J., NÝDL, T. (2006): The break-up of synclinal ridge of Ondřejník in The Podbeskydská pahorkatina foothills. Zprávy o geologických výzkumech v roce 2006. Česká geologická služba. Praha, 92–96. (in Czech)

RYBÁŘ, J., JÁNOŠ, V., KLIMEŠ, J., NÝDL, T. (2008): Structurally induced slope movements in the eastern part of the Moravsko-slezské Beskydy Mts. Zpr. o geol. výzk. v r. 2007. Česká geologická služba. Praha, 113–118. (in Czech)

SANJURJO-SÁNCHEZ, J., VIDAL ROMANÍ, J. R. (2011): Luminescence Dating of Pseudokarst Speleothems: A First Approach. Spectroscopy Letters 44(7), 543–548.

SCHROTT, L., SASS, O. (2008): Application of field geophysics in geomorphology: advances and limitations exemplified by case studies. Geomorphology 93, 55–73.

STARKEL, L. (1977): Paleogeografia holocenu. Warszawa, 363 p.

STEMBERK, J., BRIESTENSKÝ, M., JURKOVÁ, N. (2008): Displacements registered in the selected caves of Czech massif. Speleofórum 27, 141–144. (in Czech)

STEMBERK, J., JÁNOŠ, V. (2002): Slope deformations on the Radhošť ridge in the Moravskoslezské Beskydy Mts., maps 25-23-09 and 25-23-10 in the scale of 1 : 10,000. Zpr. o geol. výzk. v r. 2002, 104–106. (in Czech)

SZURA, C. (2006): Miecharska cave – the giant of Beskydy Mts. Jaskinie 2(43), 6. (in Polish)

SZURA, C. (2009): Wiślańska cave – the flysch giant. Jaskinie 3(56), 19–21. (in Polish)

TÁBOŘÍK, P. (2007): Geomorphological analysis of slope deformations on the Čertův mlýn (Moravskoslezské Beskydy Mts.). Ostrava. Diplomová práce. Ostravská univerzita. Vedoucí práce doc. RNDr. Tomáš Pánek, PhD. (in Czech)

TÁBOŘÍK, P. (2009): Use of electrical resistivity tomography in the research of mountain ridge disintegration. In: Ph.D. Workshop 2009 Proceedings. Institute of Geonics AV CR. Ostrava, 43–48.

TSUNG-LIN, L., CHING-PIAO, T., HUNG-MING, L., CHI-JEN, F. (2009): A combined thermographic analysis – Natural network methodology for eroded caves in a seawall. Ocean engineering 36, 1251–1257.

TUČNÍK, D. (1953): The caves of Radhošť. (The fissures in the Pustevny on the Radhošť Mt.) Československý kras 6, 185–186. (in Czech)

URBAN, J. (2005): Pseudokarst caves as an evidence of sandstone forms evolution – a case study of Niekłań, the Świętokrzyskie Mts., central Poland. Ferrantia 44, 181–185.

URBAN, J., MARGIELEWSKI, W., SCHEJBAL-CHWASTEK M., SZURA, C. (2007a): Speleothems in some caves of the Beskidi Mts., Poland. Nature Conservation 63, 109–117.

URBAN, J., MARGIELEWSKI, W., ŽÁK, K., HERCMAN, H., SUJKA, G., MLECZEK, T. (2007b): The calcareous speleothems in the pseudokarst Jaskinia Słowiańska-Drwali cave, Beskid Niski Mts., Poland. Nature Conservation 63, 119–128.

VARNES, D. J. (1978): Slope movements: type and processes. Landslides: analysis and control. National Academy of Sciences, Washington DC. Special report 176, 12–33.

VÍTEK, J. (1978): Types of pseudokarst caves of ČSR. Česko-slovenský kras 30, 17–28. (in Czech)

VÍTEK, J. (1981): Morphogenetical classification of pseudokarst in Czechoslovakia. Sborník Československé geografické společnosti 3, 153–165. (in Czech)

WAGNER, J., DEMEK, J., STRÁNÍK, J. (1990): Caves of Moravskoslezské Beskydy Mts. and its surroundings. Knihovna České speleologické společnosti. Praha, 132 p. (in Czech)

WALKER, M. (2005): Quarternary dating methods. Chichester, United Kingdom: John Wiley & Son, 286 p.

ŽYTKO, K., ZAJĄC, R., GUCIK, S., RYŁKO, W., OSZCZYPKO, N., GARLICKÁ, I., NĚMČOK, J., ELIÁŠ, M. (1989): Map of the tectonic elements of the Western Outer Carpathians and their foreland. PIG Warszawa, GUDS Bratislava, UUG Praha.

RÉSUMÉ

Rozsedlinové jeskyně jako indikátory svahových poruch: Přehled s důrazem na flyšové Karpaty Česka, Polska a Slovenska

Vznik a vývoj rozsedlinových jeskyní je jedním z nejviditel-nějších fenoménů spojených s výskytem svahových deformací v nejrůznějších typech hornin. Rozsedliny se velice často vytvářejí ve flyšových horninách jako například v oblasti Karpat, které jsou tvořeny střídáním subhorizontálně uložených vrstev pískovců, pra-chovců a jílovců. Článek prezentuje propojení mezi vývojem sva-hových deformací a výskytem a vývojem rozsedlinových jeskyní, poskytuje přehled o genezi a vývoji rozsedlinových jeskyní jakožto důležitého geomorfologického elementu gravitačně rozrušených svahů flyšových Karpat, prezentuje náhled na soudobou proble-matiku výzkumu a odhaduje cesty jeho budoucího vývoje.

Jan Lenart, Tomáš Pánek
Ostrava University in Ostrava, Faculty of Science
Department of Physical Geography and Geoecology
710 00 Ostrava
Czech Republic
E-mail: jan.lenart@osu.cz, tomas.panek@osu.cz

CLIMATOLOGY OF PRECIPITATION IN THE VOSGES MOUNTAIN RANGE AREA

JANA MINÁŘOVÁ

Charles University in Prague, Faculty of Science, Department of Physical Geography and Geoecology

ABSTRACT

The aim of this work is to study the climatology of atmospheric precipitation in the study area situated in north-eastern France. It is shown that the Vosges mountain range, due to its position almost perpendicular to the prevailing western airflow, affects the spatial and temporal distribution (and thus the seasonality) of precipitation at a regional scale. This is carried out by computing the daily rainfall at 14 meteorological stations over the period 1950–2011. Different levels of rainfall resolution were examined – at first the annual rainfall which varies greatly between the windward side and the highest part of the Vosges mountain range and the Upper Rhine Plain (the difference is as large as 1700 mm per average year), then the monthly rainfall and distribution of precipitation within the year and finally the daily rainfall variability. Three categories of stations were determined according to their annual precipitation distribution: (i) mountain stations with a winter precipitation maximum, (ii) leeward slope stations with two precipitation maxima, i.e. in winter and summer and (iii) leeward stations located in the Upper Rhine Plain eastward of the Vosges with a summer precipitation maximum. Quantitative methods of ombric continentality demonstrate that the Vosges represent a limit between oceanic and a more continental climate. However, the empirical formulas are not satisfying and further research is required.

Keywords: climatology, precipitation variability, ombric continentality, leeward effect, the Vosges

1. Introduction

The distribution of atmospheric precipitation is not uniform in space and time (e.g., Prudhomme, Reed 1998). Taking into consideration the potential impact of precipitation on human beings (e.g., lack of precipitation causes drought, while its excess generates floods) and the incompleteness of knowledge about this domain (Šálek 2007), further research is required. Thus the aim of this study is to contribute to the research concerning atmospheric precipitation using the standard climatological methods (with annual, monthly and daily rainfall resolution) and studying the degree of ombric (rainfall) continentality, while taking into account the potential influence of orography on the precipitation distribution.

The studied area comprises the Vosges, a relatively low-elevation mountain range, situated in north-eastern Metropolitan France near the border with Germany and Switzerland, and their surroundings – the Upper Rhine Plain in particular. The reason for such a choice of area is, that the Vosges represent one of the first orographic barriers to the Westerlies from the Atlantic Ocean (air masses come mostly from West or South-West, in 40.5% of days out of the period 1985–1987, as explained e.g., in REKLIP 1995) which is due to their extension in the north-north-east and south-southwest direction. Another hypothesis is that a limit between oceanic and more continental climate (with a different distribution of precipitation within a year) occurs in this area. The last motivation is that the chosen area (Figure XVII in Colour appendix) presents

a considerable altitudinal variability (up to 1300 m) – the Grand Ballon, the highest vosgian peak reaches 1424 metres above sea level (thereafter ASL), while the Upper Rhine Plain keeps a relatively constant altitude of approximately 200 meters and less (Sell et al. 1998).

Among the factors influencing climate variability (and therefore precipitation variability) in the studied area are altitude, slope exposure and geographical position (in the sense of distance and direction from the Vosges), along with specifics of the local relief (convexity vs. concavity) etc. It should be noted that vosgian slopes are typically steeper on the eastern (Alsatian) side, close to the Upper Rhine Plain, than those of the western (Lorraine) part (Troux, Quillé 1951); this influences the precipitation patterns too.

As aforementioned, the orientation of the Vosges mountain range forms a perpendicular orographic barrier to the prevailing western airflow; therefore it would be expected (Barry, Chorley 2003) that on the windward side and on the mountain ridges may occur an orographic intensification of precipitation mainly due to the reinforcement of air uplift while the phenomenon of rain shadow is characteristic for the leeward side (in our case it concerns mainly the Upper Rhine Plain). However at the local scale the description of the precipitation pattern gets more complicated, as many factors and conditions need to be accounted for.

Regarding climate continentality, we recognize two types of continentality in general – thermal and ombric (relating to temperature and precipitation respectively).

This study analyses only the second one. According to the degree of continentality, we distinguish oceanic, semi-continental and continental climates (e.g., Sobíšek et al. 1993). In European mid-latitudes the oceanic climate is typically humid, with relatively high and uniform temporal distribution of precipitation (with the exception of a small peak in winter at the west coasts). In contrast, the continental climate is generally much drier (precipitation peaks during summer) and the distribution of precipitation is uneven. The semi-continental climate has some combination of the characteristics of oceanic and continental climates (Zíková 2009).

The climate of the studied area is usually classified as temperate and semi-continental and generally under the prevailing influence of western airflow rich in water vapour (e.g., Sell et al. 1998). One of the most important climate characteristics of the region is its well-marked spatial and temporal variability (Météo-France 2008). Both are related to relief (topography), degree of continentality and the related seasonal of the precipitation.

Besides, the mean annual air temperature varies between 10 °C (plain), 7 °C (800 metres ASL) and 5 °C for 1200 m in the Vosges (Sell et al. 1998; Mühr 2007). In terms of average annual rainfall, the variability is much more pronounced. The windward side and the main mountain ridge of the Vosges is the most humid (the average annual rainfall surpassing 2000 mm) whereas less precipitation falls on the leeward side. The minimal rainfall is in the Upper Rhine Plain, typical of the rain shadow (e.g., town Colmar with less than 550 mm per year considered as one of the driest place in Metropolitan France) (Sell et al. 1998). Climate patterns are more pronounced in winter, with winter cyclones more

frequent and intense in winter than in summer (Bürger 2010).

Overall, this paper emerges from the need to enhance the knowledge concerning the climatology of atmospheric precipitation in relation to orography in the Vosges area. This will be accomplished by analysing 14 meteorological stations over the studied area, there providing a potential framework for estimating atmospheric precipitation. Some of the results shown here could be specific to the study area but others could be transferable to other orographic regions.

2. Data and methods

The map output for the Vosges mountain range area was processed through the ArcGIS cartographical software (version 9.3.1) operating with geographic information systems (GIS) provided by ESRI (Environmental Systems Research Institute; available from http://www.esri.com/) – using their basemaps (e.g., towns). The topology background was adopted from the Marine Geoscience Data System (project of Columbia University in New York) using their software GeoMapApp (version 3.1.6). This application (http://www.geomapapp.org/) provides a visualisation of the Global Multi-Resolution Topography (GMRT) terrain model, with node spacing of 100-meters. For continental surfaces, NED (National Elevation Dataset) was used.

Access to the meteorological daily data was granted by the Météo-France network. The daily rainfall obtained covered the period from 1950 to 2011 (i.e. 62 years) from 14 meteorological stations (see Figure XVII

Tab. 1 Geographical position, average annual rainfall $\overline{Ra}$ and year with missing data of 14 studied meteorological stations.

Meteorological station (number | name)	Northern latitude [°]	Eastern longitude [°]	Altitude [m ASL]	Average annual rainfall $\overline{Ra}$ [mm]	Year with a missing observation
1	Sewen – Lac Alfeld	47.82	6.87	620	2,334	1952–60, 1964, 2002, 2004, 2006–08
2	Wildenstein	47.98	6.96	560	2,070	1950–56, 1957, 1958, 1960, 1961, 1992
3	Sewen – Foerstel	47.81	6.91	505	1,907	1950–58, 1968, 1974, 1975, 1977, 1978
4	Longemer	48.07	6.95	745	1,865	1961, 1962
5	Mittlach – Erbe	48.01	7.03	552	1,834	1963–72, 1974, 1975, 1976
6	Le Hohewald	48.41	7.35	785	1,226	1952, 1953, 1955, 1963, 1964, 1975, 1976, 1977, 1982, 1983, 1984
7	Aubure	48.20	7.22	796	1,084	1950–1970, 1986, 1989, 2010
8	Strasbourg	48.58	7.77	139	730	–
9	Barr	48.41	7.46	193	722	1953, 1970
10	Kayserberg	48.14	7.27	248	703	1950, 1965, 1967, 1968, 1977, 1978
11	Neuf – Brisach	48.03	7.58	195	640	2002, 2003
12	Ebersheim	48.31	7.49	164	621	–
13	Rouffach – Chs	47.95	7.29	208	612	1961, 1962, 1971, 1981, 1982, 1987, 1989, 1990, 2004
14	Oberentzen	47.94	7.38	205	606	1956, 1964

in Colour appendix). The dataset was not continuous (Table 1) – some series were interrupted within the observation period (with the exception of the stations *Ebersheim* and *Strasbourg*), mostly in winter or summer. The list of meteorological stations is presented in Table 1, which displays the geographical position of the studied stations, the average annual rainfall ($\overline{\overline{Ra}}$) as well as any years with at least one day of missing observations. While some data were available during the listed years (the listed years do not mean that for all the year we have "no data", however, data from these years were omitted when calculating the average annual rainfall). The stations are listed in order of their average annual rainfall ($\overline{\overline{Ra}}$) for the studied period, from greatest (*Sewen-Lac Alfeld*, no. 1) to least (*Oberentzen*, no. 14). The meteorological stations displayed in Figure XVII are divided according to their average annual rainfall in intervals of 500 mm. The first interval includes stations with annual rainfall between 500 mm and 1000 mm; no station had less than 500 mm.

Any time period containing missing values was discarded in the calculations. That is, for the daily resolution, only days with missing precipitation data were omitted, while for the monthly resolution, the whole (incomplete) months were discarded if data were missing, even on a single day. Listing all the days with missing values in Table 1 is beyond the scope of this paper.

It was chosen not to homogenise the data because inaccuracies may occur – especially in the case of outlying values (extreme precipitation), contrary to original data. Homogenization of the dataset may result in filtering out of the marginal values (Štěpánek 2007). Another reason is that future research will examine these extremes.

The standard climatological approach was used on the collected data. This consists in analysing rainfall from large to small temporal levels (e.g., years to days) and of the rainfall variability (Sobíšek et al. 1993). For some cases, 5 meteorological stations were selected as representative of a part of the studied area (their position is indicated in Figure XVII) – *Longemer* (no. 4), the sole representative of the windward side of the Vosges, *Sewen-Lac Alfeld* (no. 1) and *Wildenstein* (no. 2), both situated closest to the main mountain crest, *Aubure* (no. 7) located on the leeward side but still in the Vosges, and finally *Oberentzen* (no. 14), which represents purely a leeward lowland station (within the rain shadow area) in the Upper Rhine Plain.

2.1 Annual rainfall and distribution of precipitation within an average year

Firstly the average annual rainfall ($\overline{\overline{Ra}}$) was analysed using Microsoft Excel 2010 within the period 1950–2011 for each station in order to determine the general magnitude of rainfall in the examined area. Then the average monthly rainfall ($\overline{Rm}$) was studied for each station

and each month, allowing to ascertain the variability of precipitation within an average year. The calculation was based on the following equations:

$$\overline{Ra} = \frac{\sum_{i=1}^{j} Ra_i}{n} , \tag{1}$$

$$\overline{Rm_{J-D}} = \frac{\sum_{i=1}^{j} Rm_i}{n} , \tag{2}$$

where i is the i-th year; j last year with observations and n represents the total number of years with observations (J-D signifies months from January to December), while Ra_i (Rm_i) is the sum of the daily rainfall (Rd) within a year (month) i and the number of days within the year (month) i.

It is important to note that for the entire study the afore described procedure was followed.

Subsequently, the season (or day) of highest concentration of precipitation within the analysed period (1950–2011) was determined for the five characteristic meteorological stations. The method shows the intra-annual variability of precipitations. The yearly centre of gravity of rainfall was computed using the percentage of $\overline{Rm}$ in $\overline{Ra}$ expressed as a vector with a direction representing a month and magnitude equal to this percentage. The closer in value these percentages are for each month, the more uniformly the precipitation is distributed in an average year. The results were plotted into a polar chart (Figure XIX in Colour appendix) which was divided into 12 parts corresponding to each month in a year (30° for every month). The 12 coordinates for the 5 examined stations were found this way, aligned in the graph. The centre of gravity (resultant vector) for each station was calculated as the sum of 12 vectors representing 12 months for such stations. The date (placed on the "auxiliary" circle in Figure XIX) was matched with each centre of rainfall gravity, i.e., the resultant vector, to indicate the centre of gravity of the humid period.

Finally to make the graph more meaningful, a dashed "average" circle (with magnitude equal to the average of resulting vectors for five stations) was added into the graph. The radius of this circle Rm_{result} centred at the origin of the polar coordinate system was calculated as:

$$\left| Rm_{J-D} \right| = \sqrt{\left[\left(\frac{\sum_{1}^{n} Rx_{J-D}}{n} \right)^2 + \left(\frac{\sum_{1}^{n} Ry_{J-D}}{n} \right)^2 \right]} , \tag{3}$$

$$Rm_{result} = \frac{\sum_{J}^{D} \left| Rm_{J-D} \right|}{12} , \tag{4}$$

where $\left| Rm_{J-D} \right|$ means the value (calculated as a distance of a vector using the Pythagorean theorem) of a resultant average monthly rainfall for all stations from January (J) successively up to December (D). This results in 12 values. The variable n is the number of examined stations (in our case equal to 5); Rm_{result} represents the sole resultant average monthly rainfall (for all months – from January to December).

2.2 Ombric continentality

The ombric continentality was also examined. Three empirical formulas describing the degree of ombric continentality were selected: (i) the time of the half annual rainfall, (ii) the degree of continentality by Hrudička (1933) and (iii) Markham's index of uneven distribution of precipitation (F).

The time of the half annual rainfall (i) represents the time in months counted from April to reach the half of the annual average rainfall ($\overline{Ra}$). The shorter the calculated time, the greater the ombric continentality (Hrudička 1933).

The degree of continentality k (ii) proposed by Hrudička (1933) is calculated as follows:

$$k = \frac{12(l - 35)}{\sqrt{s_z}} \ [\%], \tag{5}$$

where l is the percentage of the sum of the average monthly rainfall from April to September in the average annual rainfall and s_z is the sum of the average monthly rainfall for the cold period (from October to March) expressed in milimeters.

When the increase of the k value is greater, the ombric continentality is becoming more pronounced and the distribution of precipitation in an average year less uniform.

The last approach (iii) involved the use of the precipitation seasonality index F (Markham 1970). This index has been applied in several studies to demonstrate the degree of annual inequality in the distribution of precipitation or the degree of ombric continentality (e.g., in the Climate Atlas of Czechia, Tolasz et al. 2007). In this paper, it was calculated for five selected meteorological stations as follows (Shver 1975):

$$F = \frac{R}{\sum_{i=1}^{12} r_i} \times 100 \ [\%], \tag{6}$$

where F is the percentage of the magnitude of the resultant vector R (calculated as the sum of vectors representing monthly rainfall r_i, where $i = 1, 2, \ldots, 12$) divided by the total annual rainfall (equal to the scalar sum of all monthly rainfall).

Notice that the monthly rainfalls were transformed into vectors (with two components) as in the previous case (the determination of a day with the highest concentration of precipitation) described above. In general, lower value of F means more balanced distribution of precipitation within a year and thus typically lower degree of ombric continentality (Brázdil et al. 2009).

2.3 Variability of monthly and daily rainfall

The best way to express the inter-monthly and inter-daily variability seemed to be to plot a curve resembling a cumulative distribution function. The monthly (daily) rainfall data were arranged in descending order. The largest observation was assigned the order number 1, the second largest the order number 2, and so on until all observations had an order number. A quotient of an order number and the absolute number of observations was calculated (e.g., 62 for a station measuring within the whole studied period of 62 years) – in this case identical to the largest order number. This quotient was expressed as a percentage and then subtracted from "100" (to form a complement to 100).

Using this approach, we got the values on the y-axis in Figures XXI and XXII, and the x-axis values in Figures XXIII and XXIV (Colour appendix).

In Figure XXII (in Figure XXIV), the values on the x-axis (y-axis) were equal to the monthly (daily) rainfall related to the average monthly rainfall (daily rainfall from days with observations and exceeding 0.0 mm divided by the number of days with this rainfall), expressed as a percentage. For a higher significance of results, the values on the axis expressing the monthly rainfall (Rm) or daily rainfall (Rd) were divided by the average (monthly or daily) rainfall ($\overline{Rm}$, $\overline{Rd}$). Notice that the inter-monthly variability was expressed only for five selected meteorological stations comparing the months of January and July (as is standardly used in climatological research – e.g., Votavová 2010).

3. Discussion of results

3.1 Average annual rainfall

The values of average annual rainfall ($\overline{Ra}$) calculated by (1) are recorded in the Table 1. Comparing Table 1 with Figure XVII, the mountainous stations (and mostly south-western stations) show a far greater average annual rainfall (> 1000 mm/year) than the leeward side. The average annual rainfall at *Sewen-Lac Alfeld* station (no. 1, with 2334 mm/year) is almost four times greater than at *Oberentzen* (no. 14 with 606 mm/year). This difference is significant, considering the short distance in the west-east direction (only about 70 km). The results demonstrate the important role of the Vosges mountain range as a precipitation barrier, thus leading to the phenomenon of rain shadow in the Upper Rhine Plain (making it relatively dry).

It should be noted that – despite the general trend – the stations situated easternmost in the studied area do not show low values of $\overline{Ra}$. In the case of *Strasbourg* (no. 8), this is because the Vosges are not as high in its surroundings and thus the rain shadow is less pronounced in this region (REKLIP 1995, Bürger 2010).

Neuf-Brisach (no. 11) could be perceived as a station standing at the windward side of Schwarzwald, near-by is Totenkopf (557 m ASL), part of the Tertiary volcano Kaiserstuhl (Scholz 2008).

The dependency between the altitude of a station and its $\overline{Ra}$ was not proved. One explanation is that the altitude does not represent a decisive factor influencing

the rainfall in the studied area. For example, Bankanza (2011) states that for the most humid summers in the Czech Republic (1997, 2002) the slopes and altitudes in the surrounding area were much more important than the altitude of the measuring station.

It is interesting that at *Longemer* station (no. 4), which is the westernmost station and is the only one on the windward side (Table 1, Figure XVII), the average annual rainfall is not the highest as might be expected (1865 mm contrary to, e.g., *Wildenstein* (no. 2) with 2070 mm/year). The reason could lie in the fact that the windward effect is more pronounced close to the main mountain ridge than on the windward side, because the windward western slopes are not so steep, which causes a gradual (not abrupt) air uplift. This might postpone the onset of precipitation. This relationship was described e.g., by the UTD ("upslope-time-delay") model proposed by Smith (2003). Another hypothesis is that *Longemer* station (no. 4) is not situated south-easternmost where the highest rainfall is reached because of the prevailing western and mainly south-western airflow in the studied area as mentioned above (e.g., REKLIP 1995).

3.2 Average monthly rainfall

The resulting values of the average monthly rainfall ($\overline{Rm}$) calculated using formula (2) are represented in Figure XVIII. The uneven monthly distribution of precipitation within an average year is clearly evident – the most humid month is December for the seven first meteorological stations (e.g., at *Sewen-Lac Alfeld* (no. 1) it is about 300 mm), whereas for the remaining seven stations it is the summer months (most frequently June and August, e.g., 67 mm per August at *Oberentzen* station, no. 14). This demonstrates the undeniable spatial and temporal differences in distribution of precipitation and the role of the Vosges mountain range as the most significant factor.

Three categories of stations were distinguished on the basis of the precipitation course of $\overline{Rm}$ in an average year (apparent in Figure XVIII):
 (i) stations with one peak of precipitation in winter (the five first meteorological stations – e.g., *Wildenstein*, no. 2),
 (ii) stations with two peaks – one main and one incidental (four stations), which could be divided into 2 groups according to the predominant maximum in winter (*Le Hohewald*, no. 6 and *Aubure*, no. 7) or in summer (*Barr*, no. 9 and *Kayserberg*, no. 10),
(iii) stations with one peak in summer (six stations – e.g., *Neuf-Brisach*, no. 11).

It is almost surprising that the annual course of precipitation changes almost gradually from the west (i) to the east (iii) of the studied area with the accompanying progressive decrease of $\overline{Ra}$ (curves between different categories do not cover almost each other – Figure XVIII). This could be generated by the increasing ombric

continentality in the west-east direction manifested by the progressive weakening of winter maximum and the gradual increase of summer maximum of precipitation, with the summer maximum dominating for category (iii) stations. This can be explained by a greater participation of convective precipitation in summer for this category (e.g., Sládek 2005). In category (ii) with two maxima of precipitation, the summer convection and the winter intensification of the oceanic western circulation both create local precipitation maxima (McCabe 2001) – the convection is minority for the first group of stations, whereas it prevails in the second group of this category. The higher winter's wind velocity and winter's intensified atmospheric circulation is deciding in the case of category (i) (Heyer 1993).

The role of the Vosges in the course of precipitation could lie in an intensified transition from category (i) to (iii), thus amplifying the transition from oceanic to more continental climate.

3.3 Average day of the highest concentration of precipitation

In Figure XIX the average day with the highest concentration of precipitation within the examined period (1950–2011) is identified using formulas (3) and (4). It leads to an analogous conclusion as in the previous case – meteorological stations closer to the west, that is, category (i) stations, reach the highest concentration of precipitation in winter – in December (e.g., on the 19th of December for *Wildenstein*) whereas precipitation at *Oberentzen* station, category (iii), reaches a maximum on average in July (on the 5th of July). Thus the centre of rainfall gravity is dependent on the geographical position of the stations (Figure XVII).

From Figure XIX, the increase of ombric continentality is also evident. The vectors head towards December for category (i) but get shorter gradually with decreasing $\overline{Ra}$ (Table 1) up to the smallest magnitude of vector for category (ii) – here represented by *Aubure* station (no. 7). Then for category (iii), the vector increases in its magnitude even as $\overline{Ra}$ continually decrease, but the direction is now oriented to summer months, as seen for the *Oberentzen* station (no. 14), which has its vector pointed to July. It is interesting to notice that the influence of orography must represent a very important factor for the studied area, which is manifested by the immediate weakening of winter maximum just after reaching the main crest. Thus the role of Vosges as a generator of ombric continentality can be confirmed (Bürger 2010).

Moreover, from the graph on Figure XIX the ratio between the average rainfall circle (illustrated by a dashed line) and the asymmetrical curve of monthly rainfall dependencies for individual stations can be observed.

With decreasing asymmetricity of the annual distribution of rainfall, the annual course of precipitation is more balanced and the peak of the highest concentration of precipitation is less pronounced. In an ideal case (such as

for rainfall in equatorial areas) no peak can be recognized (Kottek et al. 2006; Trefná 1970), the form of the rainfall dependency approaches a circle and the resultant vector is zero. In our case, the shape of the dependency for the *Aubure* station (no. 7) is the most similar to an average circle. Thus the rainfall at *Aubure* station (no. 7) shows the most balanced concentration – with the winter peak (on 6th of December) just a little greater than the summer secondary peak (in May). This is manifested also by the smallest resulting vector out of the list.

However, this method is not without disadvantages: the information value of the results is limited, because when adding vectors of the same magnitude but opposite directions, their sum would be equal to zero. Hence, the vector would indicate that the highest rainfall for a station occurs in another month that is not counterbalanced. This has partially occurred in the case of *Aubure* (no. 7) where the magnitude of the resultant vector pointing to winter is reduced by the secondary summer maximum.

Nevertheless, the unquestionable advantage of this method lies in accenting the real centre of gravity of precipitation which is much more representative as a result than the bare comparison of $\overline{Rm}$.

3.4 Evolution of annual rainfall

The evolution of annual rainfall (Ra) in time during the period 1950–2011 was also explored (as well as for the months January and July) as you can see in Figure XX. But the results of linear trend and moving 5-year average were not statistically significant – the index of determination was on the order of single hundredths, hence the trend curves were not represented in the graph.

Points of inflexion were also studied. The humid (or dry) year is often followed by the opposite extreme (e.g., dry year 1970 followed by a wet one in 1971 or the humid 1985 was succeeded by the dry 1986).

Afterwards, the peaks were compared with literature to see whether or not they were followed by a hydrological (or another) response (e.g., minimum by a drought, maximum by a flood). In a majority of cases, the local maxima of Ra were also followed by floods (Schäfer et al. 2012). For example, the year 2001, which was the most humid year for the majority of examined stations (the highest annual rainfall of 3170 mm was collected at *Sewen-Lac Alfeld* station, no. 1), and was also marked by an extreme rainfall in the end of December (264 mm were measured from 28th and 29th of December at *Sewen-Lac Alfeld* meteorological station, no. 1) that was followed by an overflowing of the Moselle, Meuse, Erlenbach and Thur rivers; even a landslide happened with one fatality (IHMÉC 2008).

Minima of Ra were frequently followed by a hydrological and agronomical drought. In 2003 the meteorological drought which was transformed even into a socio-economical drought was recorded in almost whole of

Western Europe (Söder et al. 2009). In Metropolitan France, it caused (with the heat wave) 15,000 casualties from the 4th to the 20th of August (Hémon, Jougla 2003). Concerning the earlier dry episodes, Amigues et al. (2006) demonstrated that the meteorological drought of 1976, 1991 and 1996 was followed by the pedological or hydrological one.

No available information was found about the adverse impact of the meteorological drought in 1971, even though the data in Figure XX suggest that this episode should have been quite significant. At *Sewen-Lac Alfeld* as well as at the *Strasbourg* station (no. 1 and no. 8) the annual rainfall for 1971 was only about half of the average (1200 mm contrary to $\overline{Ra}$ = 2330 mm at no. 1 and 432 mm in contrast to $\overline{Ra}$ = 730 mm on average at station no. 8). This could be related to the insufficiency of data or due to a systematic error resulting from the conversion of values of solid precipitation to values of liquid precipitation that was much more error-prone in the past (e.g., Štěpánek 2007). The winter period 1970/1971 was not only extremely cold but also rich in precipitation – e.g., from the 1st to the 10th of March in 1971, 25 cm of new snow cover was recorded in North-Western France (Fondevilla 2004). Another reason could lie in the anemo-orogaphic system after Jeník (1961) – the examined station could be at a non-favourable place to accumulate snow (snow could be taken away by wind) as observed for example at Giant Mountains (*Krkonoše* in Czech) situated in the Czech Republic.

3.5 Inter-monthly variability

The inter-monthly variability examined through cumulative distribution curves for the months of January and July is documented in Figure XXI. The variability between the determined categories is greater in winter than in the summer period – the curves are farther apart and oscillate more in winter (from 4 to 670 mm in January compared to 13–347 mm in July). This could be connected with the more frequent occurrence of extra-tropical cyclones in the winter period (Gulev et al. 2001). The cyclones are generally moving from west to east across the Vosges mountains and as a consequence the rain shadow is more present in winter (REKLIP 1995), so that the left outliers are missing in the January curves in Figure XXI. Hence the spatial variability of precipitation is significant in January. However since the January curves are more linear, the precipitation should be more evenly temporally distributed.

The absolute inter-monthly variability is the greatest for the mountainous (i) category of stations (e.g., *Wildenstein*, no. 2). It is interesting that for these stations a relatively few dry months of July are observed whereas dry January is much more frequent for lowland stations – category (iii). The determined categories above (see section 3.2) are evident in January in contrast to July where the differences are less obvious.

To improve data readability, five stations were selected as representatives to compare the inter-monthly variability of rainfall value months for January and July in Figure XXII. The July variability for the most frequent values is smaller than the variability in January. The divergence from the linearity becomes much more visible for the July curves. This could be related to the fact that in July, the precipitation is less predictable (e.g., Buizza et al. 2009), contrary to January where the precipitation is greater and more regular. The convection nuclei arise relatively chaotically and their temporal and spatial distribution is hard to predict (McGuffie, Henderson-Sellers 2005). The missing left outliers for January, and thus the less frequent occurrence of outliers compared to July is also better visible in the relative expression of values.

3.6 Ombric continentality

The ombric continentality was studied using three quantitative empirical formulas – the two latest calculated as indicated in (5) and (6). The resulting values are listed in Table 2.

The two first characteristics show the expected values. The degree of continentality increases with the decreasing $\overline{Ra}$ – this is shown by the simultaneous decrease of the time of half annual rainfall (precipitation is more concentrated in the summer months) and the increasing Hrudička's index k. However, contrary to what might be expected, the most continental station is not *Oberentzen* (no. 14) but *Neuf-Brisach* station (no. 11). This could be related to the fact that the highest concentration of precipitation is in the summer months but due to the effect of Schwarzwald, it is not reaching the lowest value of $\overline{Ra}$. This is in agreement with REKLIP (1995), where it

is stated that the Schwarzwald precipitation maxima are in summer months and not in winter like in the Vosges.

The three distinct categories of stations can be also clearly identified from the same two characteristics – category (ii) stations have values of the time of half annual rainfall between 5.5 to 6.5 and values of k between 5.0 and 12.0. Note that the definition of continental climate proposed by Hrudička (1933), states that the half annual rainfall time must be less than 3 months; by this strict definition, none of these stations is continental. The stations of category (i) and the first group of category (ii) are "oceanic" and the remaining stations are "continental in transition" after the author definition.

However, by the definition of k, Hrudička (1933) as well as Nosek (1972) indicated that the smallest value ($k = 0.8\%$) should have been reached at Tórnshavn, the capital city of the Faroe Islands, whereas in the studied area the meteorological station *Sewen-Foerstel* (no. 3) shows a value of 0.6%. This raises some doubts about the empirical formulas concerning the degree of ombric continentality – for example for the meteorological station Valentia in Ireland less than 35% of precipitation is attained in summer (Mühr 2011), hence the numerator in equation (5) is smaller than zero and thus the k value is then negative, which is not consistent with the interpretation of k proposed by Hrudička.

Concerning Markham's index F, the values were calculated for every year of the studied period for the five selected stations (in Table 2 only the average values are listed). The results do not correspond well with the explanation of this index normally found in literature (Tolasz et al. 2007; Brázdil et al. 2009) – for the most oceanic stations, category (i), a smaller value of F would be expected according to all the previous results, but

Tab. 2 Degree of continentality for 14 examined meteorological stations for the period 1950–2011.

	Meteorological station (number | name)	Time of the half annual rainfall [month]	Degree of continentality k [%] by Hrudička	Markham's index F [%] for five selected stations
1	Sewen – Lac Alfeld	7.4	0.9	19
2	Wildenstein	7.2	1.7	15
3	Sewen – Foerstel	7.5	0.6	–
4	Longemer	6.8	3.1	10
5	Mittlach – Erbe	7.2	1.6	–
6	Le Hohewald	6.5	5.2	–
7	Aubure	6.5	5.4	5
8	Strasbourg	4.9	17.0	–
9	Barr	5.7	11.0	–
10	Kayserberg	5.6	11.7	–
11	Neuf – Brisach	4.7	21.7	–
12	Ebersheim	4.9	18.2	–
13	Rouffach – Chs	5.1	16.2	–
14	Oberentzen	5.0	18.0	14

these stations show on the contrary the greatest value in the examined area! This could be caused by the same type of error – addition of opposite vectors – as in the case of the centre of gravity of precipitation, mentioned above. But more probably this is caused by a misinterpretation of this index F. The index represents whether or not the precipitation is distributed evenly in a year. This means that its values have to be the smallest for the category (ii) with two maxima (neither the summer nor the winter maximum significantly surpasses the other), in Table 2 represented by the *Aubure* station (no. 7). This is obvious from the form of the near-elliptical shape of the curve and the minimal magnitude of resultant vector in Figure XIX.

Thus the index F should be interpreted that it could reach high values not only for continental stations but also for purely oceanic stations that are dominated by a winter maximum of precipitation. Small values of F are obtained, with a changing time of the maximum or two regular opposing maxima. It should be noted that no relationship between F and either the altitude of the station or Ra was recognized, and no trend was identified either.

3.7 Daily precipitation totals

The variability of the daily rainfall (Rd) was examined. The results of the cumulative distribution functions are presented in Figure XXIII. In term of the absolute values, it can be assumed that a higher variability occurs for category (i) stations situated in the Vosges, compared to category (iii) stations in the Upper Rhine Plain. This statement is consistent with the results of the cumulative distribution function for January and July (Figure XXI).

It is interesting that even in the daily resolution, the effect of the Vosges mountain range is clearly present – most of the precipitation falls in the area of the main crest, somewhat less at the leeward slopes and significantly less precipitation in the Upper Rhine Plain. The curves for the three categories of stations do not cross each other, with the exception of the category (ii) and the category (iii), where outliers of *Kayserberg* station (no. 10) lay in some cases below the outliers for *Strasbourg* station (no. 8).

To make the results clearer, the curves were related to the average daily rainfall ($\overline{Ra}$) only for five selected stations (Figure XXIV). The new curves of the stations situated in the Vosges mountain range differ from the curve of the *Oberentzen* station (no. 14) situated in the Upper Rhine Plain. For *Oberentzen*, the interval of values is much smaller on the x-axis and y-axis compared to the others. Thus the variability of precipitation in the area of the rain shadow is different compared to the mountainous stations – the intensified convection in summer in the lowland stations could not surpass the maxima of category (i) stations. This is supported by the fact that the difference between the average daily rainfalls is about 7 mm:

10.9 mm at *Sewen-Lac Alfeld* (no. 1) in contrast to 3.8 mm for *Oberentzen* (no. 14).

For the category (i), i.e. oceanic stations, precipitation took place on more than 50% of the days, compared to the lowland *Oberentzen* (no. 14) with at most 40% days with precipitation. This supports the statement that for the category (iii) stations the precipitation is more concentrated.

The highest daily totals are typically situated in the Vosges mountain range and the intensified convection in summer in lowland stations could not surpass this maximum.

Nevertheless, the shape of the curves could be influenced by the outliers (extreme precipitation). Thus these outliers could be interesting for future research in this field.

With regards to the absolute daily maxima, surprisingly, in a majority of cases these do not occur at the month of maximum of precipitation. For example, for *Wildenstein* (no. 2), 157 mm of rain fell on the 30th of May in 2000, rather than in December. The very same day a total daily maximum for all the 14 examined stations and the whole study period was reached at the *Mittlach-Erbe* station (no. 5) at 190.5 mm. To examine the synoptic situation is beyond the scope of this paper. However, this is quite frequent in other areas. That is, intensification of convection in one year in summer can produce relatively higher rainfall than in a standard period of maximum rainfall (Heyer 1993). But notice that for the most humid and the driest station the absolute daily maximum occurred in the month of maximum rainfall (169.1 mm for *Sewen-Lac Alfeld* on 29th of December and 68.9 mm on 15th of August for *Oberentzen*).

4. Conclusion

This paper describes a climatological research in a region influenced by orography (the Vosges mountain range and their lee) – from annual to daily rainfall resolution. Three categories of stations are identified based on the differences in the annual temporal distribution of precipitation.

For the first time in the studied area, the ombric continentality is quantitatively described. The Vosges cause a relatively fast transition into a more continental climate in their lee with a maximum of precipitation in summer (Upper Rhine Plain) and not in winter (like in the Vosges). However, some difficulties with empirical formulas are found (e.g. Hrudička's index k). For future research in this area it would be interesting to determine a real limit between oceanic climate and climate in transition.

The analysis using the shape of the cumulative distribution function has never been applied before for this region. Nevertheless, the influence of outliers (extreme

values) can be high. Thus it is strongly recommended for future research to examine these values.

Acknowledgements

REFERENCES

AMIGUES, J. P., DEBAEKE, P., ITIER, B., LEMAIRE, G., SEGUIN, B., TARDIEU, F., THOMAS, A. (2006): Sécheresse et agriculture: Réduire la vulnérabilité de l'agriculture à un risque accru de manque d'eau. Collectif scientific analysis. France, INRA, 72.

BANKANZA, J. C. M. (2011): Time variation of the effect of geographical factors on spatial distribution of summer precipitation over the Czech Republic. IDŐJÁRÁS 115 (1–2), 51–70.

BARRY, R. G., CHORLEY, R. J. (2003): Atmosphere, weather and climate. New York, Routledge, 6, 421 p.

BRÁZDIL, R. et al. (2009): Climate fluctuations in the Czech Republic during the period 1961–2005. Int. J. Climatol. 29 (2), 223–242.

BUIZZA, R., HOLLINGSWORTH, A., LALAURETTE, F., GHELLI, A. (1999): Probabilistic predictions of precipitation using the ECMWF ensemble prediction system. Wea. Forecasting 14 (2), 168–189.

BÜRGER, D. (2010): Conference paper: "Influence of geo-factors (geology, climate) on the land-use patterns in the Upper-Rhine Graben". 26. 8. 2010 within the 4th Summer University about the environment sciences organized by EUCOR, Gunsbach, France.

EASTERLING, D. R. et al. (2000): Observed Variability and Trends in Extreme Climate Events : A Brief Review. Bull. Am. Meteorol. Soc. 81 (3), 417–425.

FONDEVILLA, W. (2004): Les intempéries de 1965 à 1985 [online]. Last modification 12th December 2011. [cit. 2013-04-06]. Available at: http://la.climatologie.free.fr/intemperies/tableau8.htm.

GULEV, S. K., ZOLINA, O., GRIGORIEV, S. (2001): Extratropical cyclone variability in the Northern Hemisphere winter from the NCEP/NCAR reanalysis data. Clim. Dynam. 17 (10), 795–809.

HEYER, E. (1993): Weather and Climate. Leipzig, B.G. Teubner Publisher, 9, 344 p.

HRUDIČKA, B. (1933): Contribution to the research of ombric continentality in Europe. Brno, Offprint from the writings of the Department of Czechoslovakian Geographical Society, rang C3.

HRUDIČKA, B. (1933): Time of the half precipitation and the annual repartition of periodic amplitude in Czechoslovakia. Brno, Documents published at Faculty of Natural Sciences, Masaryk University, 185.

IHMÉC. (2008): Mémoire des catastrophes [online]. France, IHMÉC. [cit. 2013-04-06]. Accessible at: http://memoiredescatastrophes.org/catastrophe/.

JENÍK, J. (1961): Alpian vefetation in Giant Mountains, Králický Sněžník Mts and High Ash Mountains: Theory of anemo-orographic systems. Prague, Czech Republic, NČSAV.

KOTTEK, M. et al. (2006): World Map of the Köppen-Geiger climate classification updated. Meteorol. Z. 15, 259–263.

MARKHAM, C. G. (1970): Seasonality of precipitation in the United States. Annals of the Association of American Geographers 60, 593–597.

McCABE, G. J., CLARK M. P., SERREZE M. C. (2001): Trends in Northern Hemisphere Surface Cyclone Frequency and Intensity. J. Climate 14 (12), 2763–2768.

McGUFFIE, K., HENDERSON-SELLERS, A. 2005. *A climate Modelling Primer*: University of Michigan, John Wiley & Sons. 3, 296 p.

Météo-France (2008): Climatology of the Vosges. Épinal, Météo-France au service des Vosges: le centre dépertemental d'Épinal (Departmental Centre of Météo-France in Épinal), 10 p.

MÜHR, B. (2007): Climate diagram [online]. Offenbach, DWD [cit. 2011-09-29]. Available at: http://www.klimadiagramme.de/Europa/strasbourg.html.

MÜHR, B. 2011. Klimadiagramme [online]. The latest modifications on 20th September 2012 [cit. 2012-09-29]. Available at: http://www.klimadiagramme.de/.

NOSEK, M. 1972. Methods in Climatology. Prague: Academia, 1, 434 p.

PFISTER, L. (1994): Rapport of several stations to spatialisation of precipitation in the High-Vosges [manuscript]. Strasbourg. Master's thesis at Faculty of Geography at University of Louis Pasteur in Strasbourg.

PRUDHOMME, C., REED, D. W. (1998): Relationship between extreme daily precipitation and topography in a mountainous region: a case of study in Scotland. Int. J. Climatol. 18 (13), 1439–1453.

REKLIP (Regio-Klima-Projekt). (1995): Klimaatlas Oberrhein Mitte-Süd = Atlas climatique du Fossé Rhénan Méridional. Offenbach, IFG, 1, 212 p. + annexes.

SCHÄFER, G., LANGE, J., WINTZ, M., SPARFEL-GARRELS, S., SPARFEL, J., MANGOLD, M., MINÁŘOVÁ, J., RABER, F., SPARFEL, Y. (2012): Actes de la 5ème Université d'Eté EUCOR, Gunsbach, France, EUCOR, 5th Summer University of Environmental Sciences EUCOR, 92 p.

SCHOLZ, M. (2008): Classification of Flood Retention Basins: The Kaiserstuhl Case Study. Environ. Eng. Geosci. 14 (2), 61–80.

SELL, Y. et al. (1998): Alsace and the Vosges: Geology, natural environments, flora and fauna. Delachaux et Niestlé, 352 p.

SHVER CA. (1975): Index of precipitation seasonality. Trudy GGO 303, 93–103.

SLÁDEK, I. (2005): Proposal for a new degree of continentality of climate. In: Physical-geographical proceedings 3, Masaryk University in Brno, 144–148.

SMITH, R. B. (2003): A linear upslope-time-delay model for orographic precipitation. J. Hydrol. 129, 2–9.

SOBÍŠEK, B. et al. (1993): Meteorological terminological & explanatory dictionary: with concept names in Slovak, English, German, French and Russian languages. Prague, Academia: Ministry of Environment of the Czech Republic, 594 p.

SÖDER, M., CONRAD, M., GÖNNER, T., KUSCH, W. (2009): Climate changes in the South Germany: Magnitude – Consequences – Strategies. Mainz, KLIWA, 20 p.

SUMMER, G., HOMAR, V., RAMIS, C. (2001): Precipitation seasonality in eastern and southern Coastal Spain. Int. J. Climatol. 21, 219–247.

ŠÁLEK, M. (2007): Orographic intensification of precipitation and its implications for quantitative precipitation estimation by meteorological radars. In: Proceedings from the 10 years of disastrous floods in Moravia in 1997. Brno, Czech Hydrometeorological Institute, p. 20.

ŠTĚPÁNEK, P. (2007): Control of the quality of data: Homogenization of time series. Brno, Czech Hydrometeorological Institute. 68 p.

TOLASZ, R. et al. (2007): Climate Atlas of Czechia. Olomouc, Czech Hydrometeorological Institute, 1, 256 p.

TREFNÁ, E. (1970): Climatography of the World. Prague, Hydrometeorological Institute, 60 p.

TROUX, A., QUILLÉ, A. (1951): The Vosges: Geography and History. Saint Dié, Weick, Hodapp et Cie, 8, 72 p.

VOTAVOVÁ, B. (2010): Analysis of the meteorological dates [manuscript]. Brno, 46 p. Bachelor's thesis at Faculty of Electrical Engineering and Communication, Department of Biomedical Engineering at Brno University of Technology. Supervisor: doc. Ing. Jiří Rozman, CSc.

ZÍKOVÁ, N. (2009): Spatial variability of precipitation annual cycles [manuscript]. Prague, 2009, 116 p. + 1 CD-ROM. Master's thesis at Faculty of Mathematics and Physics, Department of Meteorology and Environment Protection, Charles University in Prague. Supervisor: doc. RNDr. Jaroslava Kalvová, CSc.

Jana Minářová
Charles University in Prague
Faculty of Science
Department of Physical Geography and Geoecology
Albertov 6
128 43 Prague 2
E-mail: minarovj@natur.cuni.cz

RESUMÉ

Klimatologie srážek v oblasti Vogéz

Předmětem článku je klimatologie oblasti Vogéz na základě denních úhrnů atmosférických srážek 14 studovaných meteorologických stanic z oblasti pohoří a jeho závětří (Hornorýnská nížina) za období 1950–2010. Pro odlišnosti v ročním chodu srážek byly stanice rozděleny do tří kategorií: (i) horské s jedním výrazným srážkovým maximem v zimě, (ii) stanice na závětrných svazích se dvěma srážkovými maximy – letním a zimním a (iii) stanice ryze závětrné nacházející se v nížině východně od Vogéz s jedním letním srážkovým maximem. Metody kvantitativního hodnocení stupně ombrické kontinentality vedou ke zjištění, že Vogézy tvoří hranici mezi oceánickým a kontinentálním, resp. přechodným podnebím. Další výzkum zejména extrémních denních úhrnů srážek je však žádoucí.

POLITICAL REGULATIONS AND SOCIAL PERCEPTION OF NATURAL RISKS: "RISK SOCIETY", THE CZECH EXPERIENCE AND THE EUROPEAN CONTEXT

PAVEL RAŠKA

J. E. Purkyně University, Faculty of Science, Department of Geography

ABSTRACT

Recently, the political and social notion of natural risks and disasters has gained increasing attention, partly as a result of high-magnitude disaster events in last decades. In this regard, the concept of social vulnerability has been incorporated into international legal frameworks and strategies of disaster risk reduction, emphasizing that the effective ways to reduce natural risks are inherently related to social action at different institutional levels. The shift in research agenda towards vulnerability assessment and social notion of natural risks seems to be less intensive in Czechia, however, which is due to epistemological traditions in geosciences and regional studies in the country. Therefore, the background aim of the study is to raise a discussion on emerging research themes for geoscientists and regionalists in the country-wide perspective through the two specific aims. First, we evaluated the success of Czech political representatives in implementing the international legal frameworks and strategies into the national and regional policies. Our results of analysis of strategic documents and legal frameworks suggest that although the issue of natural risks is well incorporated into the strategic documents and legal frameworks in Czechia, these documents do not sufficiently reflect the international agreement on the necessity of a conceptual shift towards a social vulnerability concept within disaster risk reduction. Second, we analysed social perception of natural risks in a case study of the city of Ústí nad Labem in northern Czechia. On one hand, the analysis has revealed that the issue of natural risks, represents an important short-term decisive factor for local community. On the other hand, the long-term perception of natural risks, as analysed using the econometric data about the impacts of natural hazards on real estate property, has shown that the social perception of risk, during the periods between the individual disaster events and after these events is relatively weak. This may represent a significant constraint for the implementation of community-based strategies of disaster risk reduction.

Keywords: natural risk, risk society, legal documents, social perception, Czechia

1. Introduction

1.1 Social vulnerability to natural disasters

During the last three decades, the social notion of natural risks and disasters has gained increasing attention in the literature. After several papers were published since the 1950s, Hewitt's work (Hewitt 1983) became a landmark for social scientists, establishing a human ecological perspective to disaster studies. Later, the general perspective of the approach was guided by the emergence of the concept of risk society, which was introduced by Beck (1992) and further developed by Giddens (1999). In his seminal work, Giddens noted that the risk society is a society that is increasingly engaged with its future and that produces phenomena and processes that are well beyond the experiences of that society. The emergence of the risk society is then reflected by politicians, he continues, who tend to represent their social responsibility by scaremongering; however, no one is in fact specifically responsible for the impacts of risks, and the state is referred to as "organised irresponsibility". The research agenda of social sciences has encountered natural risks and their impacts as a social process (Breakwell 2001; Wisner et al. 2004), and significant effort has been made to study the social production of natural risks and their impacts. Steinberg (2000), for instance, argued that it was a common practice of local and national government in the United States to put the blame for risks on random extreme natural processes, which cannot be forecast, to avoid the responsibility for the impacts of natural risk and to justify socially unequal policies.

In this regard, studies on the social aspects of natural risks have been a counterbalance to the geologic, geomorphologic and hydrometeorologic research of natural hazards, although some issues of the social and economic impacts of natural hazards have been incorporated into the studies done in these disciplines through the economic impact analyses (Schuster, Highland 2001; Fleming, Taylor 1980) and vulnerability assessments (Alcantara-Ayala, Goudie 2010; Hufschmidt 2011). Despite bringing both the social- and geo-scientific research approaches closer together, the a priori preference of these disciplines towards certain components of the natural risk model as constructed in Genève (UNDRO 1979) is still obvious. To a certain degree, such preferences are self-evident and logical because the focal disciplines dealing with natural risks have different epistemologies resulting in various methods and techniques employed (Cutter 1996; Alcantara-Ayala 2008; Cardona 2008; Raška, Anděl 2012). The social scientific approaches have deeply criticised the natural and applied sciences for their approach

to vulnerability as a process limited to potential physical damage or to demographic determinants (cf. Blahůt and Klimeš 2011). According to these critiques, "the vulnerability cannot be defined or measured without reference to the capacity of a population to absorb, respond and recover from the impact of the event" (Cardona 2008: p. 43).

1.2 The emergence of community-based strategies and the political action

According to the above mentioned perspective, the effective ways to reduce natural risks are inherently related to social action at different institutional levels, ranging from global and national policies and across regional governance to the business sector and especially to the local communities. Lately, many authors have argued for the fundamental role of community-based (local-based) strategies to mitigate the impacts of natural disasters. These strategies were studied using various sociological frameworks and resulted in a shift from hazard-based to vulnerability-based mitigation strategies within the disaster cycle (Sarewitz et al. 2003; Pelling 2003; Peltonen in Schmidt-Thomé 2006 ed.). Drawing upon the concept of risk society and social activities in disaster risks reduction, recent studies dealing with community-based strategies have aimed at both policy frameworks (e.g., Pelling 2003; Manuel-Navarrete et al. 2011) and the social perception of natural risks (Slovic 1987; Placer, Delquie 1999; Bruen, Gebre 2001). Among other issues, the studies on risk perception have focused on the question "how natural risks are understood by public and how public perceive political action and expert discussions concerned with natural risk mitigation?" (e.g., Sjöberg 1999). These studies resulted in considerations on necessity of complex learning from disasters (e.g., Choularton 2001; Corbacioglu, Kapucu 2006), even though Bubeck et al. (2012) has shown on the example of floods that the adoption of private mitigation measures cannot be clearly statistically explained by increased social perception of natural risks.

Along with and in part as the result of the social scientific research on natural risks, the notion of natural risks has also come to be increasingly appreciated in European policies. Accordingly, due to the effort of the United Nations in identifying the most vulnerable regions, evaluating the frequencies and environmental links of natural risks and setting the strategies for disaster reduction (e.g., UNDRO 1979; UN 2005), the European Union and individual European countries have made a huge effort to include these issues in their legal documents and policies (e.g., EC 2010) by having a pro-active attitude toward disaster risk reduction in setting regional policies and within local communities. Judging from these documents, the political regulation in natural risk issues seems to be a matter-of-course. In contrast, the efficacy of implementing the legal agreements and mitigation strategies at the regional and local levels is not so clear. Ambiguities

arise when taking into account the social perception of natural risks because various communities have different experiences with natural risks due to different degrees of exposure as well as the cultural and intellectual determinants among these communities. Dostál (2010), for instance, has used the data from Eurobarometer to assess the different attitudes towards the environment and environmental policy in members states of the European Union (EU). His results indicate that, although there is a certain association of natural disasters when discussing the environment across the EU, the attitude toward the environment in the old member states is based upon post-materialistic values and abstract cognitive insights and tends to be more general, while the attitudes of people in the new member states from East-Central Europe is based upon the direct experience of material survival. Taking these results into account and drawing upon territorial inequalities in environmental quality and in the social and economic impacts of natural risks in the last few decades within the European countries (CRED 2009; MunichRe 2009), we may suppose that such perceptual differences would be observed on a regional scale of individual countries as well.

Finally, these results indicate that the general concept of a risk society can hardly be self-explanatory and useful in the practice of natural risk mitigation, if not studied at various territorial levels in different natural and cultural settings. Despite the fundamental meaning of the risk society concept for a social theory, the constraints of the risk society concept for the practice of natural risk reduction are as follows: (a) the concept tackles a broad spectre of risks without any particular emphasis on natural risks and (b) the concept explains general societal behaviours (of Western Civilisation) regardless of concrete regional setting of risks. Accordingly, the efficacy of international efforts to set out community-based strategies for disaster risk reduction must be evaluated at the regional and local levels.

1.3 Research aims

Contrarily to the situation abroad, there has been a rather limited effort to study the political and social aspects of natural risks in Czechia, however. The pioneering works of Dostál (2005, 2008), Vilímek and Spilková (2009) and Blahůt and Klimeš (2011) have focused on the theoretical considerations of methodological plurality within the (natural) risks studies and on terminological questions, but not on the social production of natural risk itself. The reason for the lack of studies dealing with social dimension of natural risks in Czechia may be explained by epistemological traditions within the geoscientific and regional studies. While the physical geographers has long pursued the geoecological and palaeoenvironmental paradigm in the study of natural environment, the social geographers and regionalists focused on interactions within the social system

itself (Hampl et al. 2007), and therefore the complex approach to natural risks has been a latecomer in the research agenda.

The aim of this study is to evaluate the level of political regulation and the social perception of natural risks in Czechia. As a member state of the EU, Czechia must act in accordance with the general legal frameworks for natural risk reduction. Therefore, our first aim is to discuss how successful the Czech political representatives were in implementing these frameworks and the latest approaches of social scientific insight into the natural risk issue into the national and regional policies. The background aim of the study is to raise a discussion on emerging research themes for geoscientists and regionalists in the country perspective.

Most of the research will be carried out in urban regions (Figure 1), which enables us to assess the links between policies at different territorial levels, on the one hand, and the massive social experience with natural risks, on the other. The country-wide analyses will be put in a European context and based upon content and discoursive analyses of legal and strategic documents. If the political acceptance of the social vulnerability concept is to be efficient in disaster risk reduction, it must in

turn be counterbalanced by the increasing social notion of natural risks in local communities (Delica-Willison, Willison 2008) and by complex organizational learning (Corbacioglu, Kapucu 2006; Innocenti, Albrito 2011). Therefore, the second aim of this study is to analyse the social response to natural risks in Czechia with the case study from the city of Ústí nad Labem, which is based on the combined methodologies of environmental geography and sociology for the analysis of both the short-term and long-term impacts of natural risks on a social system of the urban region.

2. The political regulations of natural risks: the view through legal and strategic documents

The current attention paid to natural risks by various disciplines undoubtedly results from the increasing frequency of documented disaster events in the latter part of the 20th Century. The annual report of the MunichRe (MunichRe 2009) reveals that the number of disaster events has doubled between the years 1980 and 2009. The majority of these disasters are categorised among the hydrologic and meteorological extremes. Although
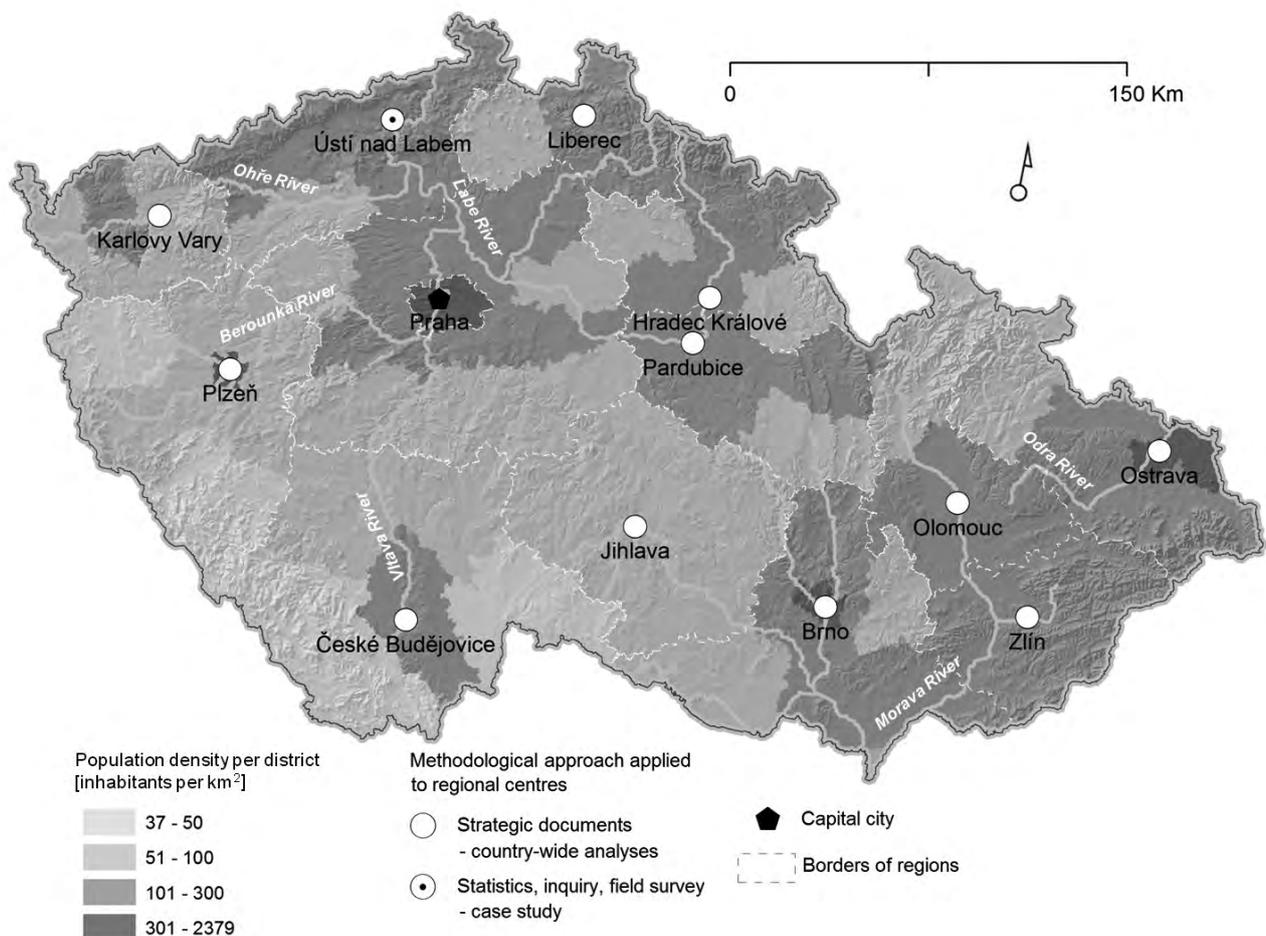
Fig. 1 Urban regions (regional centres) analysed in this study.

the increase of documented events does not necessarily represent a real increase in the frequency of the disaster events, even a stable frequency of disaster events may have larger social and economic impacts because of the greater vulnerability of societies. An increase in the social impacts of disaster events is apparently shown by the rising number of insured losses (MunichRe 2009), even though not all possible disaster impacts may be insured. During the period between 1980 and 2009, the member states of the European Environmental Agency faced approximately 4,500 disasters that caused 108,000 casualties (EEA 2010). While the majority of the casualties were caused by earthquakes and meteorological extremes (high temperature waves), the hydrologic (floods, flash floods) and meteorological (rainstorms, etc.) events are responsible for the highest economic losses. However, the quantitative data regarding losses can hardly represent the objective degree of risk, because various types of natural risks affect different societies with varying intensities (e.g., Raška and Anděl 2012).

The existing disaster statistics and recent progress in vulnerability analyses and mapping have pushed political representatives to conceptualise the fight for disaster reduction by creating legal frameworks and strategic documents for the implementation of these efforts. The Report of Expert Group Meeting of the Office of the United Nations Disaster Relief Coordinator (UNDRO 1979) has become a milestone for the political regulation of natural risks. During the next few decades, the international organisations have made an immense effort to set out the appropriate policies of disaster risk reduction. The major strategic documents resulting from this effort are summarised in Table 1.

Along with their institutional (legal) aspect, the aims of these documents illustrate the discursive shift of disaster studies toward the social vulnerability concept and the creation of community-based strategies for coping with disastrous events. The 1990s were designated as an International Decade for Natural Disaster Reduction. After the World Conference on Disaster Reduction in Yokohama, Japan in 1994, the United Nations General

Tab. 1 Selected Global and European strategic documents and reports concerned with the issue of natural hazards and risk.

Title	Source	Major focuses
Natural disasters and vulnerability assessment	The United Nations Disaster Relief Organization (UNDRO 1979)	definition of basic terms, conceptualisation of natural disasters, aims of future action
International Strategy for Disaster Reduction	The United Nations (UN 1999)	strategic and systemic approach to disaster impact reduction
The Hyogo Framework for Action	United Nations (UN 2005)	strategic and systemic approach to disaster impact reduction at different institutional levels
EU Strategy for supporting disaster risk reduction in developing countries Implementation Plan of the EU Strategy for supporting disaster risk reduction in developing countries 2011–2014	European Commission (EC 2009, 2011)	strategy of sustainable development through reducing the impacts of disasters in developing countries
Making Cities Resilient. My City is Getting Ready	The United Nations Office for Disaster Risk Reduction (UNISDR 2010)	improving knowledge and coping strategies of local urban population
Disaster Risk Management and climate Change Adaptation in Europe and Central Asia	World Bank Global Facility for Disaster Reduction and Recovery (WB 2010)	financial and insurance instruments, overview of risk mitigation measures, emergency management, public policy
Mapping the impacts of natural hazards and technological accidents in Europe: An overview of the last decade	European Environmental Agency (EEA 2010)	review and statistics of natural hazards and their impacts
A Community approach on the prevention of natural and man-made disasters	European Parliament (EC 2010), based on EC communication	research, cooperation of actors, improving legislative and financial instruments
Revealing Risk, Redefining Development – Global Assessment Report on Disaster Risk Reduction 2011	United Nations (UN 2011)	assessment of implementation and progress of disaster reduction strategies into global and regional policies, defining regional development strategies, problem of droughts as hidden risk
Humanitarian Emergency Response Review	HERR (2011), United Kingdom	report on humanitarian help
Towards a stronger European disaster response: the role of civil protection and humanitarian assistance	European Commission and Parliament (EC 2011)	increasing the efficiency of disaster response, creation of European Emergency Response Capacity, creating maps and scenarios
Prevention of natural disasters in Europe and Latin America	Euro-Latinoamerican Parliamentary Assembly (EuroLat 2013)	strategies of prevention and reduction of impacts of natural hazards, fight against climate change, monitoring and research, governmental action

Assembly adopted the International Strategy for Disaster Reduction at the turn of 1999 and 2000 and has established The United Nations Office for Disaster Risk Reduction, which is responsible for the implementation of further agreements, especially The Hyogo Framework for Action for the years 2005–2015 (UN 2005). Similar to the United Nations, The European Union institutions have conceptualised the strategy of disaster reduction through their legal frameworks with a significant focus on community-based approaches and civil protection during and between the natural risk events (EC 2010, 2011).

Within the Czech milieu, the issue of natural risks has been long incorporated into legal documents with a particular focus on crisis management during the disaster events. The process of crisis management is described mainly in Act No. 240/2000 of Crisis Management and Act No. 241/2000 of Economic Measures during the Crisis Situation. The other legal acts are devoted to (a) the strategy of an integrated emergency system (Act No. 239/2000) and the duties of public actors during the emergency, such as army forces (Act No. 219/1999) and fire departments (Act No. 237/2000), and (b) the protection against disaster events within the specific territorial and landscape features (landscape protection in Act 114/1992, water bodies in Act No. 254/2001, etc.). Most of these legal frameworks do not represent the strategy for disaster risk reduction, however. The shift toward these strategic reduction measures may be observed during the last 15 years primarily as the result of high magnitude flood events in 1997 and 2002. Since that time, the natural risk issue has been increasingly incorporated into general safety strategies (the Safety strategy of the Czech Republic, starting with 1999 and actualised in 2001, 2003 and 2011) and into strategies that are directly aimed at disaster risk reduction, e.g., the Strategy of protection against floods (Collective 2000) and Act No. 236/2002 Methods for Delimitation of Flood Areas. Moreover, Czechia has become a member of National Platforms for Disaster Risk Reduction in Europe and participated in the Natural and Technological Risk theme within the ESPON Programme (European Observation Network, Territorial Development and Cohesion). Nevertheless, the discoursive shift from hazard-based to vulnerability-based strategies (Sarewitz et al. 2003) has not been so successful. While there is rising support for research teams studying natural hazards and risks (Falc 2001), the overall mitigation strategies are still largely focused on measures after the disaster events rather than systemic disaster risk reduction (Čamrová 2006).

Considering the recent international agreement regarding the necessity for establishing community-based strategies for natural risk reduction, we have performed analyses of regional planning documents for regional centres in Czechia along with the national legal frameworks. The Integrated Plans of City Development (IPCD) have been selected as the appropriate types of documents because they represent the up-to-date strategic frameworks for the development of urban centres as created by the local authorities. In addition, the primary goal of the IPCDs is to establish a framework for obtaining the financial support from the European Structural Funds, and therefore they are clearly linked to higher territorial level strategies. We have analysed 24 IPCDs of 12 regional centres except Prague (Praha) and Central Bohemia. Although the exposure to different natural hazards in these cities varies, each of these regional centres is exposed to at least some of the hazards. Some of the IPCDs are devoted to the entire city, while part of the analysed documents deals only with certain city quarters. The results of our analysis (Table 2) indicate that the natural risk issues are mostly discussed in the IPCD designed for the whole city. Most of the comments on natural risk are related to floods, while the discussion of geologic (e.g., landslides) and meteorological (e.g., storms, heat waves) risks is absent. In 58% of the IPCDs, there is only a scarce comment on natural risks, mostly in the analytic part of the document and in the SWOT analysis, noting the presence of past natural risk events. Natural risks represent a central component of the IPCD in only a few cities (Plzeň, České Budějovice), where these risks are considered an important factor to implement the strategic aims of city development. In both Plzeň and České Budějovice, the importance given to the natural risk issue is influenced by past flood events at the Berounka and Vltava Rivers, respectively. In the IPCDs that pay detailed attention to natural risks, the comments are usually related to flood prevention, the protection against floods, economic measures during the flood events, flood and evacuation plans, and the application of flood issues to environmental education (IPCD Ústí nad Labem – Centre). In this respect, natural risk issues represent an integral, although minor, segment of the development strategies of regional centres. In contrast, only minor progress can be seen in the conceptual shift toward social vulnerability strategies of disaster risk reduction within the IPCDs, where only the IPCD of the city of Ústí nad Labem includes the example of educational goals to reduce natural risks through the vulnerability concept. In contrast to the national strategic documents and to the IPCDs, which include more or less explicit discussion of natural risk issues, the nationwide document Principles of Urban Policy, published by the Czech Department of Regional Development (Collective 2010), includes only non-specific comments concerning newly arising threats to the urban environment and the necessity for a complex approach to natural risk mitigation. Any comment on natural risk is lacking in the description of the strategic goals devoted to the urban environment, which is in strict contrast to the international documents devoted to urban development (Kreimer et al. 2003; UNISDR 2010).

Tab. 2 Results of analyses of Integrated Plans of City Development.

| | analysed IPCD | | issues related to natural hazards | | | |
| | | | brief comments | | detailed comments | |
	n	f [%]*	n	f [%]**	n	f [%]**
IPCD aimed at city	13	54,2	7	53,8	6	46,2
IPCD aimed at centre	2	8,3	1	50,0	1	50,0
IPCD aimed at quarters	9	37,5	6	66,7	3	33,3
total	24	100,0	14	58,3	10	41,7
examples of comments in documents			– reference to impacts of past hazards – brief note within SWOT analyses		– reference to impacts of past hazards – comments on present and future risks – detailed comments on mitigation measures – environmental education	

Source: analyses of public documents from 12 regional centres available in 2012 except Prague (Praha) and Central Bohemia. IPCD – Integrated Plan of City Development (see text for explanation).

3. The social perception of natural risk: the case study of the city of Ústí nad Labem

The efficiency with which the conceptual shifts in disaster studies reach territorial planning efforts and natural risk management is influenced by the social notion of natural risks from both the country-wide and community perspectives (cf. Klimeš, Blahůt 2012). Regarding the social perception of natural risks, the Special Eurobarometer survey No. 365 carried out in 2011 offers the results on the perception of the environment across the member states of the European Union, including the issue of natural hazards (Eurobarometer 2011; see also Dostál 2010 for a discussion). When discussing the environment, 26% of respondents think of natural disasters (question QB2T), which is the same number as in Czechia. In both all EU states and in Czechia, however, natural disasters were listed last, after protecting nature, climate change, man-made disasters, and the quality of life. In total, 31% of EU citizens listed natural disasters as an issue they are worried about (question QB3) compared to 34% in Czechia. However, these results give only a general view. Moreover, the survey is not able to convey the complexity of the social notion of natural disasters. That is because the answers to questions aimed directly at the subjective perception of natural disasters reflect intellectual insight into the problem during the survey but not the realistic behaviour of respondents during and between the individual disaster events, as can be seen from field observations and as tested by the assessment of indirect indices. Therefore, it was necessary to complement the general survey with a more detailed case study using combined quantitative and qualitative methodologies. In this chapter, we present the analysis of the public perception of natural risks and the short-term and long-term effects of natural risks on social systems. The analysis was carried out in a case study of the city of Ústí nad Labem.

3.1 Natural risks in Ústí nad Labem

The city of Ústí nad Labem (population of 93,747 in 2013) is located at the confluence of the Labe River and Bílina River in N Czechia (Figure 1). With its annual discharge of 308 m³ s⁻¹ at the country border in Hřensko, the Labe River is the largest river in Czechia with many documented historical flood events since the 19th Century (Figure 2; Table 3). These flood events had immense impacts on the local society functioning and on infrastructure because the whole city centre spreads within the deep valley bottom in the flooding area. The high-gradient tributaries of the Labe and Bílina Rivers suffer from flash floods, the impacts of which have resulted in further modification of the channels of these streams including protection dams. At the same time, the steep slopes built by different lithological units and exceeding 30° have been exposed due to the evolution of the Labe River valley, and these slopes are highly prone to various types of mass movements. The historical records of landslides and rock fall events within the city have been analysed by Raška et al. (2013). Finally, the peripheral sites of the city located at higher elevations are exposed to meteorological extremes, such as rainstorms and windstorms.
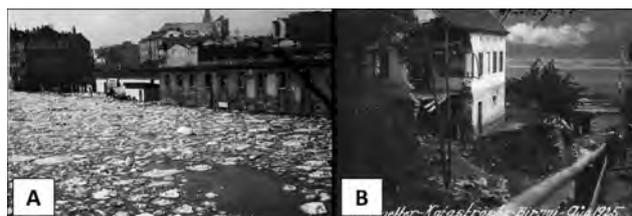
Fig. 2 Photos of historical spring flood in the city of Ústí nad Labem in 1920 (A) and summer flash flood in present-day city quarter Brná nad Labem in 1925 (B). Source: Archive of the Museum of the Ústí nad Labem city.

Tab. 3 The flood events at the Labe River in Ústí nad Labem in the 20th Century.

Flood magnitude [Q recurrence – approximate water level]	Year
Q_{100} – 1150 cm	2002
Q_{50} – 1080 cm	1845
Q_{20} – 980 cm	1862, 1890, 2013*
Q_{10} – 910 cm	1920, 1940
Q_5 – 820 cm	1923, 1941, 2006
Q_2 – 690 cm	1926, 1947, 1954, 1981, 1988, 2003

Based on the database of Povodí Ohře and Povodí Labe companies.
*current flood from June 2013, culmination at 1071 cm

During the last two decades, the city of Ústí nad Labem has been affected by several natural hazards, which are summarized in Table 4. These natural hazards included floods, flash floods, windstorms and landslides affecting both the inner city and the city periphery (Balej et al. 2007; Raška et al. 2011), but the fundamental impacts in terms of the complex character and spatial extent of the hazard have been caused by floods mainly in 2002 and 2006. Therefore, the following analyses will be primarily devoted to the short-term and long-term impacts of flood events in the city of Ústí nad Labem. The short-term impacts/effects are understood as those apparent during the disaster event or explicitly related to the event, while the long-term impacts/effects denotes the processes between individual disaster events and after them.

3.2 Short-term impacts and social perception of selected natural risks

The impacts of natural hazards in the city of Ústí nad Labem during the last two decades affected both the local communities and infrastructures. Moreover, the indirect effects of the natural risks were also apparent in city quarters, which are quite far from flood risk zones or sites of landslides, because the changes in the flow of traffic during the times of floods and other hazards resulted in the decreased accessibility of local communities to jobs and services among other effects.

The short-term effects of natural risks are well represented by changes in the local mobility of communities within the city and by the subsequent changes in the daily rhythm of localities. The issue of daily mobility has been discussed by Ellegård (1999) as an apt representation of the complex time-geographical approach to the study of the behaviour of people in concrete environments. Our assumption was that the daily mobility and rhythm of localities differentiates distinctly during anomalous events, such as natural disaster events. The daily rhythm has been analysed via repeated field survey at these sites during the flood events in 2002, 2006 and 2010. The assessment was then based on the qualitative assessment of observations and of collected photographic material according to the methods of visual sociology (Sztompka 2007), and supplemented by analysis of the Flood Protection Plan (Klenerová et al. 2004). The results of analyses of the daily rhythm at selected localities before, during and after the flood events in the city of Ústí nad Labem is shown in the Figure 3.

The major factor that influences the mobility of communities is concerned with determination of alternative corridors of mobility in areas that are not affected by floods. During the flood in 2002, the water level reached parts of the city quarters of Střekov, Ústí nad Labem – centre, Krásné Březno, Neštěmice, and Vaňov a Svádov including important traffic connections (Figure 4 for map). In turn, an alternative net of traffic lines evolved, which also included the connections that are usually not used (sidewalk across the railroad bridge). The bus traffic

Tab. 4 Major natural hazards and their impacts in Ústí nad Labem between 1990 and 2013.

Year	Type of natural hazard	Affected locality	Impacts, consequences
1994	landslide	Skalka residential zone	threat to buildings and roads
1995	landslide	Vaňov quarter	threat to buildings and roads; construction of retaining wall
2002	flood	city centre, Střekov	damage to roads and buildings, complex social impacts, limits to town traffic, indirect economic losses
2006	flood	city centre, Střekov	damage to roads and buildings, complex social impacts, limits to town traffic, indirect economic losses; completion of flood protection wall for Q_{20}
2007	windstorm (Kyrill)	higher-elevation sites	damage to forest sites; wood harvest, revegetation
2007	collapse of retaining wall (due to slope instability)	Větruše chateaux	destruction of viewpoint terrace, potential threat to visitors
2008	windstorm (Emma)	higher-elevation sites	damage to forest sites; wood harvest, revegetation
2010	flood, flash floods	city centre, Labe River tributaries	destruction of local hydrotechnical features, local limits to town traffic
2013	flood (concurrent)	city centre, Střekov	damage to roads and buildings, complex social impacts, limits to town traffic, indirect economic losses

The impacts and consequences according to town government reports, reports on city environment (Collective 2012) and rectified by own field survey.
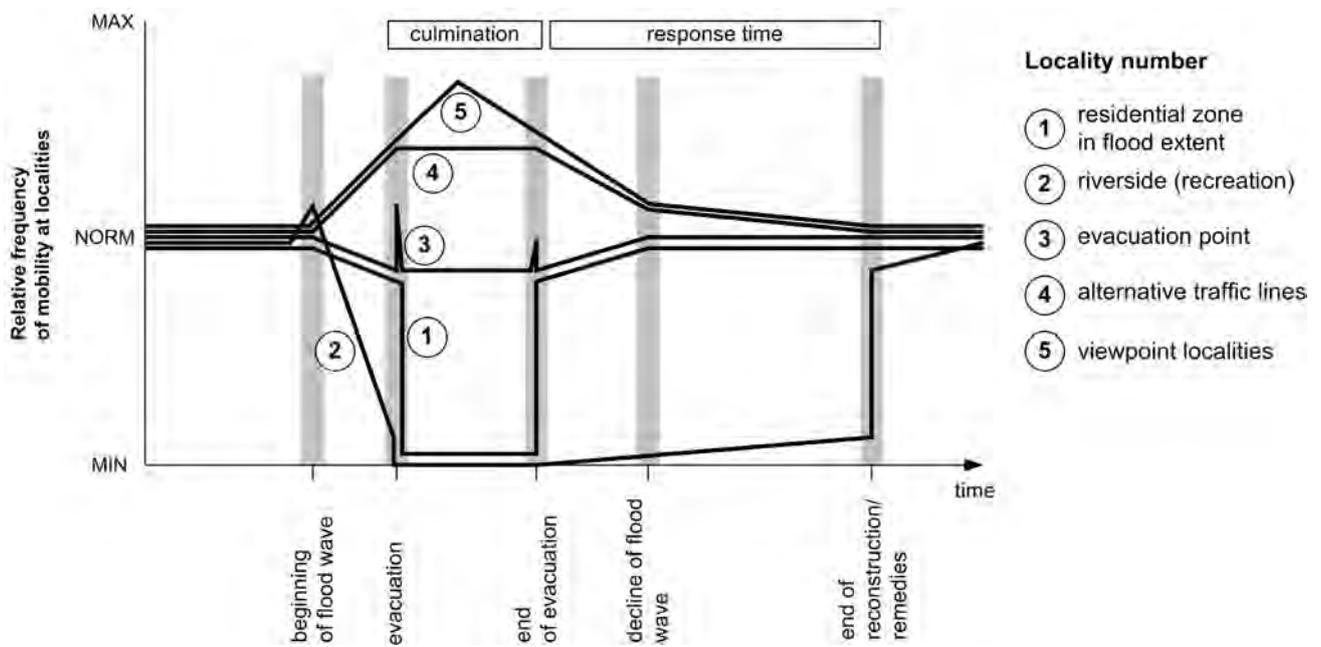
Fig. 3 Schematic representation of mobility rhythms at selected localities of Ústí nad Labem before, during and after the flood event. Based on field observation during the floods of 2002, 2006 and 2010, analyses of Flood Protection Plan and of changes in town traffic lines during the flood events. The vertical axis represents the relative change in frequency of daily mobility from the average (NORM) to the increased (towards MAX) and decreased (towards MIN) state.
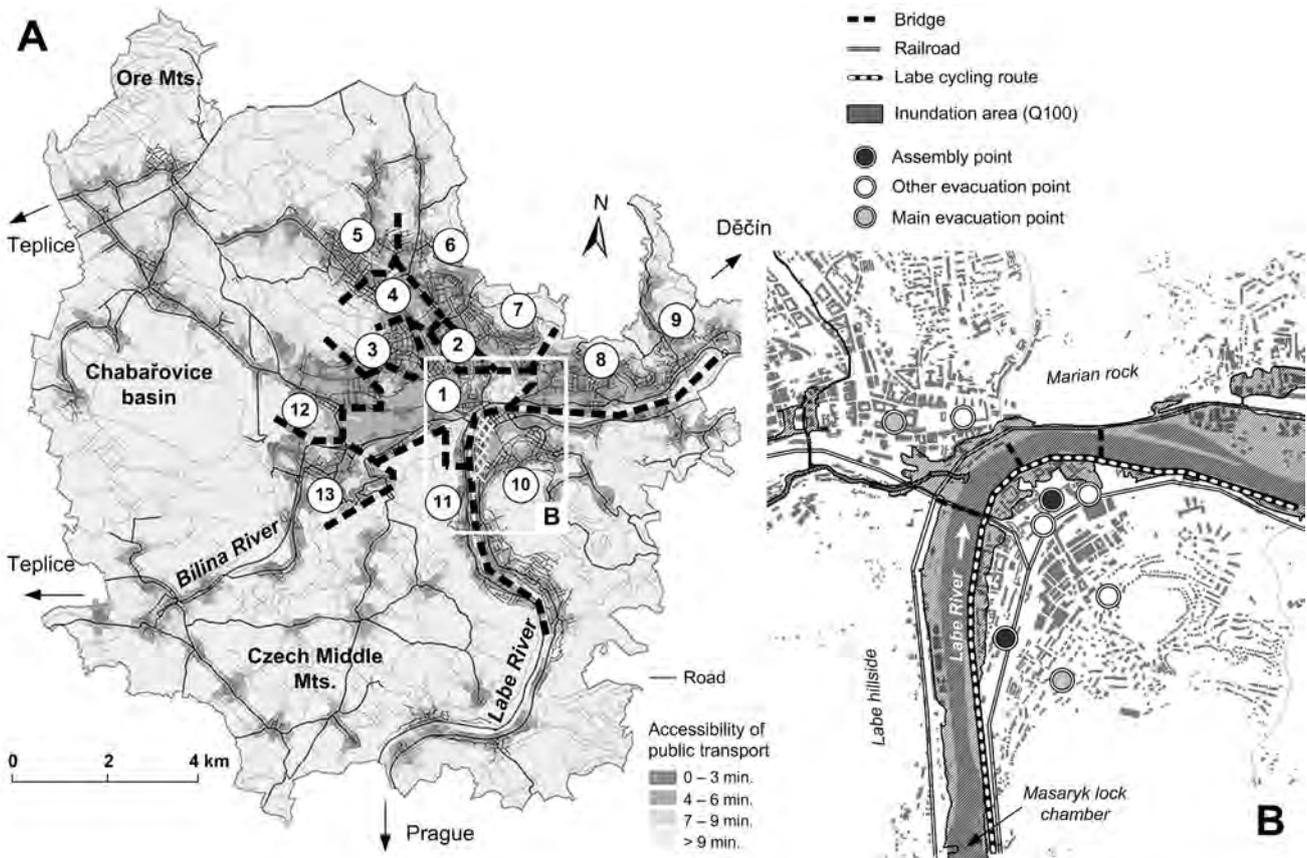
Fig. 4 A Location of city quarters in Ústí nad Labem: 1 – Centre, 2 – Skřivánek, 3 – Klíše, 4 – Bukov, 5 – Všebořice, 6 – Severní Terasa, 7 – Dobětice, 8 – Krásné Březno, 9 – Neštěmice, 10 – Střekov, 11 – Vaňov, 12 – Předlice, 13 – Trmice (the quarter of the Ústí nad Labem city before 1994). B Detailed map of the flood risk zone along the Labe River. Time accessibility to public transport published in Bartoš (2009).

lines increased their capacity in the peripheral quarters of the city, which also resulted in the increased use of services in these areas. This increased use of services together with the short-term accommodation of those who had been evacuated from their homes was negatively perceived by locals in some cases. On the other hand, even some inhabitants of flooded areas must have been frequently forced to evacuation as they did not want to leave their homes because of (a) low trust in protection of their property during the looting and (b) low confidence in seriousness of situation, which can be ascribed to uncertainty of forecast service and experts (cf. Sjöberg 1999).

The short-term increase in frequency of mobility was also characteristic for the assembly and evacuation points (Figure 4B) before the culmination of the flood wave and after its decline. The most significant changes in daily mobility have been logically identified in areas directly affected by floods (Figure 4B) and for those being evacuated or restricted for mobility. The characteristic feature of the daily mobility during the flood events is the "flood tourism" at the viewpoint sites. Along with the change of rhythm at different localities and corridors, we can also perceive differences in fluency of these changes and in the length of response time after the flood events (Figure 3). The complexity of changes in the daily rhythms and mobility of local communities indicates the increase of social notion of natural risks in a short-term horizon.

These results have also been confirmed with our previous questionnaire survey performed in 2008 (n = 108, face-to-face survey; see Raška et al. 2011 for detailed methodology). The questionnaire consisted of basic identification questions (sex, age category, education, address) and eight questions devoted to (a) the perception of relative importance of natural hazards, (b) the individual experience with the social impacts of natural hazards, and (c) effectiveness of warning system and sufficiency of information about the natural hazards. The survey indicated that certain differences exist in the perception of risk caused by various natural risks in different city quarters. Within the survey, the city was divided into five

segments. Figure 5 reveals the answers for two questions within the survey that represented the most significant factors of territorial differences of natural risk perception. We assumed that the answers would be highly influenced by individual experiences during the disaster events (Kates 1976; see Bubeck et al. 2012 for a critical discussion) as only the inhabitants that have experienced at least the 2006 flood have been interviewed. The first question was aimed at satisfaction with public information about the disaster during the event. The answers indicate that the lowest satisfaction with the quality and frequency of information about the event is typically in areas that are highly exposed to the natural hazards. Secondly, we asked about perception of risk caused by different hazard types. The results are highly variable, and contrarily to similar studies from abroad (e.g., Brilly, Polic 2005) it is not possible to find clear territorial correlation between the answers and typical hazards in individual city quarters. According to our analyses, we suggest two reasons for these results. First, the local communities ascribe more than one hazard to their city quarter because these hazards have causal relations and the locals are affected by all of them directly or indirectly. Second, although the respondents may feel risk caused only by certain types of hazards, their general view of disaster risk reduction is based upon presumption that the mitigation measures must be complex and aimed at all types of natural hazards (cf. Placer and Delquié 1999). Moreover, the perception of insufficient information about the flood risk management points out the necessity for extended public flood communication campaign (Parker, Handmer 1998; Parker et al. 2009).

3.3 Long-term impacts and social perception of natural risks

While the short-term effects of natural risks are an important factor in increasing the social perception regarding natural risks, the question arises as to whether the natural risks are perceived with the same intensity over a long-term period, i.e., also during the periods
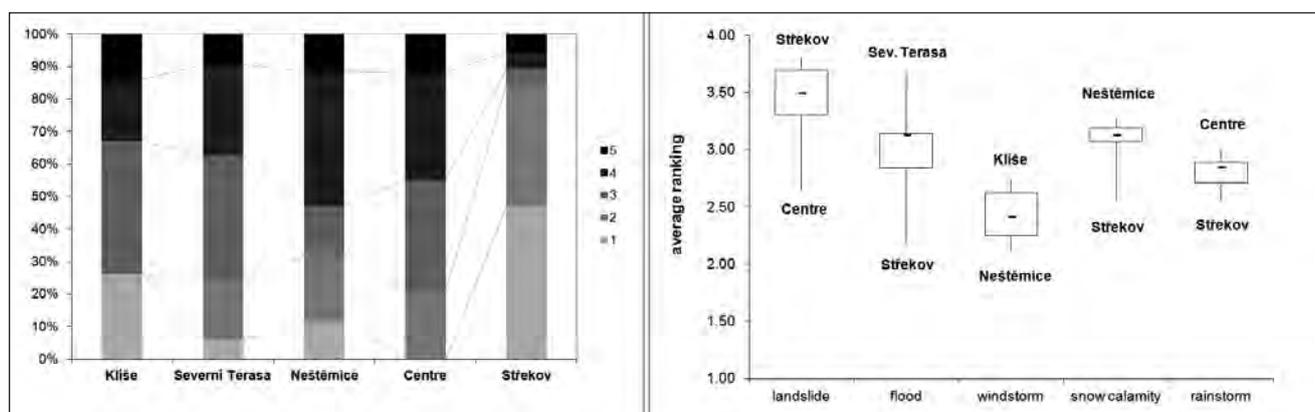
Fig. 5 Results of questionnaire survey. Left – Satisfaction with public information during the disaster events: 1 – minimum, 5 – maximum. Right – Average rank of the natural hazard according to level of risk: 1. – highest risk, 5. – lowest risk. Source: own survey, n = 108 (Raška et al. 2011). The city segments as follows: Klíše (incl. Klíše, Všebořice, Bukov), Severní Terasa (incl. Severní Terasa, Dobětice), Neštěmice (incl. Neštěmice, Krásné Březno), Město (incl. Ústí nad Labem – centre, Vaňov, Předlice), Střekov (incl. Střekov, Brná nad Labem).

Tab. 5 Statistical characteristics of the database of real estate (flats) in the Ústí nad Labem city in 2011.

	1 + k and 1 + 1	2 + k and 2 + 1	3 + k and 3 + 1	≥ 4 + k and 4 + 1	total
number of flats	19	89	62	19	189
minimal price [t. Kč]	295	419	570	450	295
maximal price [t. Kč]	1 039	1 792	2 462	2 904	2 904
average price [t. Kč]	605	878	1 320	2 049	1 113

Source: own survey from the http://sreality.cz website. Note to size categories – number stands for number of rooms + kitchen, k stands for kitchen corner.

Tab. 6 Analysis of variance for the database of two size categories of flats in Ústí nad Labem in 2011.

	n	s	min. [t. Kč]	max. [t. Kč]	F	p
2 + k and 2 + 1	89	281.23	419.00	1 792.00	3.365	0.003
3 + k and 3 + 1	62	376.38	570.00	2 462.00	2.861	0.010

The results are significant at p < 0.05. Source: own survey from the http://sreality.cz website. Note to size categories – number stands for number of rooms + kitchen, k stands for kitchen corner.

between individual disaster events. The short-term effects and social perception of natural risks are based more upon the direct evidence and experience with disasters, but the long-term social perception of natural disasters necessitates a more general and consistent intellectual insight of the local communities into the issue. Such consistent insight can be assessed through the analysis of factors other than questionnaires. Among the indicators of the long-term effects of the social perception of natural risks, the urban housing markets deserve the intense attention of both economists and environmentalists. The prices of real estate are influenced by a complex set of factors, including environmental factors (e.g., natural values and natural risks), location factors (e.g., accessibility), political and social setting (e.g., safety, social stratification, and cultural milieu) and economic factors (e.g., job opportunities and services). The significant decrease of real estate prices due to natural risks has been demonstrated with different locations. According to these studies, the decrease in price may range from less than 5% to almost 20% in floodplain locations (e.g., Hallstrom and Smith 2005; Bin et al. 2008). While some of the studies suggest only a temporary effect on real estate prices (Eves 2002; Lamond and Proverbs 2006), others indicate that the effect may be apparent for several years. The natural risks influence the price both directly, through potential social impacts and expenses for reconstruction of the house/flat after the disaster, and indirectly, through the insurance policies (e.g., Kousky 2011). To evaluate the impact of flood events in Ústí nad Labem on the long-term social perception of the natural risks, the quantitative assessment of the price of the real estate map was carried out. We performed the analysis for the year 2011, which is directly after the last flood event in 2010, and it covers the period of possible immediate impacts on the real estate map. The survey was aimed at prices of flats in

similar categories of houses and with similar legal state (personal ownership) in the entire city of Ústí nad Labem. In the event that there was a flat offered by more than one real estate agency, only the lowest price was considered. After the reduction of double records, the dataset contained 189 items (flats) in four size categories (Table 5).

The statistical analysis of variance was only possible for the size categories of two-room (n = 89) and three-room (n = 62) flats because the number of flats in other categories was not adequately representative. However, the two-room and three-room flats constitute the dominant market component. The analysis indicates that there exists statistically significant differences in the prices of flats among the city quarters at the probability level of p < 0.05 (Table 6).

Although such differences in prices exist, there is no coincidence between the lower prices and risk-exposed areas and vice versa (Figure 6). These results also partly agree with the above mentioned results of the questionnaire survey. The streets located next to the right riverbank (Střekov in the Figure 4), for instance, which were flooded up to the first floor of houses during the 2002 floods and from which the inhabitants were evacuated, represent one of the most expensive locations after the city centre and Klíše residential quarter. The results for the riverbank may be partly influenced by completion of a flood protection wall in 2008; however, the wall is designed only for Q_{20} floods, while the 2002 flood had a magnitude of Q_{100}. The highest prices were found in the city centre, despite of its partial location within the annual flooding zone. According to these results, it seems that natural risks represent only a supplementary factor for the real estate market, and the social perception of natural risks is time-dependent with a decreasing importance during the periods between individual disaster events. The real estate market, as one of the factors/
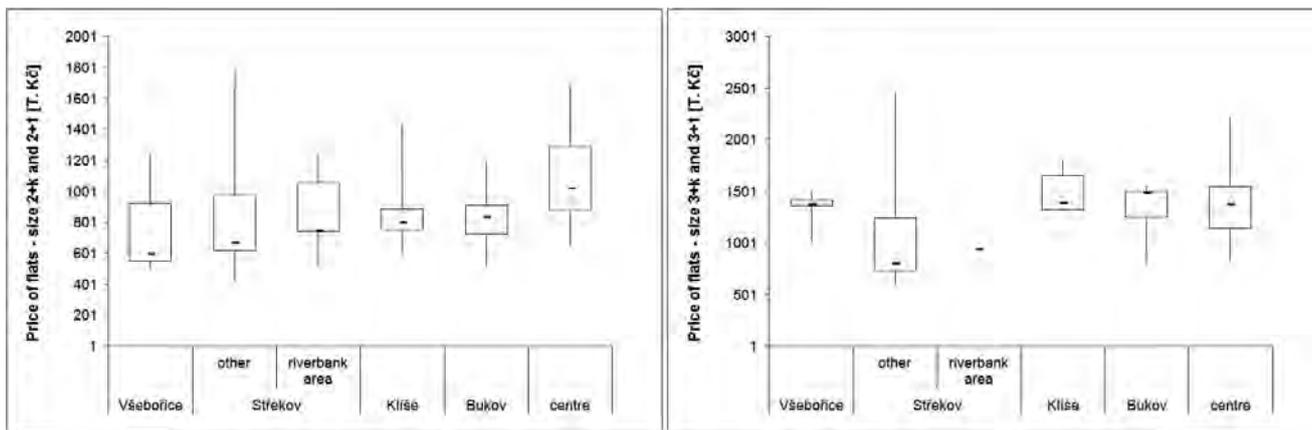
Fig. 6 Variability in the price of flats across selected city quarters. Source: own survey from the http://sreality.cz website. Note to size categories – number stands for number of rooms, k stands for kitchen. The location of city quarters is in Fig. 4.

representations of intra-urban mobility in the city of Ústí nad Labem, is generally more consistently influenced by stable long-term factors, such as job opportunities and the social structure of the city quarter (cf. Quigley and Weinberg 1977; Greenwood 1985) and by selected long-term environmental factors, such as the extent of green spaces and the level of air pollution in different parts of the city (Anděl 1999; Šašek 2008).

Although it would require further statistical analysis of the data regarding population migration within the city, the environmental intra-urban migration induced by the preference of localities due to natural risks (as discussed by e.g., Hogan a Marandola Jr. 2007; Stojanov et al. 2008) seems to be less important in Ústí nad Labem. This is partly consistent with the sociologic surveys stating that natural disasters constitute only a partial, if not minor, issue concerned with the social perception of the environment (Eurobarometer 2011). In this respect, environmental issues are more often perceived as the problems of the protection of nature, global issues, the quality of life or technological hazards. Frič (1996), for instance, has shown that, when talking about ecological disasters, most people in Czechia think of technological hazards concerned with the industrial sector. However, these results must be put in the context of the societal transition in Czechia during the last two decades. The 1990s are characterised as the beginning of the period of societal transition in Czechia, which also represents the beginning of the shift toward a post-materialistic value orientation *sensu* Dostál (2010). In that time, the environmental quality was not an important factor for 24–29% of the population of cities with more than 10,000 inhabitants, although it was generally an important factor at the national level (Drbohlav 1990). The shift toward environmental values was mostly apparent among the older population living in smaller cities and in the countryside. During the following two decades, i.e., between 1990 and 2010, there was a significant increase in positive attitudes towards the environment in Czechia, however, indicating the convergence of Czechia with other Central-European

countries (Hadler and Wohlkönig 2012). Moreover, environmental values have been increasingly perceived as important among the young population in larger cities.

4. Conclusions

The aim of this paper was to discuss the effectiveness with which the recent progress in disaster risk reduction, highlighting the role of vulnerability assessment, has been implemented in Czechia. The analysis has been performed at two territorial levels.

First, we have evaluated the political regulations in natural risk issues and vulnerability strategies through the content and discoursive analysis of the international and national strategic documents and legal frameworks. The analysis has shown that the issue of natural risks is well incorporated into the strategic documents and legal frameworks in Czechia; however, these documents do not sufficiently reflect the global and European agreement on the necessity of a conceptual shift towards a social vulnerability concept within disaster risk reduction. Natural risks represent a stable but minor issue, which is mentioned within the strategic goals of the regional development of regional centres in Czechia as defined in the Integrated Plans of City Development (IPCD). However, similar to the national level documents and legal frameworks, the IPCDs do not develop the strategic tools for vulnerability assessment and mitigation.

Second, considering that the risk society concept is gaining increased attention in the recent theoretical discourse (Giddens 1999) and the notion that an effective disaster risk reduction must be based on community strategies (Innocenti, Albrito 2011), we have assessed the social perception of natural risks in the case study of the city of Ústí nad Labem, one of the major regional centres in Czechia affected by varying natural hazard types during the last two decades. The field observations showed the complex modification of the daily rhythms of the urban population during the individual hazard

events (mainly floods). The questionnaire survey indicated that natural risks are perceived as an important issue by the public, but the respondents perceive insufficiency of information about the risk management during the disaster events. At the same time, the weak territorial correlation between the hazards perceived as the most threatening by respondents in different quarters of the city indicates that the citizens may perceive the necessity for a complex strategy in disaster risk reduction.

While the short-term effects of natural hazards (disasters) on the daily rhythm of local communities and the social perception of these hazards is clear, the long-term effects are rather ambiguous. The social and economic impacts of past floods in the city of Ústí nad Labem have resulted in the creation of a digital flood plain corresponding to the nation-wide strategies of flood risk mitigation. Nevertheless, our analysis aimed at the real estate market, which is recently considered one of the important indicators of the social perception of natural risks, indicated that there is a very limited coincidence between zones with low prices and those with a higher level of natural risks. The prices of real estate and preferences toward certain city quarters seem to be considerably more influenced by economic factors and the complex environmental perception of quarters. The increasing environmental awareness in Czechia documented by recent sociologic surveys is more related to the perception of global issues, the quality of life and technological hazards, whereas the notion of natural risk represents only a supplementary segment of the attitude towards the environment. To conclude, the long-term perception of natural risks in the studied urban centre, i.e., the notion of risk during the periods between the individual hazards and after them, is relatively weak, which may represent a significant constraint for the implementation of community strategies of disaster risk reduction.

ACKNOWLEDGEMENTS

REFERENCES

ALCÁNTARA-AYALA, I. (2008): On the historical account of disastrous landslides in Mexico: the challenge of risk management and disaster prevention. Advances in Geosciences 14: 159–164, DOI: 10.5194/adgeo-14-159-2008.

ALCÁNTARA-AYALA, I., GOUDIE, A. S. (2010): Geomorphological hazards and disaster prevention. Cambridge, Cambridge University Press.

ANDĚL, J. et al. (1999): Geografie města Ústí nad Labem. Ústí nad Labem, Acta Universitatis Purkynianae UJEP.

BALEJ, M., ANDĚL, J., ORŠULÁK, T. (2007): Environmental stressors and stress as a natural/human interdisciplinary issue (case study from the Northwestern part of the "Sudetenland"). Acta Universitatis Carolinae, Geographica, 42(1–2), 53–74.

BARTOŠ, J. (2009): Časová dostupnost zastávek MHD na Ústecku. Diploma thesis, MS, Ústí nad Labem, UJEP.

BECK, U. (1992): Risk society: towards a new modernity. London, Sage.

BERNSTEIN, P. L. (1996): Against the Gods: the remarkable story of risk. New York, Wiley.

BIN, O., KRUSE, J., LANDRY, C. (2008): Flood hazards, insurance rates and amenities: Evidence from the coastal housing market. Journal of Risk and Insurance 75, 63–82, DOI: 10.1111/j.1539-6975.2007.00248.x.

BLAHŮT, J., KLIMEŠ, J. (2011): Příspěvek k české terminologii rizik ve studiu rizik ze svahových deformací. Geografie 116, 79–90.

BREAKWELL, G. M. (2001): Mental models and social representations of hazards: the significance of identity processes. Journal of Risk Research 4: 341–351, DOI: 10.1080/13669870110062730.

BRUEN, M., GEBRE, F. A. (2001): Worldwide public perception of flood risk in urban areas and it´s consequences for hydrological design in Ireland. Flood Risk Management Proc. Irish National Hydrology Seminar, Tullamore, November 2001.

BUBECK, P., BOTZEN, W. J. W., AERTS, J. C. J. H. (2012): A review of risk perceptions and other factors that influence flood mitigation behavior. Risk Analysis 32(9): 1481–1495, DOI: 10.1111/j.1539-6924.2011.01783.x.

ČAMROVÁ, L. (2006): Jak hodnotit efektivnost veřejných výdajů na povodně? Vodní hospodářství 9, 316–318.

CARDONA, O. D. (2008): The need for rethinking the concepts of vulnerability and risk from a holistic perspective: a necessary review and criticism for effective risk management. In: BANKOFF, G., FRERKS, G., HILHORST, D. (eds.): Mapping vulnerability: disasters, development & people (37–51). London, Earthscan.

BRILLY, M., POLIC, M. (2005): Public perception of flood risks, flood forecasting and mitigation. Natural Hazards and Earth System Sciences 5: 345–355, 1684-9981/nhess/2005-5-345.

CHOULARTON, R. (2001): Complex learning: organizational learning from disasters. Safety Studies 39(1–2):61–70, DOI: 10.1016/S0925-7535(01)00026-1.

CORBACIOGLU, S., KAPUCU, N. (2006): Organisational learning and selfadaptation in dynamic disaster environments. Disasters 30(2): 212–233, DOI: 10.1111/j.0361.3666.2006.00316.x.

COLLECTIVE (2000): Strategie ochrany před povodněmi pro území České republiky. Praktická příručka 35. Praha, MZE ČR.

COLLECTIVE (2010): Zásady urbánní politiky. Praha, MMR ČR.

COLLECTIVE (2012): Ročenka životního prostředí města Ústí nad Labem. Ústí nad Labem, MMUNL.

CRED (2009): The International Disaster Databse. Centre for Research of Epidemiology of Disasters. www.emdat.be

CUTTER, S. L. (1996): Vulnerability to environmental hazards. Progress in Human Geography 20(4): 529–539, DOI: 10.1177/030913259602000407.

DELICA-WILLISON, Z., WILLISON, R. (2008) Vulnerability reduction: a task for the vulnerable people themselves. In:

BANKOFF, G., FRERKS, G., HILHORST, D. (eds.): Mapping vulnerability: disasters, development & people (145–158). London, Earthscan.

DOSTÁL, P. (2005): Socio-geographical systems, institutional mechanisms and risk processes. Acta Universitatis Carolinae – Geographica 40, 5–23.

DOSTÁL, P. (2008): Changing geographical systems and risk processes: gerenal considerations. In: DOSTÁL, P. (ed.): Evolution of geographical systems and risk processes in the global context (15–36). Praha, Charles University, P3K.

DOSTÁL, P. (2010): Environment and regional cohesion in the enlarged European Union – differences in public opinion. In: ANDĚL, J., BIČÍK, I., DOSTÁL, P., LIPSKÝ, Z., SHAHNESHIN, S. G. (eds.): Landscape Modelling: Geographical Space, Transformation and Future Scenarios (59–77). New York, Springer.

DRBOHLAV, D. (1990): Důvody regionálních a sídelních preferencí obyvatelstva v ČSR. Sborník československé společnosti geografické 95, 13–29.

EC (2010): A Community approach on the prevention of natural and man-made disasters. European Community.

EC (2011): EU Strategy for supporting disaster risk reduction in developing countries 2011–2014. European Community.

EEA (2010): Mapping the impacts of natural hazards and technological accidents in Europe An overview of the last decade. EEA Technical Report No 13/2010. Copenhagen, European Environment Agency.

ELLEGÅRD, K. (1999): A time-geographical approach to the study of everyday life of individuals – a challenge of complexity? GeoJournal 48, 167–175.

EUROBAROMETER (2011): The Special Eurobarometer Survey 365. European Community.

EVES, C. (2002): The long-term impact of flooding on residential property values. Property Management 20, 214–227.

FALC, Z. (2001): Finanční pomoc státu při stabilizaci sesuvů v letech 1997–2001 v regionech postižených následky katastrofických povodní. Praha, MŽP ČR.

FLEMING, R. W., TAYLOR F. A. (1980) Estimating the costs of landslide damage in the United States. U.S. Geological Survey. Circular 832, 21 pp.

FRIČ, P. (1996): Postoje obyvatel ČR a SR k problému životního prostředí. Sociologický časopis 32, 353–360.

GIDDENS, A. (1999): Risk and Responsibility. Modern Law Review 62: 1–10, DOI: 10.1111/1468–2230.00188

GREENWOOD, M. J. (1985): Human migration: theory, models and empirical studies. Journal of Regional Science 25: 521–544, DOI: 10.1111/j.1467-9787.1985.tb00321.x.

HADLER, M., WOHLKÖNIG, P. (2012) Environmental Behaviours in the Czech Republic, Austria and Germany between 1993 and 2010: Macro-Level Trends and Individual-Level Determinants Compared. Sociologický časopis 48, 667–692.

HALLSTROM, D., SMITH, K. (2005): Market responses to hurricanes. Journal of Environmental Economics and Management 50: 541–561, DOI: 10.1016/j.jeem.2005.05.002.

HAMPL, M., DOSTÁL, P., DRBOHLAV, D. (2007): Social and Cultural Geography in the Czech Republic: under pressures of globalization and post-totalitarian transformation. Social & Cultural Geography 8(3): 475–493, DOI: 10.1080/14649360701489029.

HEWITT, K. (ed.) (1983). Interpretation of Calamity: From the Viewpoint of Human Ecology. Boston, Allen.

HOGAN, D. J., MARANDOLA, E. JR. (2007): Vulnerability to natural hazards in population-environmental studies. Background paper to the Population-Environment Research Network Cyberseminar on Population and Natural Hazards, 1–11.

HUFSCHMIDT, G. (2011): A comparative analysis of several vulnerability concepts. Natural Hazards 58: 621–643, DOI: 10.1007/s11069-011-9823-7.

INNOCENTI, D., ALBRITO, P. (2011): Reducing the risks posed by natural hazards and climate change: the need for a participatory dialogue between the scientific community and policy makers. Environmental Science & Policy 14:730–733, DOI: 10.1016/j.envsci.2010.12.010.

KATES, R. (1976): Experiencing the Environment as Hazard, In: PROSHANSKY, H. M., ITTELSON, W. H., RIVLIN, L. G. (eds.): Environmental Psychology (401–418). New York, Holt.

KLENEROVÁ, D. ET AL. (2004): Digitální povodňový plán města Ústí nad Labem [online]. Hydrosoft Veleslavín. Available at <http://www.usti-nad-labem.cz/dpp> [cit. 2012–02–13].

KLIMEŠ, J., BLAHŮT J. (2012): Landslide risk analysis and its application in regional planning: an example from the highlands of the Outer Western Carpathians, Czech Republic. Natural Hazards 64:1779–1803, DOI: 10.1007/s11069-012-0339-6.

KOUSKY, C. (2011): Managing Natural Catastrophe Risk: State Insurance Programs in the United States. Review of Environmental Economics and Policy 5: 153–171, DOI: 10.1093/reep/req020.

KREIMER, A., ARNOLD, M., CARLIN, A. (2003): Building safer cities, the future of disaster risk. Washington, World Bank.

LAMOND, J., PROVERBS, D. (2006): Does the price impact of flooding fade away? Structural survey 24: 363–377, DOI: 10.1108/02630800610711960.

MANUEL-NAVARRETE, D., PELLING, M., REDCLIFT, M. (2011): Critical adaptation to hurricanes in the Mexican Caribbean: Development visions, governance structures, and coping strategies. Global Environmental Change A 21: 249–258, DOI: 10.1016/j.gloenvcha.2010.09.009.

MUNICHRE (2009): TOPICS GEO Natural catastrophes 2009. Analyses, assessments, positions. Munich, MunichRe.

PARKER, D. J., HANDMER, J. W. (1998): The role of unofficial flood warning systems. Journal of Crisis and Contingencies Management 6(1):45–60, DOI: 10.1111/1468-5973.00067.

PARKER, D. J., PRIEST, S. J., TAPSELL, S. M. (2009): Understanding and enhancing the public's behavioural response to flood warning information. Meteorological Applications 16: 103–114, DOI: 10.1002/met.119.

PELLING, M. (2003): The vulnerability of cities. London, Earthscan.

PELLING, M., MANUEL-NAVERRETE, D. (2011): From Resilience to Transformation: Exploring the Adaptive Cycle in two Mexican Urban Centres. Ecology and Society 16, 11.

PLACER, V., DELQUIÉ, P. (1999): Measures of social risk perception and demand for risk reduction: an experimental comparison. Risk Decision and Policy 4, 129–144.

QUIGLEY, J. M., WEINBERG, D. H. (1977): Intra-Urban Residential Mobility: A Review and Synthesis. International Regional Science Review 2: 41–66, DOI: 10.1177/016001767700200104.

RAŠKA, P., DUBIŠAR, J., CHVÁTALOVÁ, A. (2011): Přírodní rizika města Ústí nad Labem: deterministický chaos či management krajiny. In: KOUTSKÝ, J. (ed.): Ústí nad Labem – město v mlze (168–185). Ústí nad Labem, Acta Universitatis Purky nianae UJEP.

RAŠKA, P., ANDĚL, J. (2012): Přírodní rizika ve městech jejich reflexe v rozvojových dokumentech. In: KOUTSKÝ, J., RAŠKA, P. (eds.): Výzkum regionálního rozvoje – vybrané přístupy a témata (115–132). Ústí nad Labem, UJEP.

RAŠKA, P., KLIMEŠ, J., DUBIŠAR, J. (2013): Using local archive sources to reconstruct historical landslide occurrence in selected

urban regions of the Czech Republic: examples from regions with different historical development. Land Degradation and Development, DOI: 10.1002/ldr.2192.

SAREWITZ, D., PIELKE, R. JR., KEYKHAH, M. (2003): Vulnerability and risk: some thoughts from a political and policy perspective. Risk Analysis 23: 805–810, DOI: 10.1111/1539-6924.00357.

SCHMIDT-THOMÉ, P. (ed.) (2006): Natural and Technological Hazards and Risks Affecting the Spatial Development of European Regions. Espoo: Geological Survey of Finland Special Paper 42.

SCHUSTER, R. L., HIGHLAND, L. M. (2001): Socioeconomic and environmental impacts of landslides in the western hemisphere. U.S. Geological Survey Open-File Report 2001-276.

SJÖBERG, L. (1999): Risk perception by the public and by experts: a dilemma in risk management. Research in Human Ecology 6(2), 1–9.

SLOVIC, P. (1987): Perception of risk. Science 236(4799): 280–285, DOI: 10.2307/1698637.

STEINBERG, T. (2000): Acts of God: The Unnatural History of Natural Disaster in America. Oxford University Press, Oxford.

STOJANOV, R., NOVOSÁK, J., OPINIANO, J. M., GEMENNE, F., SIWEK, T. (2008): Development, Environment and Migration. Analysis of Linkages and Consequences. Olomouc, Palacký University.

SZTOMPKA, P. (2007): Vizuální sociologie: fotografie jako výzkumná metoda. Slon, Praha.

ŠAŠEK, M. (2008): Zpráva z provedeného výzkumu „Zdravé město" pro MM Ústí nad Labem. Ústí nad Labem, UJEP.

UN (2005): The Hyogo Framework for Action. New York, United Nations.

UNDRO (1979): Natural disasters and vulnerability assessment. Report of expert group meeting. Geneva: Office of the UN Disaster Relief Coordinator.

UNISDR (2010): Making Cities Resilient. My City is Getting Ready. New York, UN.

VILÍMEK, V., SPILKOVÁ, J. (2009): Natural hazards and risks: the view from the junction of *natural* and social sciences. – Geografie–Sborník ČGS 114, 332–349.

WILKINSON, I. (2004): Suffering: a sociological introduction. Cambridge, Polity.

WISNER, B., BLAIKIE, P., CANNON, T., DAVIS, I. (2004): At risk: natural hazards, people's vulnerability, and disasters. London, Routledge.

Legal acts:
Act No. 114/1992 o ochraně přírody a krajiny.
Act No. 219/1999 o ozbrojených silách eské republiky.

Act No. 237/2000 o požární ochraně.
Act No. 239/2000 o integrovaném záchranném systému.
Act No. 240/2000 o krizovém řízení.
Act No. 241/2000 o hospodářských opatřeních pro krizové stavy.
Act No. 254/2001 o vodách.
Act No. 236/2002 o způsobu a rozsahu zpracovávání návrhu a stanovování záplavových území

RÉSUMÉ

Politická regulace a společenské vnímání přírodních rizik: „riziková společnost", česká zkušenost a evropský kontext

Důsledkem výrazných přírodních pohrom v posledních desetiletích začalo být stále více pozornosti věnováno společenské dimenzi přírodních rizik. Výzkumy sociální dimenze přírodních rizik v tomto ohledu přispěly k implementaci konceptu společenské zranitelnosti do mezinárodních právních rámců a strategií zmírňování přírodních rizik. V sociálně vědní perspektivě je efektivní cesta ke zmírňování škod způsobených přírodními pohromami spatřována ve společenské aktivitě (akci) realizované na různých institucionálních úrovních. Prvním cílem této studie je zhodnotit, do jaké míry česká politická reprezentace přijala a implementovala zmíněné legislativní rámce a strategie do národních a regionálních politik. Druhým cílem je pak analyzovat sociální odezvu na přírodní rizika v Česku a dokumentovat ji na případové studii města Ústí nad Labem. Politická deklarace přijetí konceptu přírodních rizik a koncepcí zmírňování zranitelnosti společnosti byla hodnocena na základě obsahové a kritické diskursivní analýzy strategických a legislativních dokumentů a rámců. Provedená analýza indikuje, že problematika přírodních rizik je do těchto dokumentů velmi dobře zakomponována, avšak dostatečně se v nich neodráží současný posun blíže ke konceptu sociální zranitelnosti, který je stále běžněji přijímán v Evropě a ve světě. Výsledky výzkumu sociální percepce přírodních rizik a terénní šetření v případové studii zaměřené na město Ústí nad Labem ukazují, že problematika přírodních rizik představuje významný krátkodobý rozhodovací faktor pro denní aktivity obyvatel města. Na druhou stranu, analýza dlouhodobé percepce přírodních rizik obyvateli města, provedená prostřednictvím analýzy cenové mapy nemovitostí po povodňové situaci, naznačila, že vnímání přírodních rizik mezi jednotlivými událostmi a po jejich odeznění je vcelku slabá. Tato skutečnost může představovat významnou bariéru v implementaci komunitních strategií zmírňování dopadů přírodních pohrom.

Pavel Raška
Department of Geography
Faculty of Science, J. E. Purkyně University
České mládeže 8
400 96 Ústí nad Labem
Czech Republic
E-mail: pavel.raska@ujep.cz,
tel.: +420 475 283 300

COLOUR APPENDIX

Fig. I The Nepal Himalaya and its neighbouring regions.
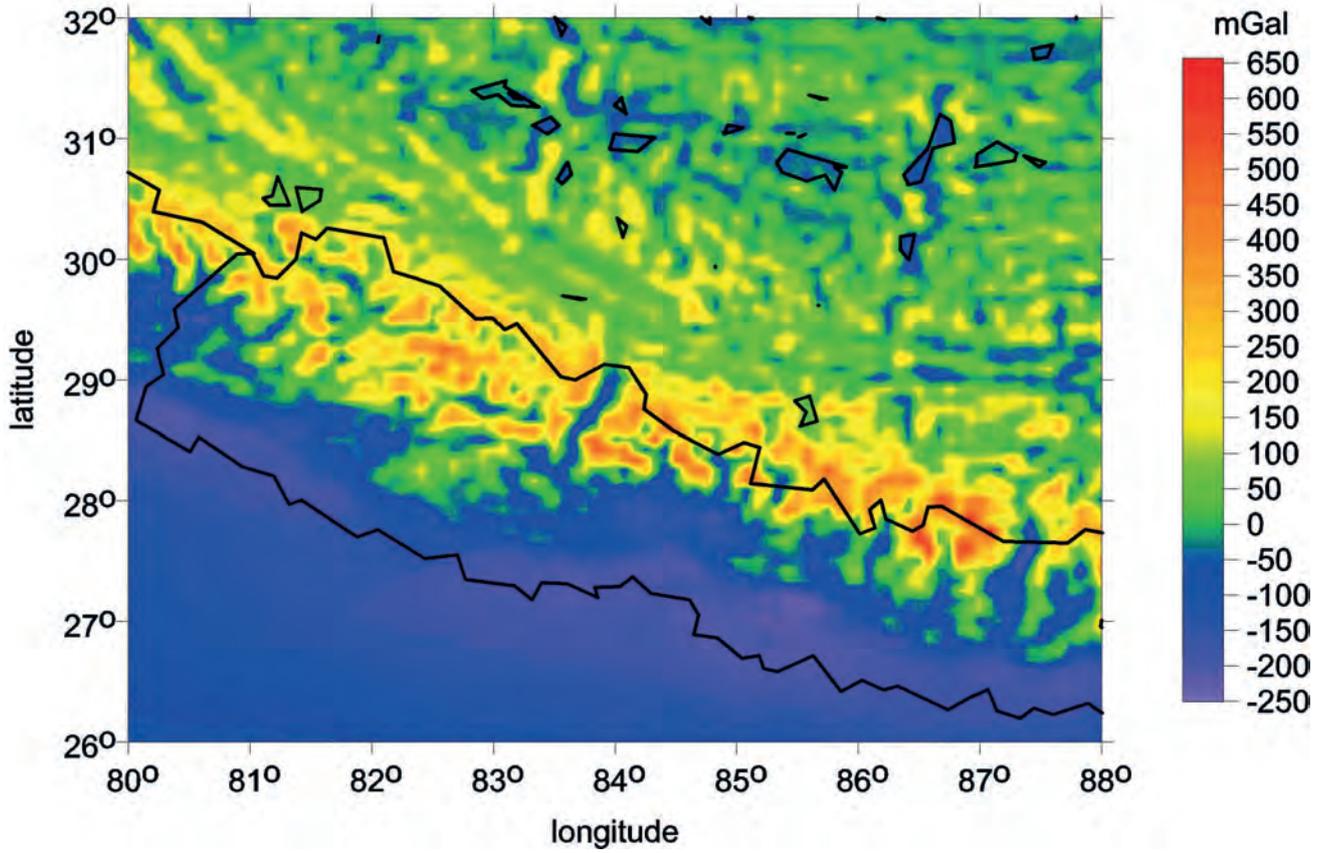
Fig. Ia The gravity anomalies Δ*g*.
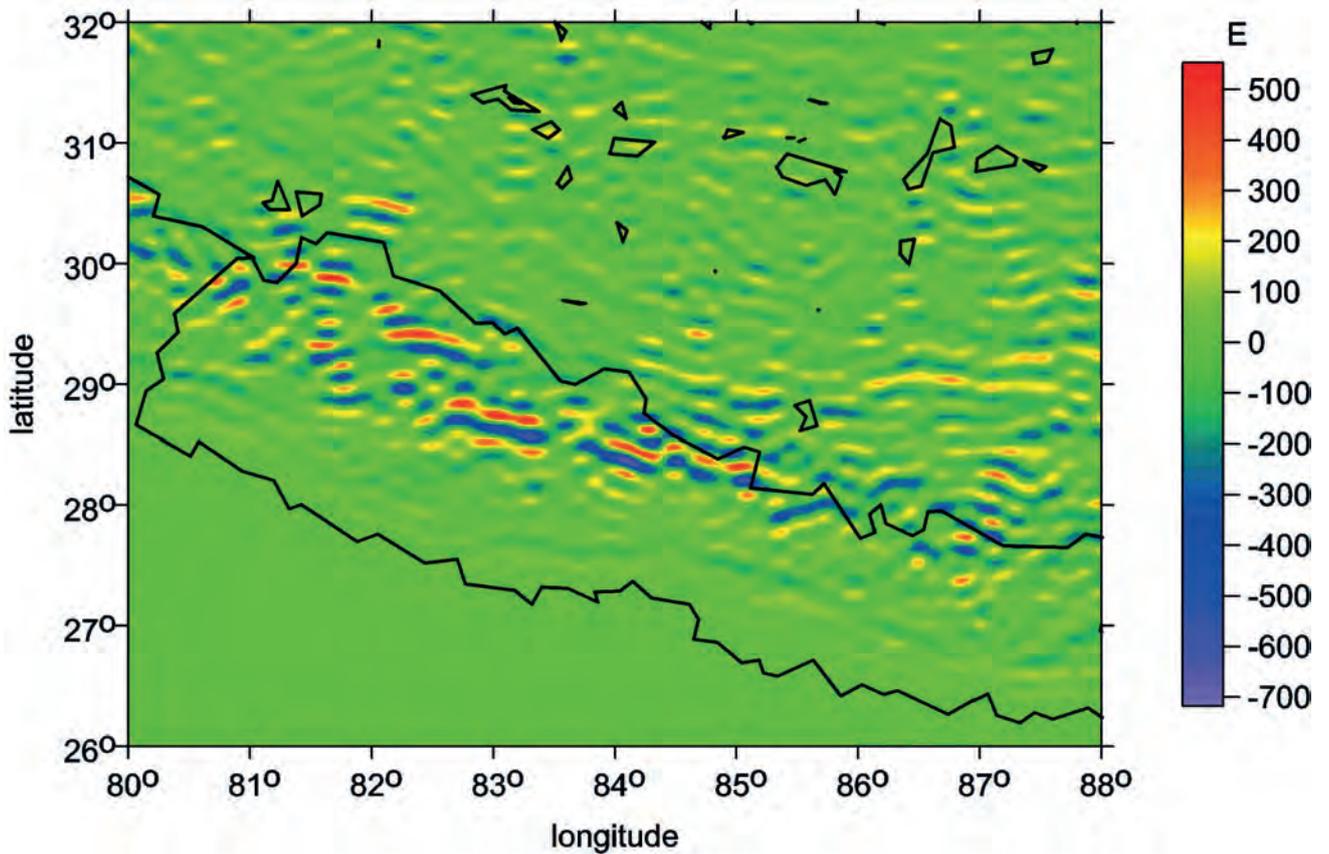
**Fig. Ib** The second derivative Γ_{11} of the disturbing gravitational potential.
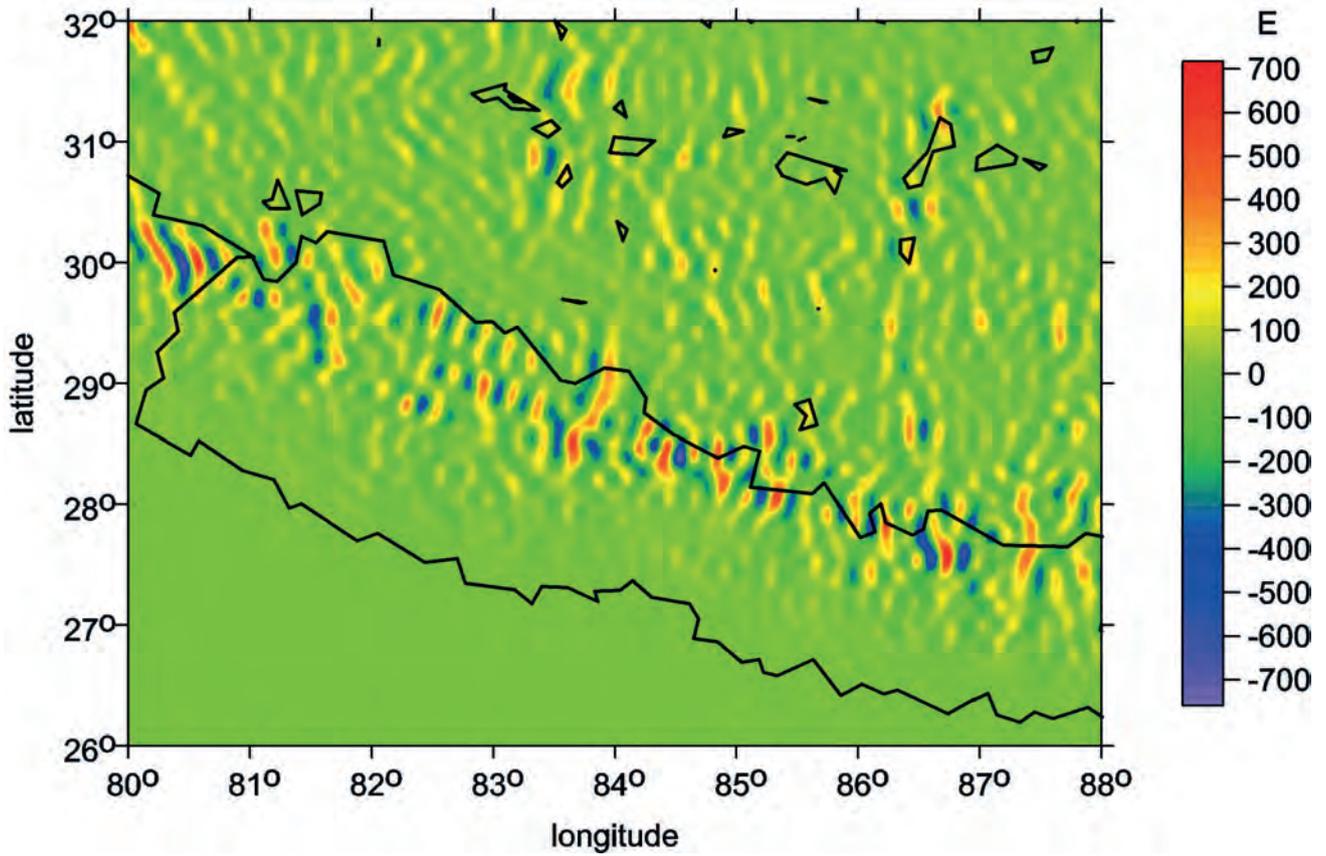
Fig. Ic The second derivative Γ_{22} of the disturbing gravitational potential.
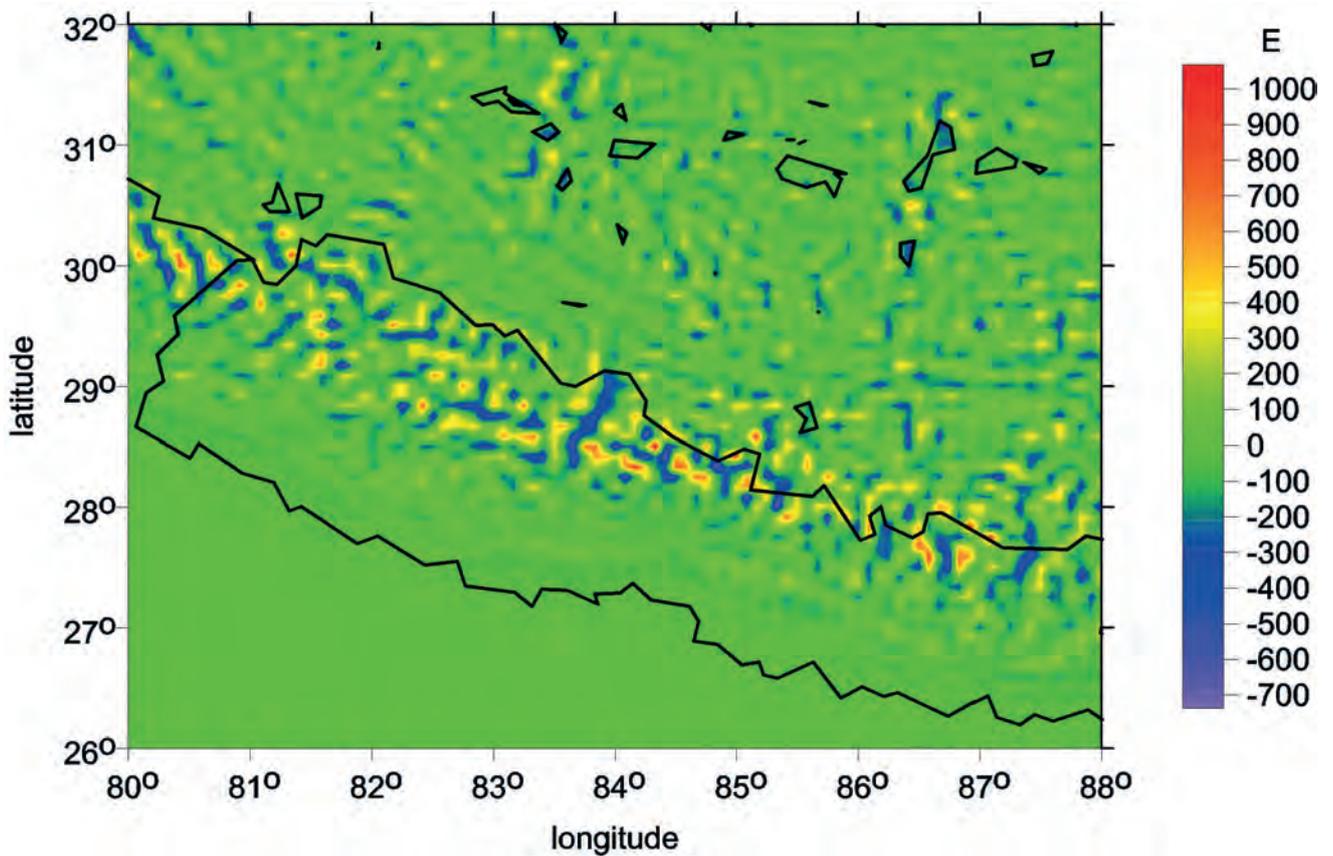
Fig. Id The second derivative Γ_{33} of the disturbing gravitational potential.
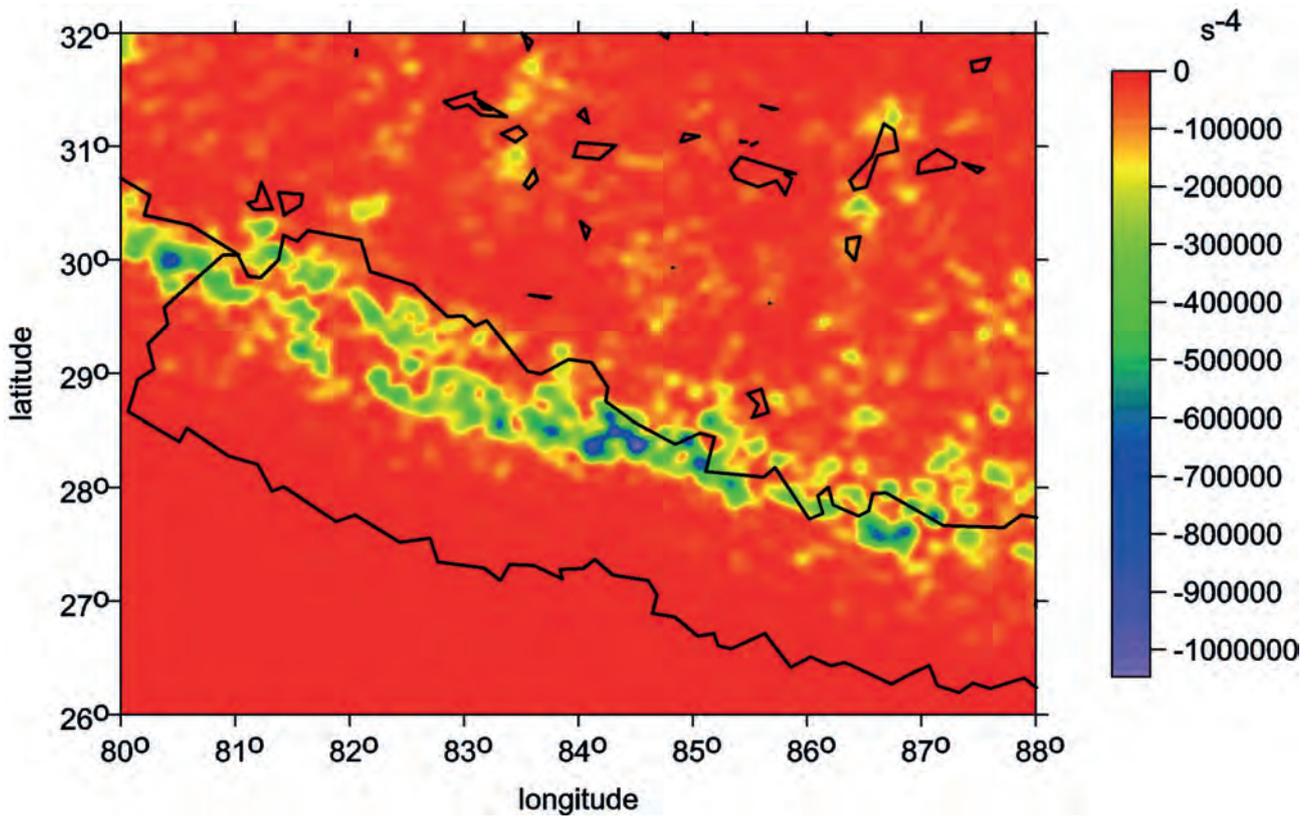
Fig. Ie The invariant I_1.
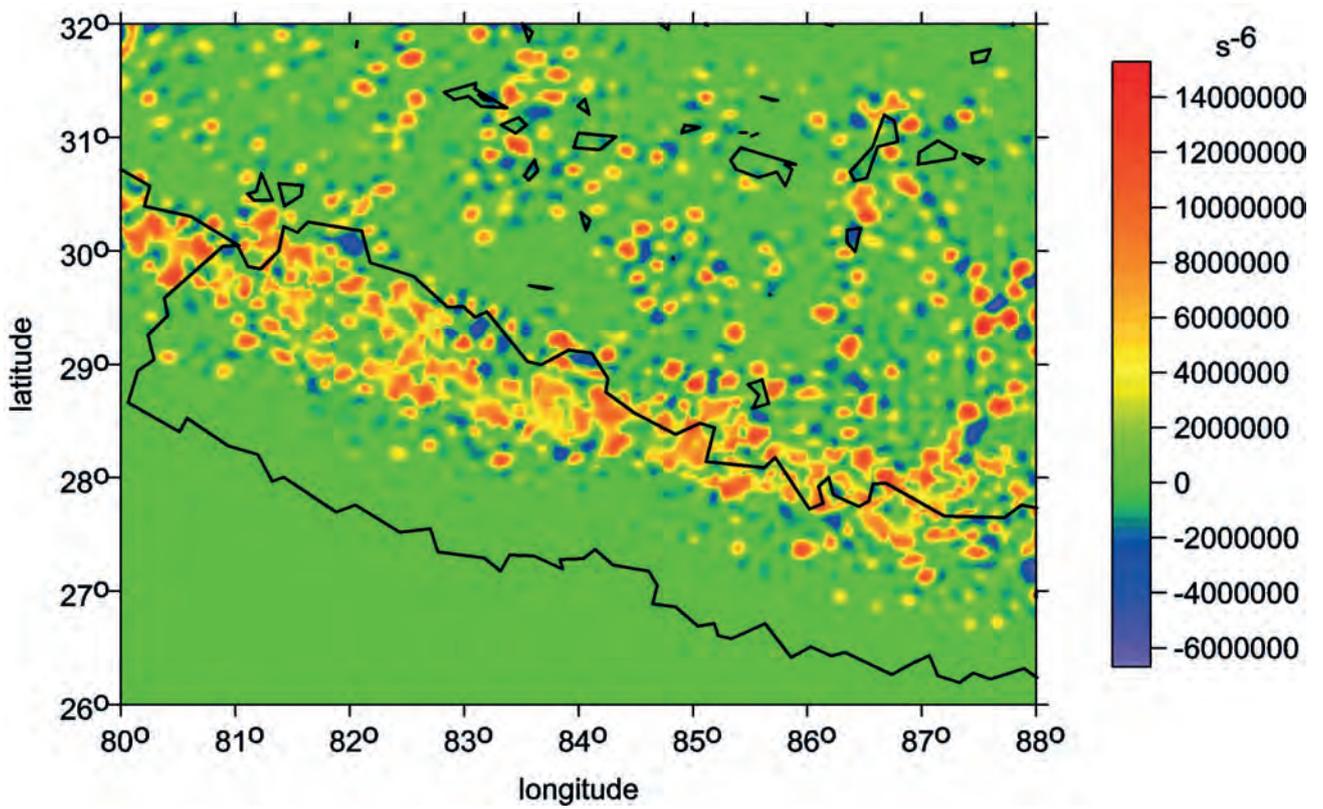
Fig. If The invariant I_2.
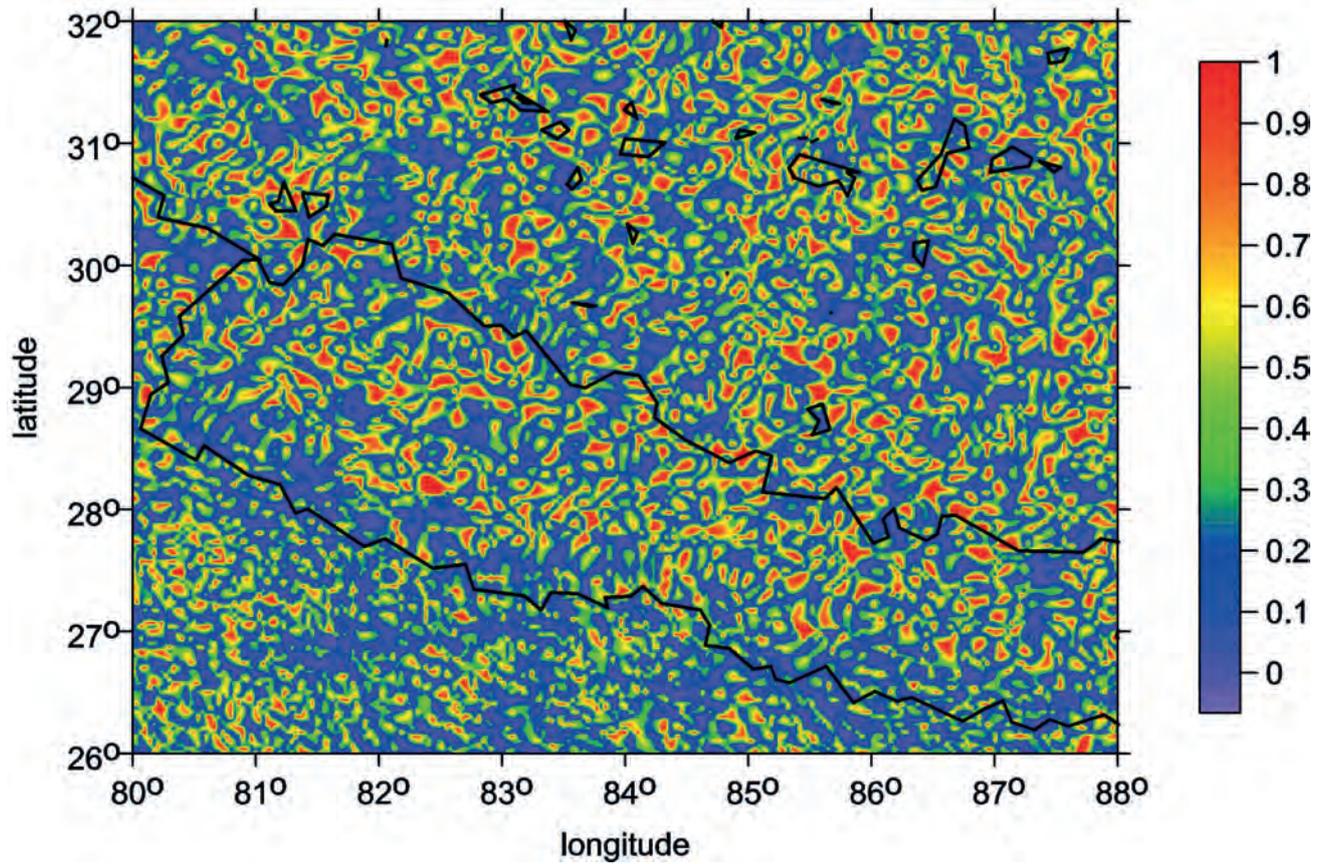
Fig. Ig The ratio I of the invariants I_1 and I_2.
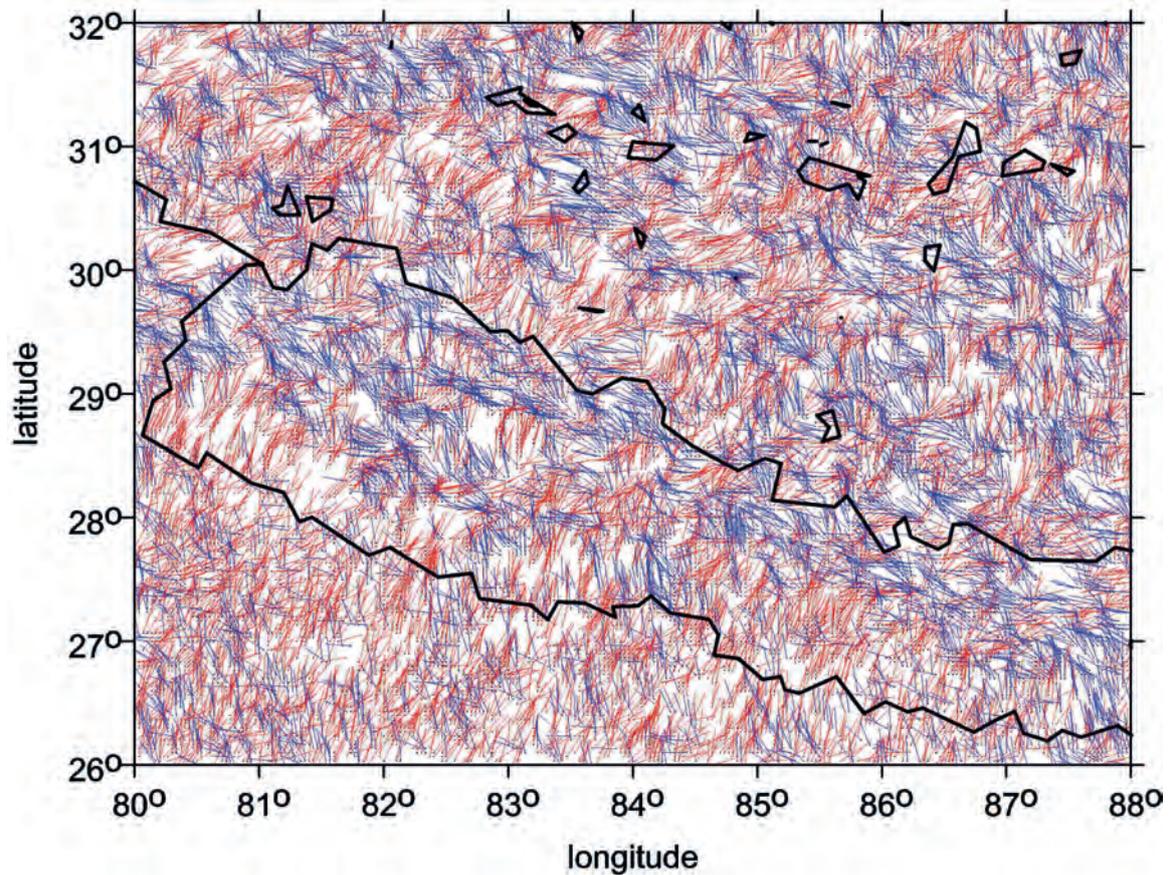
Fig. Ih The strike angle θ_S for $I > 0.3$.
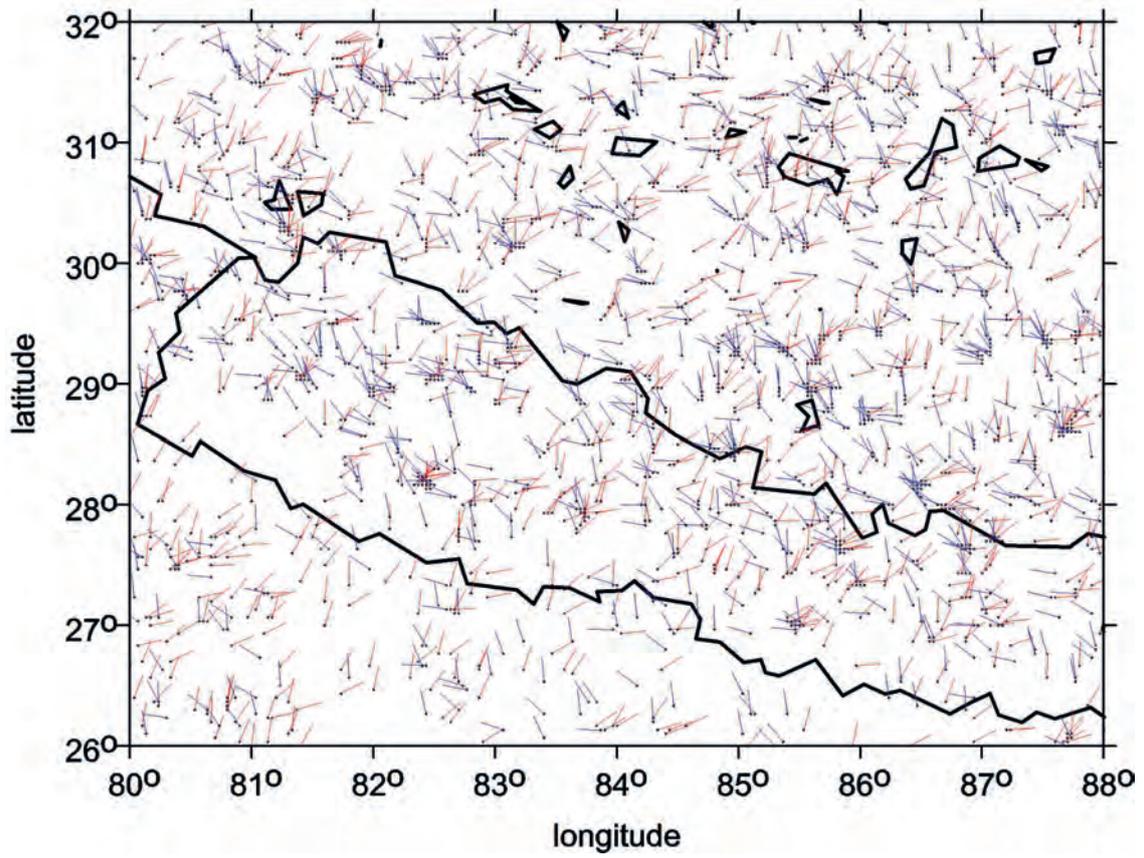
Fig. Ii The strike angle θ_S for $I > 0.9$.
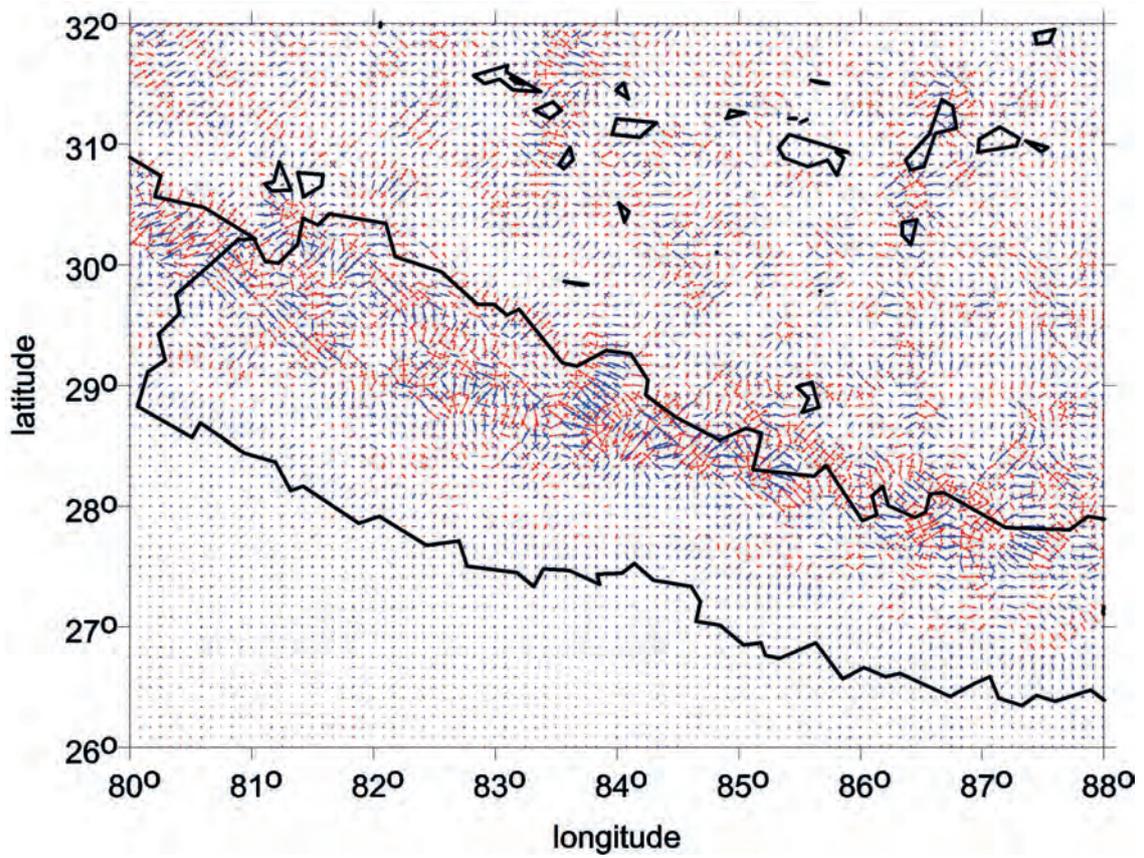
Fig. Ij The virtual deformations (red – dilatation, blue – compression) of the ellipse of deformation.

Fig. II The Japanese Islands in the wide collision zone of the East-Asian and West-Pacific lithospheric plates.
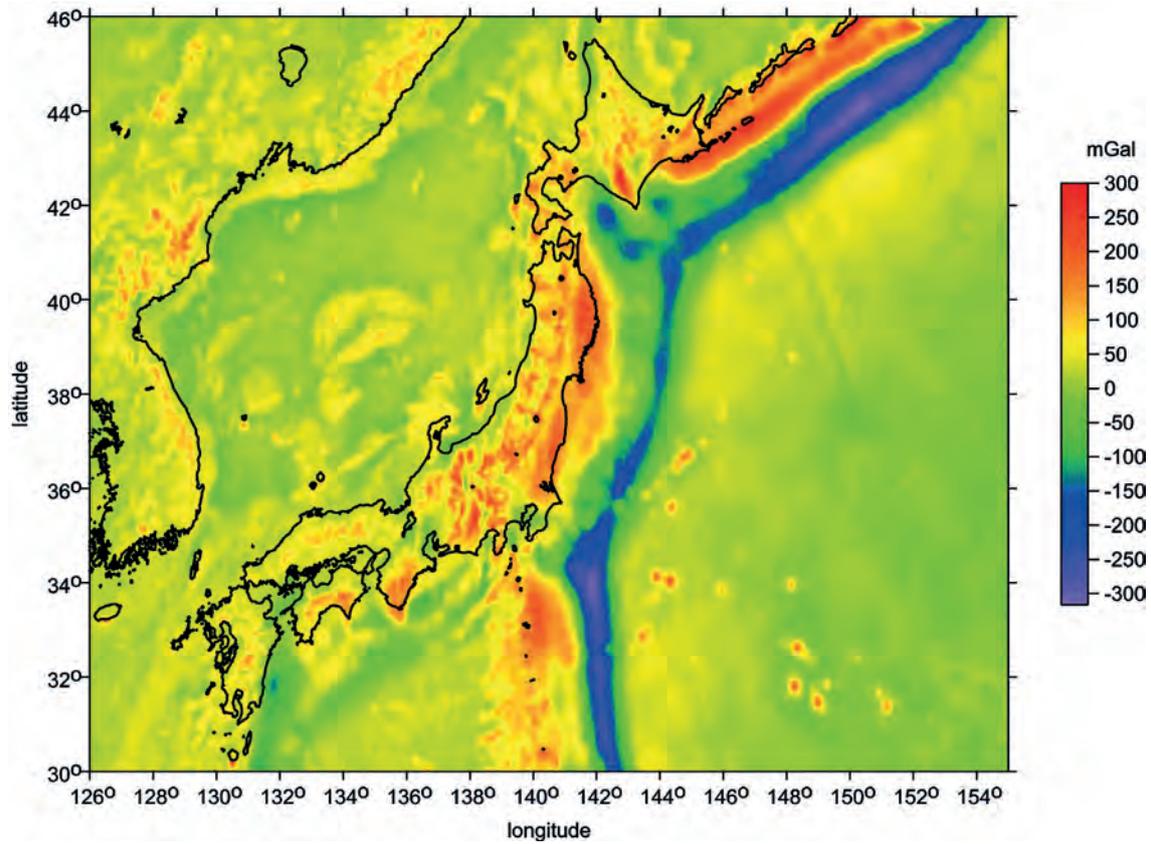

Fig. IIa The gravity anomalies Δ*g*.
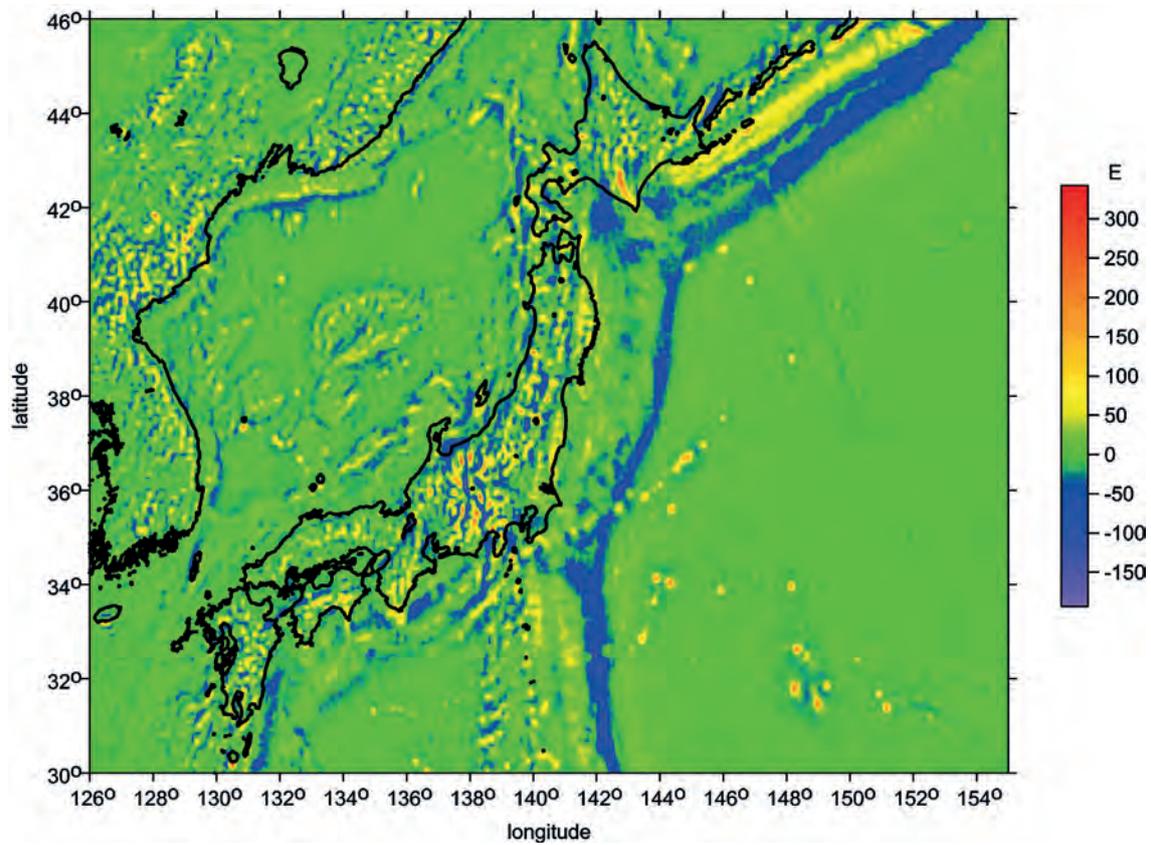
Fig. IIb The second derivative Γ_{33} of the disturbing gravitational potential.
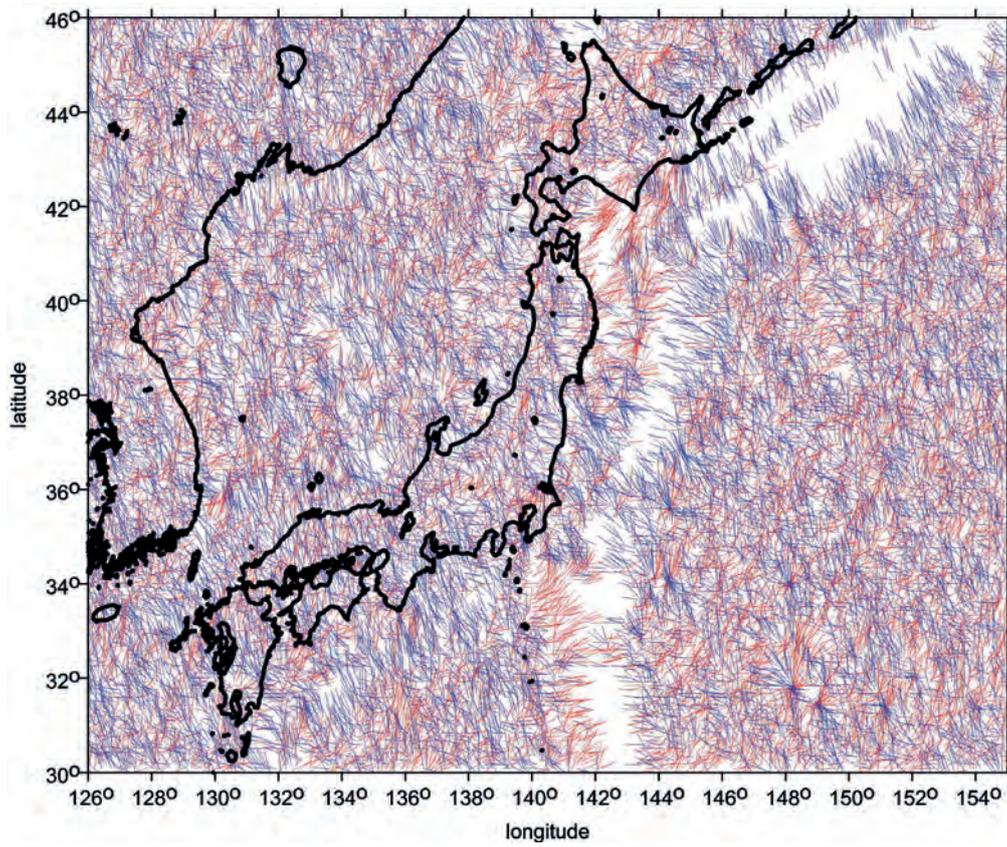
Fig. IIc The strike angle θ_S for $I > 0.3$.
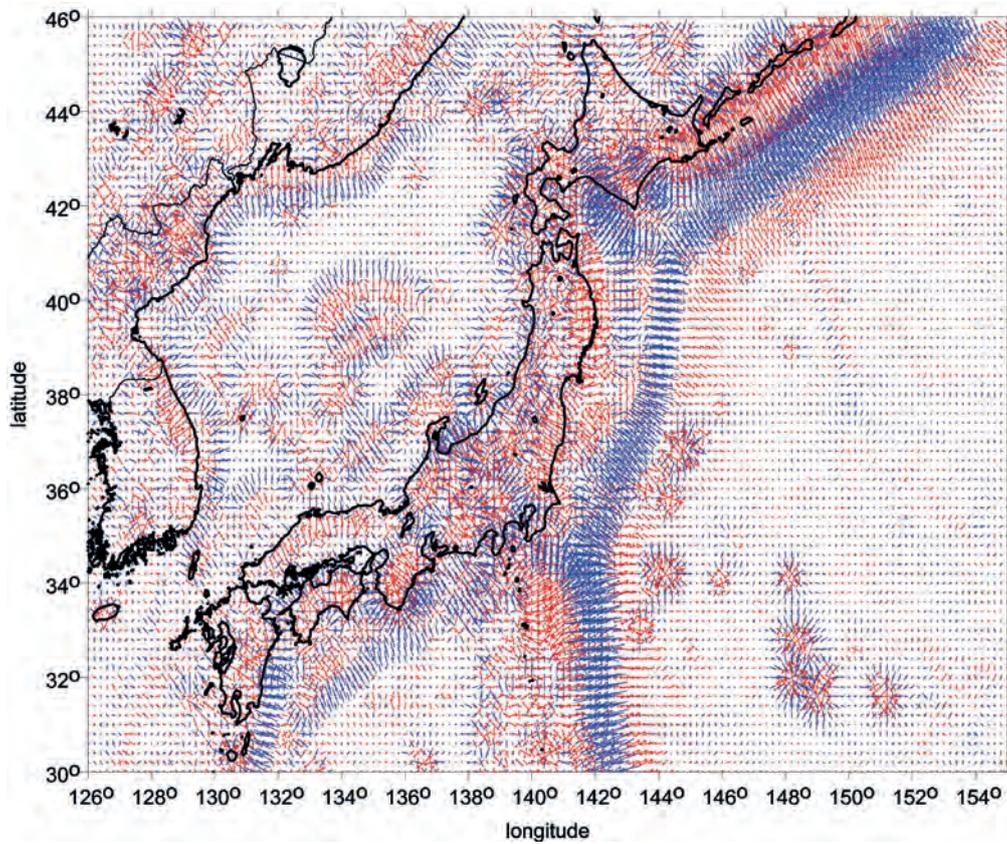
Fig. IId The virtual deformations (red – dilatation, blue – compression) of the ellipse of deformation.

Fig. III The broad contact region of north-eastern Africa, south-western Asia and south-eastern Europe.
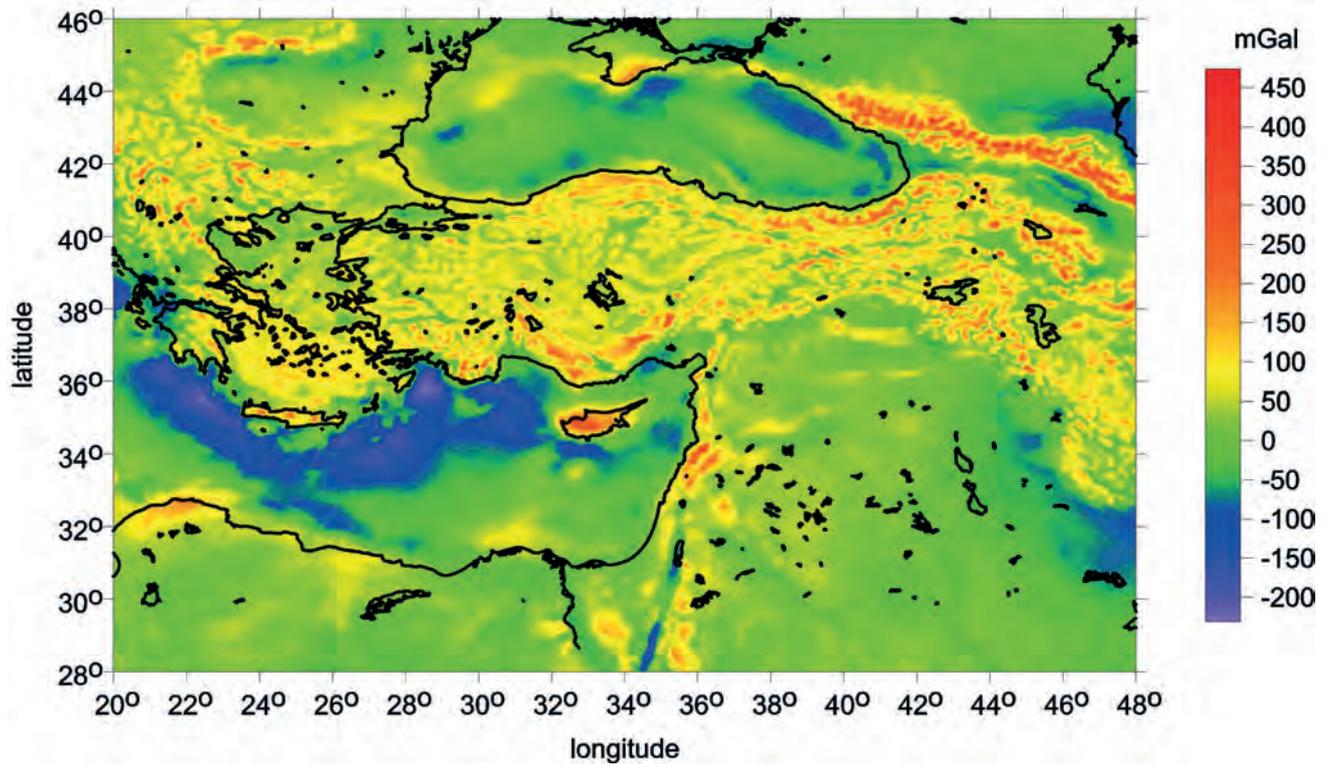
Fig. IIIa The gravity anomalies Δg.
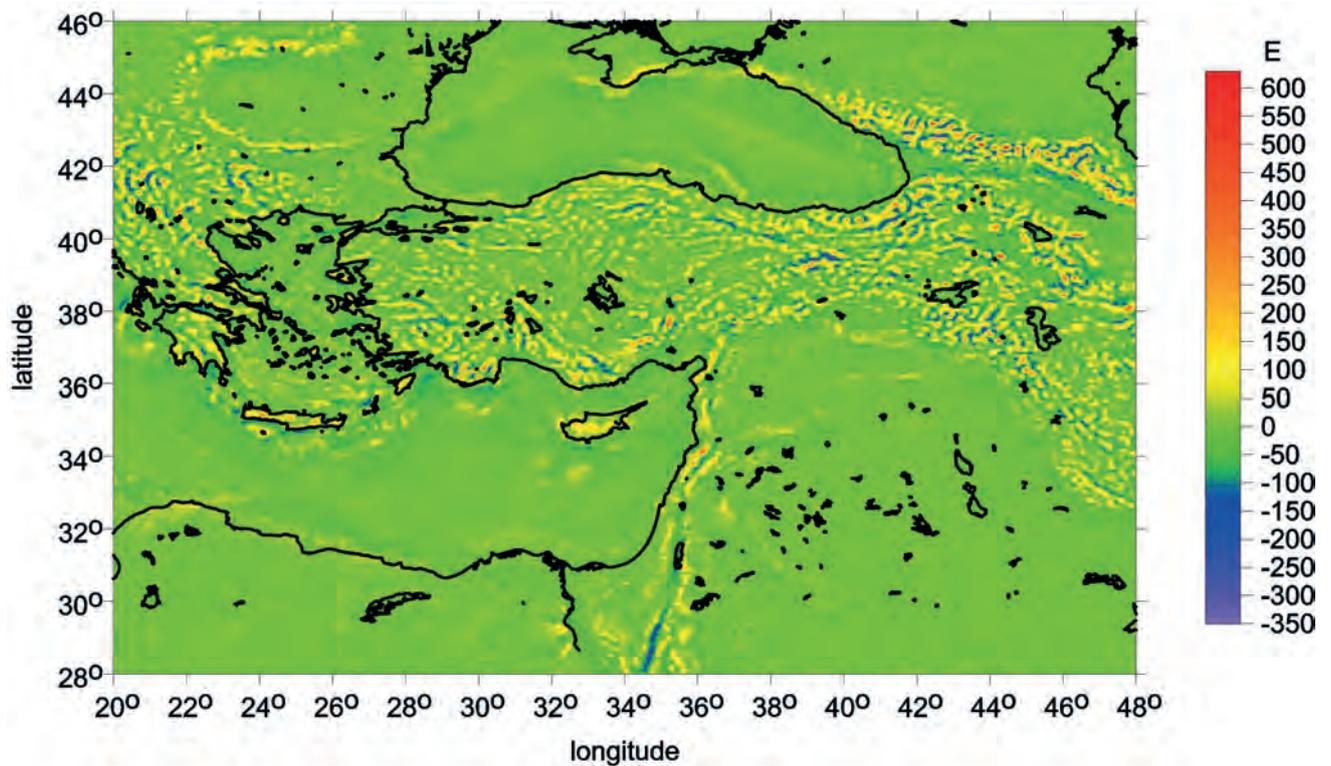
Fig. IIIb The second derivative Γ_{33} of the disturbing gravitational potential.
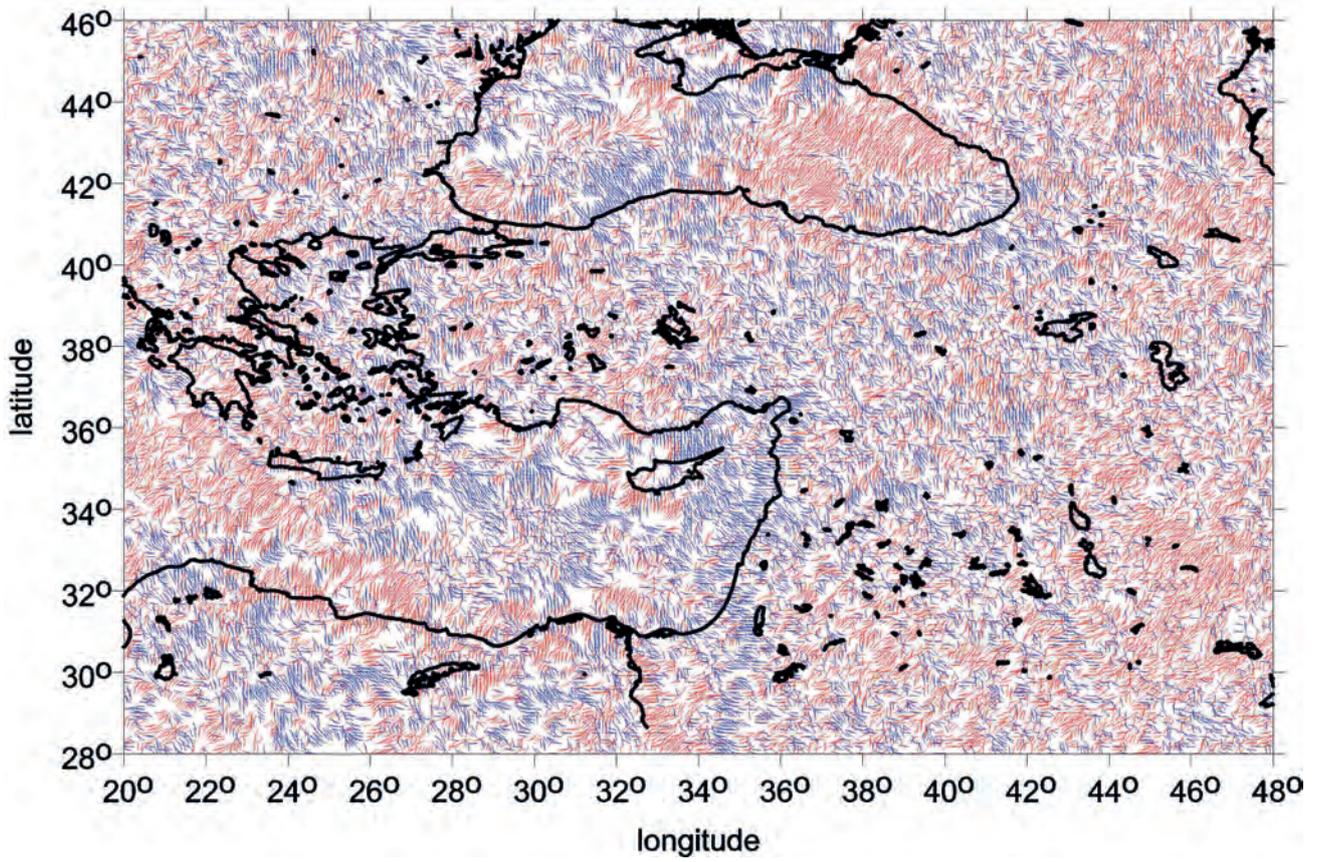
Fig. IIIc The strike angle θ_S for $I > 0.3$.
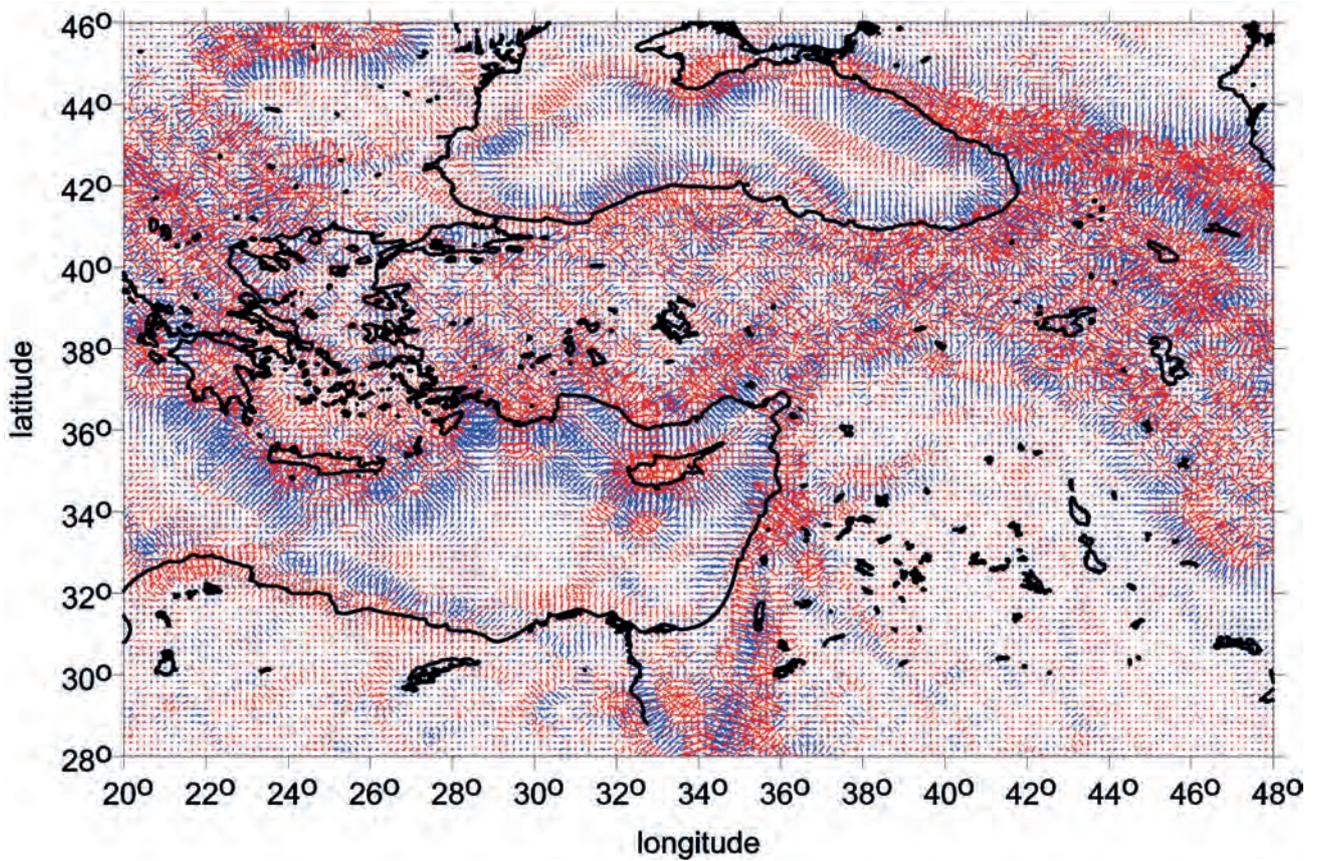
Fig. IIId The virtual deformations (red – dilatation, blue – compression) of the ellipse of deformation.

Fig. IV Central Europe with conspicuous contacts between the three extensive orogenetic units: the Eastern Alps, the Bohemian Massif and the Western Carpathians.
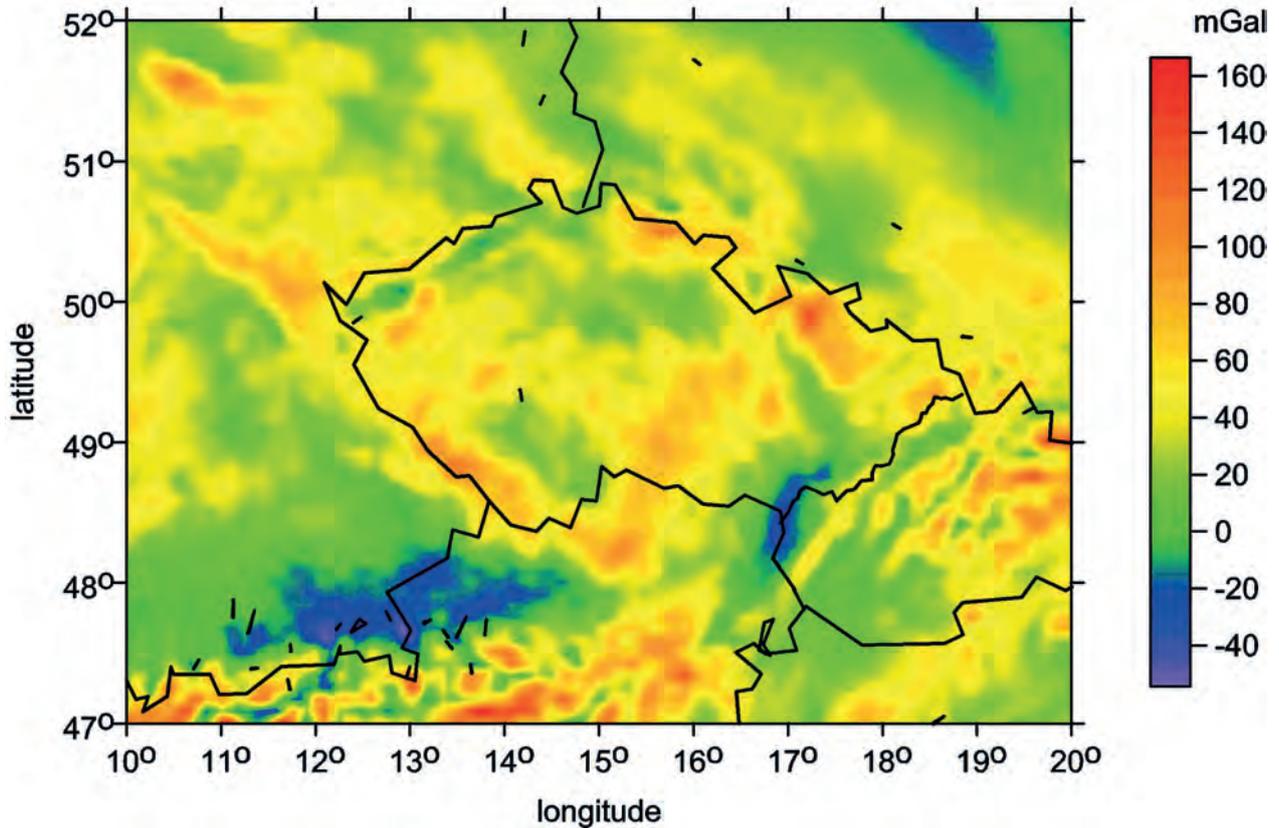
Fig. IVa The gravity anomalies Δg.
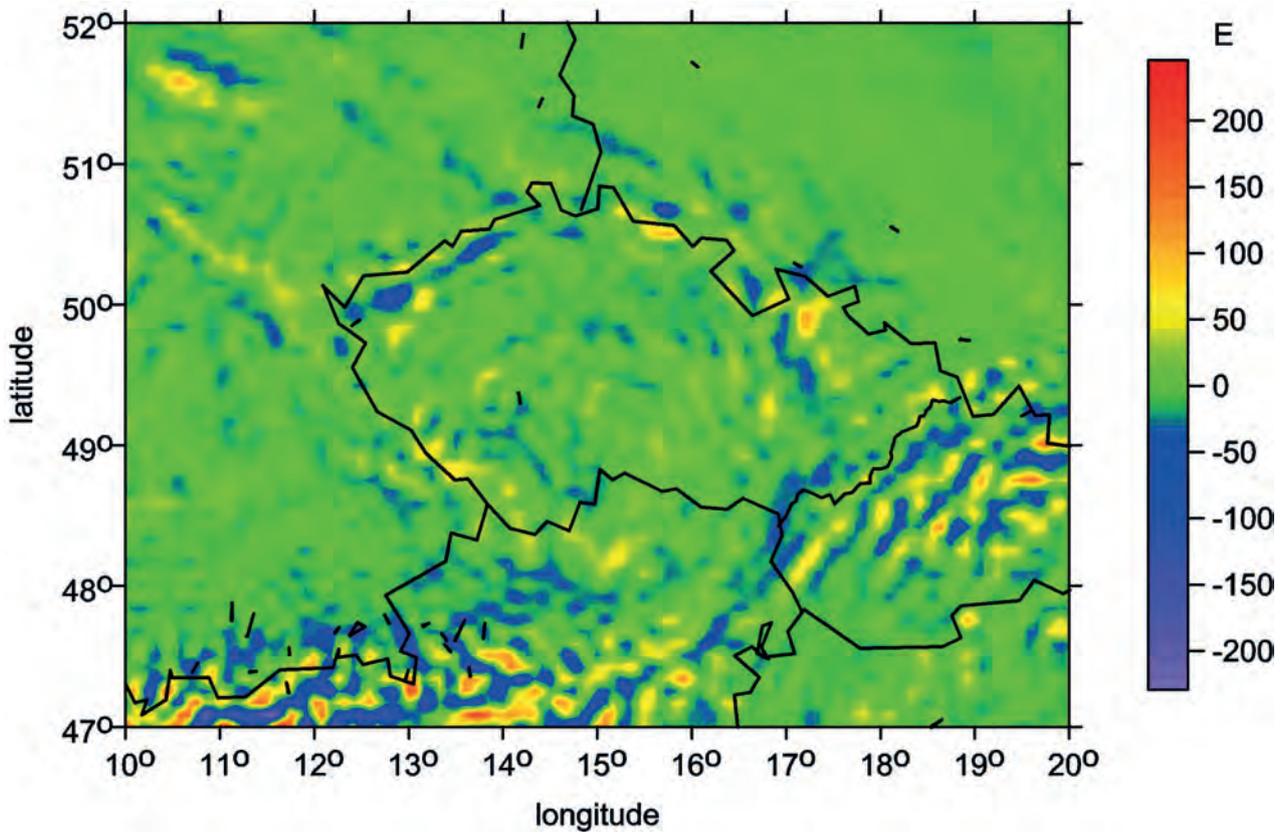
Fig. IVb The second derivative Γ_{33} of the disturbing gravitational potential.
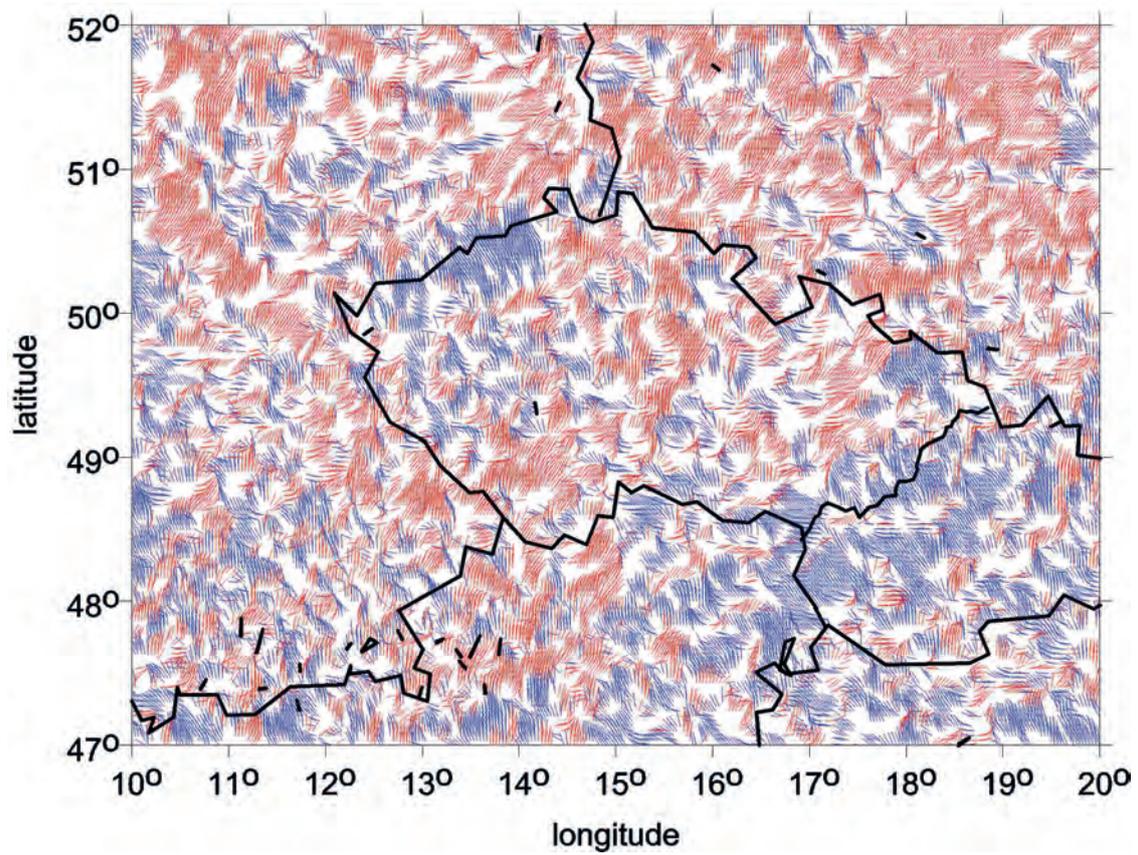
Fig. IVc The strike angle θ_S for $I < 0.3$ (looking for flat objects).
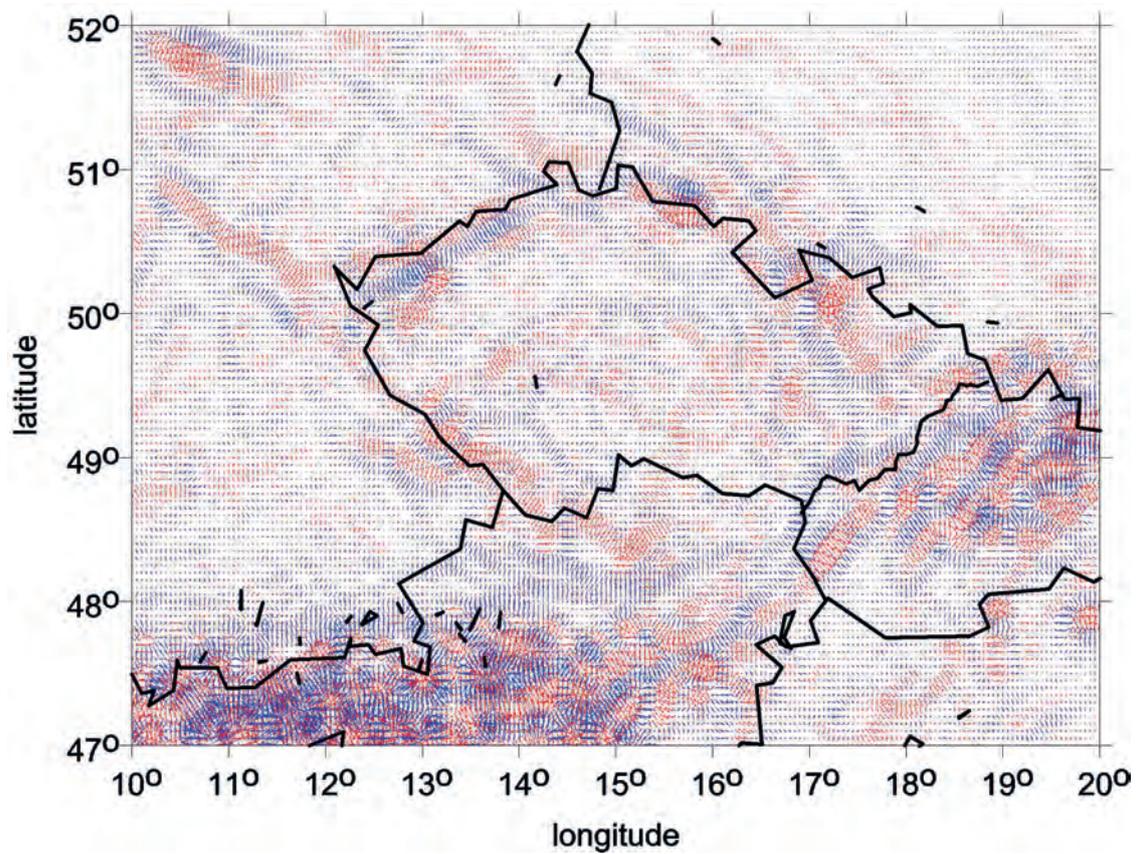
Fig. IVd The virtual deformations (red – dilatation, blue – compression) of the ellipse of deformation.

Fig. V The Vredefort impact crater in South Africa.
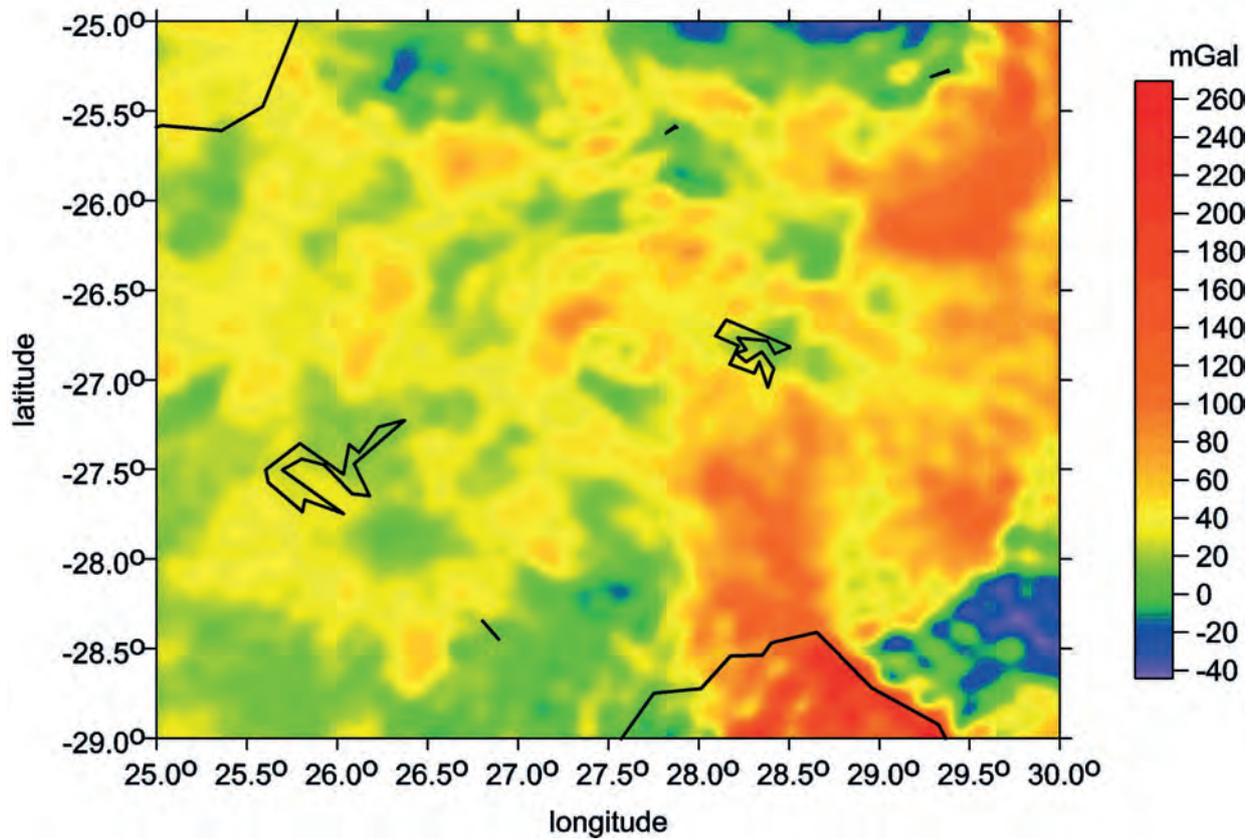
Fig. Va The gravity anomalies Δ*g*.
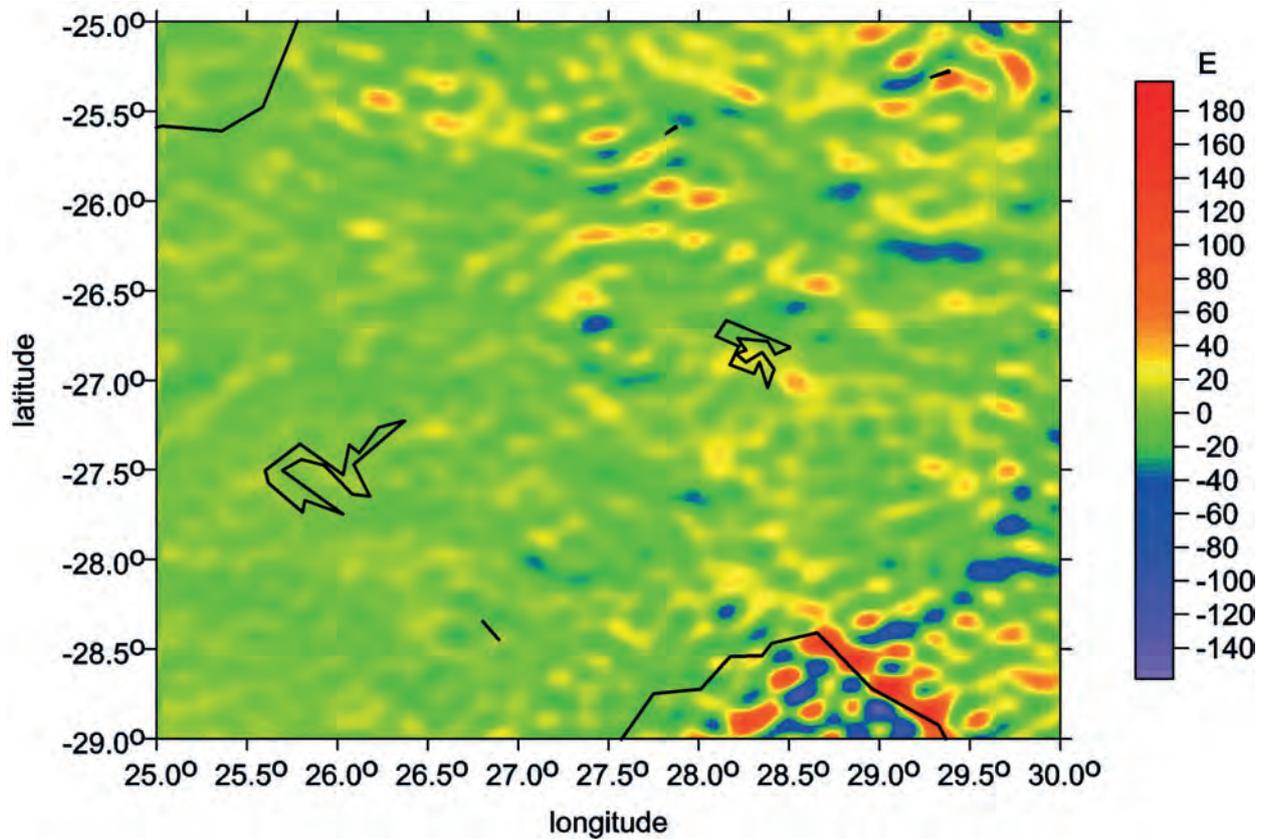
Fig. Vb The second derivative Γ_{33} of the disturbing gravitational potential.
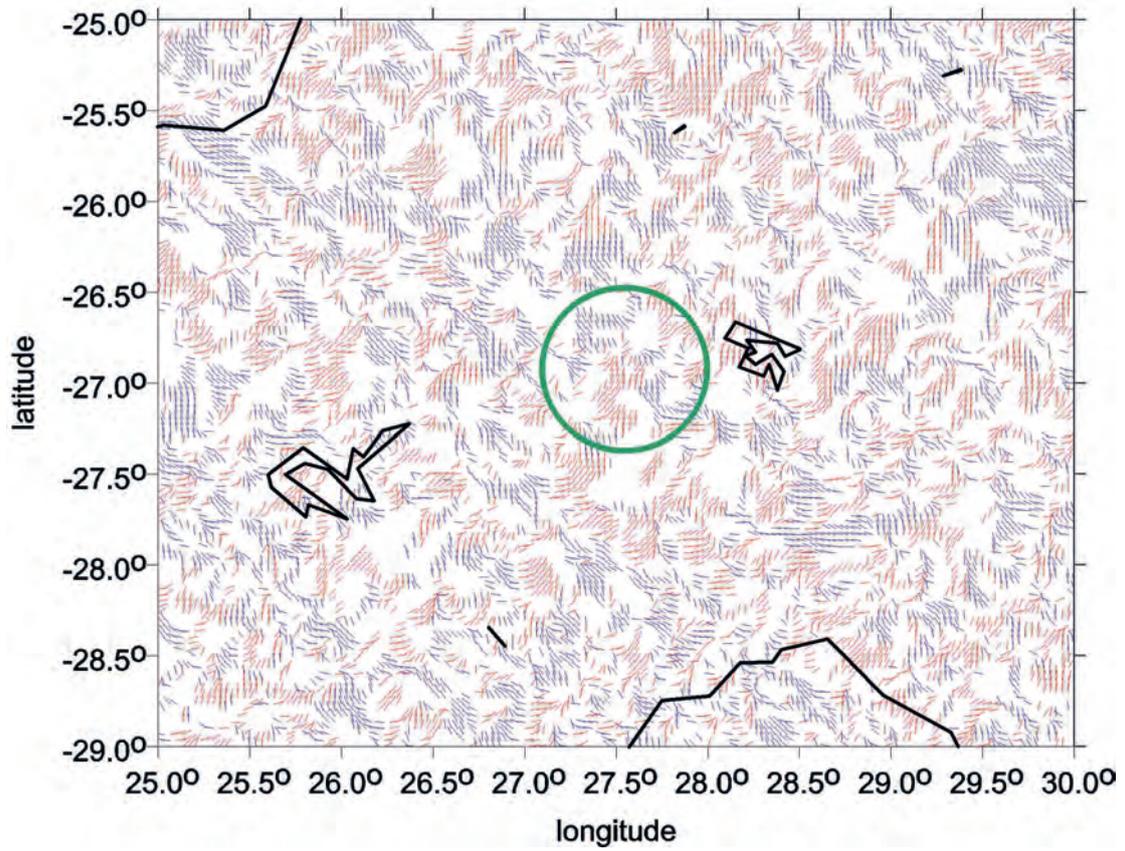
Fig. Vc The strike angle θ_S for $I < 0.3$ (looking for flat objects).
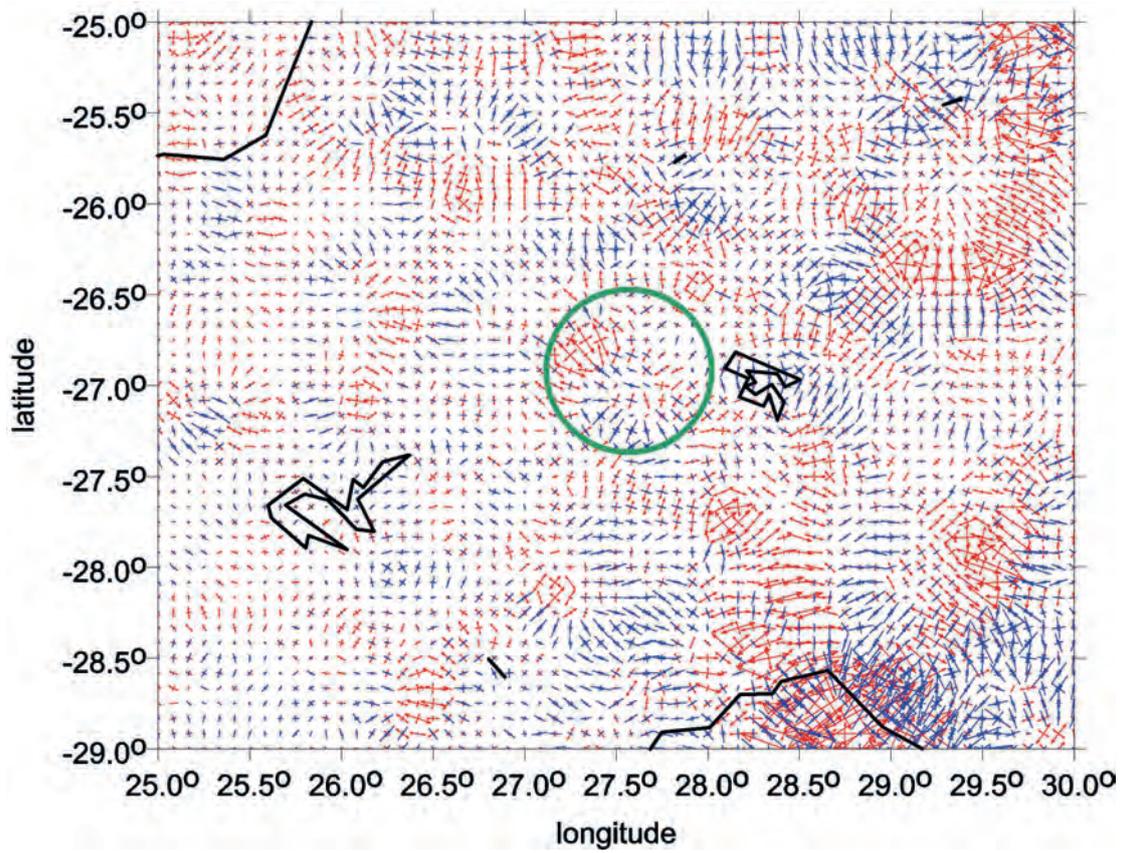
Fig. Vd The virtual deformations (red – dilatation, blue – compression) of the ellipse of deformation.

Fig. VI The Chicxulub impact crater, Yucatan.
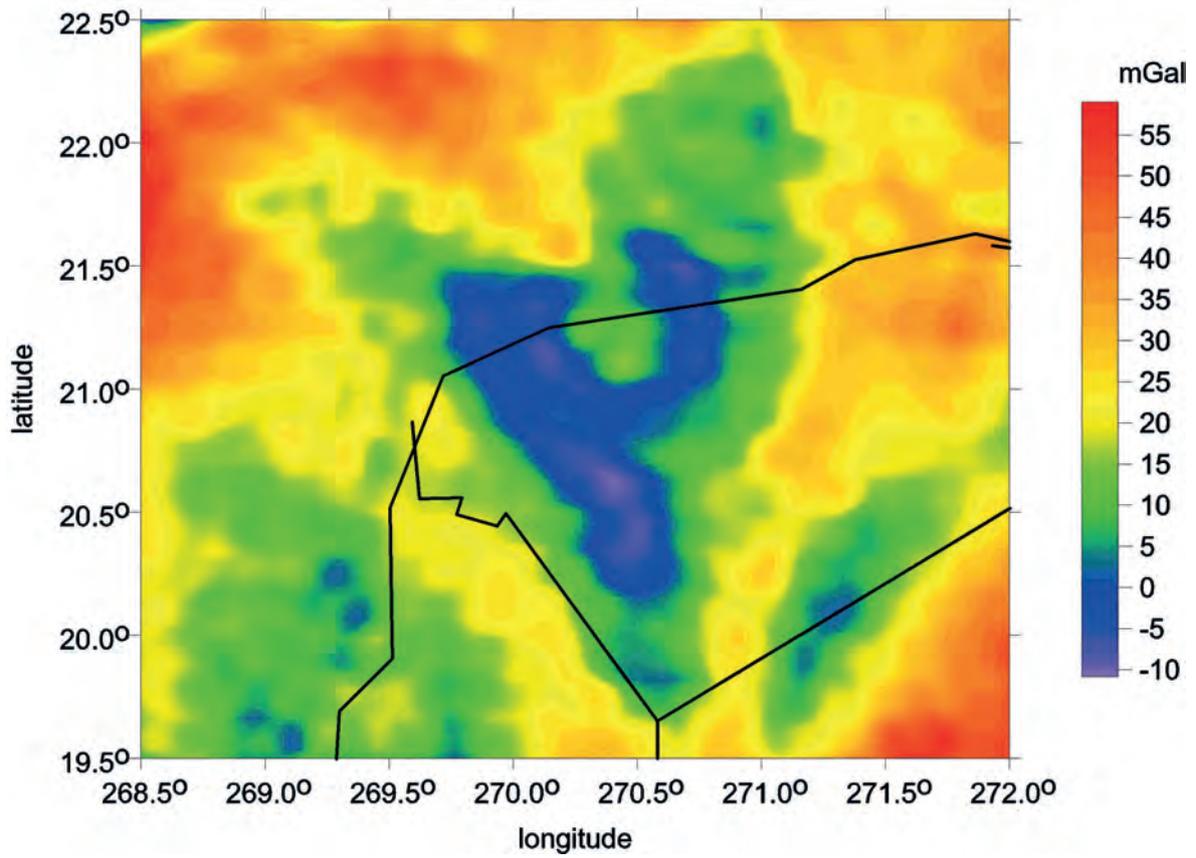
Fig. VIa The gravity anomalies Δ*g*.
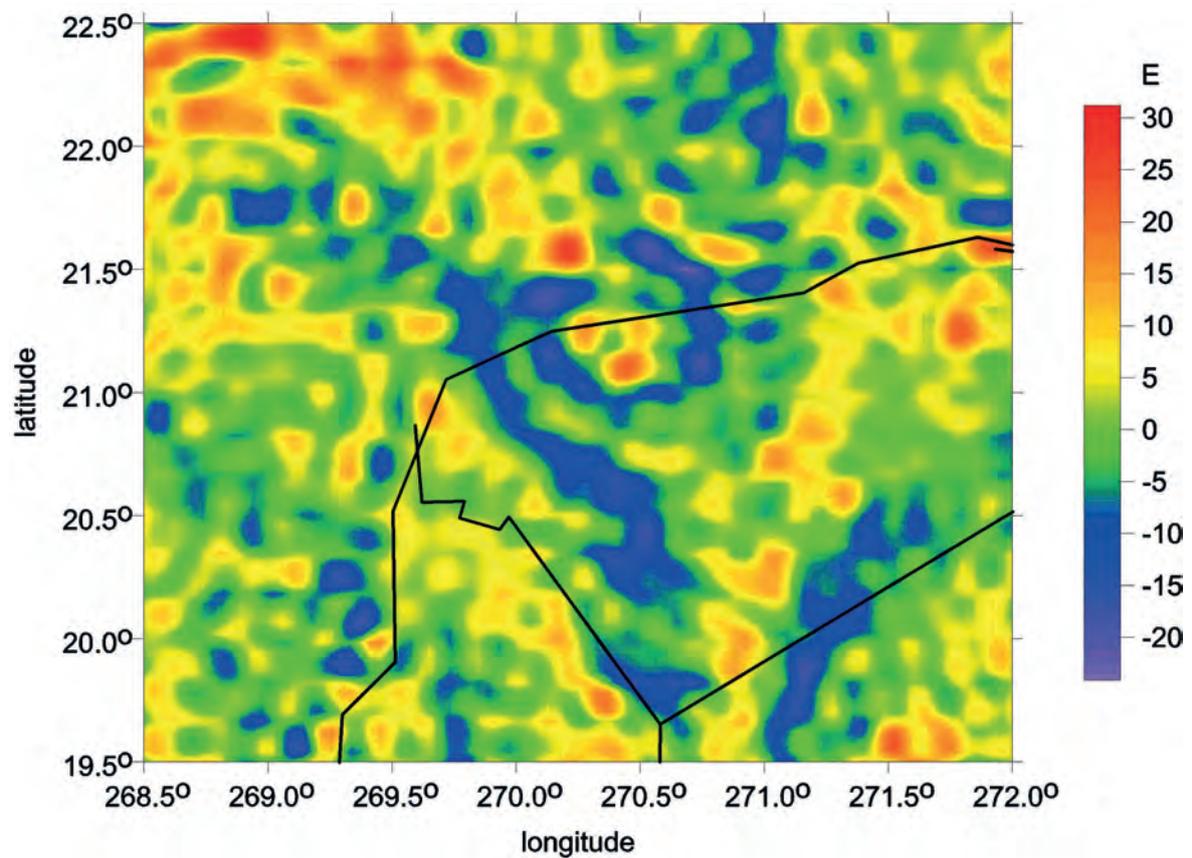

Fig. VIb The second derivative Γ_{33} of the disturbing gravitational potential.
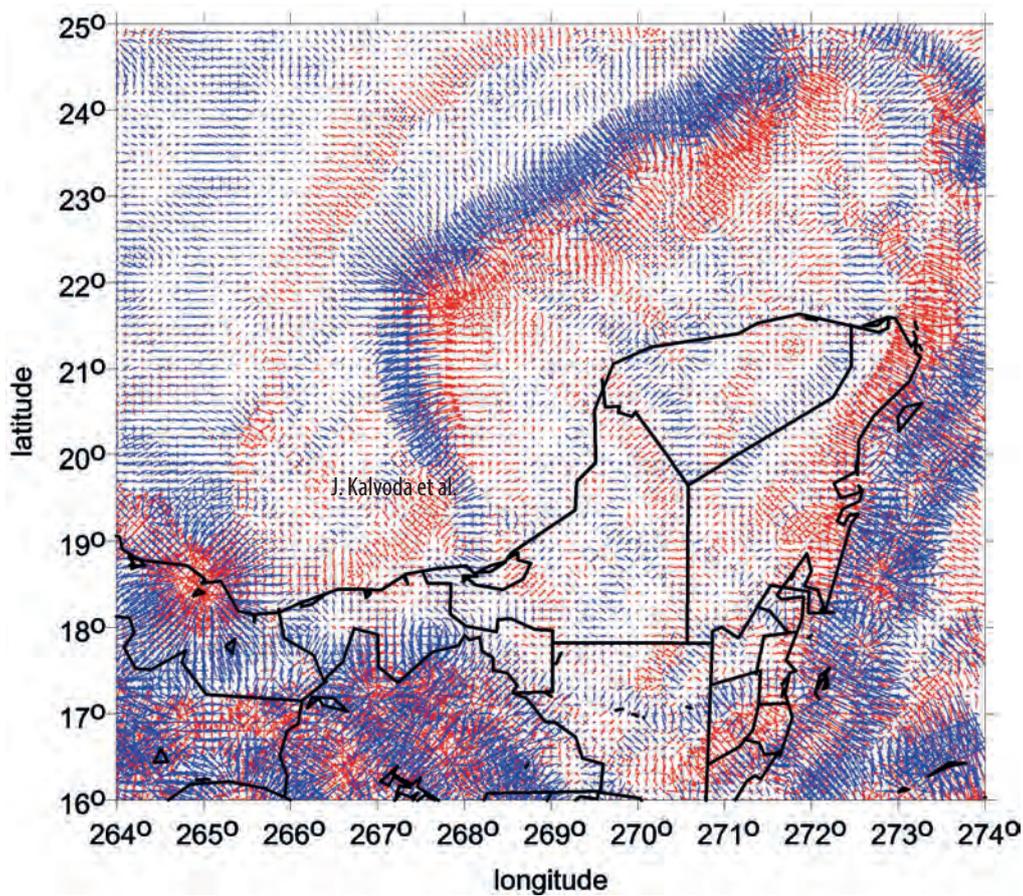
Fig. VIc The virtual deformations of the ellipse of deformation (red – dilatation, blue – compression) in the Mexico area and the Caribean (Campech bank).
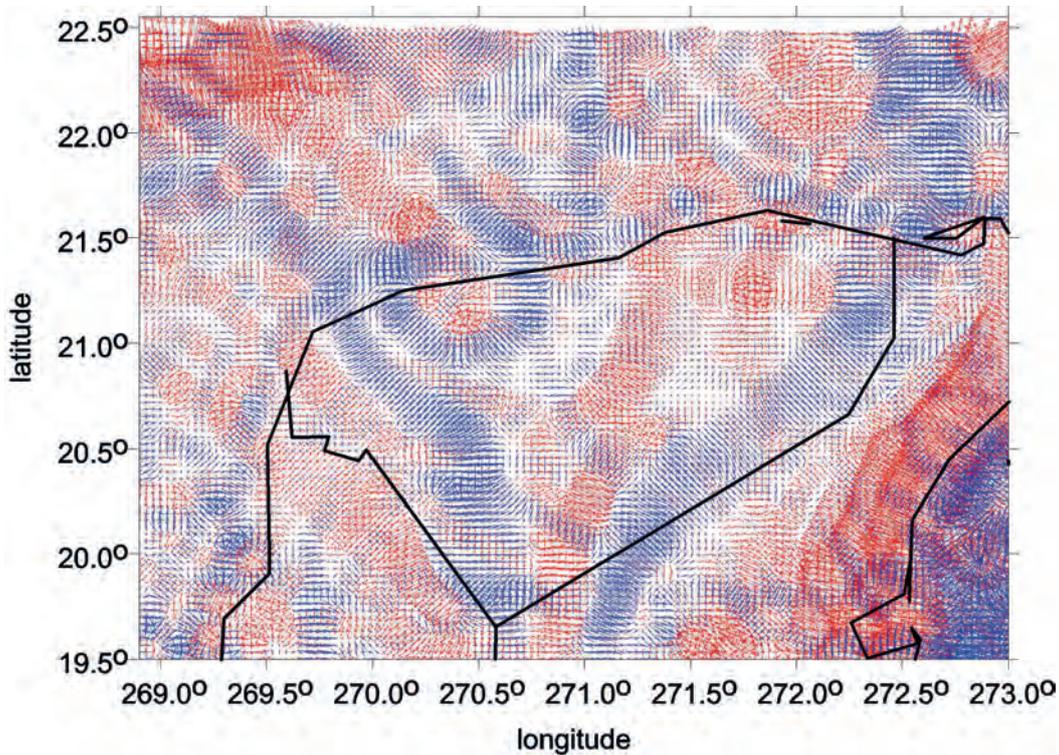
Fig. VId A detail of the round structure of the Chicxulub crater expressed by the virtual deformations of the ellipse of deformation (red – dilatation, blue – compression).

Fig. VII The Popigai impact crater, Siberia.
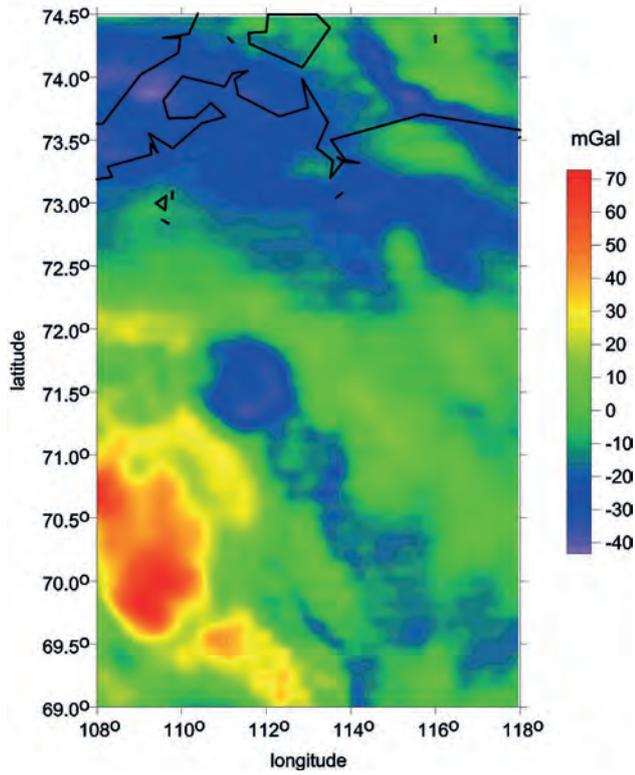
Fig. VIIa The gravity anomalies Δ*g*.
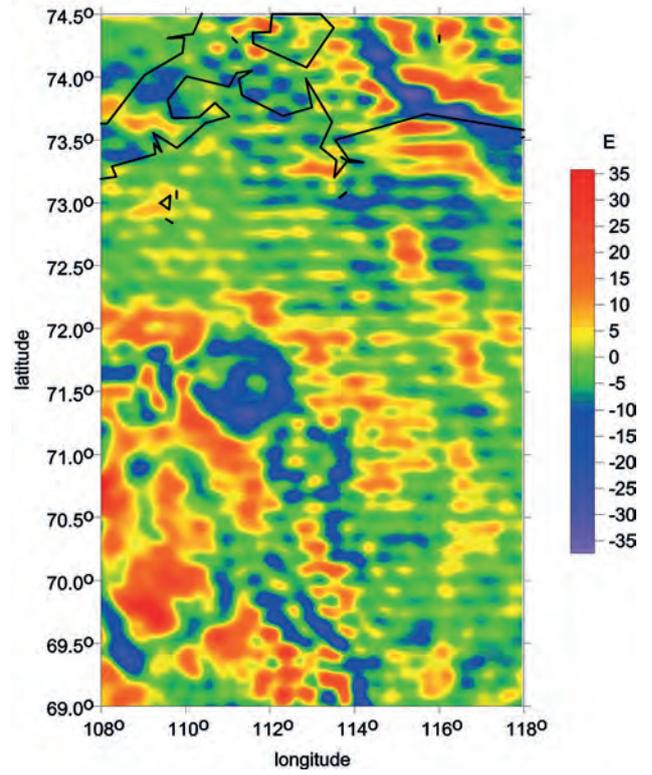
Fig. VIIb The second derivative Γ$_{33}$ of the disturbing gravitational potential.
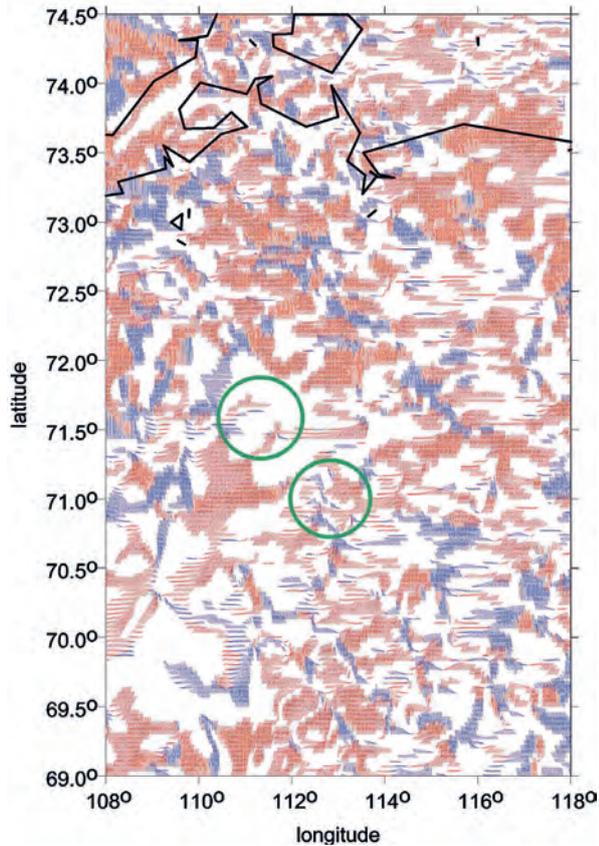
**Fig. VIIc** The strike angle θ_S for *I* < 0.3 (looking for flat objects).
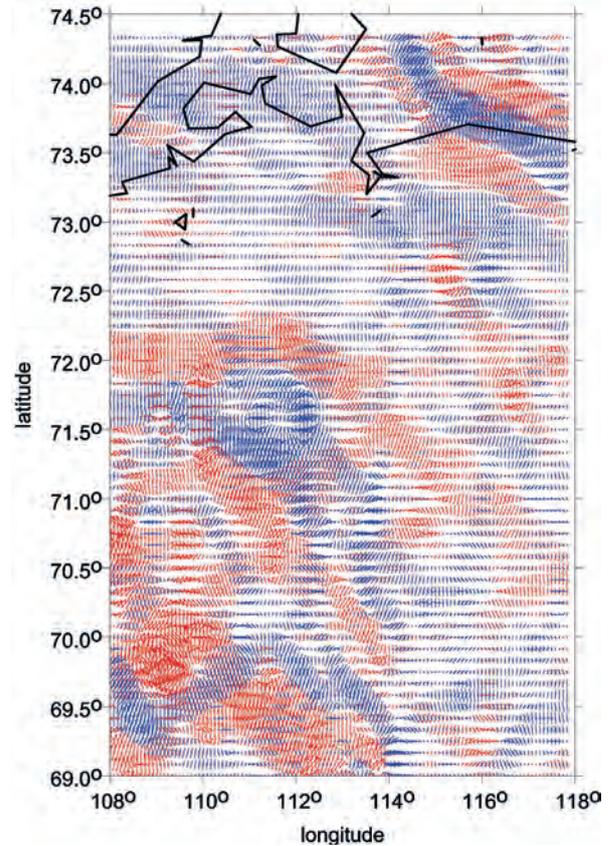
Fig. VIId The virtual deformations (red – dilatation, blue – compression) of the ellipse of deformation.

Fig. VIII The Lake Baikal region.
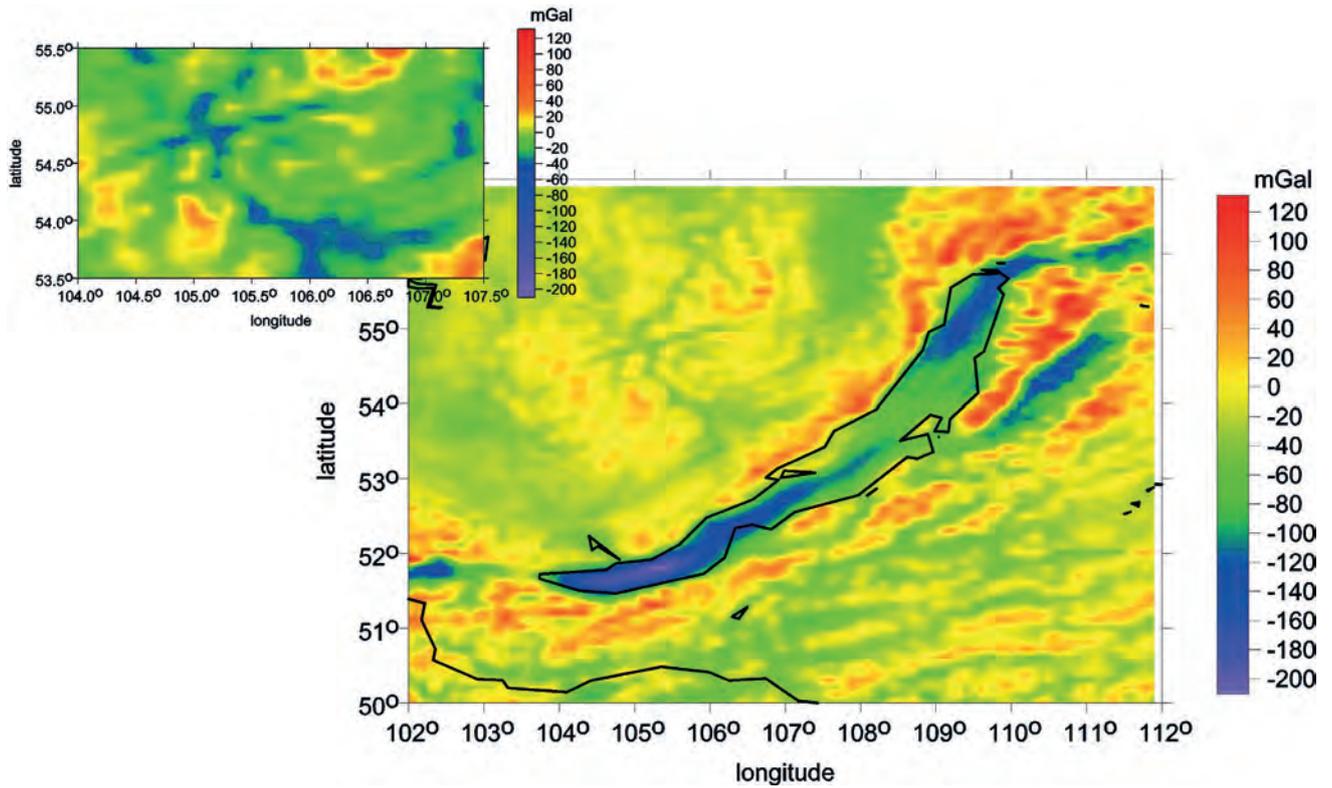
Fig. VIIIa The gravity anomalies Δ*g*.
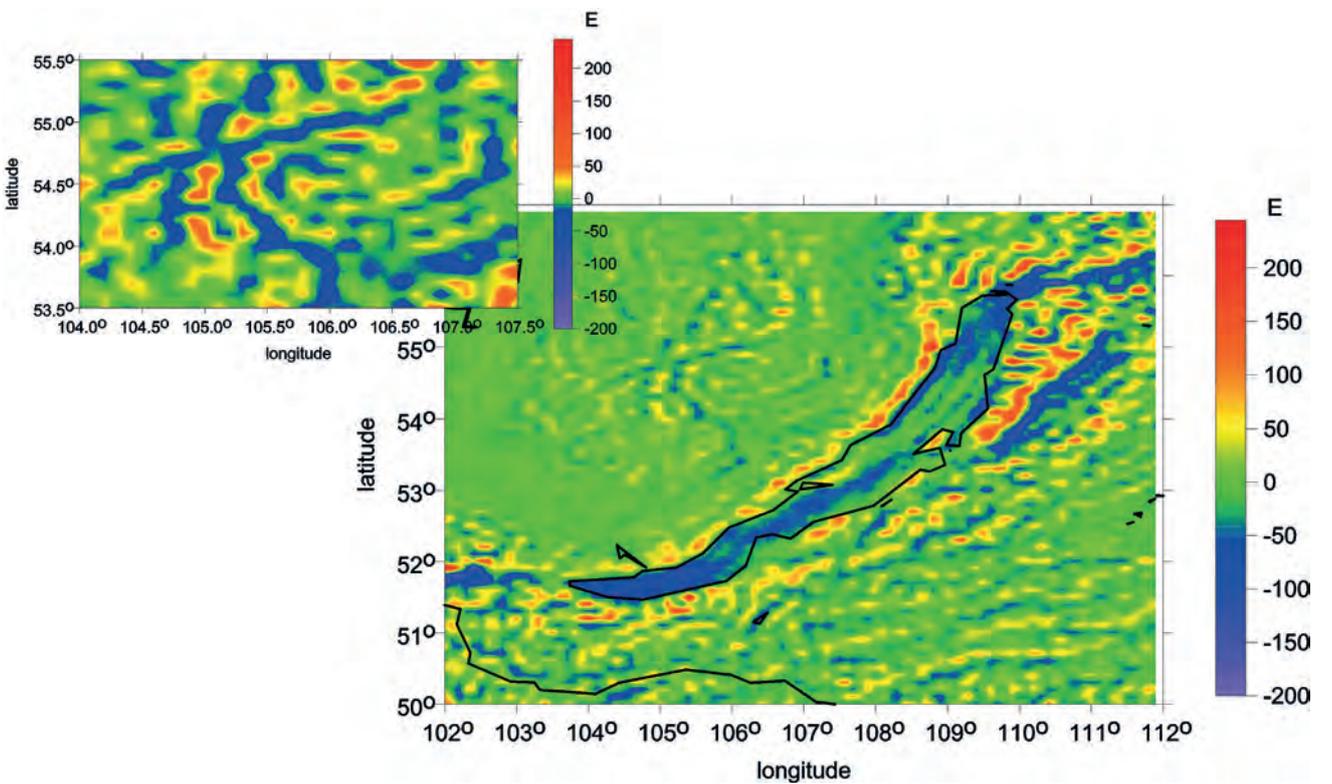
Fig. VIIIb The second derivative Γ$_{33}$ of the disturbing gravitational potential.

Fig. IX The area of the Grand Canyon in Arizona. (Part of the Colorado River is shown by red lines).
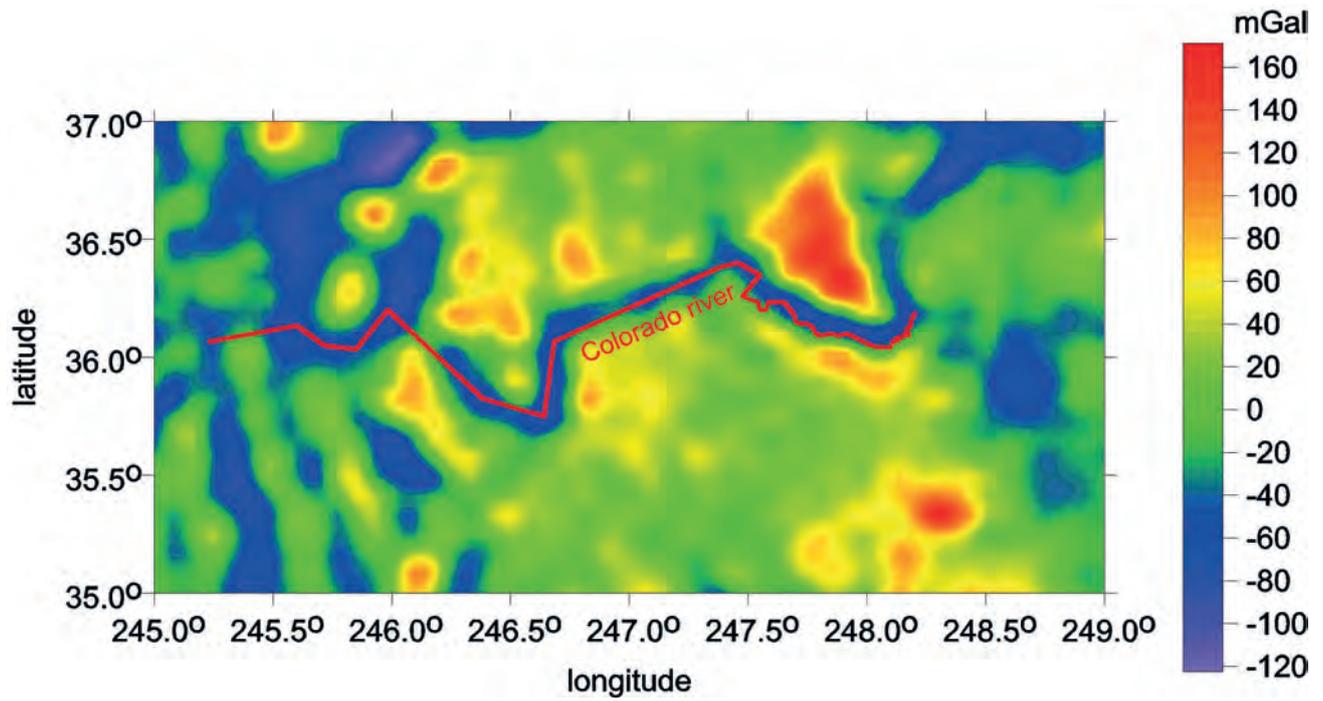
Fig. IXa The gravity anomalies Δg.
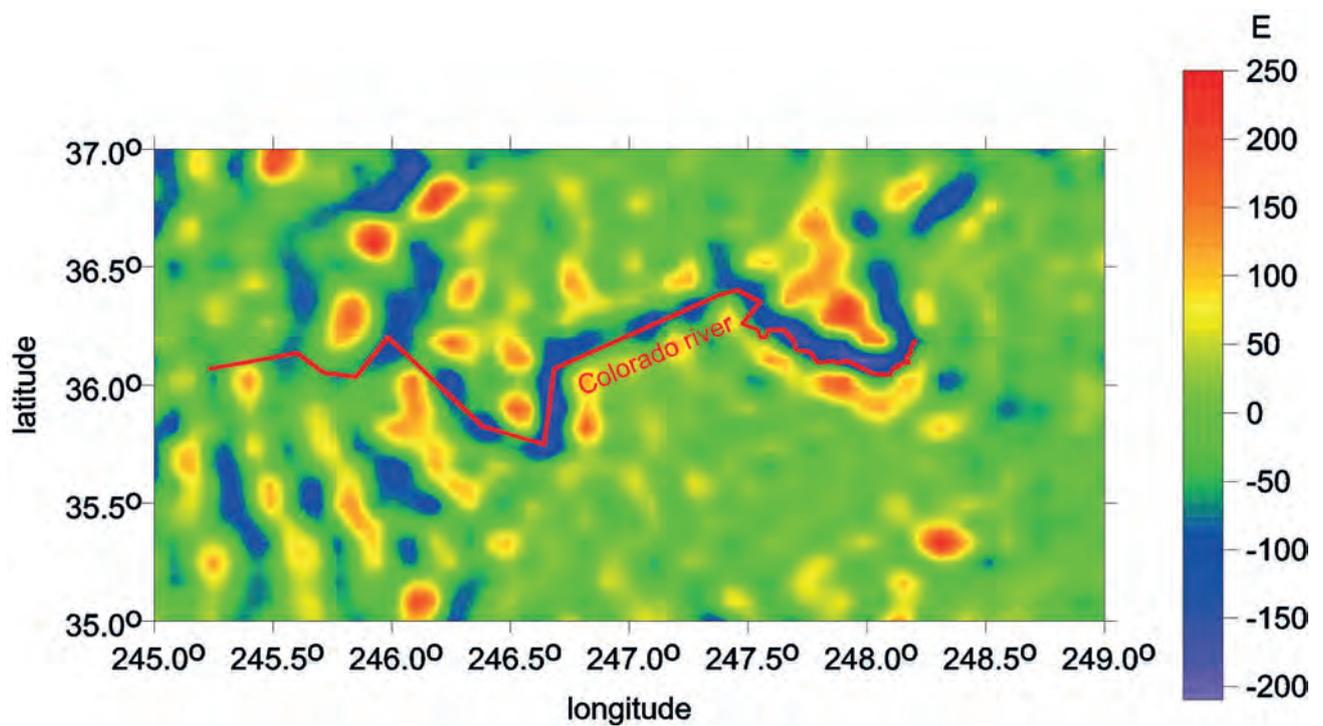
Fig. IXb The second derivative Γ_{33} of the disturbing gravitational potential.

Fig. X The area of the stratovolcanoes Popocatepetl (5426 m, P) and Iztaccihuatl (5230 m, I) in Mexico.
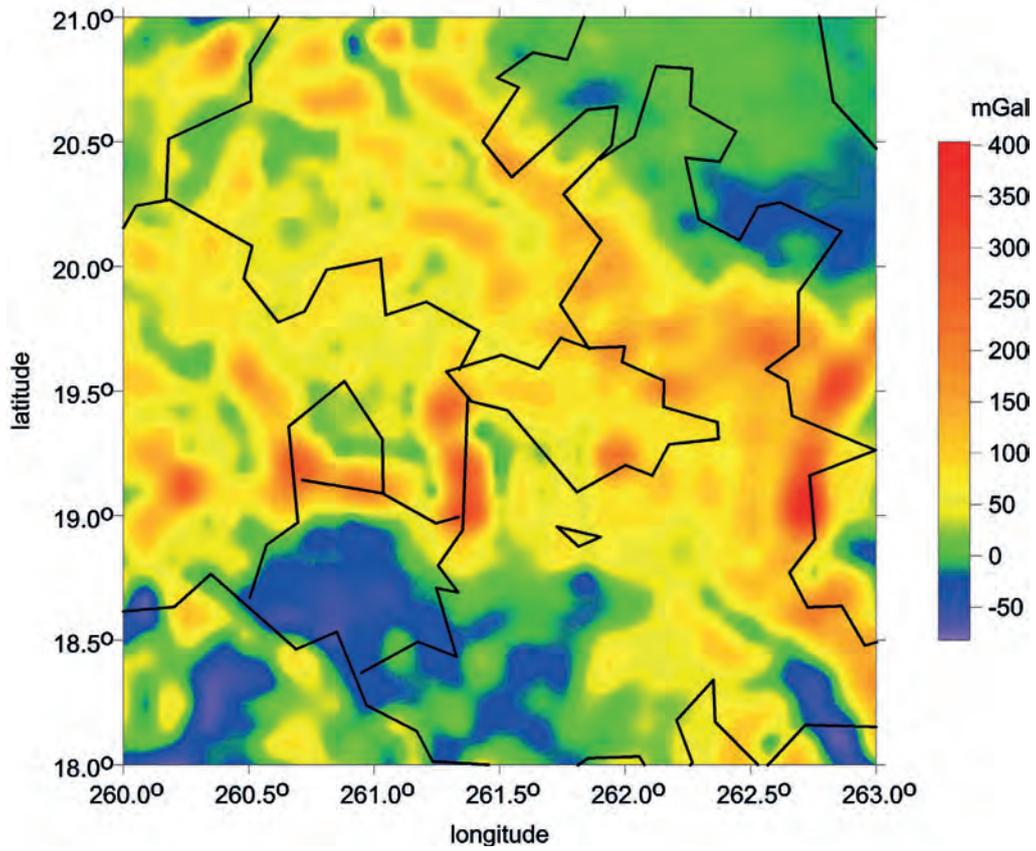
Fig. Xa The gravity anomalies Δ*g*.
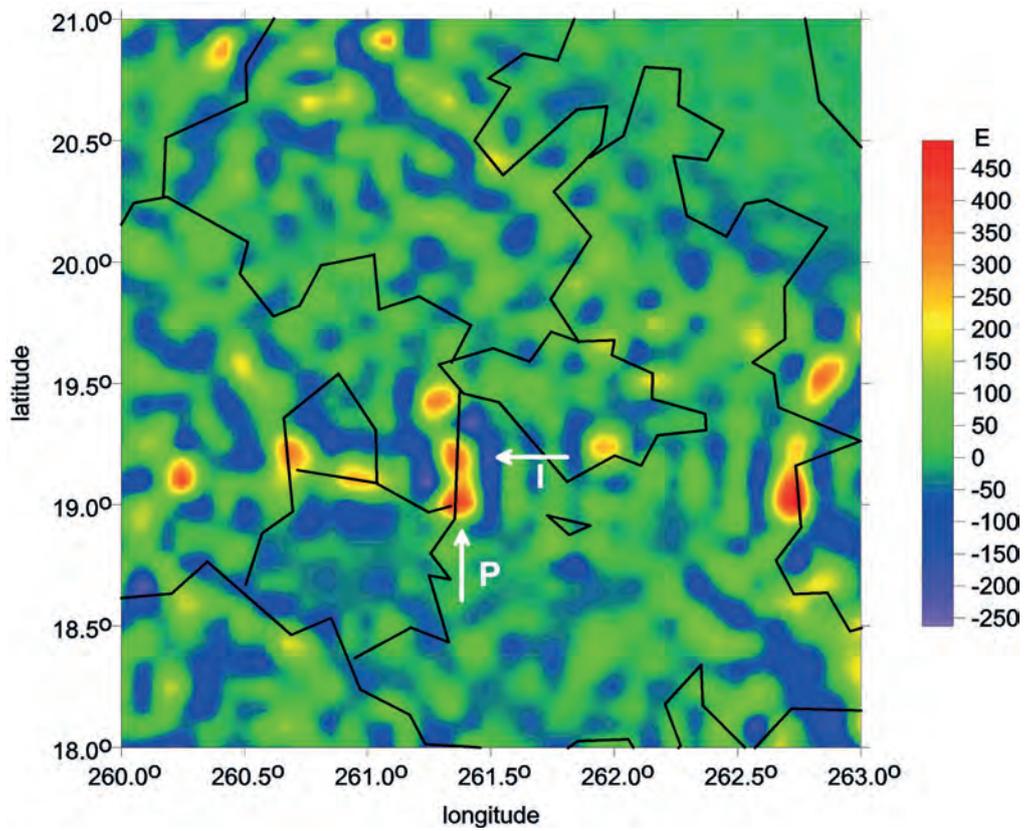
Fig. Xb The second derivative Γ_{33} of the disturbing gravitational potential.

Fig. XI Southern parts of the Caspian Sea and its neighbouring areas.
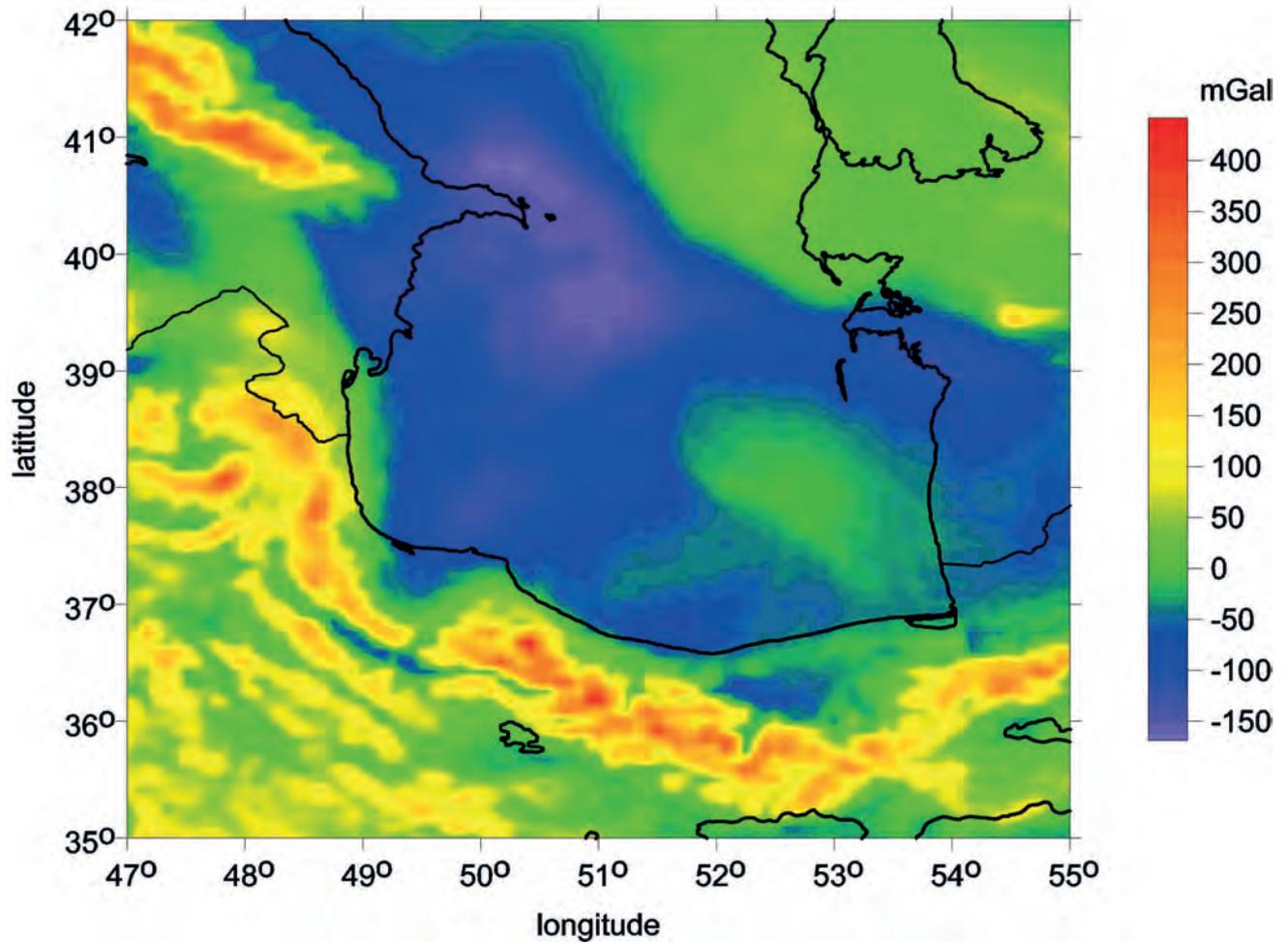
Fig. XIa The gravity anomalies Δ*g*.
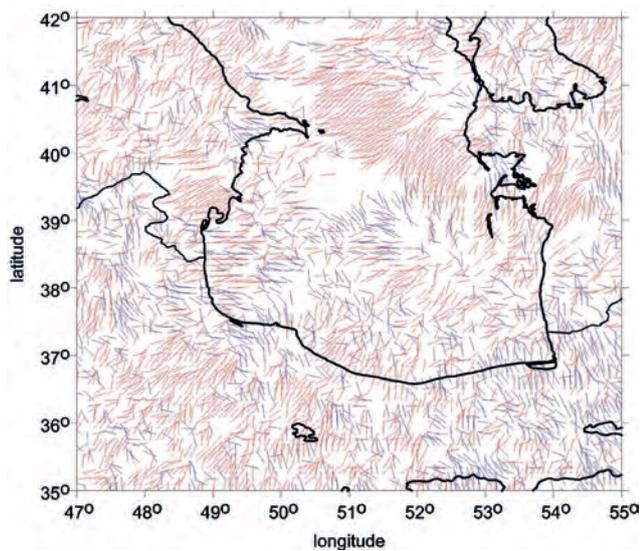
Fig. XIb The strike angle θ_S for *I* < 0.3 (looking for flat objects). Note the belt of vectors oriented to one side crossing the central part of the Caspian Sea.
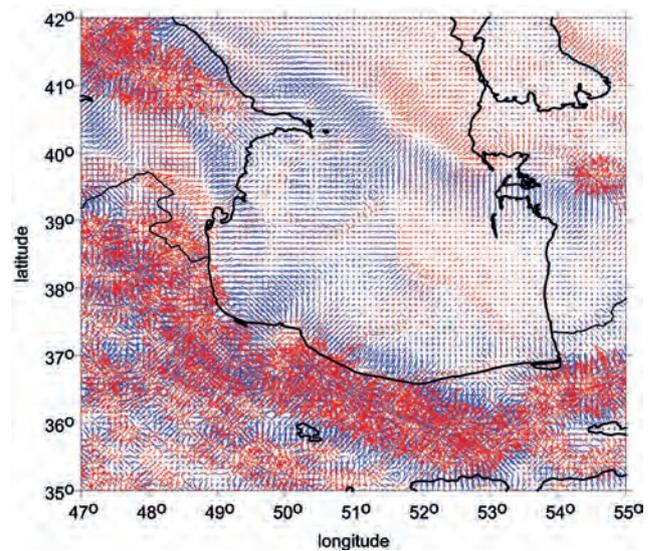
Fig. XIc The virtual deformations (red – dilatation, blue – compression) of the ellipse of deformation. A clear "belt" going roughly from West to East across the Caspian Sea.

Fig. XII The area of the Ghawar oil fields, Saudi Arabia.
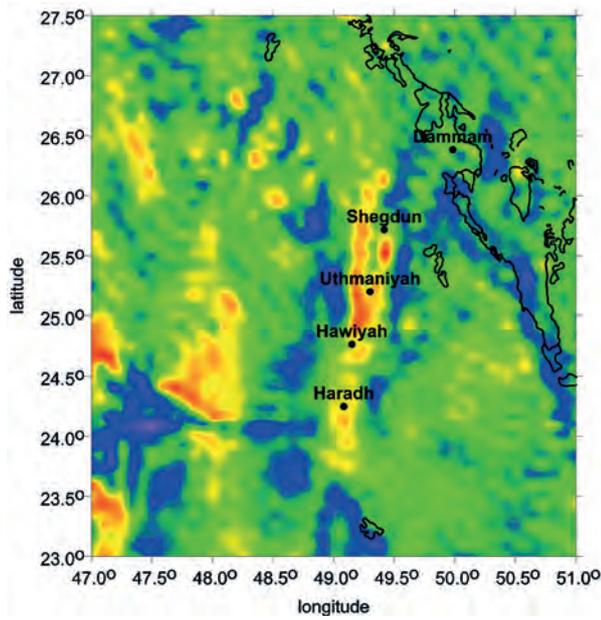
Fig. XIIa The second derivative Γ_{33} of the disturbing gravitational potential.
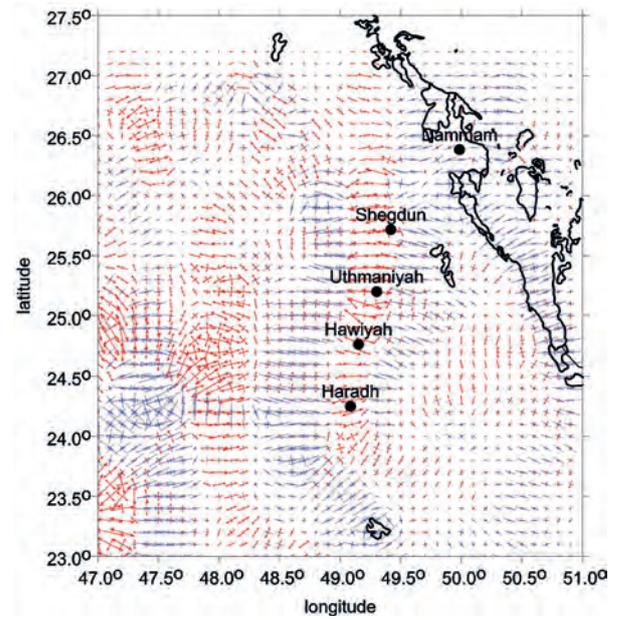
Fig. XIIb The virtual deformations (red – dilatation, blue – compression) of the ellipse of deformation.
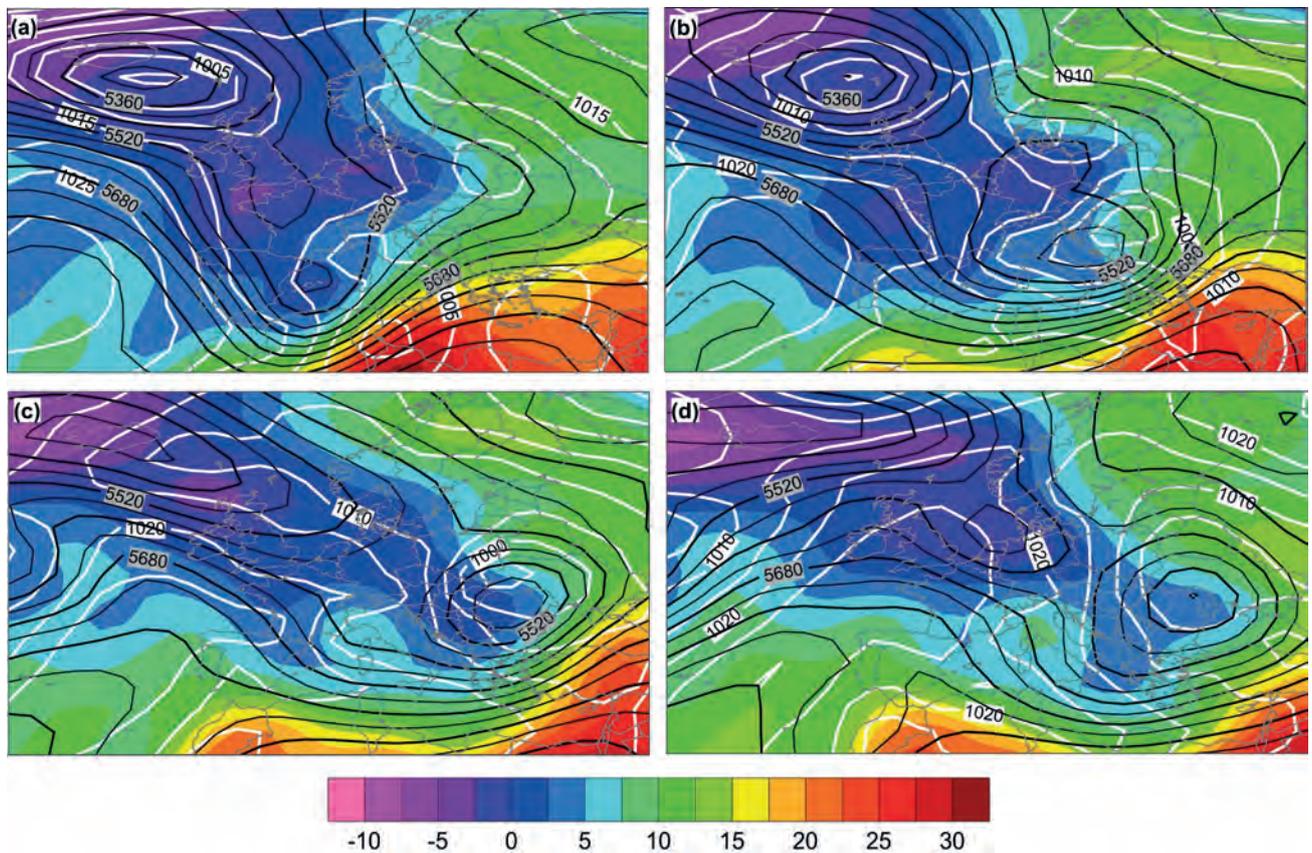
Fig. XIII NCEP-NCAR re-analyses of temperature [°C] at 850 hPa, geopotential height [m] of 500 level and sea level pressure [hPa] in Euro-Atlantic region just before and during the May 2010 event: (a) 14 May 2010 at 18 UTC, (b) 15 May 2010 at 18 UTC, (c) 16 May 2010 at 18 UTC, and (d) 17 May 2010 at 18 UTC.
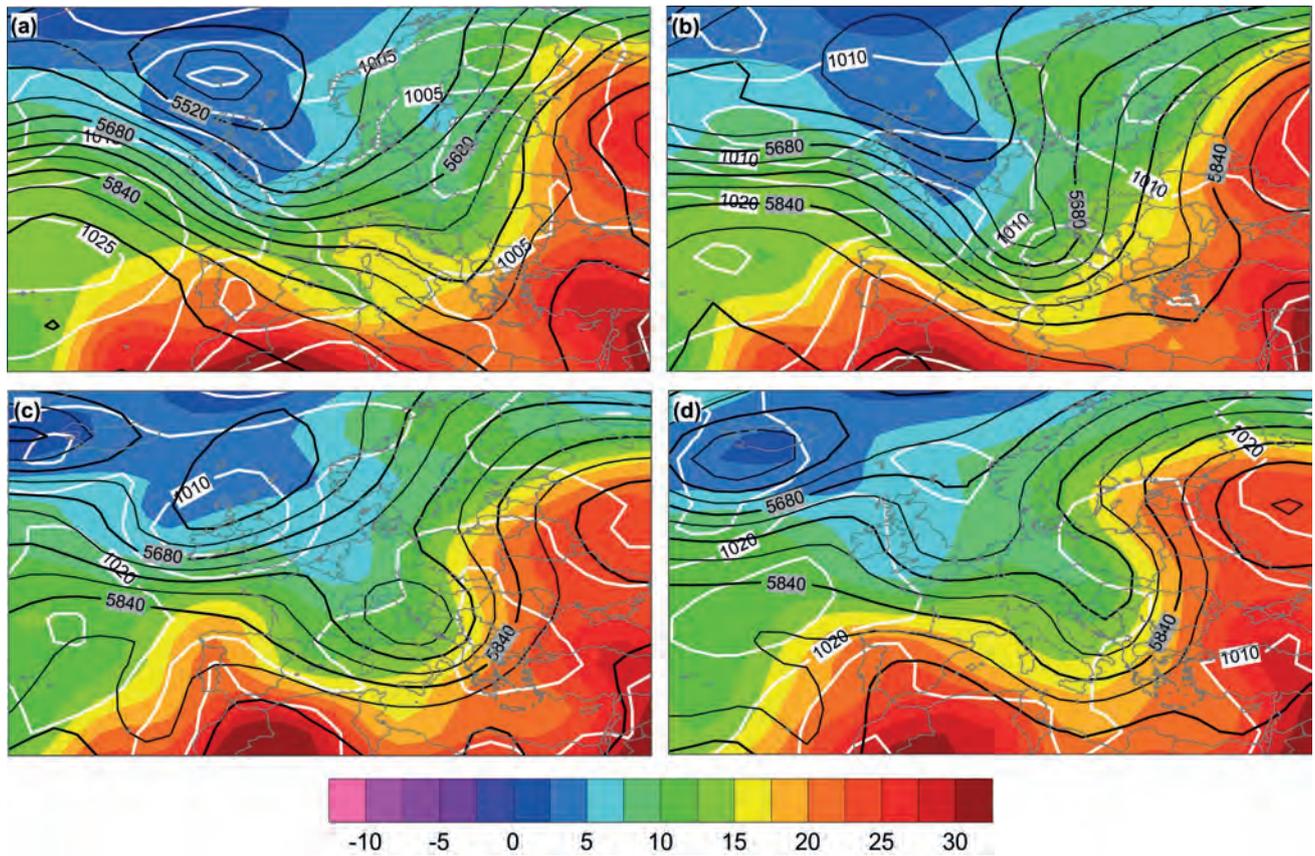
Fig. XIV Same as Figure 2, but for the August 2010 event: (a) 4 August 2010 at 18 UTC, (b) 5 August 2010 at 18 UTC, (c) 6 August 2010 at 18 UTC, and (d) 7 August 2010 at 18 UTC.
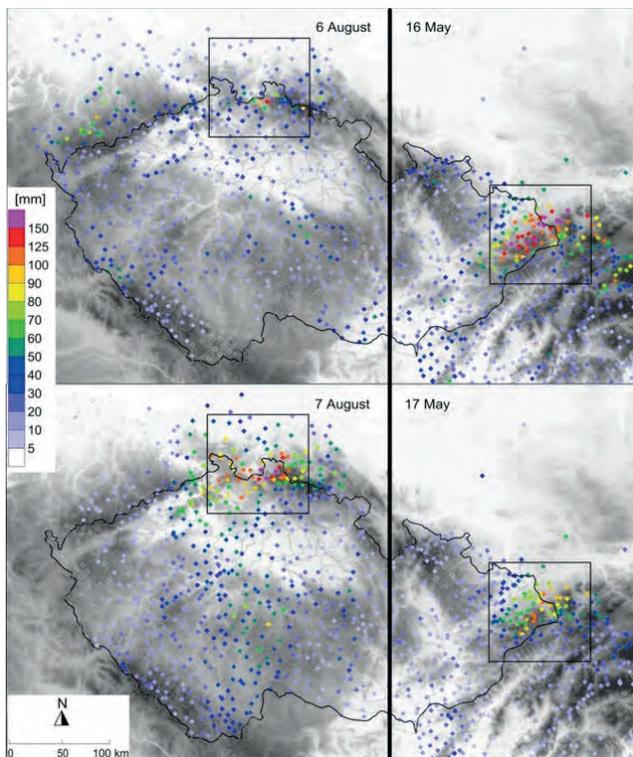
Fig. XV Daily precipitation totals in May 2010 and in August 2010 (the right and the left part of the figure, respectively); days with less intense precipitation are not depicted. The boxes indicate the most affected areas further studied in Figure IV.
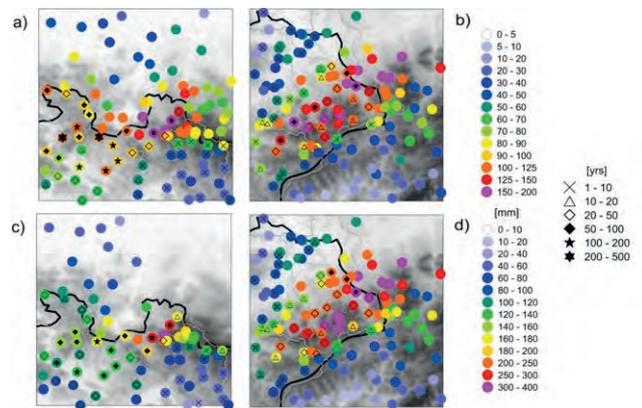
Fig. XVI Maximum 1-day (a,b) and 3-day (c,d) precipitation totals in the most affected areas in May (b,d) and in August (a,c) 2010. The position of the studied areas is depicted in Figure III.
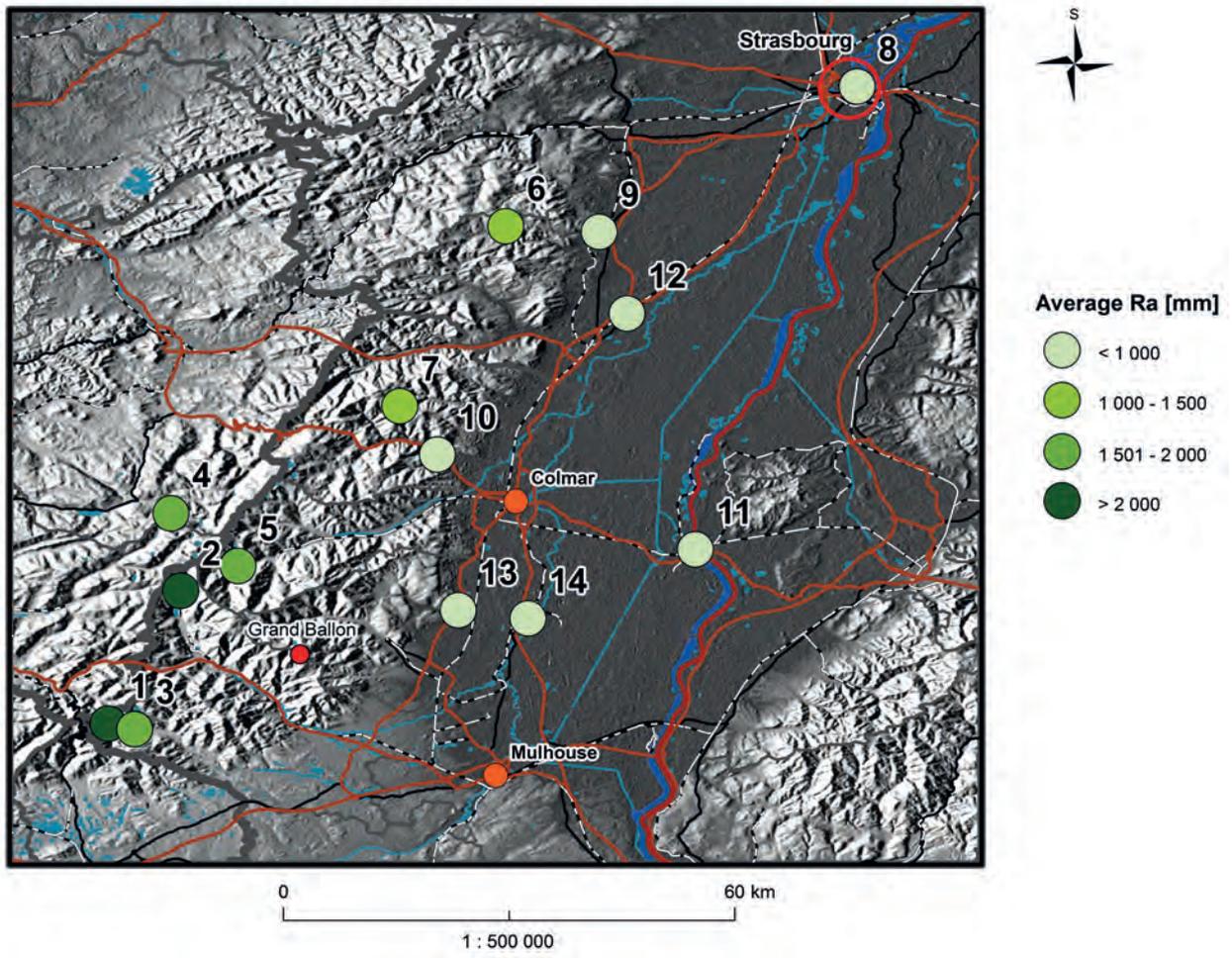
Fig. XVII Geographical position and the average annual rainfall ($\overline{Ra}$) of the 14 examined stations. Numbers represent stations listed in Table 1. The real values of $\overline{Ra}$ are recorded in this table too.
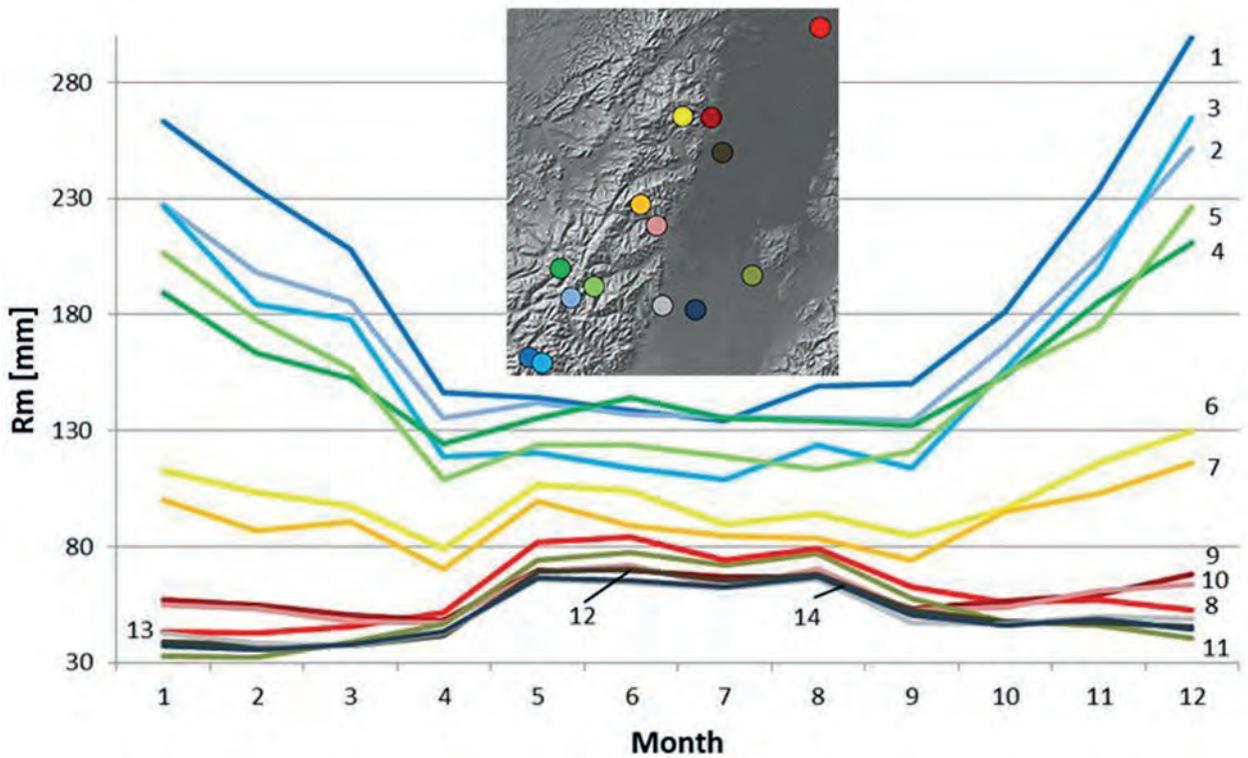

Fig. XVIII Average monthly rainfall ($\overline{Rm}$). Numbers represent stations listed in Table 1.
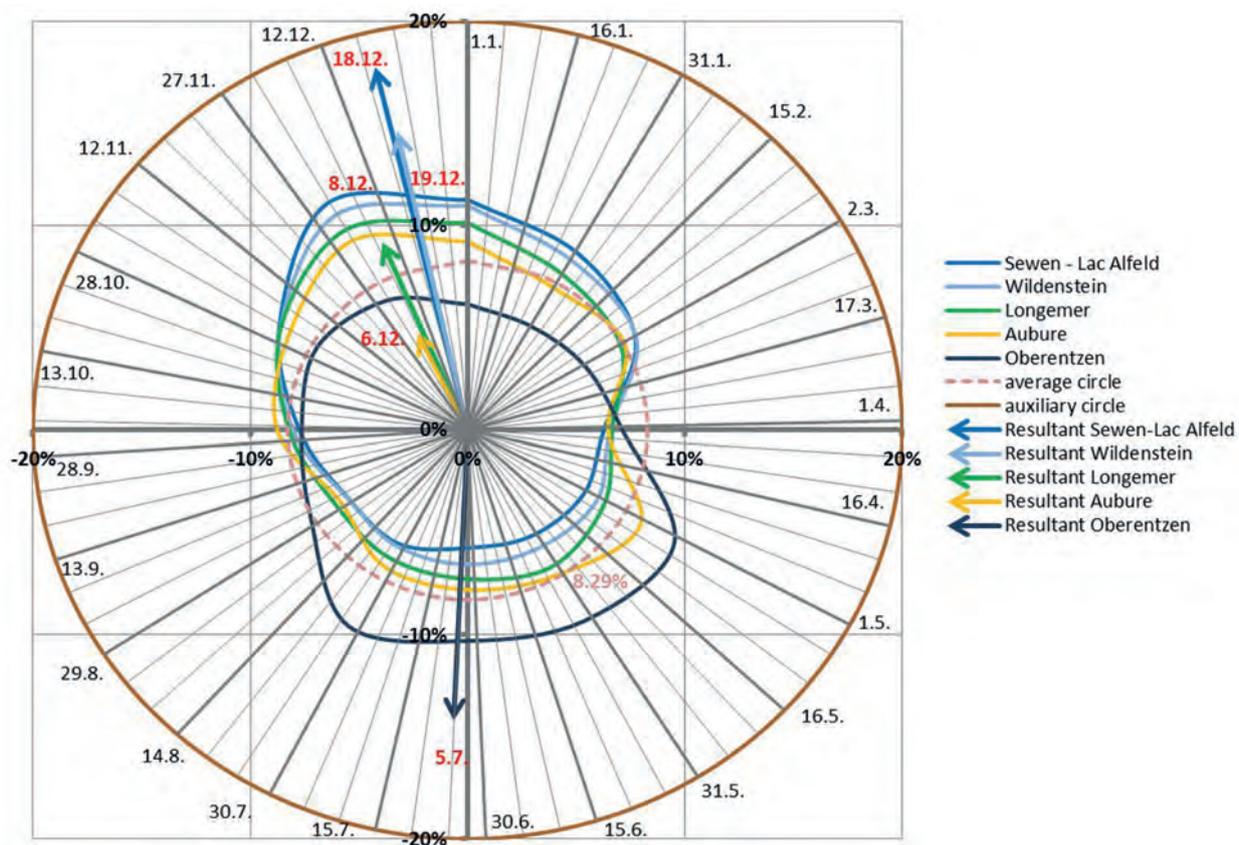
Fig. XIX Intra-annual variability of rainfall at 5 selected stations. The curve links the mean monthly rainfalls and the vector points in the direction of the date representing the centre of gravity of humid period.
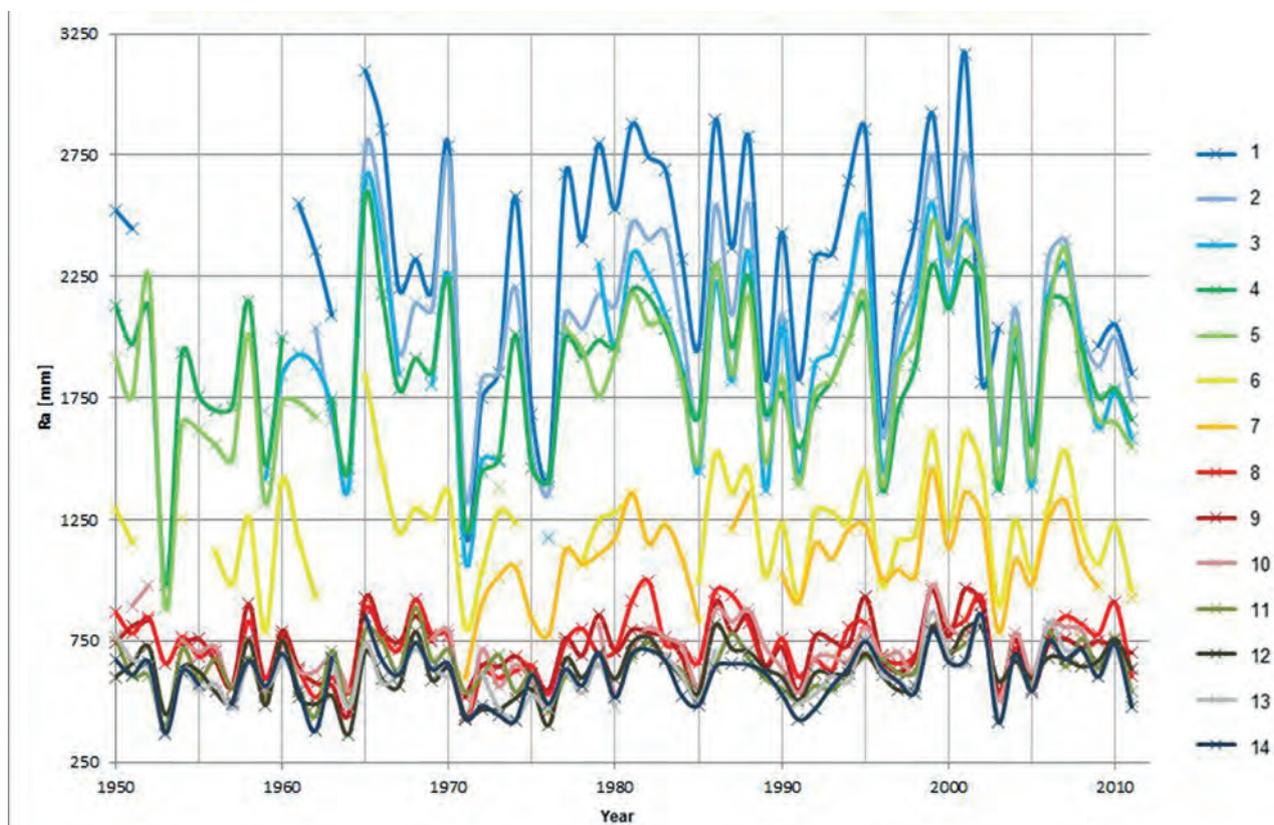
Fig. XX Inter-annual variability of annual rainfall *Ra* for the period 1950–2011. The graph shows the evolution of *Ra* in time. Gaps correspond to years with missing data (Table 1). Stations are listed in the order of descending *Ra*. Station numbers are identified in Table 1.
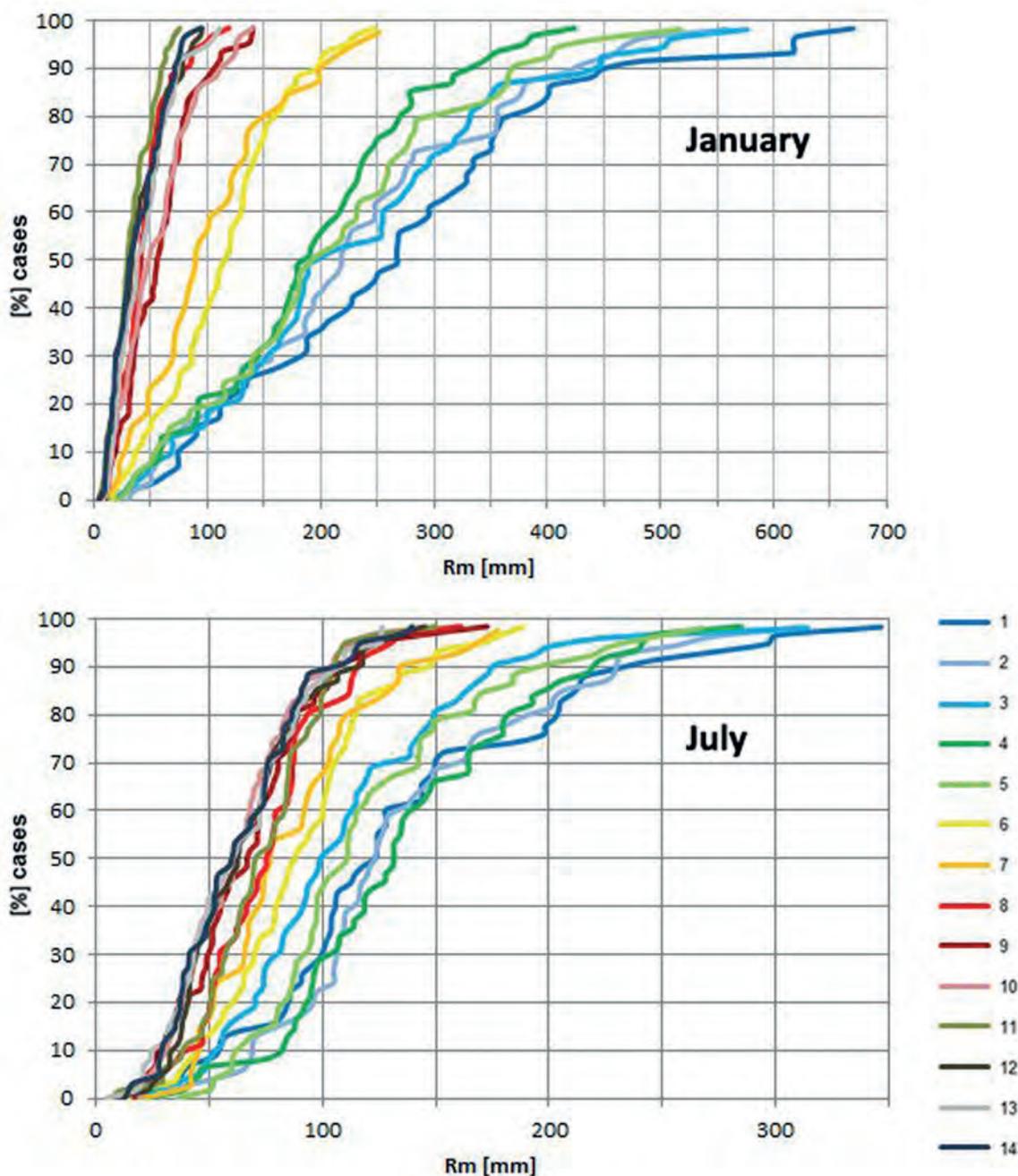
Fig. XXI Inter-monthly variability of monthly rainfall *Rm* for January and July. The cumulative distribution function for January (on the upper graph) and July (on the lower graph) for 14 meteorological stations and are presented for 1950–2011. Numbers represent stations listed in Table 1.
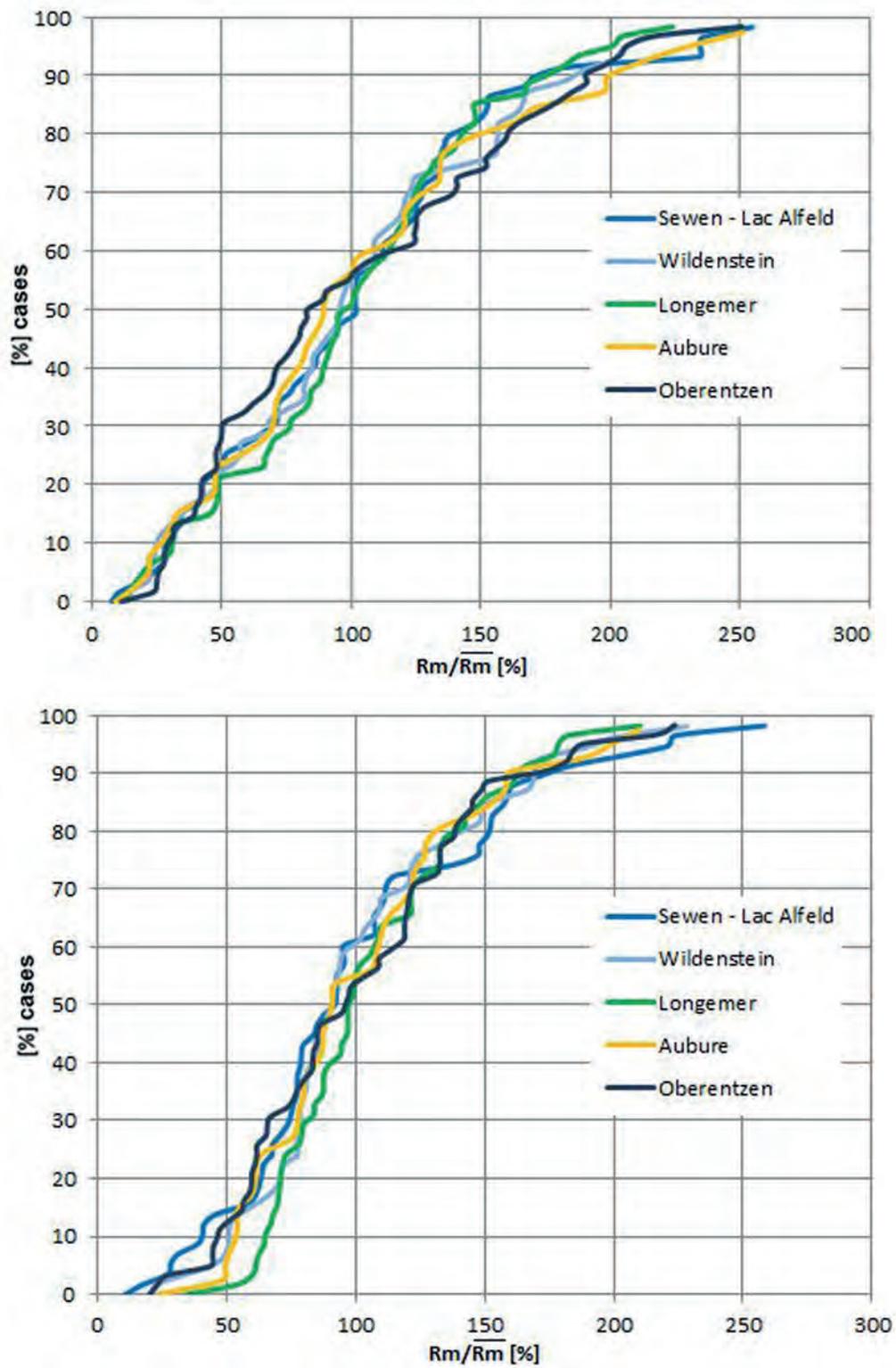
Fig. XXII As in Figure 5 but related to the average monthly rainfall for 5 selected stations.
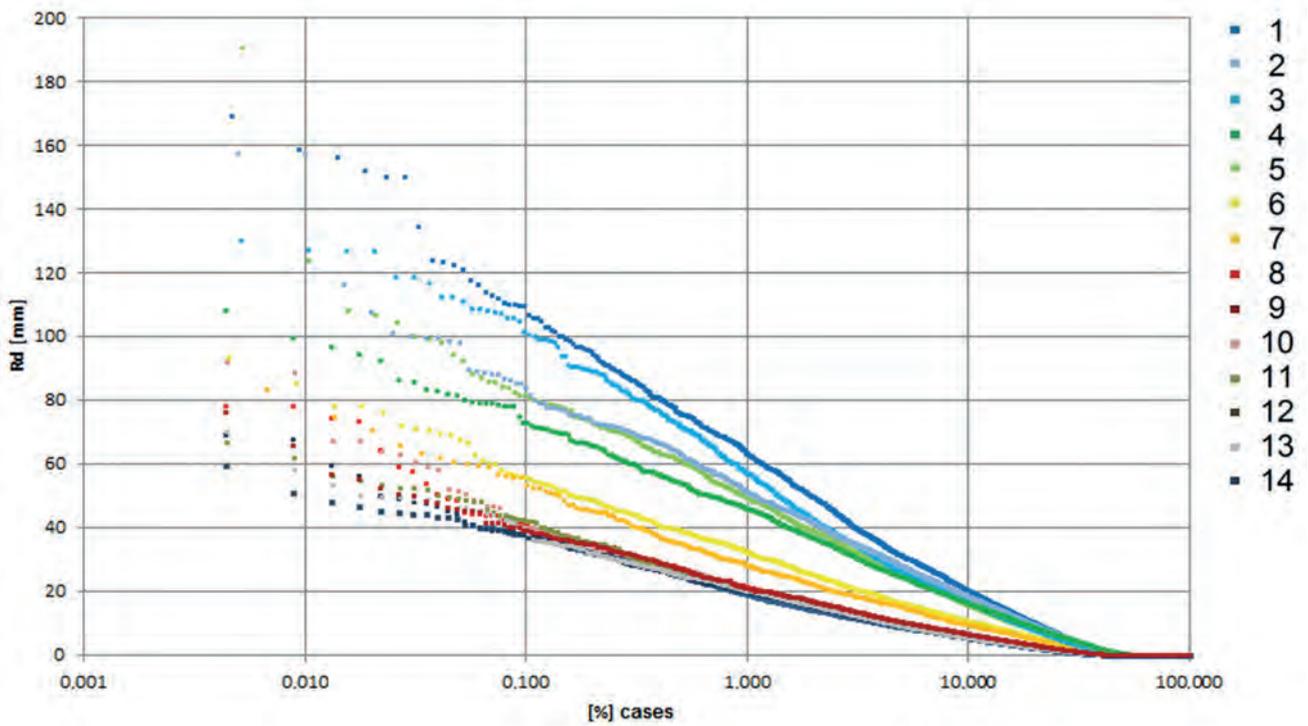
Fig. XXIII The variability of daily precipitation totals (*Rd*). Stations are listed in the order of descending annual rainfall, station numbers are identified in Table 1. The x-axis is expressed in logarithmic scale.
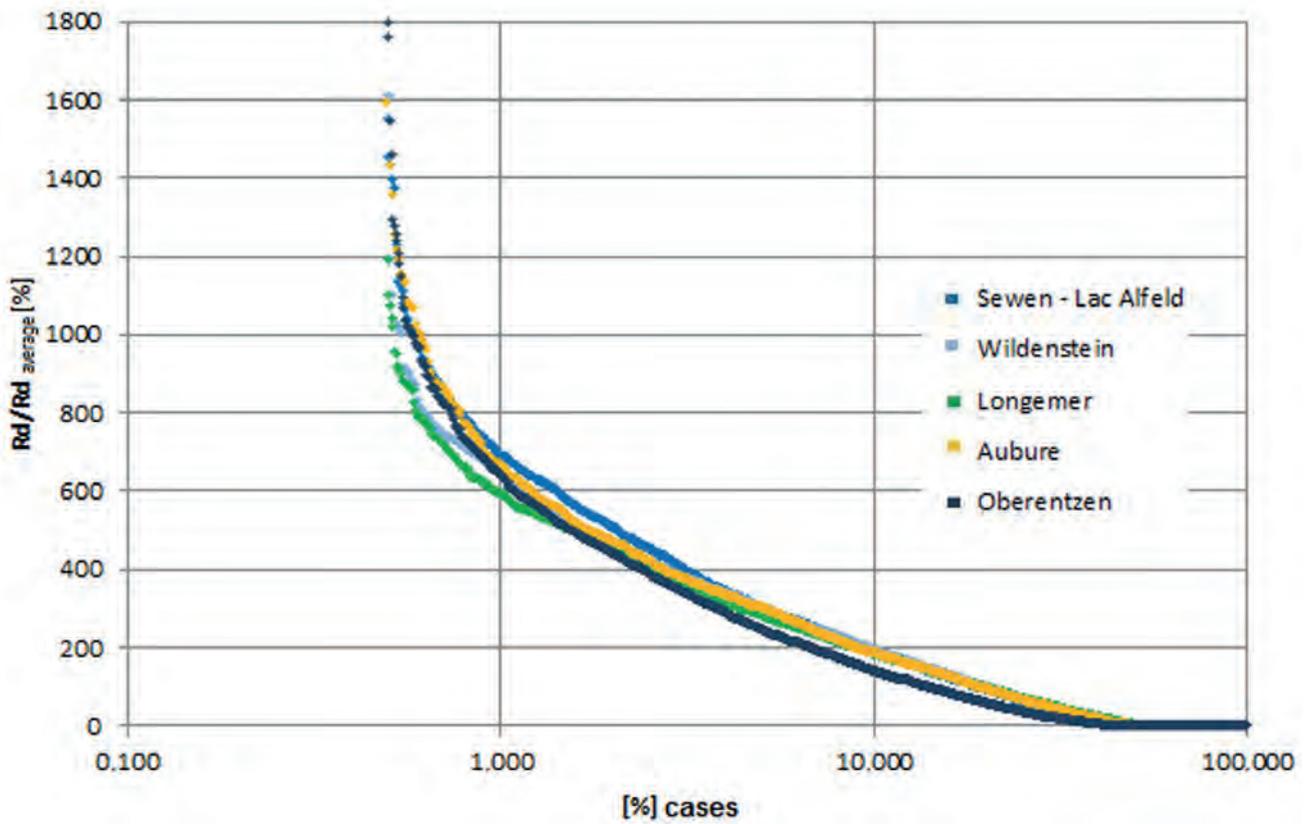

Fig. XXIV As in Figure 7 but related to the average daily rainfall for 5 selected stations. The x-axis and y-axis are expressed in logarithmic scale.
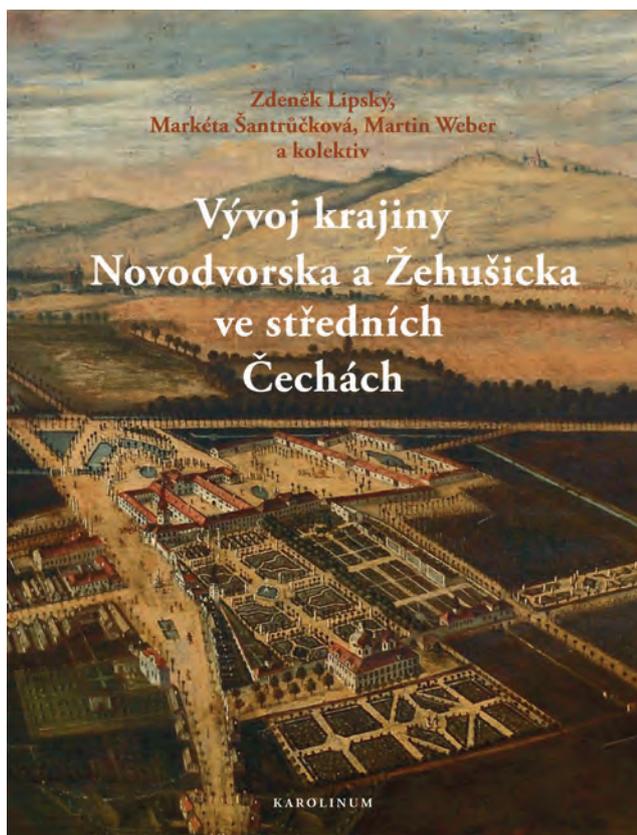
Zdeněk Lipský, Markéta Šantrůčková, Martin Weber a kolektiv: Vývoj krajiny Novodvorska a Žehušicka ve středních Čechách
Praha, Karolinum 2011, brožovaná, 204 str., 1. vydání, cena: 300 Kč

Bohatě ilustrovaná kniha přibližuje historický vývoj staré kulturní krajiny ve středních Čechách, zhruba na území bývalého novodvorského a žehušického panství (dnešní okres Kutná Hora), v níž se zachovaly četné stopy cílevědomých krajinářských úprav z doby baroka a klasicismu. Těžiště monografie spočívá ve zhodnocení krajinného vývoje 18.–20. století, protože v této době zde probíhaly intenzivní změny a pro jejich analýzu je možné využít historické mapy a jejich zpracování v prostředí geografického informačního systému. Ojedinělost publikace je dána nejen tématem, ale také interdisciplinárním přístupem: představuje výsledek společné práce odborníků přírodovědného, humanitního, technického i uměnovědného zaměření.

ISBN 978-80-246-1905-7
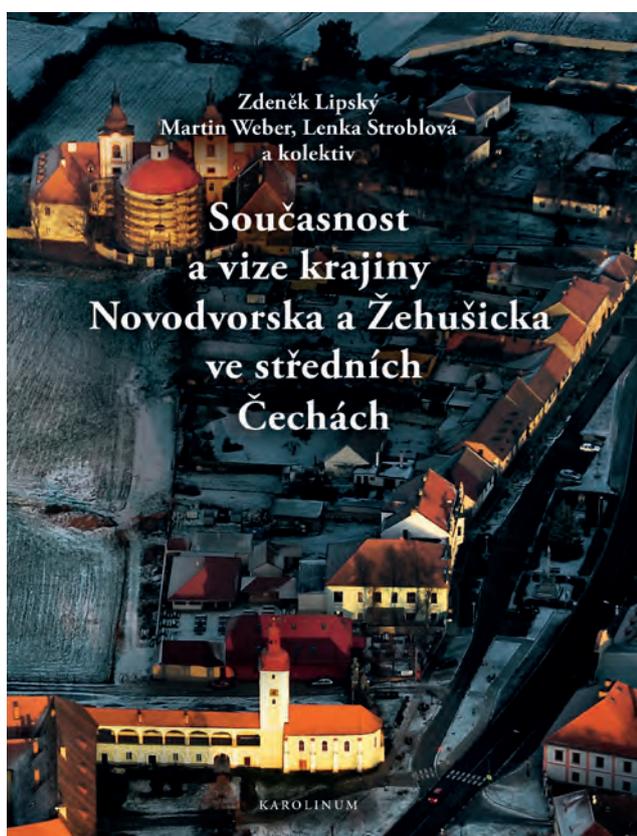
Zdeněk Lipský, Martin Weber, Lenka Stroblová a kolektiv: Současnost a vize krajiny Novodvorska a Žehušicka
Praha, Karolinum 2013, brožovaná, 408 str., 1. vydání, cena: 390 Kč

Monografie navazuje na knihu *Vývoj krajiny Novodvorska a Žehušicka ve středních Čechách*, vydanou v roce 2011. Podrobně rozebírá přírodní podmínky i stávající způsob využívání krajiny Novodvorska a Žehušicka s aktuálními problémy, které z něj vyplývají. Provádí důkladnou SWOT analýzu současného stavu území a na jejím základě předkládá variantní scénáře budoucího vývoje krajiny a její cílové charakteristiky. Text je doplněn velkým počtem map, grafů, tabulek a fotografií.

ISBN 978-80-246-2075-6